

Alma Mater Studiorum – Università di Bologna

DOTTORATO DI RICERCA IN

SCIENZE BIOTECNOLOGICHE E FARMACEUTICHE

Ciclo XXXI

**Settore Concorsuale: 03/D2**

**Settore Scientifico Disciplinare: CHIM/09**

DESIGN AND MANUFACTURE OF MICROPARTICLES CONTAINING  
SMALL MOLECULES OR BIOLOGICS FOR OPTIMIZED DRUG RELEASE

**Presentata da: Serena Bertoni**

**Coordinatore Dottorato**

Prof. Santi Mario Spampinato

**Supervisore**

Prof.ssa Nadia Passerini

**Co-supervisore**

Prof.ssa Beatrice Albertini

**Esame finale anno 2019**

**DESIGN AND MANUFACTURE OF MICROPARTICLES CONTAINING  
SMALL MOLECULES OR BIOLOGICS FOR OPTIMIZED DRUG RELEASE**

**Serena Bertoni**

## Abstract

Oral delivery is the preferred and the most common route of drug administration. In view of the increasing amount and chemical diversity of active compounds, new strategies are required to develop oral efficient drug products with optimized pharmaceutical performances, limited side effects and improved therapeutic outcomes. The present work includes distinct research projects having as common feature the development of innovative drug delivery systems to improve the oral bioavailability of drugs characterized by different pharmaceutical limitations. Microparticles (MPs) mainly produced by a solvent-free technology, *spray congealing*, have been evaluated as delivery platform to address some of the most important challenges in the area of oral drug delivery.

The first two case studies addressed the issue of low oral bioavailability of poorly water soluble drugs by the development of solid dispersion of the drug into Gelucire-based MPs. This strategy (Case study I) allowed to enhance the solubility and dissolution rate of the non-steroidal anti-inflammatory drug indomethacin, as well as to significantly increase (about 2.5 times) its oral bioavailability *in vivo*. The application of these Gelucire-based formulations to three model poorly soluble drugs (Case study II) enabled to gain new insight on the mechanisms of bioavailability enhancement. The bioavailability improvement depends on multiple effects, which include effects given by the hydrophilic carrier and effects resulting from changes in the drug crystalline original state, specifically amorphisation, conversions into metastable polymorphs and crystals size reduction.

Very different are the technological challenges in case of oral *non-systemic* small molecules drugs used for diseases involving the gastrointestinal tract, such as intestinal bowel disease (IBD), where a local delivery with limited systemic effect is desired. The Case study III, carried out at the University of Helsinki under the supervision of Prof. H. A. Santos, focused on the development of nano-in-micro composites based on a combination of responsive materials: a reactive oxygen species (ROS)-responsive polymer was used to prepare polymeric drug-loaded nanoparticles, and a pH-sensitive polymer was employed to produce the MPs.

The last part of the project focused on the oral delivery of biologic drugs. It is well known that the delivery of macromolecules through oral route is extremely difficult due to the multiple barriers of the gastrointestinal tract (GIT), mainly the acidic pH of the stomach and the digestive enzymes, which both can easily cause modifications in the protein structure. Solid lipid microparticles (SLMs)

produced by spray congealing were chosen as system for oral delivery of biologics owing to their biocompatibility and biodegradability.

After oral intake, lipid formulations are subjected to various changes in the GIT, which can deeply affect the drug release. In Case study IV, the influence of SLMs size and composition on the release performance of a model hydrophilic compound was studied in *biorelevant* dissolution media simulating the conditions of the whole GIT (gastric tract and proximal human intestine).

In Case study V the study continued evaluating the effect of pancreatic lipases on the emulsification and digestion of glycerides-based SLMs. Dynasan 114 (trimyristin) was the lipid subjected to the highest extent of lipolysis, and thus suitable to encapsulate the biologic molecule, retain it until the intestinal environment and then release it upon lipolysis. Therefore, Dynasan 114-based SLMs were explored as oral delivery system for two different biologic drugs with local action in the intestine:  $\beta$ -Galactosidase, an enzyme used for the treatment of lactose intolerance (Case study V) and glutathione, a tripeptide with antioxidant activity (Case study VI). In both case studies, spray congealed SLMs showed encapsulation efficiency values always higher than 95% and no modification, loss or degradation of the biologic drug during the process. Specifically, the activity and the kinetic parameters of the enzyme were not affected by the encapsulation process. In parallel, the solid-state properties of the crystalline glutathione were maintained after encapsulation as well. The effectiveness of SLMs were examined simulating the pathway of SLMs throughout the GI tract: in gastric environment the protection of the active molecule from the degradation, fundamental for  $\beta$ -Galactosidase, was directly proportional to the particle size of Dynasan 114-based SLMs. In intestinal environment, the drugs were released with a faster rate in the medium simulating the fed state. Finally, the cytocompatibility of Dynasan 114-based SLMs was tested on HT29 cells, confirming to be completely safe at concentrations up to 2000  $\mu\text{g/ml}$ .

Overall, MPs can provide a solid platform for the development of a number of oral formulations, representing a versatile drug delivery system able to address the different issues related to both small molecules and biologic drugs.

## Table of contents

ABSTRACT.....	1
TABLE OF CONTENTS.....	3
LIST OF PUBLICATIONS.....	5
ABBREVIATIONS AND SYMBOLS .....	6
1. INTRODUCTION .....	7
1.1 Oral drug delivery .....	7
1.1.1 Physiology of the GIT .....	7
1.1.2 Systemic delivery .....	8
1.1.3 Local delivery .....	9
1.1.4 Factors influencing oral bioavailability .....	10
1.2 Recent challenges in oral drug delivery.....	12
1.2.1 Oral small molecule drugs.....	12
1.2.2 Oral biologic drugs .....	14
1.3 Microparticles (MPs) for oral drug delivery .....	15
1.3.1 MPs composition .....	17
1.3.2 MPs preparation methods .....	18
1.3.3 MPs characterization .....	19
1.4 Spray congealing technology.....	22
2. AIMS OF THE THESIS .....	25
3. CASE STUDIES .....	26
Case study I: Exploring the use of spray congealing to produce solid dispersions with enhanced indomethacin bioavailability: <i>in vitro</i> characterization and <i>in vivo</i> study.....	26
I. Introduction.....	26
I. Experimental section.....	27
I. Results and discussion.....	32
I. Conclusion .....	46

Case study II: Gelucire-based microparticles as a versatile strategy to improve the oral bioavailability of poorly water-soluble APIs: investigation into the mechanism of bioavailability enhancement.....	47
II. Introduction .....	47
II. Experimental section .....	49
II. Results and discussion .....	52
II. Conclusion.....	66
Case study III: pH and reactive oxygen species-sequential responsive nano-in-micro composite for targeted therapy of inflammatory bowel disease.....	67
III. Introduction .....	67
III. Experimental section .....	68
III. Results and discussion .....	73
III. Conclusion.....	83
Case study IV: An investigation into the release behavior of solid lipid microparticles in different simulated gastrointestinal fluids .....	84
IV. Introduction .....	84
IV. Experimental section .....	85
IV. Results and discussion .....	89
IV. Conclusion.....	101
Case study V: Spray congealed lipid microparticles for the local delivery of $\beta$ -galactosidase to the small intestine.....	102
V. Introduction .....	102
V. Experimental section .....	104
V. Results and discussion .....	109
V. Conclusion.....	120
Case study VI: Glutathione-loaded solid lipid microparticles as innovative delivery system for oral antioxidant therapy .....	121
VI. Introduction .....	121
VI. Experimental section .....	122
VI. Results and discussions.....	126
VI. Conclusion.....	134
4. CONCLUDING REMARKS .....	135
REFERENCES.....	136

## List of publications

This thesis is based on the following original publications:

Research articles:

- I **Bertoni S.**, Dalpiaz A., Ferraro L., Beggiato S., Albertini B., Passerini N., Exploring the use of spray congealing to produce solid dispersions with enhanced indomethacin bioavailability: *in vitro* characterization and *in vivo* study, *Eur. J. Pharm. Biopharm.*, *in revision*
- II **Bertoni S.**, Albertini B., Passerini N. Gelucire-based microparticles as a versatile strategy to improve the oral bioavailability of poorly water-soluble APIs: investigation into the mechanism of bioavailability enhancement, *manuscript in preparation*
- III **Bertoni S.**, Liu Z., Correia A., Martins J. P., Rahikkala A., Fontana F., Kemell M., Liu D., Albertini B., Passerini N., Li W., Santos H. A., pH and reactive oxygen species-sequential responsive nano-in-micro composite for targeted therapy of inflammatory bowel disease, *Adv. Funct. Mat.*, 2018, 28, 1806175.
- IV Albertini B., **Bertoni S.**, Perissutti B., Passerini N., An investigation into the release behavior of solid lipid microparticles in different simulated gastrointestinal fluids, *Colloids and Surfaces B: Biointerfaces*, 2019, 173, 276-285.
- V **Bertoni S.**, Albertini B, Dolci L. S., Passerini N., Spray congealed lipid microparticles for the local delivery of  $\beta$ -galactosidase to the small intestine, *Eur. J. Pharm. Biopharm.*, 2018, 132, 1-10.
- VI **Bertoni S.**, Facchini C., Prata C., Calonghi N., Passerini N., Albertini B., Glutathione-loaded solid lipid microparticles as innovative delivery system for oral antioxidant therapy, *manuscript in preparation*

Review articles:

- VII **Bertoni, S.**, Dolci L. S., Albertini B, Passerini N., Spray congealing: a versatile technology for advanced drug delivery systems, *Ther. Deliv.*, 2018, 9, 833-845.

Articles were reprinted and adapted with permission from the publisher.

## Abbreviations and symbols

BDDCS	Biopharmaceutics Drug Disposition Classification System
BCS	Biopharmaceutics Classification System
CBZ	Carbamazepine
CAF	Caffeine
CIN	Cinnarizine
DEX	Dextran
GIT	Gastro-intestinal tract
GRAS	Generally recognized as safe
GSH	Glutathione ( <i>reduced form</i> )
GSSG	Glutathione ( <i>oxidized form</i> )
HPLC	High-performance liquid chromatography
IBD	Inflammatory bowel disease
IND	Indomethacin
IV	Intravenous
MP(s)	Microparticle(s)
PEG	Polyethylen glycol
RIF	Rifaximin
ROS	Reactive Oxygen Species
SD	Solid dispersion(s)
SLM(s)	Solid lipid microparticle(S)
TBM	Tolbutamide
WPN	Wide Pneumatic Nozzle



## 1. Introduction

### 1.1 Oral drug delivery

The oral route is the simplest, more feasible and convenient way of drug administration. Oral administration is preferred over parenteral delivery due to its ease of administration and non-invasiveness, as well as increased patient compliance rates, all of which lead to enhanced therapeutic benefits. From the industrial perspective, pharmaceutical oral products (especially solid forms) offers the advantages of good stability and generally moderate production costs. Currently, more than 60% of marketed drugs are oral products <sup>1</sup>

#### 1.1.1 Physiology of the GIT

Gastrointestinal tract (GIT) also referred to as the alimentary canal or the gut, is a series of organs consisting in a 9 meters-long tube with the functions of taking in food, digesting it, and expelling the remaining waste. The human GIT, schematically shown in Figure 1, is divided into the upper and lower tracts. The first one consist of the mouth, pharynx, esophagus, stomach, and duodenum, while the second one includes most of the small intestine and all of the large intestine.

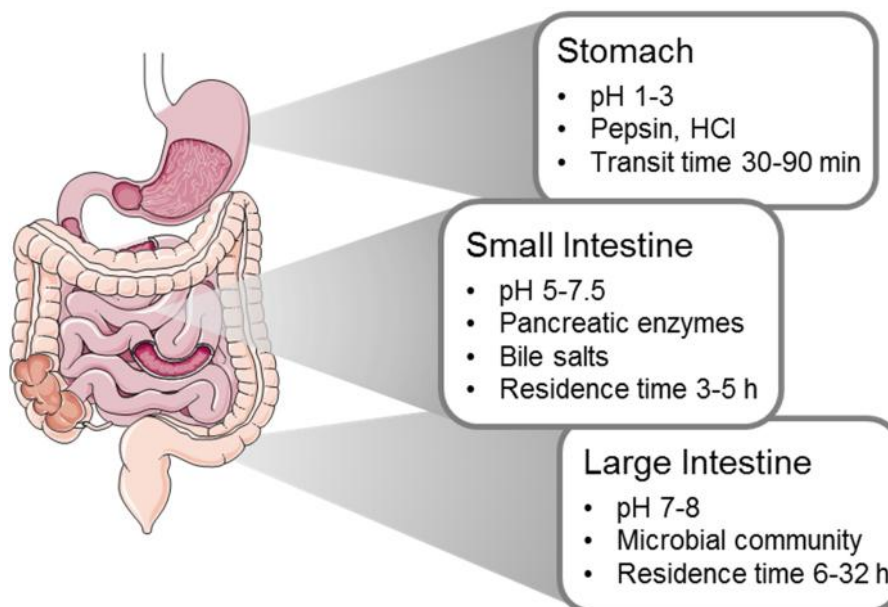


**Figure 1.** Schematic illustration of the different environments of the GI tract (stomach, small, and large intestine) encountered by a drug upon oral administration. Figure generated from Servier Medical Art.

The stomach works as a temporary food storage and mixes the food with the gastric fluid to form what is called chyme. The gastric secretions include hydrochloric acid (HCl) and enzymes that

contribute to the partial digestion of food, which mainly consists in proteolytic degradation due to the enzyme pepsin. In the empty state, the stomach is contracted and its volume is about 25-50 ml, but the size increases up to 10 times in the fed state. Spontaneous movements (contractions) of the stomach allow the formation of the chyme and the passage to the small intestine, in a process called gastric emptying. Gastric emptying occurs during fasting as well as fed states. The principal variables affecting the transit of a dosage form in the stomach are the gastric fluid volume, degree of digestive activity, rate of stomach emptying, and pH<sup>2</sup>. The drug absorption is generally limited through gastric mucosa, except from some APIs. For most drugs, the principal site of absorption is the proximal small intestine, particularly the duodenum where the epithelial surface area through which absorption can take place is very large<sup>2</sup>. Here, the intestinal mucosa is covered by a monolayer of epithelial cells, joined by tight junctions consisting mostly of enterocytes which express microvilli on the apical exterior, increasing the mean total mucosal surface of the digestive tract interior to around 260-300 m<sup>2</sup><sup>3</sup>. Although the absorption of most drugs can be explained by passive diffusion (e.g. transcellular transport or paracellular transport through the tight junctions), some compounds have specific transport mechanisms. The enteric fluid presents weakly acidic pH, digestive enzymes (mainly pancreatic) and bile salts. Bile salts are composed of water-soluble, amphipathic molecules which are formed in the liver and excreted into the small intestine, where they help emulsify dietary lipids into micelles helping their digestions and absorption<sup>4</sup>. The last part of the intestine, called large intestine, is approximately 1.5 m long and forms the colon (ascending, transverse, and descending), with a small distal part forming the rectum. Here, the environment is typically less acidic than this of the small intestine and it is characterized by the presence of a rich microbial flora, which is involved in the immune functions and in the digestion process. The intestinal microbiota plays an important role in the drug pharmacokinetic, because it can metabolize different xenobiotics including food toxicants, phytochemicals and drugs. The drug absorption in the large bowel is limited and variable because the environment shows important differences along its length and it is only in the right colon where conditions are sufficiently favourable to allow drug absorption.

### 1.1.2 Systemic delivery

The majority of drugs that are administered orally has a systemic therapeutic effect. This means that, in order to obtain the pharmacological effect, the active compound needs first to be absorbed into the systemic blood circulation. For this process to be possible, the drug formulated into a medicine must first be released from the dosage form and dissolve in the biological fluids. The

available volume of the fluids should be large enough to initiate and achieve an adequate drug dissolution. Then, the second step consists in the absorption through the gastrointestinal mucosa. Immediately after enteric absorption, the drug passes via the portal vein into the liver where it is metabolised, in a process defined *first pass metabolism*. The fraction of drug that reaches unmodified the bloodstream will be distributed in all the districts, allowing to reach the target site and exploit its action. Drug bioavailability is defined as the fraction of dose that reaches the systemic circulation after its administration. Whereas after intravenous injection the bioavailability is 100%, in case of oral administration the bioavailability of drugs is always less than 100%, because the active molecule undergo many steps before reaching the target tissue.

### 1.1.3 Local delivery

Some diseases localized in particular anatomic districts are not adequately treated by systemic drug administration. A common reason is the difficulty to reach the district itself; otherwise, the presence of the drug in the systemic circulation should be avoided for toxicity issues related to the drug systemic exposure. For example, in case of diseases involving the gastric or the intestinal tract, the target site of action consists in specific regions of the GIT. In this case, the drug needs to act locally within the gastro-intestinal lumen and/or on the gastro-intestinal mucosa, without reaching the systemic circulation. These APIs are defined as *non-systemic* or *non-absorbed* drugs. For these compounds, which are not intended to be absorbed into bloodstream, the bioavailability may be assessed by measuring the rate and extent of the active ingredient that becomes available at the site of action <sup>5</sup>. In contrast to traditional oral drugs, which are designed to be rapidly absorbed and to achieve therapeutic plasma levels, non-absorbable drugs are designed to minimize systemic exposure <sup>6</sup>. Examples of oral non-systemic drugs are polymeric resins that sequester phosphate ions, potassium ions, or bile acids for the treatment of electrolyte imbalances or hypercholesteremia. More recently, non-absorbable small molecules or peptides targeting luminal enzymes or transporters have been developed for the treatment of mineral metabolism disorders, diabetes and enteric infections. Especially for chronic syndromes such as inflammatory bowel disease (IBD), afflicting large patient populations, these drugs offer the great advantage of limited off-target systemic effects, reduced risk of drug-drug interaction and toxicity.

#### 1.1.4 Factors influencing oral bioavailability

Oral bioavailability depends on a number of different factors, which can be divided in three categories. The first category includes the physicochemical properties of the drug, such as molecular size, pKa, lipophilicity, intra and inter-molecular bonding, ionic charge and drug solid state (crystalline, amorphous or polymorphic form). Those characteristics influence mainly the drug solubility and permeability through the intestinal membrane. The Biopharmaceutics Classification System (BCS) divides the orally administered drugs into four classes according to their dose, their aqueous solubility and their permeability across the GI mucosa. A drug compound is considered highly soluble if the highest dose strength is soluble in 250 ml aqueous media or less of aqueous media over a pH range of 1-7.5 at 37.5 C°, while a drug substance is considered to be highly permeable when the extent of absorption in humans is determined to be 90% or more of the administered dose<sup>7</sup>. BCS is a widely accepted system of classification, which represent a useful tool with application in the academic, industrial, and regulatory pharmaceutical area<sup>8</sup>. Drugs belonging to BCS class I present ideal properties of solubility and permeability, thus, they can be formulated into traditional dosage forms leading to desirable oral bioavailability. Differently, BCS class II drugs have good permeability but poor solubility and they are defined as poorly water soluble drugs. Opposite properties are those of BCS class III drugs, presenting high water solubility and low permeability. Finally, the most critical category is represented by the class IV, where both solubility and permeability are limited and represent an obstacle to oral bioavailability.

Various physico-chemical properties contribute to make a compound poorly soluble. Lipinski's rule of five (Ro5) has probably been the most influential concept in preclinical drug discovery during the last decades correlating data of orally administered small molecule drugs with their molecular structure. Lipinski's Ro5 predicts that poor oral absorption is more likely when the compound presents more than 5H-bond donors, 10H-bond acceptors, the molecular weight is greater than 500, and the calculated Log P is greater than 5<sup>9</sup>. However, the Ro5 only holds for compounds that are not substrates for active transporters. When this rule was developed, information about drug transporters was very limited, but in recent years many new insights on drug transporters have been gained. Thus, more recent classification systems have been proposed<sup>10</sup> and were able to provide useful predictions for development of new drugs. For example, the Biopharmaceutics Drug Disposition Classification System (BDDCS) builds upon the Ro5 criteria and can successfully predict drug disposition characteristics for drugs, including routes of drug elimination and the effects of efflux and absorptive transporters on oral drug absorption<sup>11</sup>.

The second category consists on the external physiological characteristics of the GIT. The interaction of an oral medicine with the GIT is highly complex and dynamic. During transit down the GI tract, the active molecule is subject to a variety of physiologic factors, such as action of digestive enzymes, bile salts and metabolism of intestinal microbiota. Moreover, the drug transits through environments with different pH and composition. All these variables can profoundly affect the drug release, its chemical stability and its intestinal permeation. The presence or absence of food when the drug is administered should also be considered, because the intestinal motility, gastric transit time, intestinal resident time and fluid properties are a function of the digestive period. Additionally, the characteristics of the patient (e.g. age, genre, healthy or pathological conditions) have a crucial impact on the final drug bioavailability<sup>12</sup>.

The third category regards the specific dosage form used for the API administration. Although some aspects of the oral bioavailability depend exclusively on the first two categories (e.g. the first pass metabolism), the characteristics of the oral dosage form can influence other important processes, primarily the dissolution step and the permeation through the intestinal membrane. Differently from liquid formulations where the API is already in solution, in case of solid dosage forms (e.g. tablets) more events are necessary. As illustrated in Figure 2, these events are schematized in three steps: disintegration of the solid form into granules or smaller particles, dissolution of the particles of API into the biological fluids and absorption of the API through the biological membranes. Particularly, the processes of dissolution and absorption are often difficult to control and represent a technological challenge for the formulators. As a consequence, an oral formulation able to achieve optimal drug dissolution and permeability is considered as an ideal pharmaceutical product.

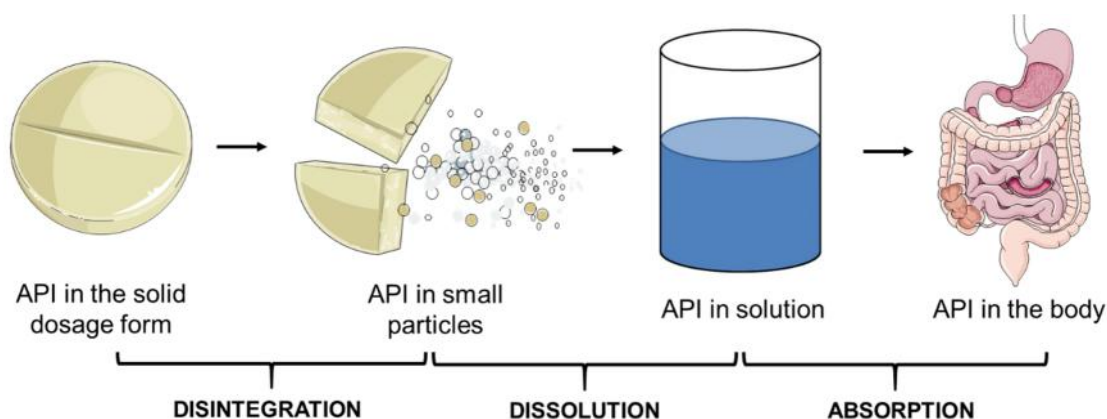


**Figure 2.** Schematic illustration of the steps necessary for an API contained in an oral solid dosage form to reach the systemic circulation. Figure generated from Servier Medical Art.

## 1.2 Recent challenges in oral drug delivery

As described in the previous paragraph, the GIT presents various chemical and enzymatic barriers that can affect oral delivery of drugs. For example, the acidic pH of the stomach can easily cause chemical degradation of many drugs with significant influences to their oral bioavailability. The presence of enzymes might result in degradation of active compounds containing hydrolyzable groups. Furthermore, poor oral absorption through the intestinal membrane represents one of the most common reasons impeding the development of oral pharmaceutical products <sup>13</sup>. Oral bioavailability of some drugs is considerably low because of high degree of pre-systemic metabolism or first pass (hepatic) metabolism. Finally, drug efflux transporters are also responsible for efflux of various drugs from the site of absorption leading to poor oral bioavailability <sup>14</sup>.

Poor oral bioavailability leads to high variability, poor control over drug plasma concentrations and weak therapeutic effect, thus limiting the development of orally effective medicines. It is well established that poor oral bioavailability is one of the leading causes of compound failure in preclinical and clinical development <sup>15</sup>. Understanding the causes of low oral bioavailability is fundamental to find the right approach to address the problem.

The application of formulation strategies to improve oral bioavailability is often the approach of choice, particularly for compounds in development or for drugs already marketed <sup>16</sup>. Compared to other approaches based on chemical modifications, such as the use of prodrugs or the lead-optimization, formulation design is preferred due to its advantages of low cost and reduced time. Moreover, the possibility to use generally recognized as safe (GRAS) materials represents a benefit in terms of safety risks and development requirements. Thus, the design and development of innovative effective oral formulations is currently one of the major challenges in the area of the pharmaceutical research. At last, the formulation need to be designed basing on the particular API.

### 1.2.1 Oral small molecule drugs

Due to the recent advances in combinatorial chemistry and high-throughput screening methods, the new molecular entities (NMEs) today are frequently large-molecular-weight lipophilic compounds. Nowadays poorly water-soluble drugs, belonging to the class II and IV of the BCS, constitute the 70% of new drug candidates and approximately the 40% of the marketed oral drugs are categorised as practically insoluble (<100 µg/mL) <sup>17</sup> (Figure 3).

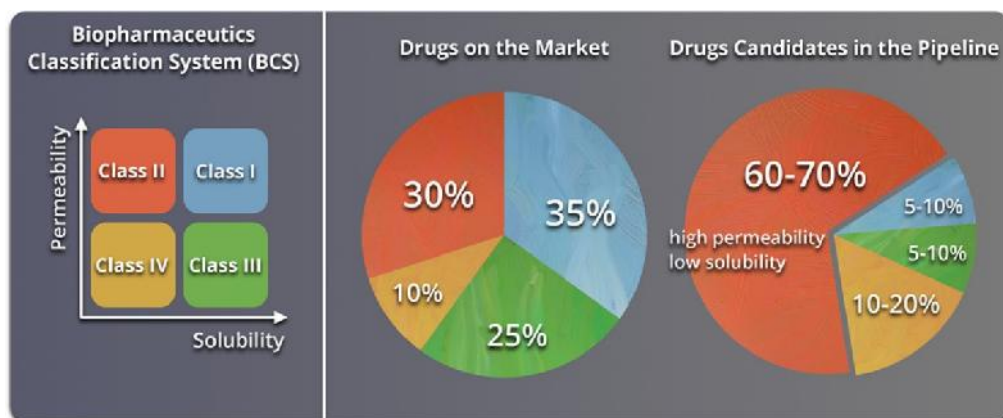


**Figure 3.** Representation of the Biopharmaceutics Classification System (BCS). The circle charts to the right show the estimated distribution of marketed and pipeline drugs by BCS classes. Reprinted with permission from “Advances in Polymer Design for Enhancing Oral Drug Solubility and Delivery” Jeffrey M. Ting, William W. Porter, III, Jodi M. Mecca, Frank S. Bates, and Theresa M. Reineke *Bioconjugate Chemistry* 2018 29 (4), 939-952.” Copyright 2018 American Chemical Society.

This problem represents one of the major challenges for the pharmaceutical industry in the recent years. Different strategies have been proposed over the years to address the issue of poorly water soluble drugs and they include particle size reduction, formation of nanocrystals and cocrystals, pH adjustment, use of cosolvents, self-emulsifying drug delivery systems (SEDDS), inclusion complexes, nanosuspensions and solid dispersions (SD). Among them, solid dispersion (SD) is one of the most common approaches and has proved to be an effective strategy for the formulation of different compounds belonging to class II of the BCS<sup>18</sup>. In SD the drug is incorporated in an inert hydrophilic carrier in the solid state. The success of SD lies in the potential to (i) decrease the drug particle size even up to molecular level (ii) modify the drug solid state from a thermodynamically stable form to a high-energy one and (iii) improve drug particles wettability by the aid of the hydrophilic excipient. A concern with SD is the possibility of the high-energy drug substance undergoing changing to the more stable form during storage (e.g. crystallization of amorphous SD). Efforts to overcome this challenge include proper excipient selection, drug loading optimization and appropriate manufacturing technologies<sup>19</sup>.

Very different are the technological challenges in case of *non-systemic* small molecules drugs used for diseases involving the stomach or the intestine. For example, Inflammatory Bowel disease (IBD) is a chronic inflammation of the GIT affecting millions of patients worldwide. In IBD, the challenge involve the formulation of a system with a localized drug delivery in the diseased site of the GIT.

Current therapeutic products specifically indicated for IBD are based on the delivery of prodrugs, colonic microflora activated systems, pH dependent and time dependent systems. However, these approaches are associated with inconsistent efficacy and inter-patient variability due to the lack of selectivity between diseased and healthy sites. The critical step in the development of a reliable drug delivery system for IBD treatment is to achieve improved localization and controlled release of the API at the site of inflammation, minimizing the premature release and subsequent absorption in the blood stream <sup>20</sup>.

### 1.2.2 Oral biologic drugs

The application of biologic drugs (i.e. proteins, peptides, enzymes, nucleic acids, hormones, etc.) as therapeutic agents has emerged over the past few decades as one of the most impactful areas of medicine <sup>21</sup>. After recombinant insulin was approved for use in 1982, over 150 different protein-based drugs for various therapeutic applications have received FDA approval <sup>22</sup>. The increasing interest of the pharmaceutical industry towards biologic drugs is due to the several benefits they can offer, if compared to conventional drugs, such as high activity and specificity, low toxicity and minimal drug-drug interactions. <sup>23</sup> Moreover, thanks to the advances in biotechnology, which enabled large-scale manufacturing, various therapeutic biomolecules have become recently available <sup>24</sup>. Despite the potential advantages of biopharmaceutics, nearly all protein therapeutics are currently administered by intravenous, subcutaneous, or intramuscular injection. Although oral pharmaceutical forms are much more convenient and non-invasive compared to injections, the delivery of macromolecules through oral route is extremely challenging. There are a number of major hurdles that must be overcome before active biomolecules can be successfully delivered via the oral route <sup>25</sup>. In particular, the main obstacles are represented by the acidic pH of the stomach and the digestive enzymes of the GI tract, which both can easily cause modifications in the protein structure, as well as a very low absorption through the mucus cell layer of the intestine epithelium <sup>26</sup>.

Biological drugs can be classified in two groups according to the therapeutic target: the first type has systemic effect, while the second type needs to act locally in the GIT. The latter one is recently moving into focus because local delivery avoids the problem of reaching the systemic compartments and, as a consequence, fewer restrictions regarding molecular size, polarity and charge <sup>27</sup>. Besides, other advantages of locally-delivered biologics include a potentially more favourable safety profile



due to minimal systemic exposure, reduced immunogenicity, and the absence of permeation-enhancing excipients, which usually implicate safety concerns<sup>28 29</sup>. However, there are currently only three marketed locally-delivered oral biological drugs: vancomycin, linaclotide and pancreatin<sup>30</sup>. The reason for this limited industrial application is probably represented by two main obstacles affecting the oral bioavailability of these drugs: the acidic pH of the stomach and the digestive enzymes of the GI tract. The gastric environment causes the protonation of proteins and their unfolding and the digestive enzymes in the stomach (pepsin) and small intestine (e.g., chymotrypsin, amino- and carboxypeptidases) cleave biomolecules into smaller fragments. The modifications in the protein structure lead often to the loss of its activity. Different strategies to protect the biologic drug from the harsh environment of the GIT have been developed: enteric coating, colon-targeting capsules, supplementation with sacrificial proteins that compete for degradation, and hindering enzymatic access using polymer conjugation<sup>27</sup>.

### 1.3 Microparticles (MPs) for oral drug delivery

Microparticles (MPs) are defined as solid particles with a size in the range of 1  $\mu\text{m}$  -1000  $\mu\text{m}$ . The drug is dissolved, entrapped, encapsulated or attached to a microparticle matrix. MPs are multiparticulate dosage form, as they consist of a multiplicity of small discrete units, each containing a fraction of the total amount of API administered. Compared to single traditional dosage forms, in the multiparticulate formulation the drug has been divided among these various delivery entities. Multiparticulate oral drug delivery systems are preferred over single unit dosage forms due to their comparatively greater dispersibility in the GIT, reduced-risk of dose dumping and systemic toxicity, decreased dosing frequency, increased patient compliance, lesser variability in concern to absorption, and accurate dosing<sup>31</sup>. Moreover, due to the small size, multiparticulates are less dependent on gastric emptying (Figure 4a), resulting in less inter and intra-subject variability in gastrointestinal transit time. Above all, they represent a flexible dosage form and, therefore, they are particularly attractive for developing patient-tailored pharmaceutical products. MPs present multiple interesting features that make them particularly attractive as drug delivery system: (i) controlled release of drugs, (ii) protection of the encapsulated materials against degradation caused by the external environment, (iii) masking the organoleptic properties such as colour, taste and odour of the API, (iv) good technological properties of the resulting powder-like materials, and (v)

safe handling of toxic encapsulated materials <sup>32</sup>. Depending upon the method of preparation, different systems can be obtained (Figure 4b). The two primary types of MPs are microcapsules and microspheres. In the first type, the API is confined within the microcapsule by a surrounding layer of excipient. In contrast, microspheres are a *matrix* system where the active compound is evenly distributed throughout the carrier. Starting from 2010, BCC Research has published a number of market research reports entitled “Microspheres: Technologies and Global Markets”, analyzing the global market for MPs from both the manufacturing and demand points of view. As shown in Figure 4c, the market for microspheres has considerably grown from 2010 and it is estimated to increase from \$ 5 billion in 2017 to \$ 6.9 billion in 2022. Specifically, the application of MPs in the pharmaceutical and the medical areas is an emerging trend and it is predicted to grow further in the next years <sup>33</sup>.

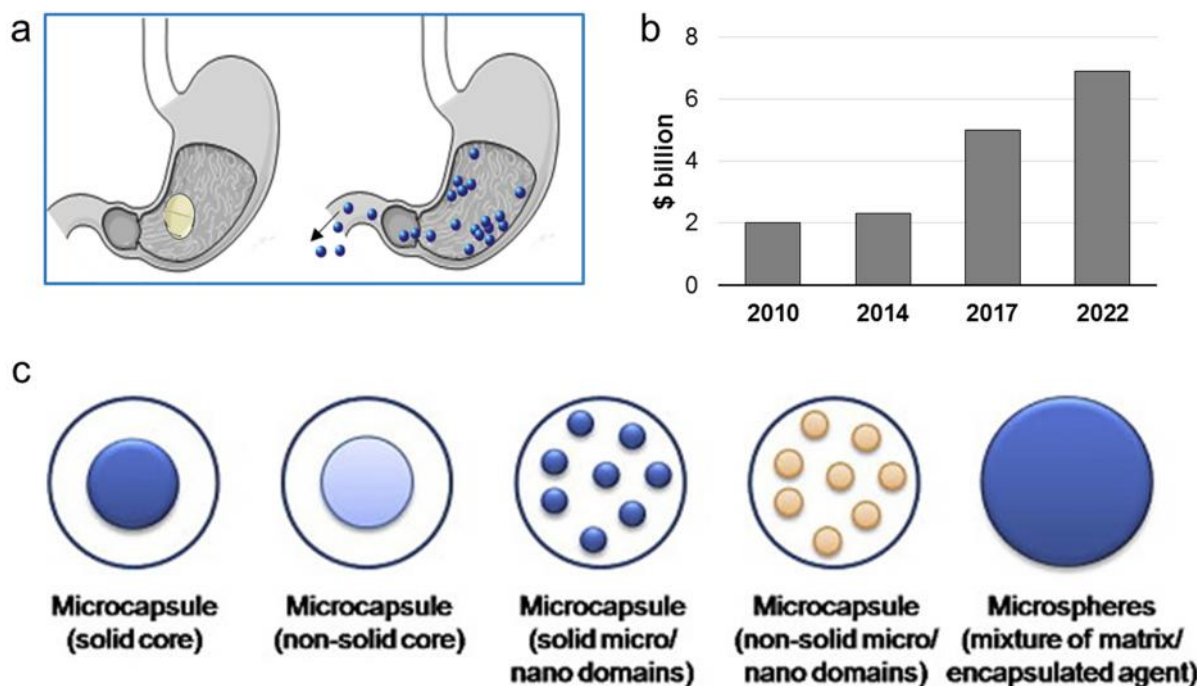


**Figure 4.** (a) Difference between single and multiparticulate solid dosage forms in the passage through the pylorus: systems with size < 2 mm are independent on gastric emptying. (b) Global industrial market for MPs in 2010 and in 2015. (c) Different categories of microparticles. Figure 4c is reprinted with permission from “Designing polymeric microparticles for biomedical and industrial applications” Elisa Campos, J. Branquinho, Ana S.Carreira, Anabela Carvalho, Patrícia Coimbra, P. Ferreira, M. H. Gil European Polymer Journal 2013, 49, 2005-2021.

### 1.3.1 MPs composition

MPs can be manufactured using a large variety of starting materials, both natural and synthetic, and by many different preparation techniques. Frequently the carrier systems used is based on polymeric materials. Polymeric MPs for biomedical application are generally prepared using biodegradable polymers. The most commonly used include poly(lactide-co-glycolide), poly(lactide), poly(glycolide), poly(caprolactone) and naturally sourced materials such as chitosan, alginate, dextran, gelatin and cellulose-based polymers.

Lipid class	Composition	Commercial name	Melting temperature (°C)	HLB
<b>Triglycerides</b>	Trimyristin	Dynasan 114	55-58	-
	Tripalmitin	Dynasan 116	65-66	-
	Tristearin	Dynasan 118	70-73	-
<b>Partial glycerides</b>	Glyceryl monostearate	Myvaplex™ 600 Myverol™ 18-04K NF	58-59	3-4
	Glyceryl distearate	Precirol® ATO 5	53-57	2
	Glyceryl dibehenate	Compritol® 888 ATO	65-70	2
<b>Fatty acids</b>	Palmitic acid	-	63	-
	Stearic acid	-	69	-
<b>Fatty alcohols</b>	Cetyl alcohol	-	49-50	5
	Cetearyl alcohol	-	50-56	4.7
	Stearyl alcohol	-	60-61	5.5
<b>PEG fatty acid esters</b>	Behenoyl polyoxyl-8 glycerides	Compritol® HD5 ATO	60-67	5
<b>Hydrogenated oils</b>	Hydrogenated castor oil	Cutina HR	83-88	-
	Hydrogenated palm oil	Softisan® 154	55-60	-
	Hydrogenated soybean oil	Sterotex HM	57-70	-
<b>Waxes</b>	Beeswax	-	62-65	-
	Carnauba wax	-	82-86	-
	Microcrystalline wax	-	60-90	-
<b>Hard fat</b>	Mixed glycerol esters	WITEPSOL H 15	33-36	-

**Table1.** Lipophilic matrix materials

As an alternative drug carrier system to polymeric MPs, solid lipid MPs (SLMs) were introduced in the early 1990s. Compared to other excipients which can be used to control the release rate of drugs, lipid components are receiving a great deal of attention due to their low cost, negligible toxicity, biodegradable properties, and versatility to be applied in solvent free-processes<sup>34</sup>. Specifically, SLMs overcome most of the drawbacks associated with polymeric particles, such as inefficient biodegradation, polymer accumulation, toxicity and the general requirement of organic solvents for their production <sup>35</sup>. The components of SLMs can be either lipophilic, such as triglycerides, fatty acids, fatty alcohols and waxes or hydrophilic, such as polyethylene glycol (PEG) and Gelucire. The most common excipients used to produce SLMs are schematized in Table 1 and Table 2.

Excipients	Composition	Commercial name	Melting temperature (°C)	HLB
<b>Polyoxylglycerides</b>	stearoyl polyoxyl-32 glycerides	Gelucire® 50/13	46-51	11
	Lauroyl Polyoxyl-32 glycerides	Gelucire® 44/14	42-48	11
<b>PEG</b>	PEG 1500	-	44-48	-
	PEG 3350	-	53-57	-
	PEG 4000	-	53-59	-
	PEG 6000	-	55-61	-
<b>Poloxamers</b>	Poloxamer 188	Lutrol® F 68 NF Kolliphor® P 188	52	>24
	Poloxamer 407	Lutrol® F 127 Pluronic F127® Kolliphor® P 407	56	18-23

**Table 2.** Hydrophilic matrix materials

### 1.3.2 MPs preparation methods

In order to obtain MPs, the API should be dissolved or dispersed into the excipient(s). The methods to prepare MPs are generally divided in two main categories: those based on the solvent evaporation and those employing on the melting of the excipient.

The solvent evaporation-based methods have been widely employed for the production of either polymeric or lipid MPs. The excipient is first dissolved in a solvent, which might be organic or aqueous, the API is added to the solution and finally the solvent is removed by evaporation. One

common technique based on solvent evaporation is the *microemulsion method*, where the organic solution of excipient is emulsified with an aqueous phase in presence of an emulsifying agent. This technique include single-emulsion methods (oil/water (O/W) or water/oil (W/O) emulsion) which are suitable to encapsulate hydrophobic drugs, whereas hydrophilic drugs are usually encapsulated using water/oil/water (W/O/W) double-emulsion methods, resulting in core-shell MPs. More recently, particles in the micro and nano-range have been prepared through *microfluidic technology*. This technique generates droplets in a device (T-junction) supplied with the excipients and drugs dissolved in immiscible solutions, followed by the solidification of the droplets by means of polymerization or solvent evaporation <sup>36</sup>. Although the principle is the same of the emulsion methods in bulk, the main advantages of using a microfluidic platforms include the smaller amount of solvents required and the highly uniform and predictable size of the particles obtained. In addition, solid particles can be obtained also by technologies such as spray drying, which involve the evaporation of the solvent.

The melting-based methods are suitable for low melting carriers, usually lipids, with melting temperatures ranging between 30 and 90°C. In the *melt emulsification method* the aqueous phase containing surfactants is emulsified with a melted excipient which was previously added with the drug. The obtained emulsion is then cooled to room temperature and the MPs are obtained by solidification. Compared to traditional solvent evaporation method, the risk of drug loss during the process is reduced. Finally, MPs with low melting carriers can be produced by spray congealing technology, which is discussed in details in chapter 1.4.

### 1.3.3 MPs characterization

- **Loading of the drug:** Drug loading (DL) and encapsulation efficiency (EE) are the two parameters used to express the loading of the active compounds in the MPs. Generally, the particles are opportunely treated (e.g. with solvents or heating) to degrade/dissolve/melt the carrier in order to release all the entrapped drug, and the amount of active compound is assayed by means of an appropriate analytical method. DL is then calculated considering the percentage ratio between the amount of loaded drug and the total weight of the formulation. Differently, EE % indicates the efficiency to entrap the drug particles within the

carrier and it is correlated to the DL as well as to the initial amount of drug added in the preparation process. DL % and EE% can be calculated according to the following equations:

$$DL (\%) = \frac{\text{mass of drug loaded in MPs}}{\text{total mass of MPs}} * 100$$

$$EE (\%) = \frac{\text{mass of drug in MPs}}{\text{starting mass of drug}} * 100$$

DL and EE are influenced by the preparation method and the formulation variables (e.g. drug and carrier characteristics). DL value can be used as quick indication to estimate the total amount of MPs to be administered, considering the therapeutic daily dose of each specific drug.

- **Morphology:** The study of MPs morphology include information about the size and the shape of the MPs, as well as surface characteristics. The shape of MPs mainly influences the technological properties of the pharmaceutical formulation, such as flowability. Microscopic analysis of the particle surface can provide important information about distribution of drug crystals, porosity or defects on the particle matrix. Moreover, by monitoring of the morphology overtime, changing in particle appearance might indicate changes in carrier (and/or drug) solid state or rearrangement of drug/carrier molecules.
- **Drug-carrier interactions:** Interaction between drug and carrier are particularly common when the API and the excipient have similar structure and establish stable bonds, such as ionic interactions, hydrogen bonds, dipole-dipole, and Van der Waals interactions. Specific analysis already in the pre-formulation phase are fundamental to exclude possible incompatibility or to observe the presence of interactions and their effect on the component mix. Moreover, by studying the nature of possible interactions between the components of the MPs, it is possible to understand the reasons for the drug physical state or for transitions from one state to another. Spectroscopic techniques are the mostly widely used for the study of interaction mechanism at a molecular level. Fourier-transform infrared (FT-IR) spectroscopy can directly monitor the vibrations of the functional groups that characterize molecular structure at the solid state reactions <sup>37</sup>.
- **Solid state properties of drug and carrier:** In the MPs, the drug can be in presence as molecular, amorphous, microcrystal or colloidal state, which is dependent on the

formulation and preparative process thereof. The evaluation of the solid physical state (amorphous, crystalline or partially amorphous) of the API is extremely important because it influences the stability during the product storage and deeply affect drug dissolution performance and therefore, drug bioavailability. Various techniques can be used to follow modifications in the solid state of drug/carrier spray congealed system. Among them, differential scanning calorimetry (DSC) and powder X-ray diffraction (XRPD) are the most commonly used for solid-state studies <sup>35</sup>.

- **Drug release studies:** The release profile of the API from the MPs is determined by *in vitro* dissolution studies. These studies are performed according to the Pharmacopoeia dissolution tests such as apparatus I, II and IV <sup>38</sup>, although non-official apparatus are also often used. The amount of drug released is assayed by an appropriate analytical method. The dissolution medium is chosen basing on the intended administration route and can have an important influence on the drug release profile. To better correlate *in vitro* data of oral formulations with the *in vivo* behaviour, media simulating the GI fluids were developed <sup>39</sup>. They are called *biorelevant media* and closely mimic the GIT environments in both fasted (without food) and fed (with food) states.
- **Studies with biological systems:** The biocompatibility of MPs can be studied *in vitro* by cell viability tests. Generally, lipid or polymeric MPs composed of biocompatible and biodegradable excipients are well tolerated. Nevertheless, the test is useful to check the tolerability of cells to different MPs concentration and it is important for MPs prepared with new materials or excipients that are not oral-approved. Cell models simulating the intestinal membrane are used to test the permeability of the API released from the MPs and permeated through the membrane. Moreover, tests of mucoadhesion can be performed in case of MPs with mucoadhesive properties. Differently from nanoparticles, MPs are unlikely to cross most biological barriers and can not be internalized by most cells because of their bigger size. For this reason, cell-particle interaction studies are rarely performed for MPs, except from small MPs (size < 10 µm) which can enter in some specialized cells (e.g., macrophages, neutrophils) by phagocytosis.

## 1.4 Spray congealing technology

Spray congealing, also known as spray chilling or spray cooling, is a process that transforms a melt into well-defined spherical solid particles<sup>34</sup>. This technology has been chosen in this thesis project as main preparation method for the production of MPs because of its multiple advantages. Firstly, it is a particularly low cost, simple and versatile method to prepare MPs. The main characteristic of this technology is the absence of solvent, either aqueous or organic, with related advantages such as low cost, possibility to load hygroscopic and water-sensitive substances and no toxicity related to the presence of organic solvents. Other advantages include the ability to obtain spherical free-flowing MPs suitable for tableting or capsule filling without the need of other downstream processes (e.g. secondary drying, milling, granulation) and high encapsulation efficiency values (90-100%). From the industrial perspective, spray congealing is easily scalable and can be adapted to the “continuous manufacturing”.

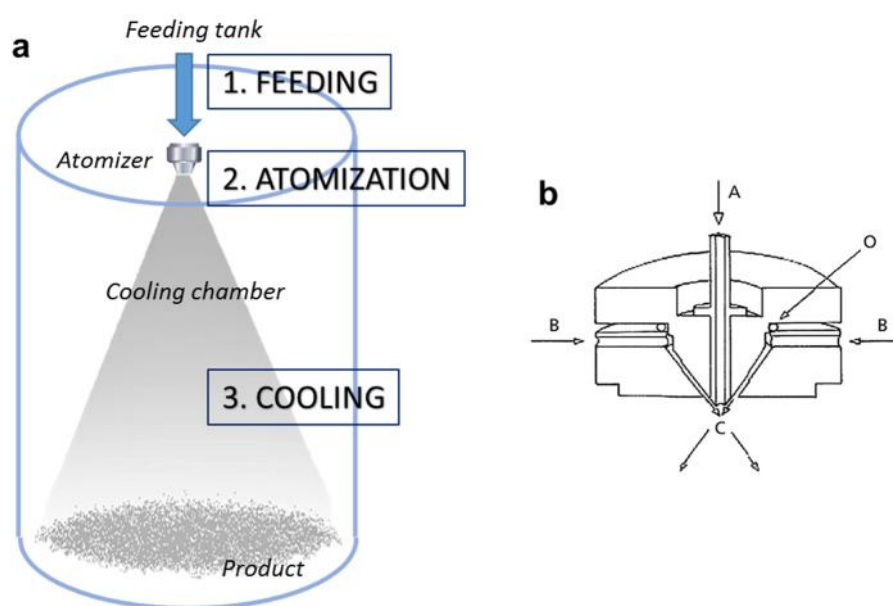


**Figure 5.** (a) Scheme of the spray congealing technology and process stages. Reprinted with permission from<sup>34</sup>. (b) Schematic representation of the wide pneumatic nozzle (WPN): A, fluid feed (molten fluid inlet); B, air inlet; C, atomisation of fluid; O, O-ring. Reprinted with permission from<sup>40</sup>.

Spray congealing technology is based on the atomization of a fluid in a chamber whose temperature is below the melting point of the carrier and a subsequent solidification of the droplets, leading to the formation of solid particles with dimensions in the micron range. Typical diameters ranges from 50 to 500  $\mu\text{m}$ . Since there is no solvent evaporation, the particles present a dense structure with no



hollow nor wide porous. The process can be schematized in three steps: feed stage, atomization stage and solidification stage (Figure 5a).

The first step of the process involves the preparation of the fluid consisting in the molten carrier, kept at a temperature above its melting point, and the active ingredient. Excipients suitable for spray congealing are substances with melting temperatures generally ranging from 35 to 90°C. The drug may be dissolved or dispersed into the molten carrier, according to its hydrophilic/hydrophobic properties. In this step it is fundamental to keep the fluid homogeneous, especially when the drug is not soluble or it is only partially soluble in the molten excipient, in order to have a uniform drug loading. During the atomization step, the molten fluid stream is breakup in small droplets. The performance of the spray congealing process strictly depends on the atomization efficiency of the molten fluid. Thus, the most important step is the atomization phase and can be performed using various type of atomizers: pressure <sup>41</sup>, two-fluids, rotary <sup>42 43</sup> and ultrasonic nozzles <sup>44 45</sup>. In the present thesis, an original pneumatic atomizer, called wide pneumatic nozzle (WPN) was used. After this step, in the cooling stage the droplets quickly solidify. The drug, if solubilized in the molten carrier, may re-crystallize in its original form, in a different polymorphic form <sup>46</sup>, in crystals with smaller size (i.e. nanocrystals), or may solidify in the amorphous form. The MPs obtained by spray congealing can be described as a solid dispersion, which is defined as a dispersion of one (or more) active ingredient(s) in an inert carrier or matrix at solid state <sup>47</sup>. More specifically, it is appropriate to discriminate between solid solutions (where the drug is molecularly dissolved in the solid excipients matrix) and solid dispersions (where the drug is dispersed as crystalline or amorphous particles within the matrix). A schematic classification of the different systems that can be obtained is reported in Figure 6.

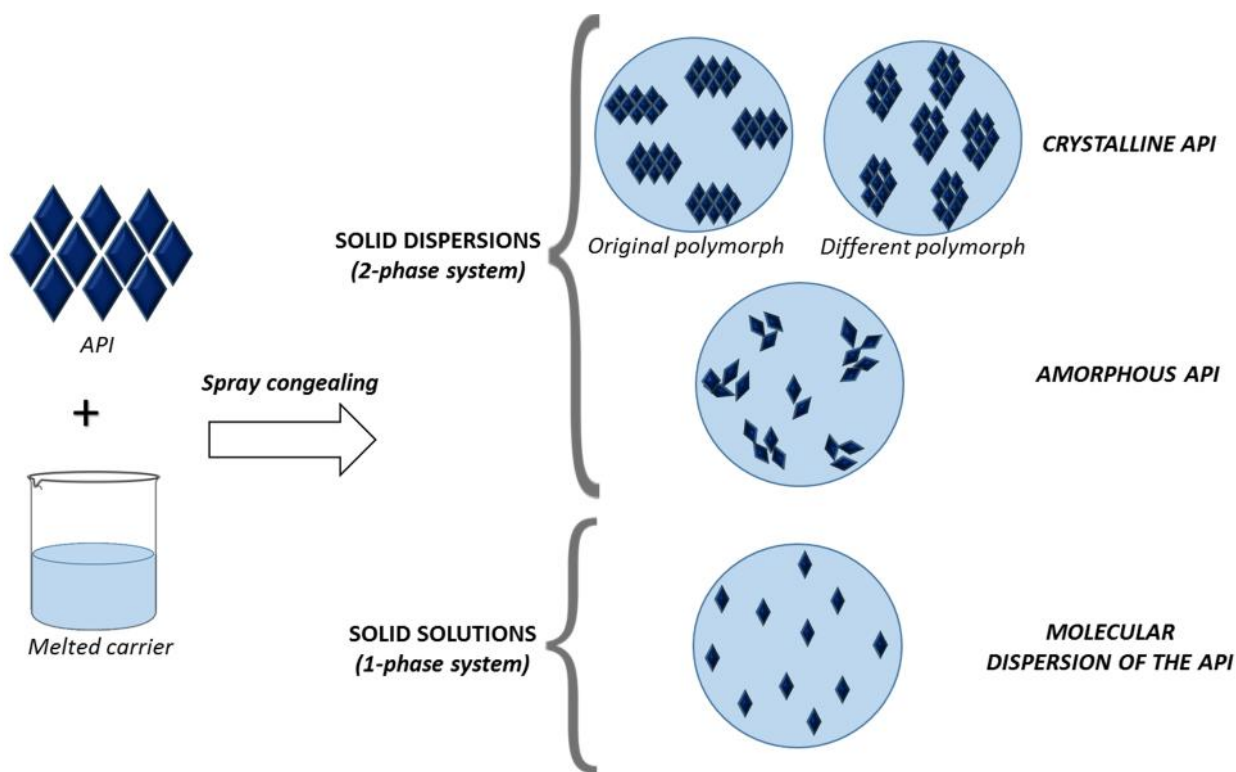


**Figure 6.** Classification of the different solid dispersions/solutions which can be obtained by spray congealing. Reprinted with permission from <sup>34</sup>.

## 2. Aims of the thesis

The aim of this thesis project is the development of microparticles (MPs) to optimize the oral bioavailability of drugs. In view of the advantages of multiparticulate systems and their versatility, MPs were employed for the delivery of different active pharmaceutical ingredients (APIs). Depending on the problem of the specific API and on the therapeutic purpose, different formulations were designed and characterized. Specifically, the six case studies of this thesis project face some of the most relevant challenges in the area of oral drug delivery.

The first part of the project is focused on the development of MPs containing small molecule drugs.

- Hydrophilic MPs were developed to enhance the oral bioavailability of poorly water soluble drugs. The MPs were characterized in terms of morphology and solid state properties and their efficacy was tested *in vitro* and *in vivo* (case study I). Moreover, the mechanism of solubility and dissolution enhancement was investigated (case study II).
- In case of diseases involving the gastrointestinal tract, such as intestinal bowel disease (IBD), a local delivery with limited systemic effect is desired. Thus, a different formulation approach was adopted. Specifically, a nano-in-micro composite was formulated to obtain a targeted delivery to the inflamed site of the intestine (case study III).

The second part addresses the problem of oral delivery of biologic drugs. Solid lipid microparticles (SLMs) are a promising carrier for oral delivery of biologic drugs owing to their biocompatibility and biodegradability.

- The influence of SLMs size and composition on the release performance of a model hydrophilic compound was studied in dissolution media simulating the conditions of the gastrointestinal tract (case study IV).
- The effect of the pancreatic lipases on the digestion of the lipid matrix was also evaluated.  $\beta$ -Galactosidase (lactase), an enzyme used for the treatment of lactose intolerance, was loaded in SLMs to achieve a local drug delivery to the small intestine (case study V).
- The tripeptide glutathione, a biologic molecule with small size, was formulated into SLMs to develop an effective oral formulation with antioxidant activity (case study VI).

### 3. Case studies

Case study I: Exploring the use of spray congealing to produce solid dispersions with enhanced indomethacin bioavailability: *in vitro* characterization and *in vivo* study

#### I. Introduction

Indomethacin (IND) is a non-steroidal anti-inflammatory drug used for rheumatoid arthritis and other chronic inflammatory diseases. Despite its long time and widespread use<sup>48</sup>, IND can cause severe gastrointestinal complications, increased blood pressure and decreased kidney function<sup>49</sup>, and the risk of developing these adverse effects increases in the case of high doses and prolonged treatments. Additionally, the poor water solubility of IND represents a major limitation for its oral bioavailability. Many attempts to increase IND solubility and dissolution rate using different formulation strategies have been reported<sup>49 50 51 52</sup>, with the ultimate objective of reducing the daily dose and/or administration frequency. Among them, solid dispersion (SD) is one of the most commonly used and promising approach<sup>53 54</sup>. However, various problems limit SD extensive applications. Specifically, the low reproducibility and consistency in the quality of SD often lead to variations in the bioavailability<sup>55</sup>. In addition, due to the intrinsic characteristics of SD, the stability of the dosage form during manufacturing and storage (i.e. chemical instability and physical instability) is probably the main issue that still need to be totally addressed<sup>56</sup>. For the aforementioned reasons, managing the commercial production of SD-based products is more challenging than traditional products containing drugs in their most stable solid form<sup>57</sup>. Generally, the methods for the preparation of SD are classified in *solvent-based methods* and *melting-based methods*. An important reason of concerns in view of an industrial application of SD is the toxicity related with the use of organic solvents. On the other hand, the melting-based methods (e.g. hot melt extrusion) also presents some drawbacks, such as need of multiple downstream processes and, thus, higher production costs. Therefore, there is increasing need of simple, inexpensive technologies combined with feasible and stable formulations.

This research proposes an original oral delivery system for the bioavailability enhancement of IND, a BCS class II drug, which can address the multiple demands, desirable for a successful SD, of reproducible *in vitro* and *in vivo* performance, easily scaled-up manufacturing technology, non-toxic

and low-cost formulation and prolonged stability. Specifically, spray congealing technology was used for the manufacturing of IND-containing SD in the form of MPs with high encapsulation efficiency. A commercially available mixtures of mono, di and triglycerides with PEG esters of fatty acids, called “Gelucires” were chosen as hydrophilic low-melting temperature carriers. Gelucires are a family of vehicle including different excipients, all GRAS and oral-approved, wherein Gelucire 50/13 is probably the most studied for preparing matrix system such as particles, granules<sup>58</sup>, minitabets<sup>59</sup> and solid dispersions<sup>60</sup> and successfully employed in spray congealing<sup>61</sup>. In this study Gelucire 48/16, a new excipient recently marketed, was evaluated as suitable carrier to prepare MPs by means of spray congealing. Hence, the initial focus of our research was to investigate the ability of Gelucire 48/16 to enhance the dissolution performance of IND as well as to demonstrate whether it is a more efficient dissolution enhancer than Gelucire 50/13. Moreover, being SD complex binary systems where each component might influence the behavior of the other, the physicochemical properties of both components may determine the overall performance of the final formulation<sup>62</sup>. Therefore, a detailed solid state characterization was performed to understand the physicochemical properties of IND-loaded MPs after manufacturing and during storage. *In vitro* investigation on the MPs biopharmaceutical properties and *in vivo* study on rats after oral administration were performed to assess the benefits of the proposed formulation on oral bioavailability. Finally, the long-term stability (18 months) of the best formulation was studied.

## I. Experimental section

**Preparation of IND-loaded MPs:** MPs were produced by spray congealing using an external-mix two-fluid atomizer, called Wide Pneumatic Nozzle (WPN). Initially, the excipient of the formulation (Gelucire 50/13 and Gelucire 48/16 in different ratio, Gattefossè, Milan, Italy) was heated up to a temperature 5 °C above the melting point. IND (10% w/w, Sigma Aldrich, Steinheim, Germany) was added to the molten carrier and magnetically stirred until complete solubilization, and then loaded into the feeding tank. The temperature of the feeding tank of the nozzle and the inlet air pressure were set at 65°C and 3.5 bar, respectively. The atomized molten droplets hardened during the fall into a cylindrical cooling chamber, which was held at room temperature and the MPs were collected from the bottom of the cooling chamber. Three different drug-loaded formulations (MPs A, MPs B, MPs C) were produced. For comparison purposes, physical mixes of IND and excipients in the same weight ratio as the loaded MPs were prepared by mixing 10% of IND with 90% of unloaded MPs.

### ***IND-loaded MPs characterization:***

*Morphological analysis.* Shape and surface morphology of IND and MPs were observed by Scanning Electron Microscopy (SEM). Samples were fixed on the sample holder with double-sided adhesive tape, sputter coated with Au/Pd under argon atmosphere performed using a vacuum evaporator (Edwards, Crawley UK) and examined by means of a scanning electron microscope (ESEM Quanta-200) operating at 20,0 kV accelerating voltage.

*Particle size analysis.* Size distribution of MPs was evaluated by sieve analysis using a vibrating shaker (Octagon Digital, Endecotts, London UK) and a set of six sieves ranging from 75 to 500  $\mu\text{m}$  (Scientific Instrument, Milan, Italy).

*Determination of drug content.* IND content was determined by dissolving 20 mg of MPs accurately weighed in 50 mL of ethanol. The solution was shaken for 24h at 25°C. Finally, the solution was filtered, diluted with the same solvent, and the drug content was assayed spectrophotometrically at 320 nm. Each formulation was analysed in triplicate and the mean  $\pm$ SD was reported.

*Differential scanning calorimetry (DSC) studies.* DSC analysis were performed using a Perkin Elmer DSC 6 (Perkin Elmer, Beaconsfield UK) with nitrogen as purge gas (20mL/min). The instrument was calibrated with indium and lead for temperature, and with indium for the measurements of the enthalpy. Samples of pure IND, unloaded MPs and IND-loaded MPs, weighing 8-9 mg, were placed in an aluminium pan and heated from 25 to 220°C at a scanning rate of 10°C/min.

*Fourier transform-infrared spectra (FT-IR) analysis.* Studies of infrared spectra of pure drug, unloaded MPs and IND-loaded MPs were conducted with an IR spectrophotometer (Jasco FT-IR A-200) using the KBr disc method. The samples were mixed with KBr and compressed into tablet (10mm in diameter and 1 mm in thickness) using an hydraulic press (Perkin Elmer, Norwalk USA). The scanning range was 650-4000  $\text{cm}^{-1}$  and the resolution was 1  $\text{cm}^{-1}$ .

*Hot Stage Microscopy (HSM) analysis.* Physical changes in the samples during heating were monitored by HSM studies using a hot stage apparatus (Mettler-Toledo S.p.A., Novate Milanese, Italy) mounted on Nikon Eclipse E400 optical microscope connected to a Nikon Digital Net Camera DN100 for the image acquisition. The samples were equilibrated 25°C for 1 min and then heated at a scanning rate of 10°C/min in the 25-200°C range of temperature. The magnification was set at 10x.

*Powder X-Ray Diffraction (PXRD) analysis.* Single components, MPs and corresponding physical mixtures were studied by X-ray powder diffraction technique using a Philips X'Pert powder

diffractometer equipped with a graphite monochromator in the diffracted beam. CuK $\alpha$  radiation was used (40 mA, 40 kV). The spectra had been obtained in the 3°–35° 2 $\theta$  range using a 0.05° step and a 0.216°/s speed.

**Solubility and dissolution studies:** Solubility measurements of pure IND and of IND-loaded MPs were performed in 10 mL of phosphate buffer (0.2 M, pH 5.8) at 25°C. The samples were magnetically stirred for 48h, equilibrated for 2h and the suspensions were then centrifuged at 10.000 rpm for 10 minutes. The supernatant was filtered through a 0.20  $\mu$ m membrane filter. Finally, the filtrates were suitably diluted with the same solvent and analysed at 266 nm by UV-Visible spectrophotometer. The study was performed in triplicate. The results were expressed as mean  $\pm$  standard deviation (S.D.). One-way analysis of variance (ANOVA) followed by the Bonferroni posthoc test (GraphPadPrism, GraphPad software Inc., CA, USA) was used to analyse the data and the level of significance was set at the probabilities of \*p < 0.05, \*\*p < 0.01 and \*\*\*p < 0.001.

A dissolution paddle apparatus (Pharmatest, Steinheim, Germany) was used with a stirring rate of 50 rpm, according to the European Pharmacopoeia<sup>63</sup>. The dissolution medium (phosphate buffer 0.2 M, pH 5.8) was maintained at a temperature of 37°C. Samples of IND, physical mixtures and IND-loaded MPs (size fraction 100-150  $\mu$ m) containing a suitable amount of IND for sink conditions (C < 0.2 Cs) were added to 500 mL of dissolution medium. The aqueous solution was filtered and continuously pumped (12.5 mL/min) to a flow cell in a spectrophotometer (UV2 Spectrometer, Unicam) and absorbance values were recorded at 266 nm. The dissolution tests were performed in triplicate. Dissolution profiles were individually compared using the “similarity factor, f2”, which could be defined as follows:

$$f2 = 50 * \log \left\{ 1 + \left[ \frac{1}{n} * \sum_{t=1}^n (R_t - T_t)^2 \right]^{-0.5} * 100 \right\}$$

Where n is the sample number, R<sub>t</sub> and T<sub>t</sub> are the reference assay and test assay at time point t, respectively.

#### ***In Vivo Studies:***

***HPLC Analysis.*** The IND quantification for bioavailability studies was performed by HPLC. The chromatographic apparatus consisted of a modular system (model LC-10 AD VD pump and model SPD- 10A VP variable wavelength UV–vis detector; Shimadzu, Kyoto, Japan) and an injection val

with 20  $\mu\text{L}$  sample loop (model 7725; Rheodyne, IDEX, Torrance, CA, USA). Separation was performed at room temperature on a reverse phase column Hypersil BDS C-18, 5U, equipped with a guard column packed with the same Hypersil material (Alltech Italia Srl BV, Milan, Italy). Data acquisition and processing were accomplished with a personal computer using CLASS-VP Software, version 7.2.1 (Shimadzu Italia, Milan, Italy). The detector was set at 319 nm. The mobile phase consisted of a mixture of methanol and 0.2% phosphoric acid (75:25 v/v). The flow rate was 1 mL/min. The compound 9-phenyl-carbazole was employed as internal standard in extraction procedures of indomethacin from rat blood (see below). The retention times for IND and 9-phenyl-carbazole were 3.9 and 14.7 minutes, respectively. The chromatographic precision for each compound was evaluated by repeated analysis ( $n = 6$ ) of the same samples. For IND and 9-phenyl-carbazole dissolved in mobile phase the values were obtained for 50  $\mu\text{M}$  (0.018 mg/mL and 0.012 mg/mL, respectively) solutions and were represented by the relative standard deviation (RSD) values ranging between 0.61% and 0.72%, respectively.

The efficacy of indomethacin extraction from blood samples was determined by recovery experiments, comparing the peak areas extracted from 10  $\mu\text{M}$  (3.6  $\mu\text{g}/\text{mL}$ ) blood test samples at 4° C with those obtained by injection of an equivalent concentration of the drug dissolved in their mobile phase. The average recovery  $\pm$  SD of indomethacin from rat blood resulted  $85.8 \pm 3.6\%$ . The concentrations of this compound were therefore referred to as peak area ratio with respect to the internal standard 9-phenyl-carbazole. The precision of the method based on peak area ratio, calculated for 10  $\mu\text{M}$  (3.6  $\mu\text{g}/\text{mL}$ ) solutions, was represented by RSD values of 0.91%. The calibration of indomethacin was performed by employing nine different concentrations in whole blood at 4 °C ranging from 2  $\mu\text{M}$  (0.72  $\mu\text{g}/\text{mL}$ ) to 80  $\mu\text{M}$  (28.6  $\mu\text{g}/\text{mL}$ ) and expressed as peak area ratios of the compounds to the internal standard versus concentration. The calibration curve resulted linear ( $n = 9$ ,  $r = 0.992$ ,  $P < 0.0001$ ).

*In Vivo Administration of Indomethacin: Intravenous Infusion.* Male Sprague Dawley rats (200–250 g) provided by Charles-River (Milan, Italy), kept fasting since 24 hours received a femoral intravenous infusion of 0.90 mg/mL indomethacin dissolved in a medium constituted by 20% (v/v) DMSO and 80% (v/v) physiologic solution, with a rate of 0.2 mL/min for 5 min. Four rats were employed for femoral intravenous infusions. At the end of infusion and at fixed time points within 24 hours blood samples (300  $\mu\text{L}$ ) were collected and inserted in heparinized test tubes that were centrifuged at 4°C for 15 min at 1,500 x g; 100  $\mu\text{L}$  of plasma were then withdrawn and immediately



quenched in 300  $\mu\text{L}$  of ethanol (4  $^{\circ}\text{C}$ ); 100  $\mu\text{L}$  of internal standard (100  $\mu\text{M}$  9-phenyl-carbazole dissolved in ethanol) was then added. After centrifugation at 13,000  $\times g$  for 10 min, 400  $\mu\text{L}$  aliquots were reduced to dryness under a nitrogen stream and stored at  $-20^{\circ}\text{C}$  until analysis. The samples were dissolved in 150  $\mu\text{L}$  of mobile phase (methanol and 0.2% phosphoric acid 75:25 v/v), and, after centrifugation, 10  $\mu\text{L}$  was injected into the HPLC system for indomethacin assay. All the values obtained were the mean of four independent experiments. The *in vivo* half-life of indomethacin in the blood was calculated by nonlinear regression (exponential decay) of concentration values in the time range within 24 hours after infusion and confirmed by linear regression of the log concentration values versus time. The area under the concentration-time curve (AUC) value was calculated by the trapezoidal method within 24 hours, the remaining area was determined as the ratio between the indomethacin concentration detected at 24 hour and the elimination constant ( $k_{el}$ ), that was obtained from the slope of the semilogarithmic (-slope  $\cdot 2.3$ ). All the calculations were performed by using the computer program Graph Pad Prism.

*In Vivo Administration: Oral Administration of Indomethacin.* Powders constituted by  $\gamma$ -indomethacin, or its physical mixture with unloaded MPs C or by IND loaded MPs C were mixed with palatable food in order to induce their oral assumption by male Sprague Dawley rats (200–250 g) kept fasting since 24 hours. The dose of orally administered IND was 2 mg for each type of powders. Four rats/group were employed for the oral administration experiments. At the end of administration and at fixed time points within 8 hours blood samples (300  $\mu\text{L}$ ) were collected, then extracted and analyzed as above described. All the concentration values obtained for IND were the mean of four independent experiments. All *in vivo* experiments were performed in accordance with the European Communities Council Directive of September 2010 (2010/63/EU), a revision of Directive 86/609/EEC, the Declaration of Helsinki, and the Guide for the Care and Use of Laboratory Animals as adopted and promulgated by the National Institutes of Health (Bethesda, Maryland, USA). The protocol of all the *in vivo* experiments was approved by the Local Ethics Committee (University of Ferrara, Ferrara, Italy). Efforts were made to reduce the number of the animals and their suffering.

The AUC values referred to each orally administered treatment were calculated by the trapezoidal method within 8 hours, the remaining area was determined as the ratio between the indomethacin concentration detected at 8 hour and the elimination constant ( $k_{el}$ ). The absolute bioavailability values of indomethacin, referred to the oral administered samples, were obtained as

the ratio between their oral AUC values and AUC of the intravenous administration of the drug, normalized with respect to their doses, according to the following equation <sup>64</sup>:

$$F = \frac{AUC_{oral}}{AUC_{IV}} \cdot \frac{dose_{IV}}{dose_{oral}}$$

All the calculations were performed by using the computer program Graph Pad Prism.

Statistical Analysis about in Vivo Administration of Indomethacin. Statistical comparisons between AUC values obtained by oral administrations were performed by one way ANOVA followed by Bonferroni post-test. P < 0.001 was considered statistically significant. All the calculations were performed by using the computer program Graph Pad Prism.

**Stability studies:** The MPs were stored in polyethylene closed bottles at 4 ± 2°C. After 18 months, the physical stability of the IND loaded into the MPs was assessed by FT-IR analysis and by measuring the drug content. The solid state properties of the MPs were studied by means of X-ray powder diffraction analysis. Moreover, dissolution studies were repeated to examine possible changes in the biopharmaceutical properties of the MPs.

## I. Results and discussion

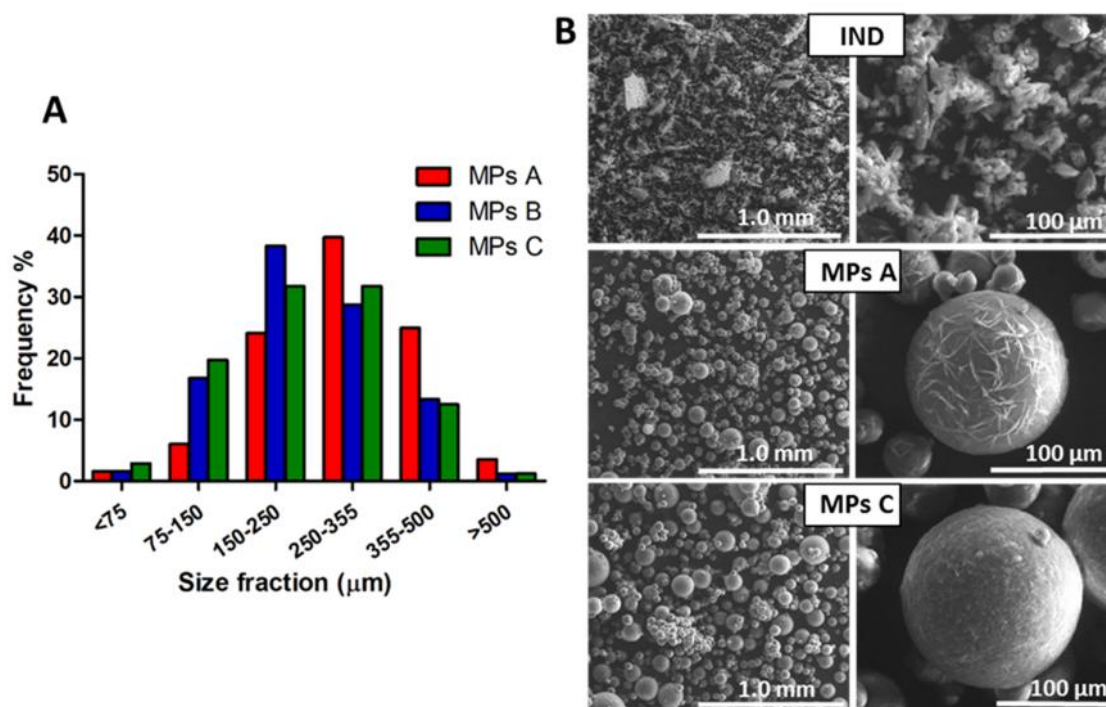
**MPs morphology and drug loading.** Spray congealing (SC) technology allows the preparation of solid microparticles (MPs) by solidification of the atomized molten fluid along the palling pathway. Preliminary SC experiments showed that it was not possible to obtain solid MPs using Gelucire 48/16 as the only carrier: infact, after atomization, the droplets could not harden during the fall into the cooling chamber, kept at room temperature. However, a binary system of Gelucire 48/16 and Gelucire 50/13 was identified as suitable for SC production. Different weight ratios between the carriers were tested (Table 1) and the formulation with the highest possible amount of Gelucire 48/16 was MPs C, containing 70% w/w of Gelucire 48/16. It is also important to highlight that during SC process, IND completely solubilized in the molten Gelucires forming a bright yellow fluid.

All MPs exhibited an experimental drug loading (DL) similar to the theoretical one (10% w/w), hence the encapsulation efficiency (EE) was very close to 100%. Notably, excellent EE values are usually obtained with SC technology <sup>61</sup>, representing one of the major advantages of this method.

Sample	Costituents (% w/w)			DL (% w/w $\pm$ SD)	EE (%)
	Gelucire 50/13	Gelucire 48/16	IND		
MPs A	90	-	10	10.73 $\pm$ 0.14	107.26
MPs B	45	45	10	9.91 $\pm$ 0.22	99.06
MPs C	27	63	10	10.06 $\pm$ 0.20	100.61

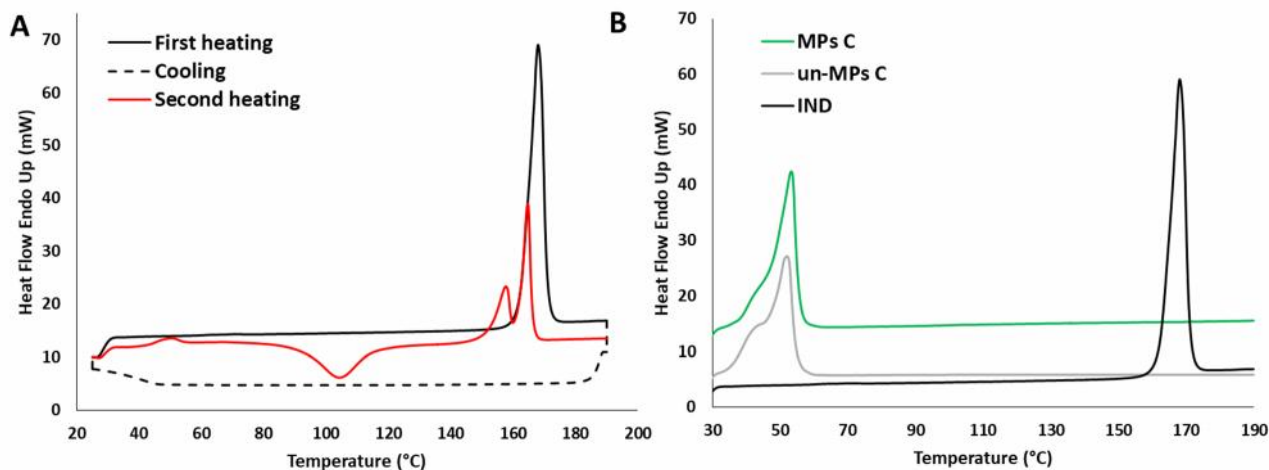
**Table I.1.** Composition, drug loading (DL) and encapsulation efficiency (EE) values of IND-loaded MPs

Figure I.1a shows an unimodal Gaussian particle size distribution for all formulations. More than 90% of MPs presented average diameter between 75 and 500  $\mu\text{m}$ , with minor differences regarding the prevalent size fraction, which was 250-355  $\mu\text{m}$  for MPs A and 150-250  $\mu\text{m}$  for MPs B and MPs C. SEM images of IND and particles (MPs A and MPs C) are reported in Figure 1b (on the left: low mag. and on the right: high mag.). SEM analysis revealed the successful formation of spherical MPs, with a slight tendency to aggregate. Interestingly, the particle surface of MPs A showed some needle-like crystals, which were absent in MPs C.



**Figure I.1.** (a) Particle size distribution of MPs A, MPs B and MPs C. (b) SEM images of pure IND, MPs A and MPs C after preparation. Images were taken at magnifications of 150x (left) and 1200x (right).

**Solid state characterization.** IND is known to have a complex solid phase behaviours which include an amorphous form and more than 4 polymorphic forms<sup>65</sup>. Notably, the fact that IND solubilized in melted Gelucire might indicate the formation of MPs as solid solutions, with the drug molecularly dispersed into the carrier. Otherwise, the drug might have undergone re-crystallization or amorphisation during the solidification step, leading to the formation of solid dispersions. To have a clear and precise vision of the physicochemical properties of the loaded drug and understand their influence on the biopharmaceutical properties of the final formulation, a detailed solid state characterization was carried out. In order to gain information about the original polymorphic form of IND, a DSC cycle (Figure I.2a) was performed by a first heating step followed by a cooling step and then a second heating step. In the first step of the cycle, a single sharp melting endotherm was observed at 161.2 °C (onset=157.5°C) with heat of fusion of 119.11 J/g. During the cooling step, no event correlated to IND crystallization was detected, suggesting the conversion in the amorphous form. Indeed, in the following re-heating step the amorphous IND exhibited a  $T_g$  at 40.7 °C followed by recrystallization at 101.6 °C (onset temperature and  $\Delta H$  were 89.1 °C and -66.23J/g, respectively). In addition, two melting endothermic peaks were observed at 151.8°C (onset=147.4°C) and 158.5 °C (onset=156.2°C). Those results were in accordance with the literature<sup>65 66</sup> and revealed that original IND was the stable  $\gamma$ -form. Figure I.2b shows the DSC results of the MPs C, with and without drug. The thermogram of *un*-MPs C displayed a broad endothermic event characterized by a small pre-transition and a main transition at 45.9 °C (onset=40.8°C), indicating the melting of the particles. The DSC profile of the particles containing 10% of IND (MPs C) is very similar to the unloaded one, with a broad endothermic peak corresponding to the carrier melting, showing that the presence of IND had no effect on the carrier melting temperature and suggesting the crystallization of Gelucire during MPs solidification in the same crystalline form. Nevertheless, in MPs C the melting peak of the drug was absent, and the same was noted for formulations A and B (data not shown). The disappearance of the IND melting peak suggests the conversion of the drug in the amorphous form when loaded into the MPs. However, also the dissolution of the drug crystals into the molten carrier during the DSC analysis may cause the melting peak disappearance, as already noticed in the case of Gelucire 50/13 as carrier<sup>67 68</sup>.



**Figure I.2.** (a) DSC profiles of MPs C, unloaded MPs C (un-MPs C) and pure IND. (b) DSC cycle of IND.

More information on the solid state and physicochemical properties of the drug-loaded MPs can be obtained by observing the morphology of MPs during thermal treatment. Thus, HSM study was performed on pure drug, MPs A and MPs C (Figure I.3). The study confirmed the melting of IND between 160 and 165 °C. Afterwards, the sample was cooled back down to 25°C, and interestingly the solidification occurred without evident recrystallization of the drug. In the case of MPs A, the particle started to melt at 60°C and the melting was complete at 65°C, in agreement with the melting point of Gelucire 50/13. Although small crystals were observed immediately after carrier melting, they completely disappeared as soon as the temperature was above 80°C. Differently, MPs C melted at a lower temperature (from 50 to 55°C) and no crystal was observed thereafter. The results suggested the absence of IND crystals into the MPs, and thus the presence of molecularly dispersed or amorphous IND was hypothesized. However, as also noticed in the DSC study, another possible explanation consists in the progressive melting of IND in the molten Gelucire during analysis, and the consequent lack of clearly visible crystals.

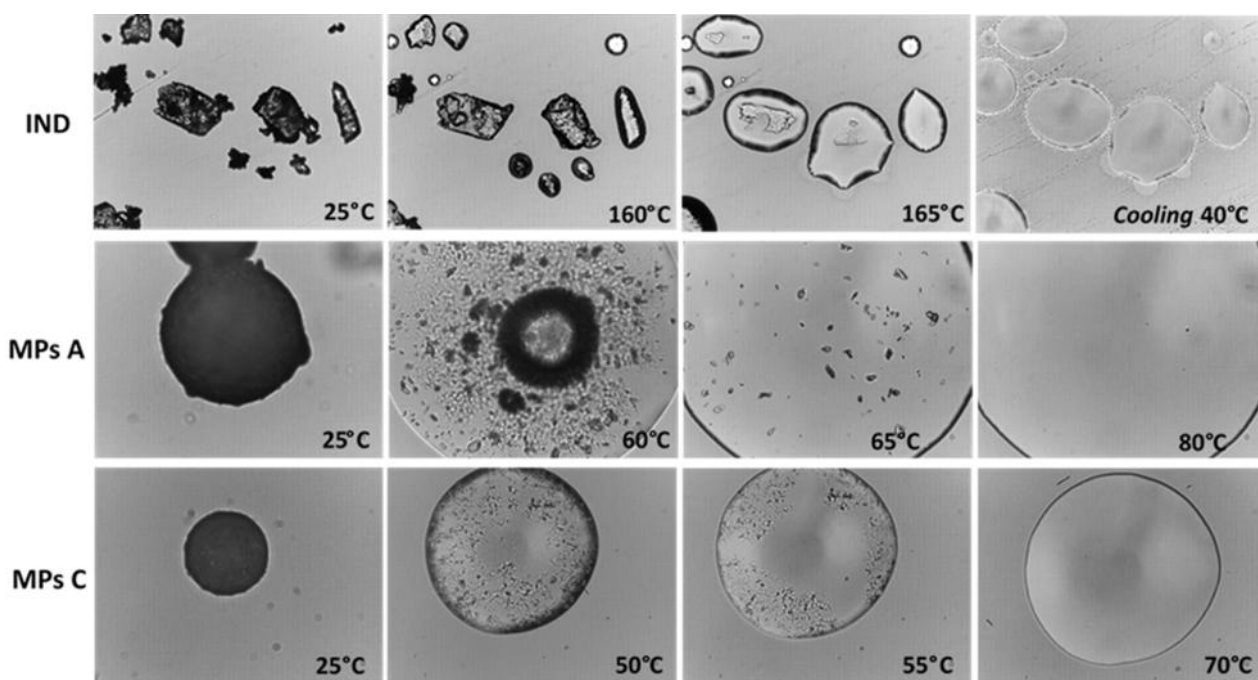


**Figure I.3.** HSM images of pure IND, MPs A and MPs C during heating. For all images the magnification was set at 20x.

FT-IR analysis was performed to investigate the possible interactions between drug and carrier as well as to gain other information regarding IND physical state inside the MPs. All formulations were analysed and in Figure I.4a is reported, as example, the spectra of MPs C, Phy mix C, *un*-MP C and pure drug. IND spectrum showed sharp bands at the wavenumbers ( $1716.3$ ,  $1691.3$ ,  $1613.2$ ,  $1588.1$  and  $1599.6$   $\text{cm}^{-1}$ ) characteristics of the  $\gamma$  form<sup>65 69</sup>, confirming again that the pure drug was in the stable polymorphic form. Specifically, unloaded particles showed bands typical of Gelucire:  $3100$ - $3600$   $\text{cm}^{-1}$  (broad, stretching of free OH groups),  $1738.5$   $\text{cm}^{-1}$  (stretching C=O group),  $1469.5$   $\text{cm}^{-1}$  (C-H deformation of alkyl group),  $1113.7$   $\text{cm}^{-1}$  (C-O stretching), and  $963.3$   $\text{cm}^{-1}$  (double band, characteristic of the polyethylene glycol groups)<sup>67 70 71</sup>. MPs and Phy mix present FT-IR spectra similar to the unloaded particles but with some extra band that can be ascribed to the presence of drug, although with lower intensity due to the limited content of drug in the sample (10%). To allow a better analysis of the results, the spectra of MPs and Phy mix were compared in the region between the wavenumbers  $1800$ - $1500$   $\text{cm}^{-1}$ , specific for the carbonyl stretching. As visible in Figure I.4b, the carrier gives only one band at  $1720$ - $1750$   $\text{cm}^{-1}$  with no other bands in this region. Thus, all other bands in this region can be ascribed to IND containing in Phy mix and MPs. Interestingly, various differences were detected between the two samples. Notably, the specific bands positions of IND in the Phy mix C corresponded with the original IND crystalline form  $\gamma$ , and the same bands

were observed for Phy mix A and B (data not shown). The bands of IND were observed at different wavenumbers in case of all MPs formulations (Figure I.4b for MPs C, data not shown for MPs A and MPs B). The differences in the carbonyl stretching region depend on the hydrogen-bonding of the carboxylic acid and amide carbonyl group of IND, which can have different arrangements in the various polymorphic forms <sup>72</sup>, as reported in the table in Figure I.4c.  $\alpha$ -IND shows four specific vibration modes in the carbonyl stretching region. Differently, amorphous IND possesses two main signals at 1679 and 1707  $\text{cm}^{-1}$ , and a minor band at 1735  $\text{cm}^{-1}$  <sup>65 72</sup>. The bands detected in the MPs in this region (at wavenumbers of 1649, 1681 and 1692  $\text{cm}^{-1}$ ) were similar to the characteristic signals of the  $\alpha$ -form, but the strong band at 1734  $\text{cm}^{-1}$  assigned to the non-hydrogen bonded carboxylic acid was missing. However, other bands at 1591 and 1610  $\text{cm}^{-1}$  correspond to the typical bands of IND amorphous form <sup>73</sup>.

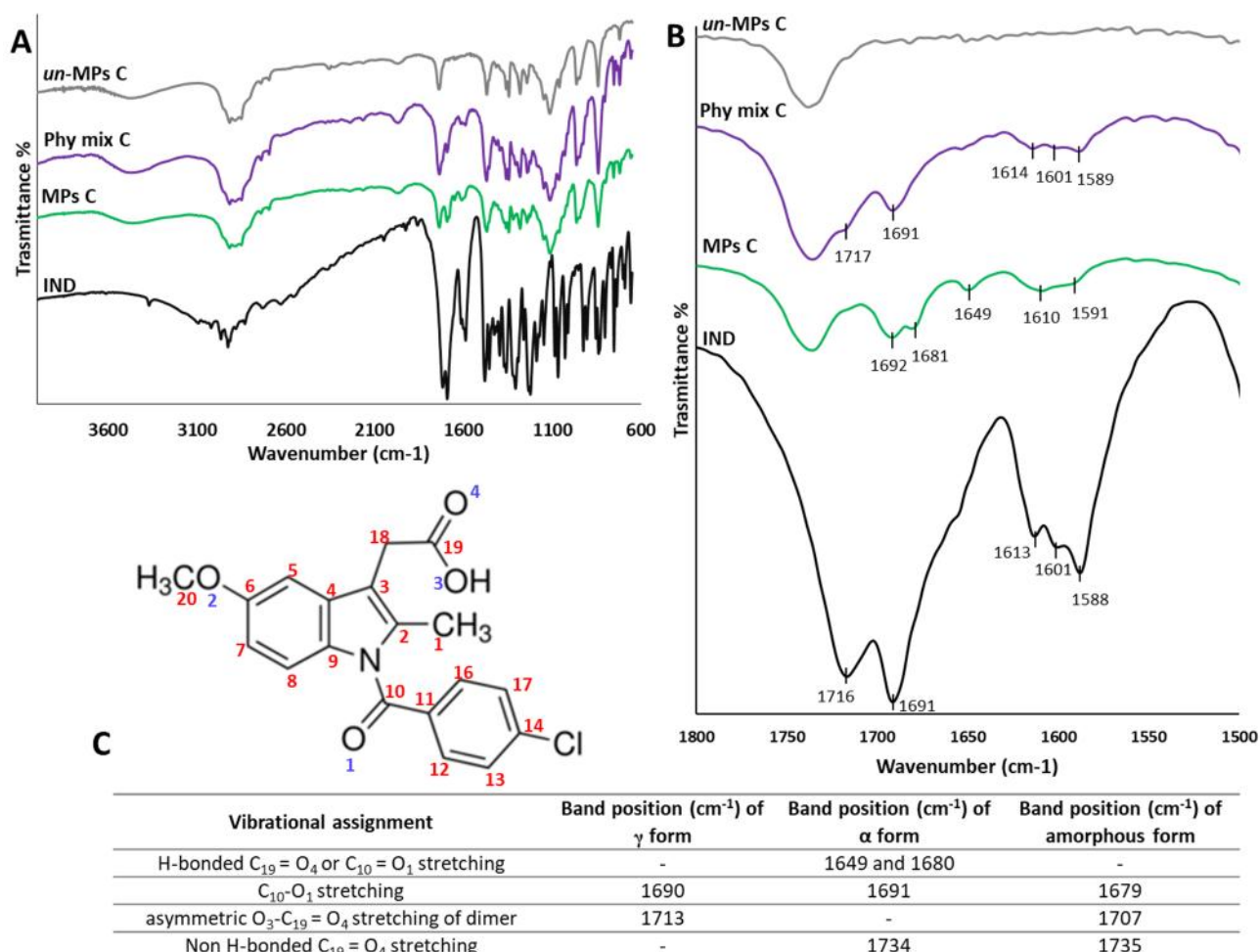


**Figure I.4.** (a) FT-IR spectra of IND, MPs C, Phy mix C and *un*-MPs C in the spectral region between 4000 and 400  $\text{cm}^{-1}$ . (b) Focus on the carbonyl stretching region between the wavenumbers 1800-1500  $\text{cm}^{-1}$ . (c) The band positions reported in literature <sup>73</sup> for  $\gamma$  form,  $\alpha$  form and amorphous form of IND. The numbering system of IND molecular structure follows that used by Kirstenmacher and Marsh <sup>74</sup>.

Although interesting indications on the solid state of IND-loaded MPs were given by thermal analysis (DSC and HSM) and FT-IR analysis, a more precise information about the drug solid form can be provided exclusively by PXRD analysis, whose results are shown in Figure I.5. The diffractogram of IND confirmed the characteristic pattern of form  $\gamma$ , with main peaks at  $2\theta$  equal to 11.6, 17.1, 19.7, 21.9, 26.7 and 29.4<sup>65</sup>. Gelucire showed two main peaks at  $2\theta$  of 19.3 and 23.5, in accordance with literature data<sup>60 68</sup>, observed in the MPs samples as well as in the physical mixture samples. In both formulations A and C, the physical mixtures showed a XRD pattern consisting in the sum of the pure components. All the IND main peaks were in the same position, although less intense because of the relative smaller amount (10% w/w) with regard to the pure IND, thus indicating no modification in IND solid state when physically mixed with Gelucire. Differently, in the diffractograms of MPs only the peaks correspondent to the carrier appeared, and no distinct peak of IND was detected, indicated a loss of IND crystallinity when formulated into spray-congealed MPs.

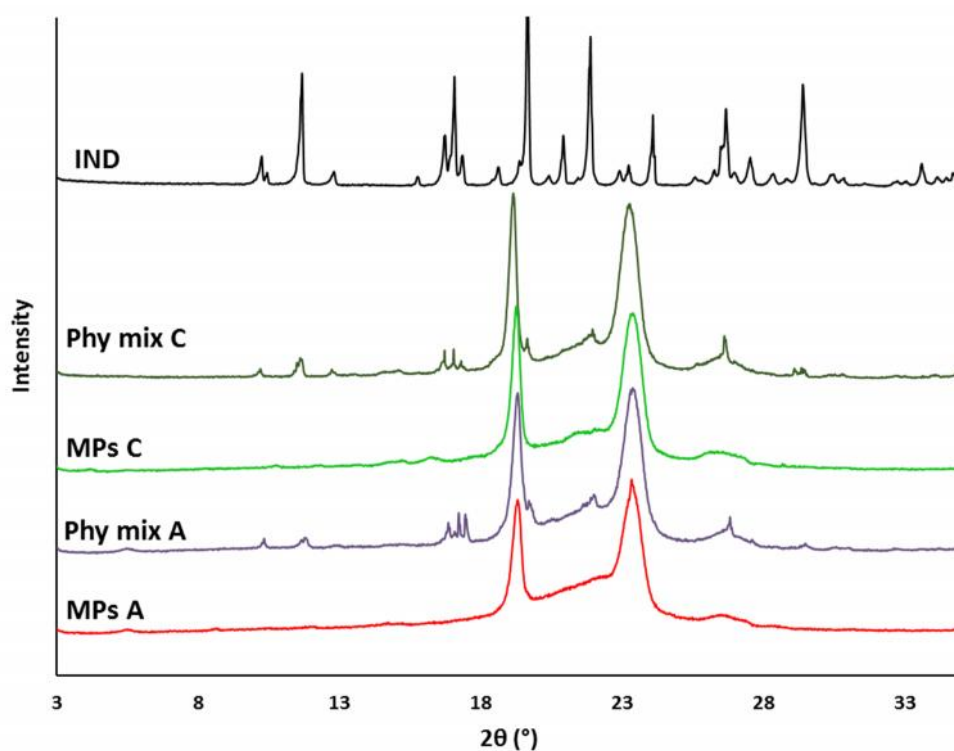


**Figure I.5.** Powder X-Ray diffractograms of pure IND compared with MPs and with the correspondent physical mixture (formulations A and C).

Overall, the solid state characterization data indicate that the spray congealed Gelucire based-SD of IND resulted in semicrystalline SD with the drug mainly amorphous dispersed in a crystalline carrier.



***In vitro* dissolution and solubility studies.** IND (pKa 4.5) can be considered practically insoluble in simulated gastric fluid (pH 1.2) and slightly soluble in simulated intestinal fluid (pH 7.4)<sup>75</sup>. Since IND solubility increases with the raising of the pH, the drug absorption is facilitated in intestinal environment, where the pH is higher compared to the gastric fluid. However, intestinal pH values weakly acidic are not uncommon, especially in fed conditions, where the average pH is reported to be around 5.8<sup>76</sup>, thus leading to a difficult drug dissolution. For this reason, in the present research all dissolution and solubility studies were performed in weakly acidic buffer (pH 5.8) rather than at neutral pH (i.e. pH 6.8 or 7.4), in order to simulate the least favourable (and more challenging) pH condition.

Blending of IND with highly hydrophilic polymers such as Gelucire or polyethylene glycol (PEG) might increase IND dissolution rate and the reason is attributed to the improvement of wettability of IND particles<sup>77</sup>. Therefore, in the dissolution studies, beside pure IND and MPs, physical mixtures of Gelucire and IND were analysed as well, in order to verify the effect of Gelucire 50/13 and Gelucire 50/13-58/16 mixtures on the drug dissolution. *In vitro* dissolution profiles are reported in Figure 1.6a. Dissolution profiles were individually compared using the “similarity factor,  $f_2$ ”. IND powder showed the slowest dissolution rate, with 53% of drug dissolved in the first 30 min and 64% after 60 min. All three Phy mix moderately improved IND dissolution rate, with an effect more evident in the beginning of the test, probably attributed to the improvement of wettability. The calculated  $f_2$  between IND and the three physical mixtures ( $f_2= 39.3, 39.2$  and  $36.3$  for Phy mix A, B and C, respectively) confirmed that the dissolution profile of each Phy mix was significantly different from that of the pure drug. MPs A considerably enhanced IND dissolution rate, leading to 80 % of drug dissolution within 30 minutes. The highest dissolution rate improvement was achieved by MPs B and MPs C, with 89 and 87% of drug dissolved in the first 30 min, respectively. Specifically, the dissolution performance of MPs resulted different from both the correspondent physical mixtures ( $f_2= 26.7, 20.3$  and  $22.7$  for formulation A, B and C, respectively) and IND with  $f_2$  values lower than 20 ( $f_2= 17.1, 12.8$  and  $13.6$  for MPs A, B and C, respectively). Differently, the dissolution profiles of the different MPs formulations resulted not significantly different ( $f_2 \geq 50$ ) indicating no substantial influence of the different Gelucire ratio on IND dissolution rate. Overall, the results suggested a moderate effect on dissolution rate given by the presence of hydrophilic excipient on the hydrophobic drug powder. The best enhancement in dissolution rate was achieved by spray congealed-MPs. This could be attributed to the amorphous state of IND in Gelucire-based system, as demonstrated by solid state studies.

The solubility of IND, MPs A, MPs B and MPs C (Figure I.6b), evaluated in phosphate buffer (pH 5.8), was  $29.1 \pm 11.6$ ,  $1.6 \pm 0.6$ ,  $541.4 \pm 3.6$   $\mu\text{g}/\text{mL}$ , respectively. The solubility of IND formulated into MPs A, B and C was approximately 4-, 19-, and 31-fold higher, respectively, than that of IND powder. The increasing in solubility with the higher amount of Gelucire 48/16 in the formulation indicates a better solubilisation ability of this excipient. The MPs C formulation was therefore selected for oral administration studies.

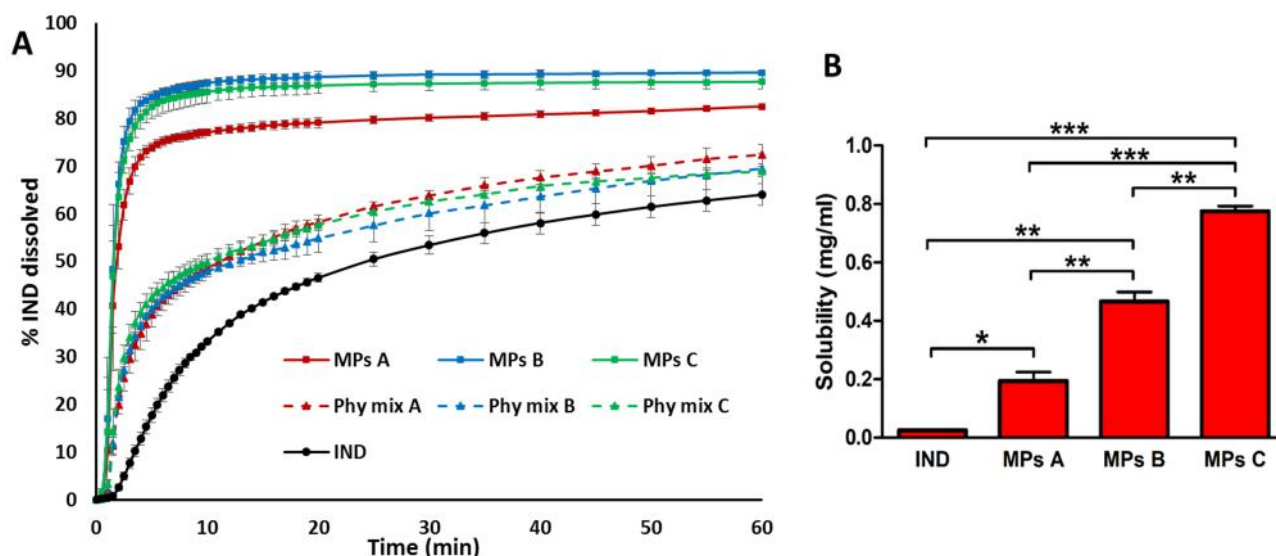


**Figure I.6.** (a) Dissolution profiles of IND, MPs and physical mixtures (Phy mix) in phosphate buffer pH 5.8. (b) 48 h solubility of IND and MPs in phosphate buffer pH 5.8. Data represent mean  $\pm$  S.D. ( $n = 3$ ), and the level of significance was set at the probabilities of  $*p < 0.05$ ,  $**p < 0.01$ , and  $***p < 0.001$ .

***In vivo* bioavailability studies.** After intravenous (IV) infusion of 0.90 mg IND, the drug concentration in the rat bloodstream was  $13.43 \pm 0.9$   $\mu\text{g}/\text{mL}$ . This value decreased during time with an apparent first order kinetic (Figure 7) confirmed by the linearity of the semilogarithmic plot reported in the inset of Figure 7 ( $n = 8$ ,  $r = 0.996$ ,  $P < 0.0001$ ), showing an half-life value of  $8.84 \pm 0.31$  hours. These data are in good agreement with those obtained by previous studies on indomethacin pharmacokinetics <sup>78</sup>.

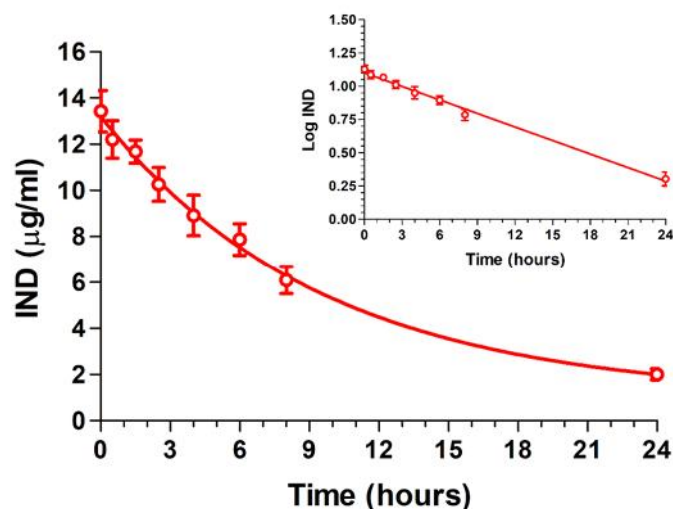


**Figure 1.7.** Elimination profile of indomethacin after 0.90 mg IV infusion to rats. The elimination followed an apparent first order kinetic, confirmed by the semilogarithmic plot reported in the inset ( $n = 8$ ,  $r = 0.996$ ,  $P < 0.0001$ ). The half-life of indomethacin was calculated to be  $8.84 \pm 0.31$  hours. Data are expressed as the mean  $\pm$  SD of four independent experiments.

The rat blood indomethacin concentrations within 8 hours the oral administration of 2.0 mg of drug (about 8 mg/kg) as powders of free  $\gamma$ -indomethacin (IND), its physical mixture with unloaded MPs C (Phy mix C), or IND-loaded MPs C (MPs C) are reported in Figure 1.8. It can be observed that the free  $\gamma$ -indomethacin powder induced a concentration peak in the rat bloodstream of about 10  $\mu\text{g/mL}$  two hours after the administration ( $T_{\text{max}}$ ) and a similar profile was obtained with the physical mixture. These data appear in agreement with those obtained by previous studies, indicating IND peak concentrations in bloodstream of rats of around 30  $\mu\text{g/mL}$  two hours after the administration of 22.5 mg/kg of indomethacin suspended in methyl cellulose<sup>79</sup>. In addition, it is reported that the oral administration of free  $\gamma$ -indomethacin as solid powder to rats induces peak concentrations in the bloodstream near to 5  $\mu\text{g/mL}$ , with a corresponding  $T_{\text{max}}$  value of two hours<sup>78</sup>.

On the other hand, the profile resulting from loaded MPs C showed a peak concentration of about 24  $\mu\text{g/mL}$  two hours after its administration (Figure 1.8).

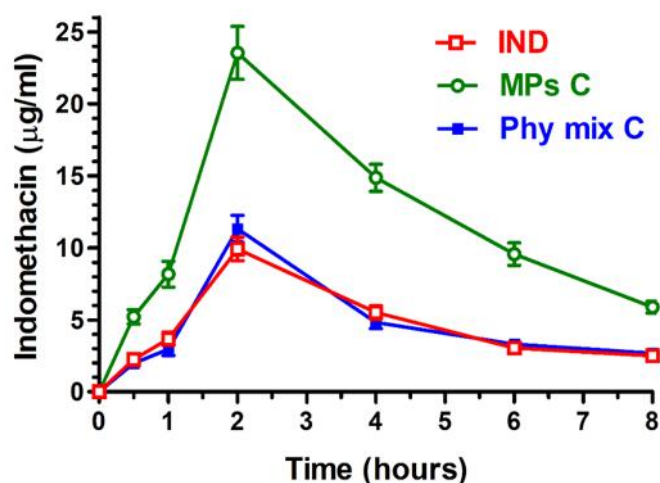


**Figure I.8.** Blood indomethacin concentrations ( $\mu\text{g}/\text{mL}$ ) obtained by oral administration of 2.0 mg dose to rats within 8 hours. The formulations were constituted by the powders of free  $\gamma$ -indomethacin (IND), its physical mixture with unloaded MPs C (Phy mix C), or IND-loaded MPs C (MPs C). All data reported in Figure are expressed as the mean  $\pm$  SD of four independent experiments.

As reported in Table I.2, it can be observed that the AUC value obtained by the oral administration of free  $\gamma$ -indomethacin ( $70.55 \pm 2.26 \mu\text{g}\cdot\text{mL}^{-1}\cdot\text{h}$ ) is not significantly different ( $P > 0.05$ ) from the AUC value obtained by the physical mixture administration ( $76.99 \pm 2.26 \mu\text{g}\cdot\text{mL}^{-1}\cdot\text{h}$ ), whereas a significant difference ( $P < 0.001$ ) was detected between the AUC values obtained by the oral administration of free  $\gamma$ -indomethacin and the loaded MPs C.

Formulation	IND dose	AUC ( $\mu\text{g}\cdot\text{mL}^{-1}\cdot\text{h}$ )	Absolute Bioavailability (F)
IND (IV)	0.9 mg	$165.06 \pm 6.2$	--
IND (oral)	2.0 mg	$70.55 \pm 2.26$	<b>19.20%</b>
Phy mix C	2.0 mg	$76.99 \pm 2.26^*$	<b>20.98 %</b>
MPs C	2.0 mg	$174.3 \pm 5.8^{**}$	<b>47.51%</b>

**Table I.2.** AUC values obtained by intravenous (IV) infusion of 0.9 mg indomethacin (IND IV) or by the oral administration of 2 mg of indomethacin as free  $\gamma$ -drug (IND oral), its physical mixture with unloaded MPs C (Phy Mix IND), or encapsulated in MPs C (MPs C IND). All the AUC values are reported as the mean  $\pm$  SD of four independent experiments. The absolute bioavailability values were calculated by the AUC data normalized with respect to their IND doses.  $p > 0.05$  versus IND (oral);  $** p < 0.001$  versus IND (oral).

In particular, the AUC value of the microparticulate formulation was  $174.3 \pm 5.8 \mu\text{g}\cdot\text{mL}^{-1}\cdot\text{h}$ , about 2.5 times higher than the AUC value of the free  $\gamma$ -indomethacin. These data indicate that the administration of the MPs C sample allows to sensibly increase the amounts of IND absorbed in the bloodstream, even if no significant effects were observed on the absorption rate of IND in the bloodstream, being 2 h the  $T_{\text{max}}$  values for all the powders tested. A similar behaviour was previously registered with IND formulations constituted by self-emulsifying systems<sup>79</sup>. The ability of the MPs C IND sample to increase the IND absorption in the bloodstream appears attributable to the microparticulate formulation and not to the simple presence of their excipients, being the AUC value of the physical mixture not significantly different to that of free  $\gamma$ -indomethacin. In this case, the potential improvement of wettability of IND promoted by the presence of Gelucire did not seem to induce a significant effect (as instead observed for dissolution of IND) on the drug absorption in the bloodstream. In fact, this effect might be induced either way by components of the GIT, such as bile acid salts, released by the gall bladder in order to emulsify hydrophobic compounds during digestion<sup>80</sup>.

The AUC values of the profiles reported in Figures I.7 and I.8 were used for the calculation of absolute bioavailability (F) values of the solid formulations, which are reported in Table I.2. The F values were calculated by the AUC data normalized with respect to their IND doses. In this case the IND dose for the IV administration was 0.9 mg for each rat (about 3.6 mg/kg), being the maximum amount allowing to obtain solubilized indomethacin in 1 mL of the medium constituted by 20% (v/v) DMSO and 80% (v/v) physiologic solution. The IND dose for the oral administration was 2 mg for each rat (about 8 mg/kg), a value included between 1.85 mg/kg and 22.5 mg/kg, a range normally used for oral bioavailability studies of this drug<sup>64 78 79 81</sup>.

The F values of  $\gamma$ -indomethacin in the free form, or mixed in the physical mixture with unloaded MPs C, were about the 20%, in accordance with previous studies about oral administration of this drug<sup>78</sup>. According to these previous studies we evidenced that an approach of co-crystallization of indomethacin can induced the increase of both water solubility and oral bioavailability of this drug. As an example, the co-crystallization of indomethacin with saccharin or 2-hydroxy-4-methyl-pyridine induced a drug bioavailability increase from the 23% to the 34% or 38%, respectively<sup>78</sup>. Unfortunately, 2-hydroxy-4-methyl-pyridine is characterized by acute toxicity for our body.

According to the measurements here reported, the oral administration of the loaded MPs C IND allowed to obtain a F value of 47.51%, about 2.5 times higher than that obtained with the free  $\gamma$ -

indomethacin, indicating the ability of this formulation to sensibly increase the oral IND bioavailability. It is important to remark that this bioavailability enhancement was obtained with a formulation characterized by high biocompatibility, being Gelucire recognized as Safe (GRAS) and oral-approved.

**Stability studies.** No statistical change in drug content was found for all samples ( $p > 0.05$ ) (data not shown), indicating that all the formulations were physically stable with no loss or degradation of the drug during storage. Moreover, the FT-IR analysis of MPs C (data not shown) showed all the characteristic peaks correspondent to IND and excipient kept unchanged, suggesting the absence of interaction between carrier and drugs during long term storage. The stability of the drug in the amorphous form, however, represents a major challenge for this system. Therefore, IND solid state in MPs A and MPs C after 18 months was characterized by XRPD. As shown in Figure I.9, the diffractograms showed no evident change in the pattern compared to the zero time samples, therefore suggesting a good stability of the systems with no change in IND solid state form. Additionally, the dissolution profile of the formulation C (Figure 3 SI) resulted unchanged after 18 months storage, thus confirming the stability of the pharmaceutical performance of this formulation.

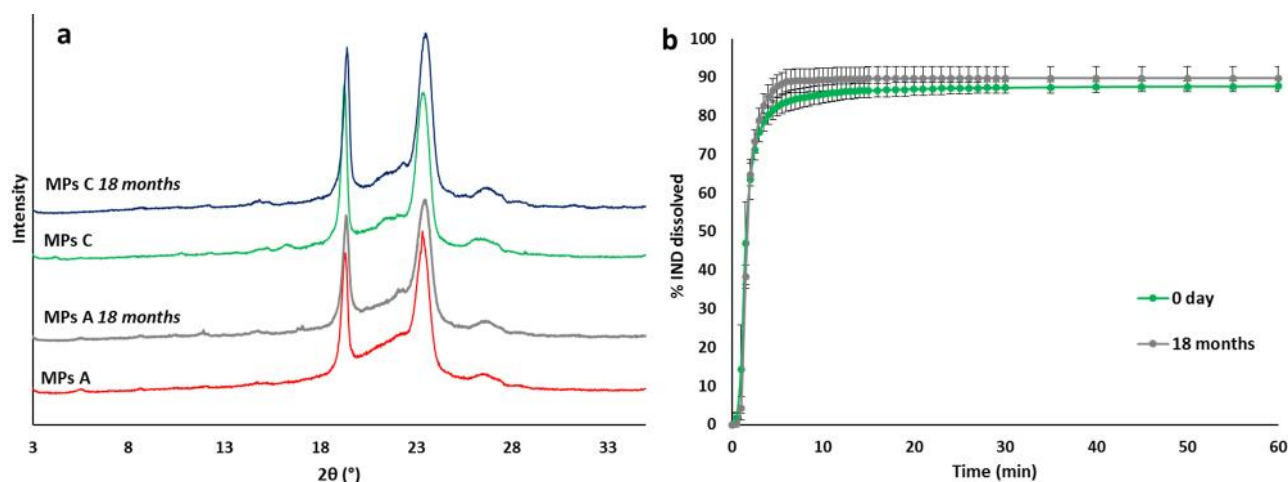


**Figure I.9.** (a) Powder X-Ray diffractograms of MPs A and MPs C immediately after preparation and after 18 months of storage. (b) Dissolution profiles of MPs C immediately after preparation and after 18 months of storage in phosphate buffer pH 5.8. Data represents mean  $\pm$  SD (n=3).

Changing in polymorphic form of IND in dispersion with hydrophilic carrier has been previously reported. Recently, Van Duong et al. reported the study of semicrystalline dispersions of IND in PEG where the crystallization of the drug was observed in either the  $\alpha$ -form or  $\tau$ -form, a new polymorph, or a mixture of the two forms, depending on the drug loading in the dispersion <sup>72</sup>. The SD with 10% of IND, the same drug loading of our system, showed the longest time for IND recrystallization compared to the SD with higher drug loadings. In this study, the SD in cold storage maintained the amorphous state of IND for long time (18 months). The reason can be found in the composition and preparation process of the SD: in spray congealing process, we observed that IND solubilized in the molten carrier. The formation of a liquid solution implies that the self-interactions of the API in the crystals are disrupted and replaced by drug–carrier interactions. When the solidification occurs, the arrangements of the drug-carrier molecules determine the microstructure of the SD. In case of low drug loadings, the amount of drug is generally insufficient to affect the carrier crystallization during solidification from the melt <sup>82 72</sup>. Thus, the dispersions exhibits instant crystallization of Gelucire (Figure 2b) with amorphous drug entrapped in the ordered crystalline matrix (Figure 5). The mobility of IND molecules would be thus extremely low in the highly viscous crystalline Gelucire matrix. Therefore, we hypothesize that the crystallization of IND in the SD was retarded because of the lack of molecular mobility required for nucleation and crystal growth. Moreover, the storage at low temperature (4°C) further contributed to maintain the long-term stability of the SD.

## I. Conclusion

In this work, spray congealed MPs containing a recently marketed excipient (Gelucire 48/16) have been explored to improve oral bioavailability of indomethacin (IND) and decrease the required daily dose to optimize its clinical use. Spray congealing enabled the preparation of MPs with encapsulation efficiency values closer to 100%. The incorporation of IND into MPs led to the amorphisation of the drug, as confirmed by PXRD analysis. The new excipient Gelucire 48/16 showed great potential for the bioavailability enhancement of IND. Specifically, the formulation with 30% Gelucire 50/13 and 70% Gelucire 48/16 led to an important increase in drug solubility and a considerable enhancement of drug dissolution rate compared with the pure drug. *In vivo* pharmacokinetic studies indicate that this formulation allows to sensibly increase (about 2.5 times) the oral bioavailability of  $\gamma$ -indomethacin. The bioavailability enhancement was due to both the wetting ability of the hydrophilic carrier and the high-energy state of amorphous IND. Overall, the developed MPs showed good *in vitro* and *in vivo* performance as well as ideal technological properties. In fact, spray congealed MPs were spherical and free flowing, thus ready-to-use for tableting or capsule filling. Moreover, beside the characteristics of biocompatibility and low-cost of the proposed formulation, the major advantage of our strategy resides in the long-term stability (18 months) achieved by the MPs, showing consistent and reproducible pharmaceutical performances, a key issue in view of an industrial application.



## Case study II: Gelucire-based microparticles as a versatile strategy to improve the oral bioavailability of poorly water-soluble APIs: investigation into the mechanism of bioavailability enhancement

### II. Introduction

Gelucires are a family of inert semi-solid waxy excipients with an amphiphilic nature, characterized by two numbers, the first one referring to the melting point and the second one referring to the HLB (Hydrophilic Lipophilic Balance) value. They are polyethylene glycol (PEG) glycerides composed of mono-, di-, and triglycerides and mono- and diesters of PEG, as well as a defined amount of free PEG (Figure II.1). Because of their unique composition with surfactants (esters of PEG), cosurfactants (monoglycerides), cosolvents (free PEG) and oily phase (di- and triglycerides), Gelucires present interesting properties<sup>83</sup>.

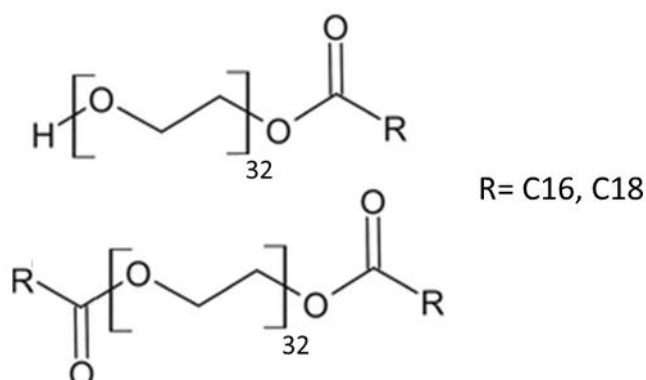


**Figure II.1.** Structure of the main components of Gelucire 50/13: PEG-32 mono- and diesters of palmitic (C16) and stearic (C18) acids.

The previous case study has showed the success of spray congealed MPs based on Gelucire in improving the oral bioavailability of the BCS class II drug IND. Specifically, the recently marketed Gelucire 48/16<sup>84</sup> demonstrated excellent properties in enhancing the solubility and dissolution rate of the drug. However, very few applications of this oral-approved excipient have been explored so far. The solubility enhancement property of Gelucire can depend on different factors, such as enhanced wettability due to the hydrophilic excipient, formation of micellar structures, particle size reduction of the API and changes in the API solid state during MPs preparation. In particular, modifications in the API solid state from a stable form to a high-energy state can determine an

important increase in drug dissolution rate. In the previous case study, IND resulted to change from the stable  $\gamma$  form to the amorphous one when formulated into Gelucire based-MPs. The improvement in the dissolution rate of amorphous systems is mainly attributed to the loss of the drug crystal structure. After amorphisation, the energy normally required to break up the drug crystalline structure before it can dissolve in water is no longer a limitation<sup>55</sup>. However, this might not be the only mechanism involved. It has been suggested that Gelucire tends to form a fine emulsion or micellar solution when it comes in contact with water<sup>85</sup>. This could explain its effect in increasing both the solubility and the dissolution rate of drugs. In fact, as Gelucire contains amphiphilic components, it is likely to form micelles. Small drug molecules can be incorporated into micelles in a specific location according to their structure and hydrophobicity, in order to give raise to the system with the lowest energy. Accordingly, Gelucire 44/14<sup>86, 87</sup> and Gelucire 50/13<sup>88</sup> have been successfully employed to produce solid SEDDS by spray congealing. Although a number of studies have investigated the *in vitro* and *in vivo* release characteristics of drug dispersions in Gelucire 50/13<sup>89</sup>, very few research has been conducted to investigate the involved mechanism.

The aim of this research is to investigate oral MPs based on Gelucire 50/13 and Gelucire 48/16, prepared by spray congealing, for the bioavailability enhancement of different BCS class II drugs. In particular, in this study we addressed two issues. Firstly, the MPs were loaded with three model drugs in order to investigate the versatility of this system in improving the solubility and the dissolution rate of poorly water-soluble compounds. The selected APIs belong to class II of BCS, exhibit  $\log P$  values between 2 and 6 and present different acid-base character. Specifically, carbamazepine (CBZ), tolbutamide (TBM) and cinnarizine (CIN) were selected as neutral, acid and basic compounds, respectively. Secondly, we focused closely on the mechanism of dissolution and solubility enhancement in order to provide an explanation for the properties of this new excipient. In the first part of the study, by means of emulsification time determination and dynamic light scattering (DLS), the self-emulsification ability of the new Gelucire 48/16 was investigated. Then, systems containing the model drugs were characterized both on physicochemical and biopharmaceutical properties. The comparison between the three drug loaded-MPs allowed to gain new insights into the mechanism of improved bioavailability.

## II. Experimental section

**Preparation of samples:** MPs were produced by the spray-congealing technology using WPN atomizer. Initially, the excipient (Gelucire 50/13 and Gelucire 48/16 in different ratio, Gattefossè, Milan, Italy) was heated up to a temperature 5 °C above its melting point. The API (10% w/w) was added to the molten carrier and magnetically stirred to obtain a stable suspension or solution, which was loaded into the feeding tank. All APIs were obtained from Sigma Aldrich, Steinheim, Germany. The temperature of the feeding tank of the nozzle and the inlet air pressure were set at 55°C and 3 bar, respectively. The atomized molten droplets hardened during the fall into a cylindrical cooling chamber, which was held at room temperature. Finally, the MPs were collected from the bottom of the cooling chamber and stored in polyethylene closed bottles at 25°C. Three different formulation were produced for both unloaded (Figure II.1) and-loaded MPs (Table II.1). For comparison purposes, physical mixes (Phy mix) of API and excipients in the same weight ratio as the loaded MPs were prepared by mixing 10% of API with 90% of unloaded MPs.

### **Study of the MPs self-emulsification ability:**

**Emulsification time.** The self-emulsifying time of the MPs was evaluated using the turbidity method, as proposed by Xiao *et al.*<sup>90</sup> and following the same procedure used by Albertini *et al.*<sup>88</sup>. Three different dissolution media were used: water; gastric buffer pH 1.2; intestinal buffer pH 6.8. The dissolution media, previously filtered through 0.45 µm filter membrane, were continuously stirred at 50 rpm and 37°C with a rotating paddle. Unloaded MPs were added onto the surface of the stirred solution, which was filtered and continuously pumped (12.5 ml/min) to a flow cell in a spectrophotometer. The absorbance (A) of the sample was measured at the wavelength of 600 nm (UV2 Spectrometer, Unicam) and compared to the blank medium. The transmittance (T) and the Relative Absorbance (A %) was then calculated using the following equations:

$$T(\%) = 10^{2-A}$$

$$A(\%) = \frac{A}{A_{max}} \times 100$$

where A is the absorbance at t time, and A<sub>max</sub> is the final value of absorbance, when A does not change with time. The self-emulsifying time is considered the time necessary for the system to reach a constant value of transmittance, and therefore of Relative Absorbance.

*Droplet size determination.* At the end of the emulsification time test, the resulted microemulsion was characterized by DLS (Brookhaven 90-PLUS, Holtsville, NY), using a procedure previously described.<sup>88</sup> Briefly, samples were collected and filtered through a 0.8 µm filter in order to remove particulate materials without affecting the dimension of the micelles. Samples were then diluted with the same solvent to reach an ideal Average Count Rate and analysed at 25°C by DLS setting the wavelength at 600 nm and the scattering angle at 90°. Water; pH 1.2 buffer; pH 6.8 buffer previously filtered through 0.45 µm filter membrane were also analysed as blank medium, respectively. Mean diameter sizes are expressed as mean and standard deviation of six consecutive measurements of each sample. The polydispersity index (PDI) from intensity distribution was also measured.

***Morphological analysis of MPs and drug content determination:***

*Morphological analysis.* Shape and surface morphology of APIs and MPs were observed by Scanning Electron Microscopy (SEM). Samples were fixed on the sample holder with double-sided adhesive tape, sputter coated with Au/Pd under argon atmosphere performed using a vacuum evaporator (Edwards, Crawley UK) and examined by means of a scanning electron microscope SEM (Philips XL 30) operating at 20.0 kV accelerating voltage. Size distribution of MPs was evaluated by sieve analysis using a vibrating shaker (Octagon Digital, Endecotts, London UK) and a set of six sieves ranging from 75 to 500 µm (Scientific Instrument, Milan, Italy).

*Analytical methods.* In case of CBZ and TBM, a spectrophotometric method was used. Due to its very limited water solubility, a reverse phase HPLC method was used for the quantification of CIN. The HPLC system consisted of two mobile phase delivery pumps (PU 2089 plus, Jasco) and a multiwavelength detector (MD 2010, Jasco). A Luna C18 column (150 mm x 4.60 mm, 5 µm) was used with a mobile phase consisting of phosphate buffer (pH 2.5):methanol:acetonitrile (30:30:40, v/v). The injection volume was 20 µl, the flow rate was 1 mL/min and the detection wavelength was set at 251 nm.

*Determination of drug content.* The drug loading was determined by dissolving or melting a variable quantity of MPs accurately weighed in a suitable solvent. In case of CBZ, MPs were added to 100 mL of distilled water. The sample was heated to 60°C to melt the carrier and then shaken for 24h at 25°C. Finally, the solution was filtered, diluted with the same solvent, and the drug content was assayed spectrophotometrically at 285 nm. TBM content was determined by dissolving MPs in 10 mL of ethanol. The solution was shaken for 24h at 25°C. After filtration and dilution, the drug content was assayed spectrophotometrically at 229 nm. CIN content was determined by adding MPs in 10

mL of acidic water, heating to 60°C to melt the carrier and then shaken for 24h at 25°C. The solution was filtered, opportunely diluted with the mobile phase and assayed by HPLC. Each formulation was analysed in triplicate and the mean  $\pm$ SD was reported.

### ***Solid state characterization of MPs:***

*Differential scanning calorimetry (DSC) studies.* DSC analysis were performed using a Perkin Elmer DSC 6 (Perkin Elmer, Beaconsfield UK) with nitrogen as purge gas (20mL/min). The instrument was calibrated with indium and lead for temperature, and with indium for the measurements of the enthalpy. Samples of APIs, unloaded MPs and loaded MPs, weighing 8-9 mg, were placed in an aluminium pan and heated from 25 to 220°C at a scanning rate of 10°C/min.

*Fourier transform-infrared spectra (FT-IR) analysis.* Studies of infrared spectra of pure drugs, unloaded MPs and loaded MPs were conducted with an IR spectrophotometer (Jasco FT-IR A-200, Milan, Italy) using the KBr disc method. The samples were mixed with KBr and compressed into tablet (10mm in diameter and 1 mm in thickness) using a manual hydraulic tablet presser (Perkin Elmer, Norwalk, USA) at 4000 kg/cm for 4-6 minutes.

*Hot Stage Microscopy (HSM) analysis.* Physical changes in the samples during heating were monitored by HSM studies using a hot stage apparatus (Mettler-Toledo S.p.A., Novate Milanese, Italy) mounted on Nikon Eclipse E400 optical microscope connected to a Nikon Digital Net Camera DN100 for the image acquisition. The samples were equilibrated 25C for 1 min and then heated at a scanning rate of 10°C/min in the desired ranges of temperature. The magnification was set at 10x.

*Powder X-Ray Diffraction (PXRD) analysis.* Single components, MPs and corresponding physical mixtures were studied by X-ray powder diffraction technique using a Philips X'Pert powder diffractometer equipped with a graphite monochromator in the diffracted beam. CuK $\alpha$  radiation was used (40 mA, 40 kV) and the spectra was obtained in the range 3°–35° 2 $\theta$ .

***Biopharmaceutical properties of MPs:*** The tests have been performed in three different media depending on the model API: CBZ was tested using purified water because its dissolution is independent of the pH of the medium<sup>67, 91</sup>; in case of the acid and basic model APIs, the media has been selected in order to simulate the least favourable (and more challenging) pH condition and to better evaluate the effect of the formulation. Accordingly, TBM was tested in gastric simulated conditions (HCl solution pH 1.2) and CIN in intestinal simulated conditions (phosphate buffer solution pH 6.8).

Solubility studies. Solubility measurements of APIs and of loaded MPs were performed in 10 mL of the respective media at 25°C. The samples were magnetically stirred for 48h, equilibrated for 2h and the suspensions were then centrifuged at 10.000 rpm for 10 minutes. The supernatant was filtered through a 0.20 µm membrane filter. For CBZ and TBM, the filtrates were suitably diluted and analysed by UV-Visible spectrophotometer at 285 nm and 231, respectively. For CIN, after suitable dilution the samples were analysed by HPLC. The study was performed in triplicate.

Dissolution studies. The USP rotating paddle apparatus (Pharmatest, Steinheim, Germany) was used with a stirring rate of 50 rpm and was maintained at a temperature of 37°C. For CBZ and TBM, samples of pure drug, physical mixes and loaded MPs (size fraction 100-150 µm) were added to 500 mL of dissolution medium. The aqueous solution was filtered and continuously pumped (12.5 mL/min) to a flow cell in a spectrophotometer (UV2 Spectrometer, Unicam) and absorbance values were recorded at 285 nm and 231 nm for CBZ and TMB, respectively. In case of CIN, samples of pure drug and loaded MPs (size fraction 100-150 µm) were added to 1 L of dissolution medium. At specific time points, 2 ml of the medium were withdrawn using a 800 µm filter to avoid the removal of the SLMs and the amount of drug was quantified by HPLC. 2 ml of fresh medium were added to keep the volume constant. The dissolution tests were performed in triplicate.

**Statistical Analysis:** All results were expressed as mean ± standard deviation (S.D.). One-way analysis of variance (ANOVA) followed by the Bonferroni post-hoc test (GraphPadPrism, GraphPad software Inc., CA, USA) was used to analyze the data and the level of significance was set at the probabilities of \*p < 0.05, \*\*p < 0.01 and \*\*\*p < 0.001.

## II. Results and discussion

**Study of the self-emulsification ability of MPs.** Unloaded-MPs were prepared in three different Gelucire 48/16:Gelucire 50/13 ratio, as shown in Figure II.2. The previous study showed that the highest amount of Gelucire 48/16 appropriate for spray congealing technology is formulation C, containing 70% w/w of Gelucire 48/16. Using WPN atomizer, non-aggregated and spherical MPs were obtained, with prevalent fraction having particle size of 150-250 µm. In Self Emulsifying Drug Delivery System (SEDDS), the efficiency of self-emulsification could be estimated by determining the rate of emulsification and particle size distribution. The latter is the most important factor in self

emulsifying performance because it determines the rate and extent of drug release, as well as absorption<sup>92</sup>. For that reason, emulsification time studies and particle size determination by DLS were set up.

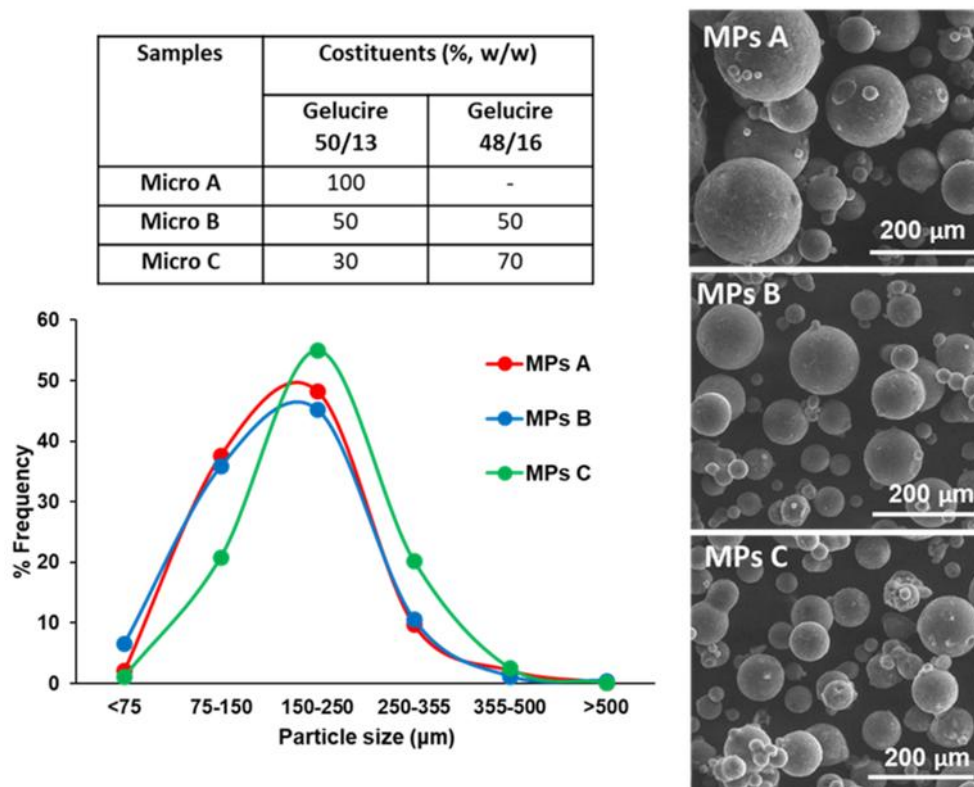


**Figure II.2.**Composition, particle size distribution and SEM images of unloaded MPs.

Figure II.3 shows the results of the emulsification time test of the formulation containing only Gelucire 50/13 (MPs A) and the formulation with the majority of Gelucire 48/16 (MPs C). MPs A completely emulsified within 115 minutes at pH 6.8, 120 minutes in water and 140 minutes in acidic media (pH 1.2). Thus, no significant variation in the self-emulsification time of formulation A was noticed on varying the medium. Moreover, in all environment MPs A formed a slightly cloudy micellar solution which was stable over time, since the measured value of absorbance did not change after the emulsification time was reached. Differently, MPs C needed only 14 minutes in pH 6.8 media and 18 minutes in water or acidic media to form the emulsion. Nevertheless, in this case the emulsion was not stable and after few minutes the micellar system started to change, as suggested by a gradual decreasing of the Relative Absorbance. The turbidity of the solution reached a final value after 55 minutes in buffer at pH 6.8 and after about 80 minutes in water and in buffer at pH 1.2.

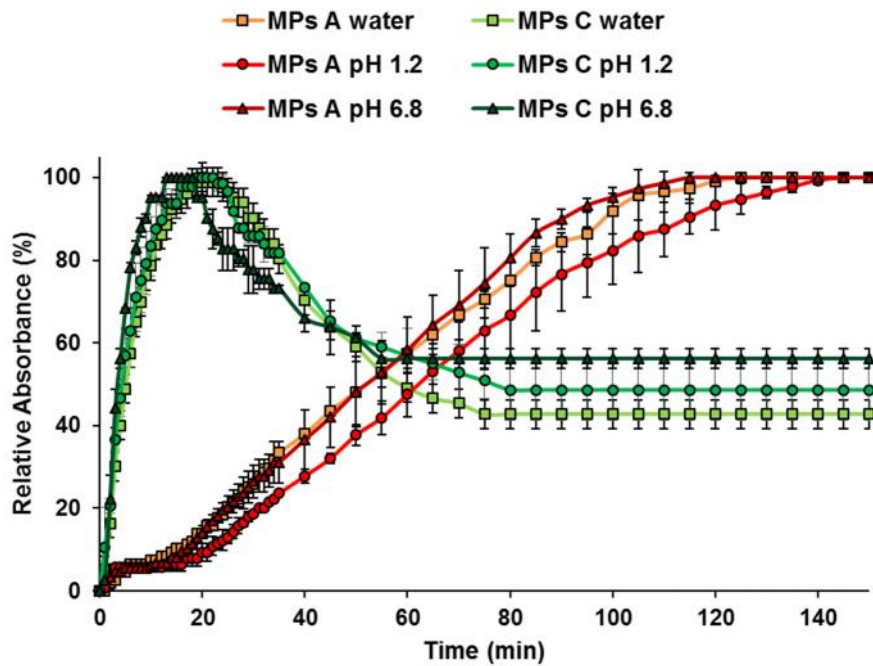


**Figure II.3.** Emulsification time of MPs A and MPs C in three different media: distilled water, buffer pH 1.2 and buffer pH 6.8. Values are expressed as means ( $n = 3$ )  $\pm$  SD.

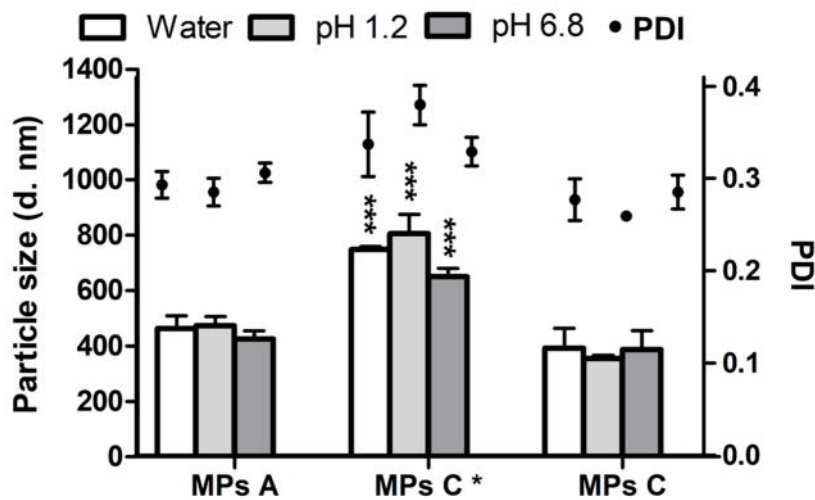


**Figure II.4.** Globule size of the emulsion formed from MPs A and from MPs C at the end of the emulsification-time test; the emulsion formed from MPs C at the highest value of absorbance (indicated as MPs C\*) was also analysed. Three media were evaluated: water, buffer pH 1.2 and buffer pH 6.8. Polydispersity index (PDI) was also measured. Values are expressed as means ( $n = 3$ )  $\pm$  SD, and the level of significance was set at the probabilities of \*\*\* $p < 0.001$ .

After the emulsification time analysis, the size of the micelles obtained from the solubilisation of MPs A and MPs C was evaluated by means of DLS and the results are reported in Figure II.4. The globule size of the emulsion obtained from MPs A solubilisation in the three media (distilled water,



buffer pH 1.2 and buffer pH 6.8) were  $424.3 \pm 2.7$  nm,  $438.5 \pm 1.4$  nm and  $387.1 \pm 34.9$  nm, respectively. Low PDI values ( $0.294 \pm 0.018$ ,  $0.240 \pm 0.031$  and  $0.282 \pm 0.003$ , respectively) indicated that the system had narrow size distribution. In view of the difference in the emulsification time between the two formulations, in the case of formulation C the size of micelles was assessed in two different times: when the highest value of absorbance was reached (maximum turbidity of the system) and at the end of the test, when the absorbance value was no longer varying. The results showed that also in the case of formulation C, the behaviour was not affected by the medium. Differently, a significant difference was noted ( $p < 0.001$ ) comparing the globule size of formulation C at the highest value of absorbance with those at the end of the test. In the first time point, where the maximum absorbance was detected, the system was characterized by big globule size and high PDI, indicating a higher instability compared to the same system after 90 min. However, when the constant value of absorbance was reached, the micellar solutions formed by MPs C showed similar globule size and PDI to MPs A.

Overall, both formulations formed a micellar solution in relatively short times, thus acting as SEDDS. Considering the composition of Gelucire, it is reasonable to suppose that the polar portion (free PEGs, PEG fraction of the PEG esters, hydroxyl group of monoglycerides) would constitute the outer part of micelles, whereas the apolar portion (hydrocarbon chains of PEG esters and mono-di-tri glycerides) would constitute the inner part of micelles, which is not in direct contact with water. Results showed that the presence of Gelucire 48/16 led to faster emulsification, probably due to its higher hydrophilicity (HLB of 16). Previous studies<sup>93 94</sup> demonstrated that as the concentration of hydrophilic components increased in the formulation, the emulsification ability of the system increased and the mean droplet size decreased. It is therefore reasonable to hypothesize that MPs C showed a better performance on drug bioavailability in virtue of their higher percentage of hydrophilic carrier. Although the final globule size of the microemulsion were similar for both formulations, it should be noticed that the value of absorbance at the end of the test was quite different. Mukherjee and Plakogiannis<sup>95</sup> showed that droplet size and the turbidity of the emulsions were affected by the oil concentration within the formulations. Accordingly, the different composition of Gelucire 50/13 and Gelucire 48/16 might result in a microemulsion with different micelle structure and therefore with different potential for drug incorporation and release.

**Loaded MPs: morphology and drug content.** All formulations, containing 10% w/w of drugs, were successfully prepared by spray congealing resulting in spherical and non-aggregated MPs. Particle

size distributions of the loaded-MPs were similar to those of the unloaded. SEM analysis (Figure II.5) of pure drugs showed crystals with different morphology.

CBZ crystals appeared as principally plate shaped, typical of the stable polymorphic form III<sup>96, 97</sup>, with some needle-like crystals, probably attributed to a different polymorphic form. TBM corresponded to prismatic crystals similar to its stable polymorphic form I<sup>L 98</sup> and CIN appeared as long regular crystals.

The morphological analysis of the MPs revealed mainly spherical particles with a smooth surface. The composition and the drug content in the three formulation of MPs are reported in Table II.1. For all model APIs, the actual drug loading were similar to the theoretical one (10%), hence the encapsulation efficiency was very good. This is due to the spray congealing technology that ensures high efficiency of encapsulation without loss of drug during process<sup>34</sup>. Slightly lower drug loading values were observed for CIN compared to the other two APIs. The reason might be in the particle size of the commercial API. As visible on the SEM images of the pure drugs (Figure 4), CIN particle size was rather bigger than those of CBZ and TBM. Thus, the inclusion of the as-received drug powder into the MPs during spray congealing process can result more difficult.

Samples	Costituents (% w/w)			Drug loading (% w/w)		
	Gelucire 50/13	Gelucir e 48/16	API	CBZ	CIN	TBM
MPs A	90	-	10	10.32 ± 0.13	9.38 ± 0.76	10.72 ± 0.87
MPs B	45	45		10.14 ± 0.06	9.37 ± 0.97	9.76 ± 0.11
MPs C	27	63		9.71 ± 0.37	8.19 ± 0.94	9.76 ± 0.27

**Table II.1.** Composition and drug loading of the MPs A, MPs B and MPs C loaded with CBZ, CIN and TBM.

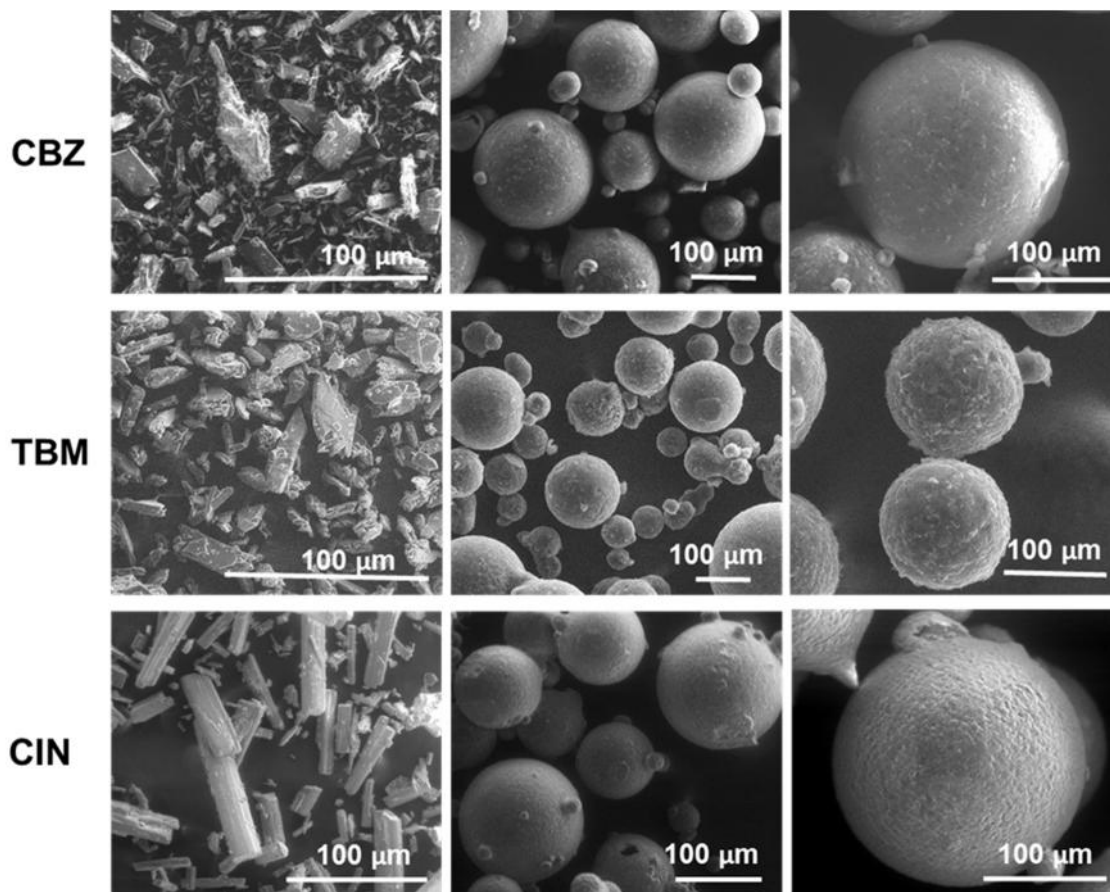


**Figure II.5.** SEM images of pure APIs (left) and MPs C at two different magnification (centre and right).

**Loaded MPs: dissolution and solubility studies.** The results of dissolution and solubility studies are shown in Figure II.6. All MPs considerably increased the release profile of CBZ (Figure II.6a), confirming the effectiveness of Gelucire-based MPs. Gelucire 48/16 showed a better performance than Gelucire 50/13 in improving the drug dissolution rate. By observing the profiles of Phy mix CBZ, we can notice that an increase of dissolution rate was achieved simply by mixing the drug and the carrier, as result of a better wettability of the drug in presence of Gelucire. However, the highest enhancement was achieved with MPs. Up to 80 % of CBZ was released within 10 minutes by the MPs, but it took 40 and 50 minutes, for the same amount of CBZ to be released in the case of the Phy mix and the pure drug, respectively.

The acid model drug TBM (Figure II.6b) showed similar behaviour, confirming that the formulation with the best performance was MPs C. In this case, however, whereas only a low increase in dissolution was achieved by the Phy mix, a marketed difference was achieved by MPs. Notably, although the tests were performed at acidic pH where TBM dissolution is unfavourable, the increase in dissolution rate form MPs was remarkable.

A different result was obtained in the case of CIN (Figure II.6c), the model basic API. CIN has an extremely low water solubility, equal to 2.5 µg/ml at 37°C<sup>99</sup>. Moreover, its solubility and dissolution behaviour is highly pH dependant, with the solubility value decreasing with the increasing of pH<sup>100</sup>. Accordingly, at pH 6.8 the release of pure CIN was extremely low. The effect of the MPs on drug dissolution was effective only in the first 5 minutes of the test whereas a decrease in CIN concentration was observed afterwards. These results suggested that at unfavourable pH conditions, where the dissolution of the drug is prevented, the MPs led to the formation of a supersaturated solution followed by a precipitation of the fraction of CIN solubilized in the beginning of the test.

The solubility of the APIs was enhanced in the order MPs C>MPs B>MPs A for all the three drugs. The solubility achieved from MPs A and MPs C resulted significantly different in all model APIs. In particular, the solubility of CBZ, TMB and CIN increased about 1.3, 2.3, 8.2-fold respectively with the formulation with only Gelucire 50/13 (MPs A) and 4.5, 3.9, 12.7-fold respectively with the MPs having the highest amount of Gelucire 48/16 (MPs C). Thus, the same trend observed in the dissolution studies was evident for the solubility, as result of the wetting effect and auto-emulsifying properties of the excipient. The marked differences between the three formulations is probably due to the differences between Gelucire 50/13 and Gelucire 48/16, which involve their hydrophilic characteristics and their auto-emulsifying properties.

Overall, the potential of Gelucire-based MPs for the bioavailability enhancement of BCS class II drugs was evident for all three model APIs showing a good increase in solubility, whereas the increase in dissolution rate was good for the neutral and acid model APIs and inconsistent in case of the basic API characterized by a highly pH-dependent behaviour.

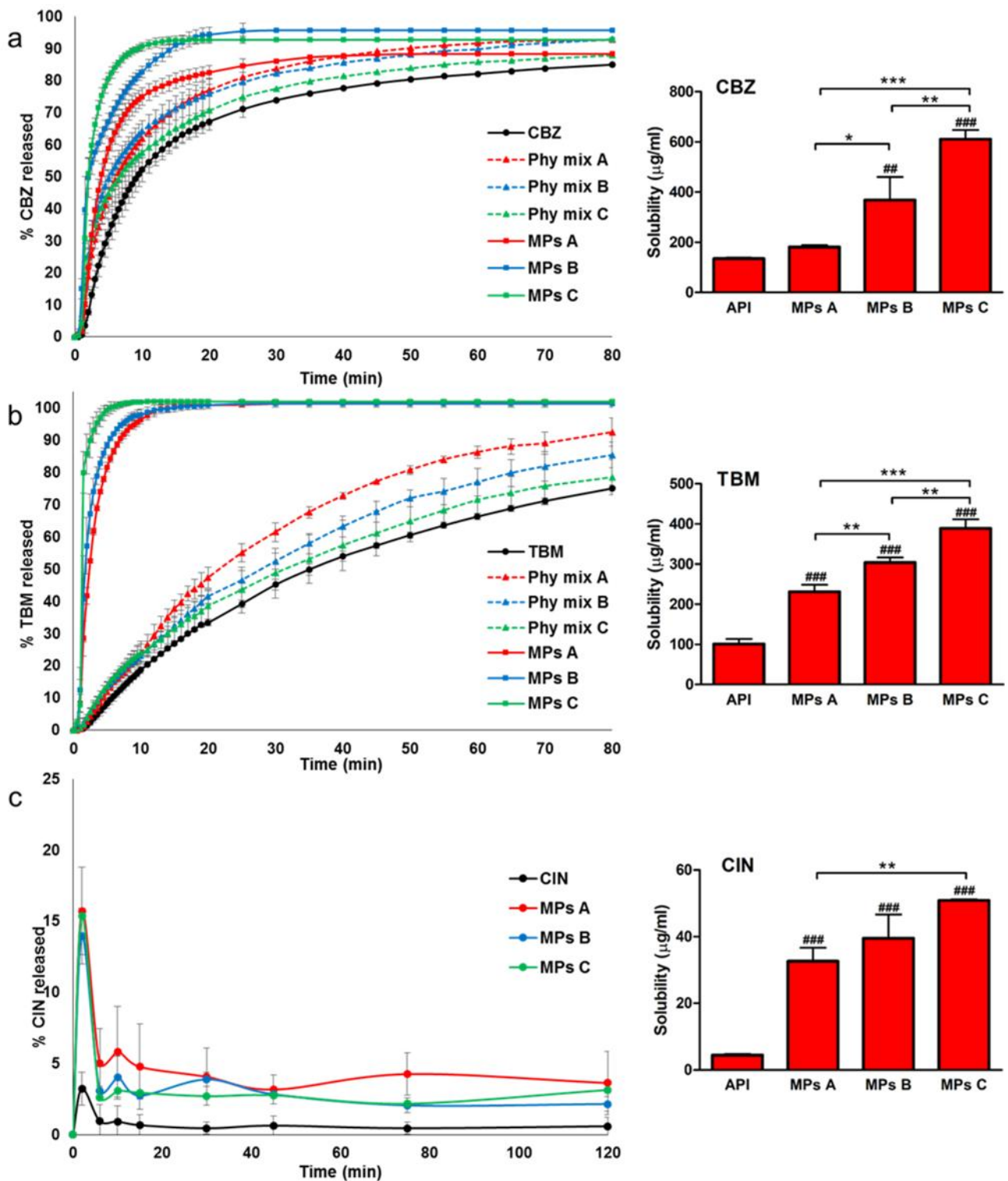


**Figure II.6.** Dissolution profiles and solubility studies of MPs A, MPs B and MPs C compared to the pure drugs for CBZ (a), TBM (b) and CIN (c).

**Loaded MPs: solid state characterization.** The solid state properties of the APIs in the MPs strongly influence important attributes such as chemical stability, hygroscopicity, dissolution rate and ultimately affect the bioavailability of the drug. Considering that the performance of the delivery

systems depends on the form of the API formulated into MPs, knowledge about the original polymorphic form of commercial drugs, and about the solid state of the APIs inside the MPs are needed.

CZB-loaded MPs: For CBZ, at least four polymorphs and a dehydrate form have been described in the literature. There has been much confusion about the naming of CBZ polymorphs. In this study we have adopted the nomenclature used by Grzesiak *et al.*<sup>101</sup>; the polymorphs/pseudopolymorphs known so far are listed in **Table II.2**.

Nomenclature	Crystal structure	Morphology	XRD diagnostic peaks (°, 2θ)	Characteristics
I	Triclinic	Fine needles	7.9, 8.6, 9.4, 12.2, 13.1, 19.9	Stable form at high temperature
II	Trigonal	Long and thick needles	8.7, 13.3, 15.0, 18.5, 20.1, 24.5	Metastable form, considered an impurity of form III
III	<i>P</i> -Monoclinic	Plate-shaped prisms	15.3, 15.9, 17.2, 19.5, 25.0	Commercial form. Stable form at room temperature, highly hygroscopic
IV	<i>C</i> -Monoclinic	Spherical plates	14.1, 17.9, 21.8, 33.1	Considered an impurity of form III, less soluble
dihydrate	-	Fine needles	8.8, 12.1, 18.8, 19.4	Formed in humid conditions, less soluble than form III

**Table II.2.** Nomenclature and main properties of the four CBZ polymorphs and the dehydrate

HSM and XRD analysis were performed to investigate possible modifications of the carrier and/or the drug after the spray congealing process. During HSM analysis (Figure II.7a), the optical examination of CBZ confirmed the presence of the two main crystal habits of the drug, form III and form I, already observed by SEM analysis. After heating, between 160 and 180 °C, some drug crystals evolved from form III (prismatic) into form I, with needle-shaped morphology, in a transition already reported<sup>102, 103</sup>. The melting of the drug occurred at 190 °C, in agreement with the endothermic event observed by DSC. During the HSM analysis of MPs C CBZ, Gelucires melted from 45 to 50 °C and CBZ was easily recognized as long needle-like crystals dispersed within the molten carrier. Unexpectedly, no prismatic crystals was detected in all MPs observed (analysis performed on three samples). From about 80 °C, CBZ crystals started getting smaller, as they gradually dissolved in the molten Gelucire; the dissolution was complete at about 135 °C, as previously observed<sup>67</sup>.

In order to better clarify the polymorphic form of CBZ in the MPs, XRPD analysis was performed. Figure II.7b reported the XRPD the on the raw CBZ, Micro C CBZ and the Phy mix C. The XRPD pattern

of pure CBZ showed diffraction peaks at  $2\theta = 7.9, 8.6, 9.3, 12.2, 13.1, 13.9$  whose positions and intensities are characteristic of form I, but also some peaks with lower intensities at  $2\theta = 15.2, 15.8, 17.2, 24.9$  typical of form III. These results confirmed that the starting drug sample was a mixture of the two stable forms of CBZ. The two PXRD of the Phy mix C presented the typical signals of triglycerides, observed at  $19.1$  and  $23.3^\circ 2\theta$ <sup>104</sup>, as well as the distinctive peaks of the drug, obviously less intense, due to the lower content of CBZ in the samples, equivalent to 10%. Moving to the analysis of MPs, it can be clearly seen that the pattern of MPs C CBZ was radically different from the corresponding Phy mix. This suggested a modification of CBZ crystals occurred during the spray congealing process. Beside the same two intense peaks of the carrier, which showed no modifications, the peaks of the drugs appeared as clear peaks at completely different positions:  $2\theta = 5.1, 8.7, 13.3, 15.1, 18.5, 20.1$  and  $24.5$ . These values of  $2\theta$  positions and relative intensities were compared to the diagnostic peaks of the four polymorphs of CBZ, and it was evident that they perfectly matched the pattern of CBZ form II. The anhydrous form II of CBZ has been observed during processing, contributes to the decreased purity of CBZ Form III<sup>96</sup> and morphology corresponds to long needles<sup>105</sup>. These findings were supported by the results previously obtained by HSM, which showed long regular needle-shaped crystals inside MPs. This particular change in the CBZ solid state has been previously noticed by Martins *et al.*<sup>106</sup> in a paper focused on the comparison between the influence of ultrasound and high-shear mixer on the properties of MPs produced by spray congealing. Although the form II is unstable, XRPD carried out after 6 months from the MPs production showed no changing in MPs C CBZ, proving that Gelucire-based MPs can stabilize this polymorph. The same results were obtained for formulation A (graph not shown).

FT-IR spectra analysis of pure CBZ, unloaded MPs C, MPs C CBZ and the correspondent Phy mix is reported in Figure III.7c. CBZ spectrum presented a sharp peak at  $3483\text{ cm}^{-1}$ , due to the  $-\text{NH}$  vibration, carbonyl stretching vibration in the primary amide group at  $1686\text{ cm}^{-1}$  and the  $-\text{NH}_2$  bending vibration at  $1488\text{ cm}^{-1}$ , in agreement with those reported in other studies.<sup>107</sup> The IR spectrum of the MPs C CBZ is similar to the physical mix ones and showed all the CBZ and carrier characteristics bands, suggesting the absence of interaction or complexation between drug and carrier in both systems. However, they are not completely superimposable: for the MPs containing CBZ, the characteristic signal at  $1686\text{ cm}^{-1}$  was noted at  $1691\text{ cm}^{-1}$ , indicating a peak shift to higher wave numbers, compared to the correspondent Phy mix, in which the peak moved to the original position at  $1686\text{ cm}^{-1}$ . This could indicate that in the MPs the double carbonyl bond of CBZ is less

involved in intermolecular interactions, as the stretching frequency increases with bond strength.<sup>108</sup> Moreover, this characteristic stretching band of CBZ has been reported to increase to higher wavenumbers passing from the forms III and I to the form II<sup>101</sup>.

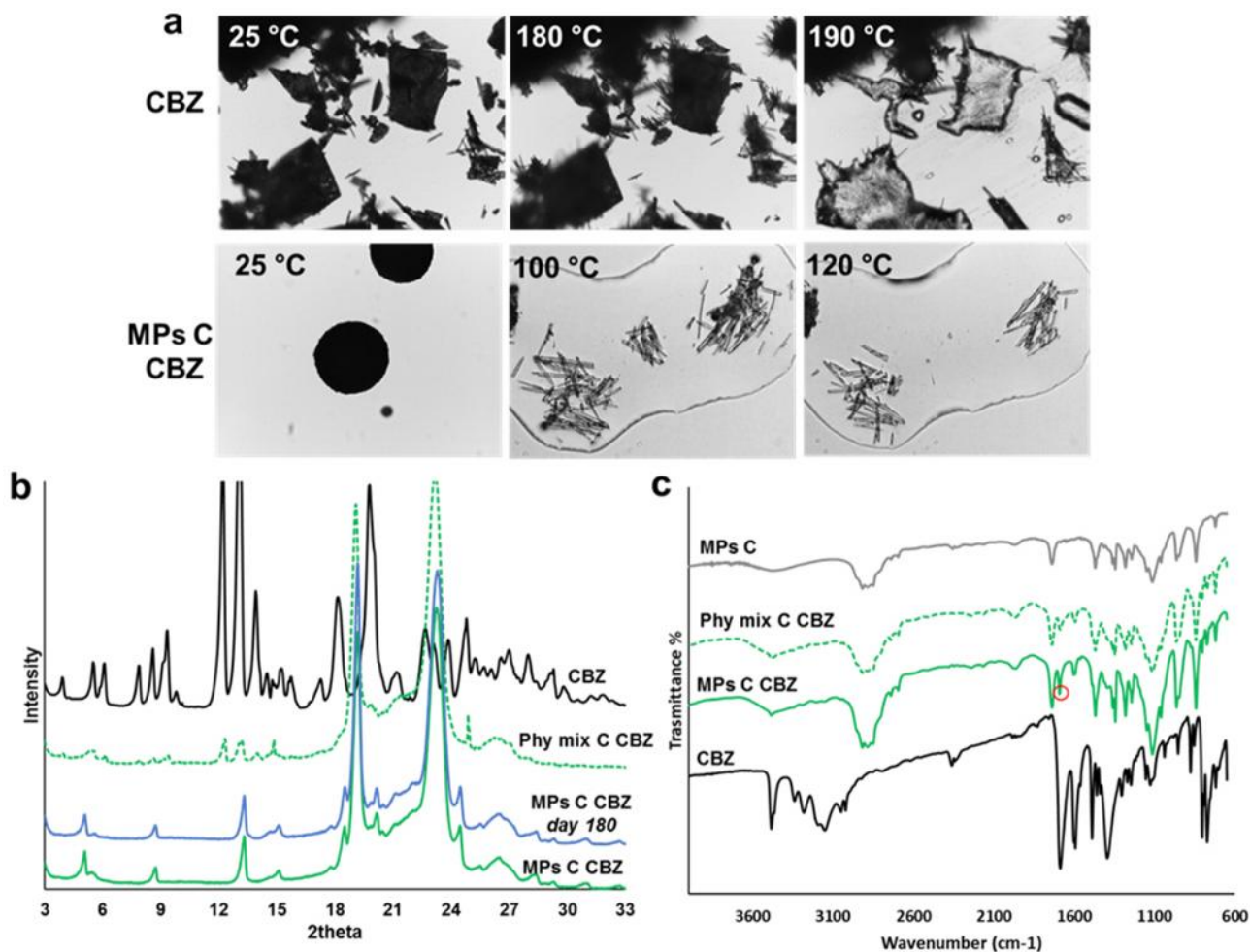


**Figure II.7.** (a) HSM images of CBZ and MPs C CBZ. The magnification was 20x for the pure drug (first line) and 10x for the MPs (second line) images. (b) XRPD spectra of CBZ, Phy mix C CBZ and MPs C CBZ immediately after preparation and after 6 months of storage. (c) FT-IR spectra of CBZ, unloaded MPs C, MPs C CBZ and Phy mix C CBZ.

TBM-loaded MPs: TBM is characterized by different polymorphs, schematized in Table II.3. HSM analysis (Figure II.8a) of TBM showed prismatic crystals which melt at 130 °C. TBM-loaded MPs melt between 45 and 55 °C, depending on the formulation, and no crystal was observed into the Gelucire molten matrix. This result suggested the transformation of the drug into the amorphous form with loss of crystal structure. Otherwise, it is possible that drug crystals, although present in the solid particles, solubilized within the molten Gelucire during the analysis and were therefore not visible. TBM as-received was characterized to have information about its original crystal properties. DSC



(Figure II.8b) shows a transition peak at  $T = 44.8\text{ }^{\circ}\text{C}$  with an enthalpy of melting of  $\Delta H = 9.5\text{ J g}^{-1}$ . According to the literature, this transition peak is due to the transition of form I<sup>L</sup> to I<sup>H</sup> <sup>98 109</sup>. The second endothermic event at  $T_m = 130.0\text{ }^{\circ}\text{C}$  ( $\Delta H = 98.1\text{ J g}^{-1}$ ) correspond to the data of form I<sup>H</sup>, which report a melting temperature between 125.5 to 131.5  $^{\circ}\text{C}$  and a  $\Delta H$  ranging from 88.0 to 100.6  $\text{J g}^{-1}$  <sup>110</sup>. Thus, DSC analysis of the unprocessed material suggested that the drug was mainly in its most stable form I<sup>L</sup>. The melting of the carrier is represented by an endothermic event between 35 and 55 $^{\circ}\text{C}$ , both in the thermograms of unloaded MPs C and TBM-loaded MPs. It should be noted that the endothermic signal of TBM melting in the drug loaded-MPs C was absent. This phenomenon has been previously observed in Gelucire based- dispersion, and could be due to loss of API crystal structure during spray congealing process or during DSC analysis <sup>67 68</sup>.

XRPD analysis was performed to further investigate the solid state of TBM into MPs after spray congealing process, using formulation C as example. As shown in Figure II.8c, pure TBM is highly crystalline with diffraction peaks at  $2\theta = 8.8, 12.2, 13.2, 14.3, 17.6$  and  $20.9$ , typical of form I<sup>L</sup> <sup>98 111</sup>. In Phy mix TBM, the diffractogram showed the same sharp peaks, with low intensity due to the amount of TBM (10% w/w) in the sample. When the TBM was loaded in MPs, the peaks of the drug appeared broader and with lower intensity. This result suggested either the formation of TBM crystals with smaller size or the partial conversion in the amorphous form, with low residual crystallinity of the drug into the carrier matrix. The modification in the peaks appearance but not in their position exclude the possibility of conversion into a different polymorph as well as the complete amorphisation of the API into the SD.

Nomenclature	Crystal structure	Morphology	XRD diagnostic peaks ( $^{\circ}, 2\theta$ )	Melting point ( $^{\circ}\text{C}$ ), $\Delta H_{fus}$ (kJ/mol)	Transition point ( $^{\circ}\text{C}$ )
I <sup>H</sup>	-	-	-	128, 23.8	-
I <sup>L</sup>	Orthorhombic	Prism	8.7, 12.1, 19.9, 20.9	-	40
II	Monoclinic	Plate	10.3, 11.3, 19.6	117, 26.0	-
III	Monoclinic	Needle	11.2, 15.4, 18.2	-	106
IV	Monoclinic	Needle	10.6, 18.0, 18.9	-	88

**Table II.3.** Nomenclature and main properties of the TBM polymorphs

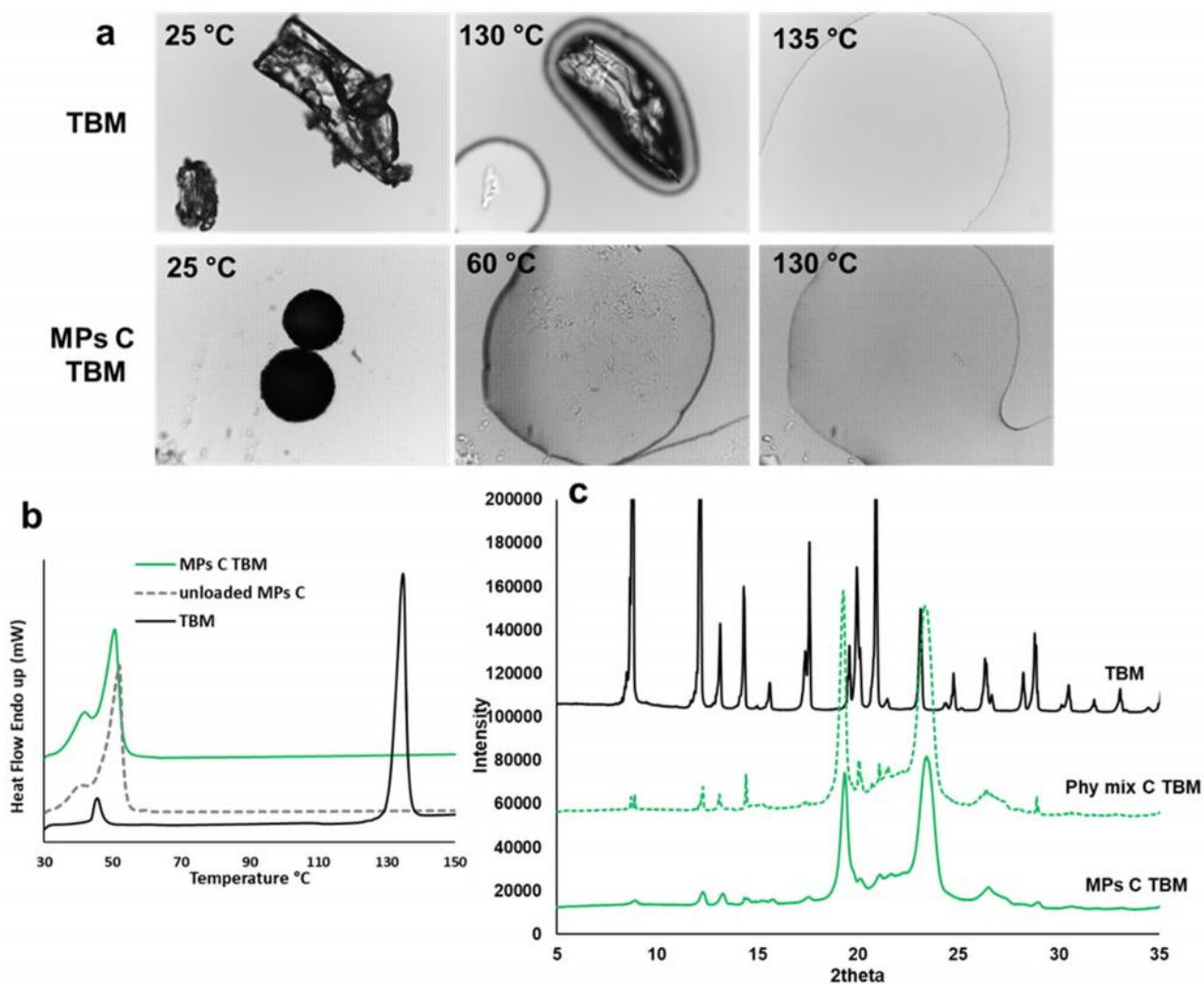


**Figure II.8.** (a) HSM images of TBM and MPs C TBM. The magnification was 40x for the pure drug (first line) and 10x for the MPs (second line) images. (b) DSC of TBM, unloaded MPs C and MPs C TBM (c) XRPD spectra of TBM, Phy mix C TBM and MPs C TBM.

CIN-loaded MPs: As already mentioned, the basic drug CIN is, among the three model APIs, the most lipophilic compound with a  $\log P$  of 5.8<sup>112</sup>. It is therefore reasonable to expect lower affinity between the drug and the hydrophilic carrier Gelucire. Accordingly, during spray congealing production of CIN-loaded MPs, the drug powder did not solubilize into the molten Gelucire and a suspension was obtained. Therefore, the presence of CIN crystals in the original solid form in the MPs was expected. The HSM analysis, shown in Figure II.9, confirmed our hypothesis. CIN original crystals are regular column-shaped crystals which melted at 122 -124 °C. As expected, in case of MPs, crystals of CIN were observed upon carrier melting (red arrows in Figure II.9). Specifically, the crystals had similar morphology to the original one, but with smoother rounded borders and tended to progressively

solubilized in the carrier with the increasing of the temperature, until complete disappearance at 100-110°C.

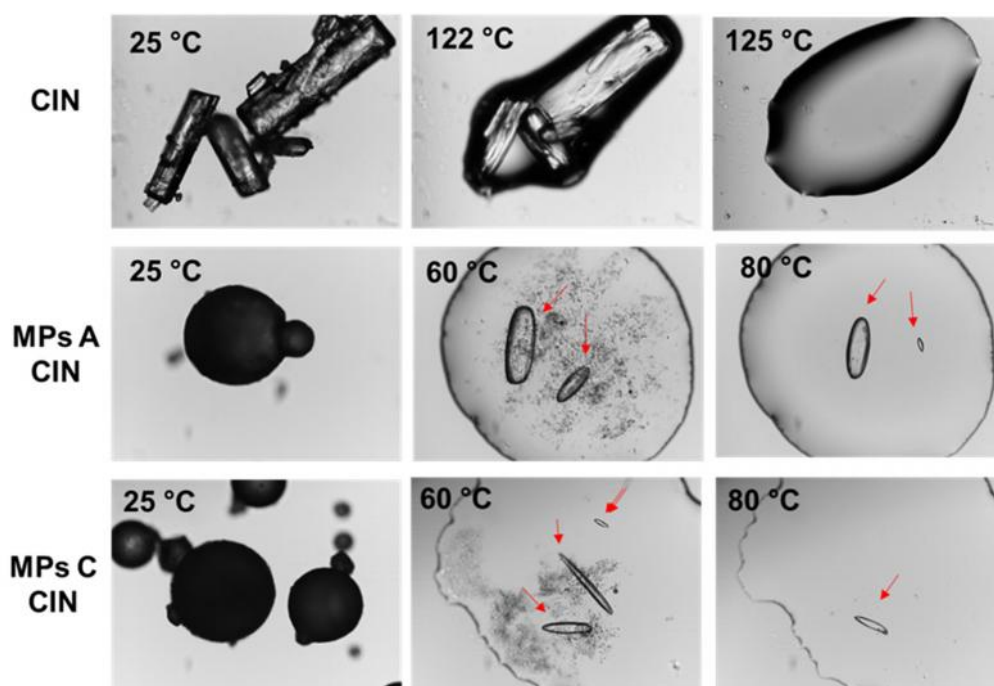


**Figure II.9.** HSM images of CIN, MPs A CIN and MPs C CIN. The magnification was 20x for the pure drug (first line) and 10x for the MPs (second and third lines) images.

This study demonstrate the suitability of spray congealing technology in the production of SD of different BCS class II APIs in form of spherical MPs, in order to increase their oral bioavailability. The results showed that each specific API can result in Gelucire-based SD with different properties. Numerous factors such as chemico-physical characteristics of the API, its crystalline state, the affinity of the API with the carrier at the liquid and solid state, possible interactions between drug and carrier influence the overall properties of the MPs. In the cooling phase of spray congealing process, the API can solidify in various forms and during storage, these forms can undergo further changes. Specifically, the spray congealed systems of Gelucire50/13 or Gelucire50/13-Gelucire 48/16 can consist in crystalline dispersions with both carrier and API in their crystalline form, with no modification of the API original polymorphic form. This was observed for the basic model API CIN, when the affinity of the API with the hydrophilic carrier is low. In this case, the dissolution rate was not efficiently enhanced by the SD because of the preservation of the API more thermodynamically stable form, as well as its extremely low and pH-dependent water solubility. Otherwise, crystalline dispersions with both carrier and API in their crystalline form, with the API in a different polymorphic form can be obtained, as in the case of CBZ. Additionally, semicrystalline

dispersions with crystalline carrier and the API partially amorphous with smaller crystals (as in the case of TBM) or even completely amorphous API (as in the case of IND, case study I) can be obtained. In these last cases, the API original crystalline form was somehow modified by the formulation into Gelucire SD, bringing the drug molecules in a thermodynamically less stable state, determining an improvement of the dissolution behaviour. This is particularly evident in the dissolution studies of CBZ and TBM, where the dissolution profiles were significantly enhanced from MPs compared to the correspondent Phy mix.

## II. Conclusion

This study highlights the complexity of Gelucire-based SD containing poorly water soluble APIs belonging to BCS class II. The bioavailability enhancement of Gelucire-based MPs depends on multiple effects, which can be divided in two main categories: (i) effects given by the hydrophilic carrier, such as improved wettability, reduction of interfacial tension between drug and water, prevented particle aggregation and solubilising effect due to Gelucire surfactant properties. These effects are independent on the API physical state inside the MPs. (ii) effects resulting from changes in the drug crystalline original state, including amorphisation, conversions into metastable polymorphs and crystals size reduction. Whereas the second category is strictly dependent on the specific API and should be therefore studied on a case-by-case basis, the first one can be ideally exploited for the bioavailability enhancement of all BCS class II drugs. In this regard, the comparison of Gelucire 50/13 with the recently marketed Gelucire 48/16 showed a superior ability of Gelucire 48/16 in improving the solubility of poorly water soluble APIs, due to the more hydrophilic chemical composition. Both carrier in contact with aqueous fluids, led to the formation of microemulsions with micelles of about 400 nm and low PDI. However, formulations containing the majority of Gelucire 48/16 showed shorter emulsification time and different micelle structure compared to the Gelucire 50/13-based system.

## Case study III: pH and reactive oxygen species-sequential responsive nano-in-micro composite for targeted therapy of inflammatory bowel disease

### III. Introduction

Oxidative stress plays an essential role in the pathogenesis and progression of IBD,<sup>113</sup> and diseased sites present abnormally high ROS level, as confirmed by biopsies of tissues taken from IBD patients showing from 10- to 100-fold increase in mucosal ROS concentrations<sup>114 115</sup>. The unusually high concentrations of ROS localized at sites of intestinal inflammation can be exploited as a selective feature to target the delivery system, and avoid the release of the drug in the healthy tissue<sup>116</sup>. Accordingly, we identified the excessive generation of ROS as a disease-specific triggering mechanism to design a responsive drug delivery system. Nano-sized delivery systems have been recognized as a promising strategy for IBD treatment, because of their preferential accumulation in the inflamed regions of the intestine<sup>117</sup>. Additionally, nanoparticles (NPs) provide the potential of tailoring drug properties, including solubility, stability, and release behavior and their surface can be easily modified in order to introduce targeting-ligands or adjust surface characteristics (e.g., surface charge or adhesive properties). Advances in polymer science have led to the development of several novel reactive oxygen species (ROS)-responsive materials in the last few years. For example, the introduction of arylboronic moieties to common polymers such as poly amino-esters<sup>118</sup>, polyesters<sup>119</sup>, cyclodextrins<sup>120</sup> provides specific sensitivity towards hydrogen peroxide (H<sub>2</sub>O<sub>2</sub>), making these polymers very attractive for the development of oxidation-sensitive systems. Within this group, an oxidation-sensitive dextran (OxiDEX) can be prepared by a simple modification of the hydroxyl groups of dextran, resulting in a responsive and biocompatible material, thus very promising for biomedical applications<sup>121</sup>. Drug delivery systems based on ROS-responsive polymers can be applied for various therapeutic purposes, as they represent a promising smart delivery vehicle for pathological disorders characterized by ROS overproduction.

Therefore, considering the potential of recently synthesized ROS-responsive polymers and the advantages of nano-sized systems in IBD treatment, it is important to evaluate these biomaterials for the development of smart high-precision medicines. The aim of this research is the development of an advanced oral drug delivery system able to meet multiple demands: protection of the responsive NPs against harsh GI environments, prevention of premature drug release and

achievement of targeted and efficient local drug delivery to the diseased sites with limited systemic absorption. For this purpose, we designed a nanoplatform based on OxiDEX NPs to achieve an oxidation-responsive drug delivery, externally modified with chitosan (CS), known for its mucoadhesive properties. Mucoadhesion can be an additional advantage for IBD targeting as it promotes better contact with the mucosal surface and reduces the clearance of nanocarriers when the intestinal motility is increased, which is common in IBD, helping to maintain high local concentration of drug<sup>122</sup>. Rifaximin (RIF), an intestine-specific antibiotic successfully used in inducing remission of IBD<sup>123 124</sup>, was chosen as model drug. NPs were then encapsulated by microfluidics in hydroxypropyl methylcellulose acetate succinate (HPMCAS), a pH-responsive polymer, to produce nano-in-micro structured particles<sup>125</sup>. The final composites were designed to protect the NPs from the harsh conditions of the upper GI tract (*e.g.*, acid pH of the stomach) and to release them in the intestine, closer to the targeted site. Thereafter, upon triggering by abnormally elevated ROS levels, the OxiDEX NPs will selectively release RIF to the inflamed tissues.

### III. Experimental section

**Preparation of OxiDEX nanoparticles:** An oxidation-responsive dextran-modified polymer (OxiDEX) was synthesized using the procedure of Broaders et al.<sup>121</sup> with minor modifications and characterized by NMR. OxiDEX NPs were prepared by nanoprecipitation method. OxiDEX (5 mg) was dissolved in dimethylsulfoxide (DMSO) (0.25 ml), and then added dropwise into the anti-solvent (ethyl acetate, 2.5 ml) under magnetic stirring. The formed NPs were collected by centrifugation at 10000 rpm for 5 min washed with ethyl acetate and dried under vacuum at room temperature overnight.

**Drug loading:** RIF loaded nanoparticles (RIF NPs) were prepared using the method described above, but adding RIF (2.5 mg) in the OxiDEX solution. The concentration of RIF in samples was determined by Agilent 1100 high performance liquid chromatography (HPLC, Agilent Technologies, USA) with a mobile phase composed of phosphoric acid (0.1%, pH 3.3) and acetonitrile (volume ratio 50:50) at a flow rate of 1mL min<sup>-1</sup>. A Gemini® 3 µm NX-C18 110 Å column (Phenomenex, USA) was used as stationary phase. The injection volume of the samples was 10 µl and the detection wavelength was 293 nm. For the drug loading determination, 1 mg of NPs was accurately weighed and stirred in a

mixture of 0.1 M of H<sub>2</sub>O<sub>2</sub> (0.5 ml) and acetonitrile (0.5 ml) for 2 h, until complete dissolution. The sample was centrifuged and the drug content in the supernatant was analyzed by HPLC.

**Coating of nanoparticles with chitosan:** After preparation, NPs were coated with CS by physical adsorption method<sup>126</sup>. Medium viscosity chitosan (Mw=190000-310000 Da, 75-85% deacetylated, Sigma-Aldrich, USA) was dissolved in 0.1 % acetic acid solution to obtain a 1% solution and the pH was adjusted to 5.5 by slowly adding sodium hydroxide solution. NPs and RIF-NPs were dispersed in 0.9 ml of MilliQ-water by sonication, 0.1 ml of CS solution was added to the NPs dispersion to have a final CS concentration of 0.1%. NPs were magnetically stirred with the CS solution for 1 h. CS-NPs and RIF-loaded CS-coated NPs (CS-RIF NPs) were collected by centrifugation and washed with MilliQ-water.

**Characterization of OxiDEX NPs:** Size distribution and surface charge of NPs and RIF NPs before and after CS coating were determined by Zetasizer Nano ZS (Malvern Instruments Ltd, UK) in MilliQ-water (pH 7.4). Transmission electron microscopy (TEM; JEOL 1400, Japan) was used to observe the morphology of NPs before and during degradation study in presence of H<sub>2</sub>O<sub>2</sub>. TEM images were obtained with 80 kV acceleration voltage in bright-field mode. The chemical composition of dextran, OxiDEX, NPs, CS-NPs and pure CS was characterized by FTIR (Vertex 70, Bruker, USA). The FT-IR (KBr) spectra were recorded in the range of 4000–650 cm<sup>-1</sup> with a resolution of 4 cm<sup>-1</sup> using OPUS 5.5 software. Differential scanning calorimetry (DSC; AG-DSC823e, Mettler Toledo, Switzerland) was performed on OxiDEX, NPs, pure drug and physical mixture (PM). Samples were heated from 25 °C to 250 °C under nitrogen flow at a heating rate of 10 °C min<sup>-1</sup>. Stability study was performed on drug loaded NPs and CS-NPs using Hanks' balanced salt solution (HBSS) as buffer to mimic the intestinal medium (pH 6.8)<sup>127</sup>.

**In vitro evaluation of oxidation-responsive degradation of the NPs:** The response of OxiDEX NPs exposed to H<sub>2</sub>O<sub>2</sub> and the consequent release of the drug were studied *in vitro*. RIF NPs (250 µg) were incubated in 1 ml of PBS buffer (pH 6.8, 37 °C) containing various concentrations (0, 0.1, 0.25, 0.5, 1.0 mM) of H<sub>2</sub>O<sub>2</sub>. At different time points, 100 µl of NPs suspension were withdrawn, centrifuged and the drug content in the supernatant was analyzed by HPLC. To study the stability of NPs in acidic conditions and the possible hydrolysis of NPs, quantitative experiments were conducted by measuring the absorbance of NPs-containing aqueous solutions (pH 1.2 and pH 6.8, 37°C) at 500 nm at various time points.

**Microfluidic assembly of nano-in-micro composites:** NPs were encapsulated by microfluidics in an enteric polymer, HPMCAS MF grade (HPMCAS-MF) with oil-in-water emulsion. The flow focusing microfluidic chip consisted of two borosilicate glass capillaries (World Precision Instruments, USA) assembled on a glass slide, as described elsewhere<sup>125</sup>. The injection rates of the inner oil fluid (HPMCAS-MF 10 mg ml<sup>-1</sup> in ethyl acetate) and the outer fluid (2% w/v Poloxamer 407 aqueous solution, pH 4) were 2 ml h<sup>-1</sup> and 20 ml h<sup>-1</sup>, respectively. RIF NPs and CS-RIF NPs were dispersed in the inner fluid before microfluidic process by tip sonication (weight ratio NPs:HPMCAS-MF 1:3). The formed droplets were collected in 1% Poloxamer 407 solution (pH 4.0). The solidified microparticles were collected by centrifugation, washed with MilliQ water (pH 4.0) and dried in a vacuum oven at 50 °C overnight. In addition to encapsulation of RIF NPs (NPs@MF) and CS-RIF NPs (CS-NPs@MF), free drug was encapsulated (RIF@MF) to obtain a reference formulation.

**Labelling of nanoparticles with FITC:** For confocal imaging, NPs were fluorescently labelled by loading of FITC. Briefly, FITC was added in the DMSO solution of the polymer to have a final concentration of OxiDEX and FITC of 20 mg ml<sup>-1</sup> and 0.2 mg ml<sup>-1</sup>, respectively (ratio FITC:OxiDEX 1:100). The obtained solution was used to prepare labelled NPs using the same nanoprecipitation method.

**Characterization of nano-in-micro composites and in vitro drug release studies:** To determine the distribution of the NPs into the microparticles of MF, CLSM was applied. FITC-labelled NPs were encapsulated in MF and Nile red was added as fluorescent dye to the inner fluid during the preparation of nano-in-micro composites. After microfluidic fabrication, the produced composites were arranged into 35 mm Petri-Dish with a thin bottom and imaged by CLSM (Leica SP5 II HCS A, Germany).

The release profiles of the nano-in-micro composites were evaluated by using pH variation method (pH 1.2 and pH 6.8), as described in the European Pharmacopoeia. NPs@MF, CS-NPs@MF (equivalent to 10 µg of RIF) were added to 1 ml of SGF (pH 1.2). After 2 h, particles were collected by centrifugation and resuspended in PBS buffer (pH 6.8) for additional 6 h. The test was conducted at 37°C with stirring at 100 rpm. At specific time points, 100 µl of the release medium were withdrawn, centrifuged to remove the solid particles and the amount of drug in the supernatant was quantified by HPLC. 100 µl of fresh medium were added to keep the volume constant. The morphology of nano-in-micro composites before and during the release study was examined by scanning electron microscopy (SEM, Hitachi S-4800, Japan). To investigate the benefits of the nano-



in-micro composites, release studies were performed also with RIF NPs and CS-NPs, following the same experimental procedure.

**Cell culture:** Human colon carcinoma Caco-2 clone C2BBE1 and human colon adenocarcinoma HT29-MTX were cultured in separate 75 cm<sup>2</sup> culture flasks in high glucose (4.5 g l<sup>-1</sup>) Dulbecco's modified Eagle's medium (HyClone, Logan, UT) containing 10% of fetal bovine serum (Gibco, Invitrogen, USA), 1% (v/v) of L-glutamine, 1% (v/v) of nonessential amino acids, 100 IU ml<sup>-1</sup> of penicillin, and 100 mg ml<sup>-1</sup> of streptomycin (HyClone, Logan, UT). Cells were grown at 37°C in 5% of CO<sub>2</sub> and 95% relative humidity and the cell medium changed every other day.

**In vitro cytotoxicity studies:** Cytotoxicity of NPs, CS-NPs and nano-in-micro composites on cells was evaluated using CellTiter-Glo (Promega Corporation, USA). C2BBE1 and HT29-MTX were separately seeded in 96-well plates at a density of  $2 \times 10^5$  cells per ml and left to attach for 24 h. Then, the medium was discarded and cells were washed with 100 µl of Hanks' balanced salt solution-4-(2-hydroxyethyl)-1-piperazinethanesulfonic acid (HBSS-HEPES, pH 7.4). Formulations were added to each well at a concentration of 50, 200, 500, 1000 and 2000 µg ml<sup>-1</sup> (NPs or equivalent) and incubated for 6 and 24 h. Afterwards, cells were washed twice with HBSS-HEPES and the number of viable cells was quantified by addition of CellTiter-Glo. Luminescence was measured using a Varioskan Flash plate reader (Thermo Fisher Scientific, USA). HBSS-HEPES without particles and Triton X-100 1% were used as negative and positive control, respectively.

**Cell model of the intestinal membrane: C2BBE1/HT29-MTX cell monolayer:** cells were seeded on 12-Transwell cell culture inserts at a seeding density of 70,000 cells per cm<sup>2</sup> with C2BBE1 and HT29-MTX cells in a ratio of 9:1, the medium was replaced every other day until the cell monolayer was formed after 21 days. TEER was measured all over the 21 days to control the development of tight junctions.

**Mucoadhesion of the particles to cell monolayers:** Cell monolayers were washed with HBSS-HEPES, then 200 µL suspension of labelled particles in HBSS-HEPES (250 µg ml<sup>-1</sup>) was added and incubated for 4 h at 37 °C. After incubation, the monolayers were washed twice with HBSS-HEPES (pH 7.4) to remove the particles not attached and fixed with 4% paraformaldehyde at room temperature for 15 min. Wheat Germ Agglutinin-Alexa Fluor 594 conjugate (WGA-AF 594) (10 µg mL<sup>-1</sup>) was incubated 10 minutes to stain the mucus. After washing, the Transwell filter was excised, embedded in a mounting medium containing DAPI and mounted on glass slides for confocal imaging. The particle-cell interactions were observed using CLSM (Leica SP5, Leica Microsystems, Germany).

**Drug permeability across cell monolayer:** The permeability of RIF across the cell monolayers was investigated from the apical (0.5 mL) to basolateral direction (1.5 mL) at 37 °C with shaking at 100 rpm. HBSS–HEPES buffer solution pH 7.4 was used in the received compartment, whereas HBSS–HEPES buffer (pH 6.8) with or without 1 mM of H<sub>2</sub>O<sub>2</sub> was employed in the donor compartment to simulate healthy and oxidative extracellular medium conditions, respectively. Samples were added on the apical part to have a final RIF concentration of 6 µg ml<sup>-1</sup>. At specific time points (15, 30, 60, 90, 120 and 180 min) 100 µl of the release medium were withdrawn from the basolateral part and replaced with fresh medium. The amount of drug permeated in the basolateral compartment was quantified by HPLC and the  $P_{app}$  was calculated<sup>128</sup>. The experiments were carried out in triplicate.

**Flat embedding TEM:** After permeability studies, the cell monolayers were fixed with 2.5% glutaraldehyde (Sigma-Aldrich, USA) in 0.1 M of phosphate buffer saline (PBS) (pH 7.4) for 20 min at room temperature. Then, the wells were washed twice with sodium cacodylate buffer (NaCac) for 3 min. After that, the cell monolayers were post-fixed with 1% of osmium tetroxide in 0.1 M of NaCac buffer (pH 7.4) and then dehydrated and embedded in epoxy resin. Ultrathin sections (60 nm) were cut perpendicularly to the inserts, post-stained with uranyl acetate and lead citrate, and examined with TEM.

**Statistical Analysis:** All results were expressed as mean ± standard deviation (S.D.). Analysis of variance (ANOVA) followed by the Bonferroni post hoc test (GraphPadPrism, GraphPad software Inc., CA, USA) was used to analyse the data and the level of significance was set at the probabilities of \* $p < 0.05$ , \*\* $p < 0.01$  and \*\*\* $p < 0.001$ .

### III. Results and discussion

**Characterization of nanoparticles.** A H<sub>2</sub>O<sub>2</sub>-responsive material (OxiDEX) was synthesized and used to prepare NPs, which were subsequently coated with CS. The preparation procedure of the particles is schematically shown in Figure III.1.

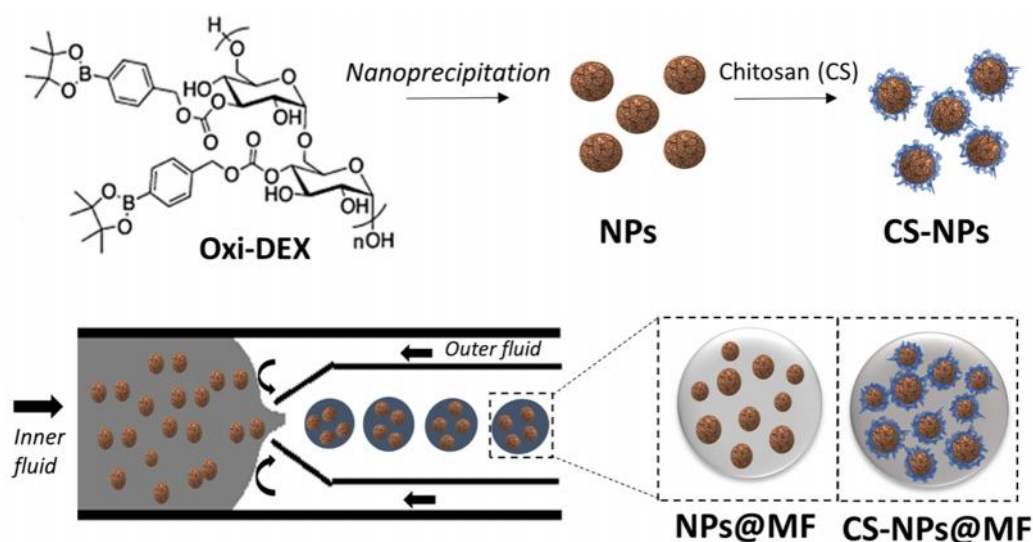


**Figure III.1** Scheme of the production procedure of NPs and CS-NPs and schematic illustration of the fabrication process of the nano-in-micro composites by microfluidics: NPs and CS-NPs were encapsulated in MF grade HPMCAS (MF) to form, respectively, the composites (NPs@MF and CS-NPs@MF). NPs or CS-NPs were dispersed in an ethyl acetate solution of MF, which served as inner oil fluid. The outer continuous fluid was 2% w/v P-407 aqueous solution (pH 4).

The size and polydispersity index (PDI) of OxiDEX NPs were evaluated by dynamic light scattering (DLS). The hydrodynamic average size was 100-200 nm (Figure III.2a), and it was not affected by the CS coating. Moreover, a relatively similar particle size distribution was observed for NPs and CS-NPs (Figure III.2c); however, a slightly wider particle size distribution was detected in the case of CS-NPs, due to the presence of CS layer on the particle surface, which led to a size distribution moved towards higher values and to an increased polydispersity. This trend was confirmed by a small increase in the PDI (Figure III.2a), which passed from 0.303 to 0.363 after CS coating in the case of unloaded particles. Similarly, for RIF-loaded particles the PDI increased from 0.344 to 0.412 after CS coating. The presence of CS on the particle surface was confirmed by the measurement of zeta-potential, that changed from negative ( $-24.4 \pm 1.7$  mV) to positive ( $+11.6 \pm 0.5$  mV) (Figure III.2b), because of the positively charged amino groups of CS. The morphology of OxiDEX particles was studied by transmission electron microscopy (TEM). TEM images (Figure III.2c) show highly spherical

particles in case of uncoated NPs, while a more irregular particle shape due to surface covering of CS was noticed for CS-NPs. The size of dried particles observed in TEM images was slightly larger than the average hydrodynamic diameter obtained from the DLS experiment, but still consistent with the DLS results if observing the size distribution.

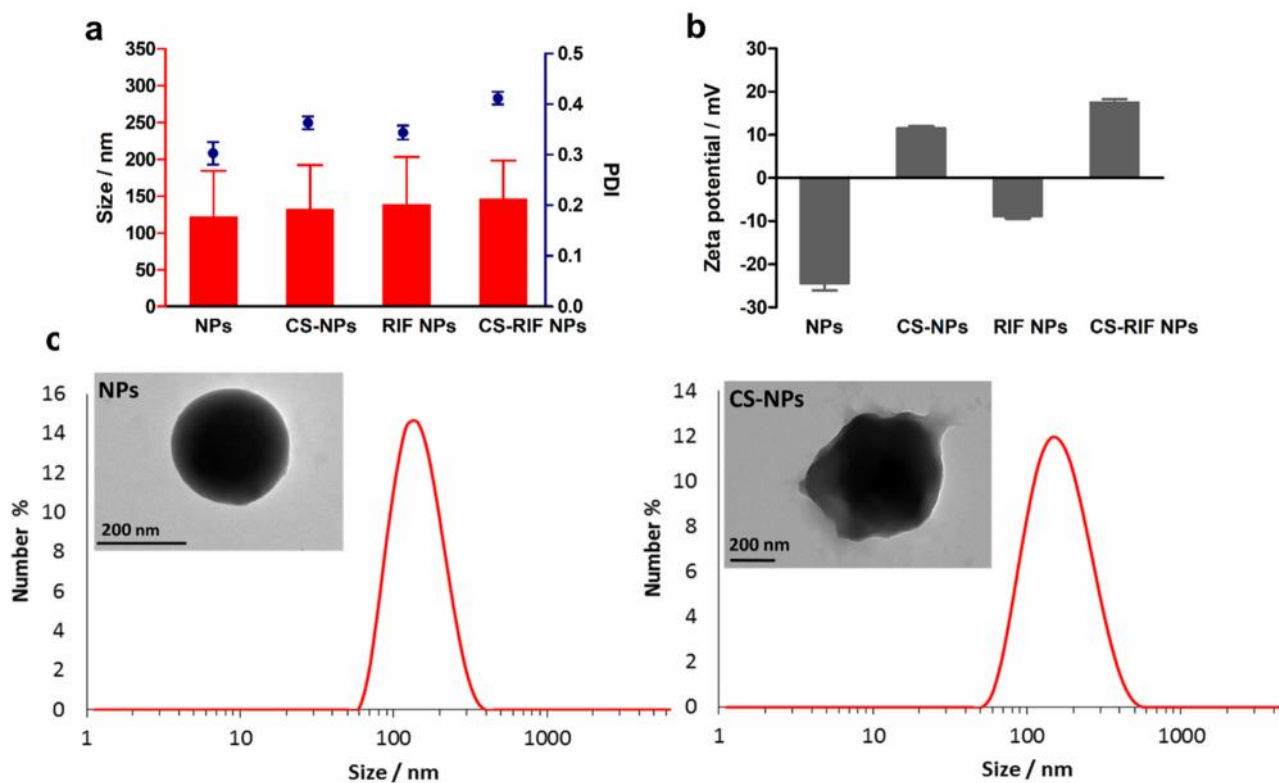


**Figure III.2.** (a) Size and PDI and (b) zeta-potential of NPs and CS-NPs both unloaded and loaded with RIF. (c) TEM images of NPs and CS-NPs and correspondent particle size distribution measured by DLS.

Fourier transform infrared (FTIR) spectroscopy results are reported in Figure III.3a. Dextran showed characteristic bands at 3400, 2923, and 915  $\text{cm}^{-1}$ , attributed to O-H bonds, C-H bonds, and the  $\alpha$ -glucopyranose ring, respectively<sup>129</sup>. After the boronic ester modification, we observed the presence of new bands at 1640, 1610 and 1540  $\text{cm}^{-1}$  due to the C-H stretching vibrations of the aromatic groups. Moreover, after modification, the broad band at 3400  $\text{cm}^{-1}$  due to dextran hydroxyl groups was markedly reduced and an extra strong band appeared at 1747  $\text{cm}^{-1}$ , which can be related with the C=O stretching of the newly formed ester groups. These characteristic bands of OxiDEX can be found with minor shift in the NPs. Comparing the spectra of NPs before and after CS coating, in the CS-NPs extra bands (1541, 1560, 1653, 1676 and 1684  $\text{cm}^{-1}$ ) appeared, which were absent in the spectrum of NPs. In particular, the bands ranging from 1510 to 1650  $\text{cm}^{-1}$  represent a distinctive feature of CS and may be attributed to its amide groups<sup>130</sup>. In this region, the two strongest signals

(1676 and 1684  $\text{cm}^{-1}$ ) can be found in the spectrum of CS-NPs. In addition, compared to the FTIR spectrum of NPs, the carbonyl band (1650  $\text{cm}^{-1}$ ) was shifted to higher wavenumbers (1653  $\text{cm}^{-1}$ ) after CS coating. This strong band at 1653  $\text{cm}^{-1}$ , which can be seen in the spectrum of pure CS, is characteristic of the polymer and attributed to the  $-\text{C}=\text{O}$  stretching vibration of its secondary amide

131.

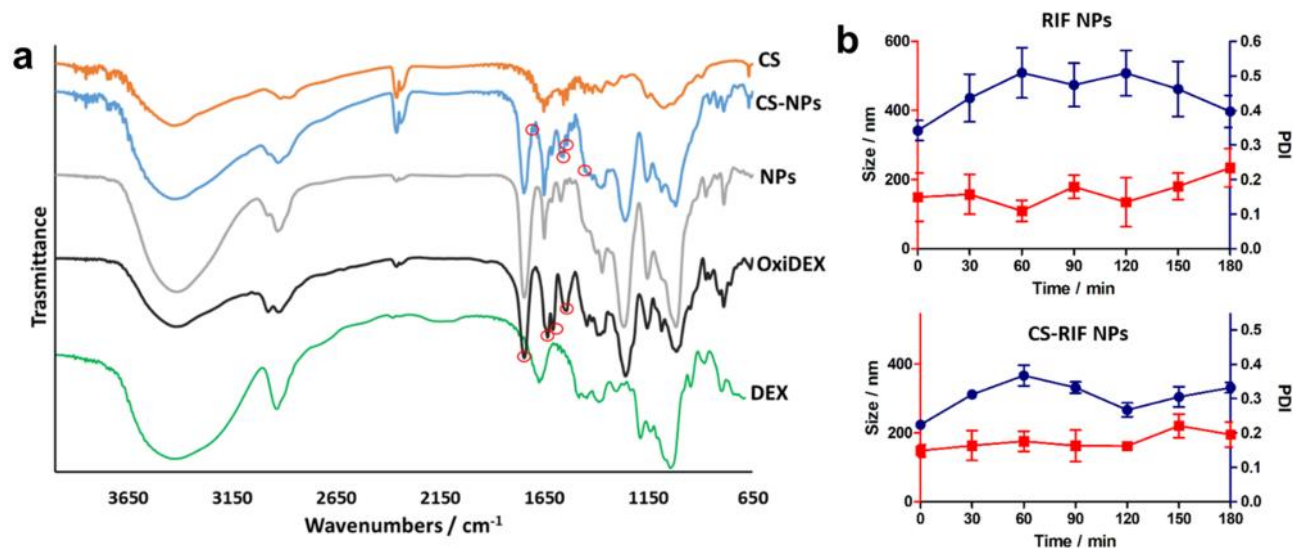


**Figure III.3.** (a) FTIR spectra of dextran (DEX), OxiDEX, NPs, CS-NPs and pure CS. (b) Evolution of the nanoparticle size and polydispersity index (PDI) during incubation in simulated intestinal buffer. Data represent mean  $\pm$  S.D. ( $n = 3$ ).

The RIF loading values were  $3.3 \pm 0.1\%$  and  $2.9 \pm 0.2\%$  for NPs and CS-NPs, respectively. Since the NPs are designed to deliver the drug locally on the intestinal membrane, the formulation needs to be stable the time necessary to reach the inflamed mucosa and to be degraded by the local ROS. Hence, the colloidal stability of RIF NPs and RIF CS-NPs was studied in a medium simulating intestinal conditions (Figure III.3b). The average sizes of NPs showed fluctuations between 110 and 230 nm and the PDI, approximately 0.4, had also moderate variations. We found that the presence of CS on the NPs surface led to more stable particle size and lower PDI, which was around 0.3. Comparing these results with the ones obtained in MilliQ-water (Figure III.2a) we can deduce that in the presence of saline buffer, the OxiDEX particles were less stable than in water. However, after CS coating, the stability in buffer increased significantly. In particular, the average size was stable at 180 nm for the first 120 min, and only a small increasing in size (to around 200 nm) was observed in the third hour, suggesting that the NPs' tendency to aggregate in buffer was attenuated by the addition of CS coating.

**H<sub>2</sub>O<sub>2</sub>-responsive degradation of NPs.** The hydrolysis of OxiDEX NPs was examined in PBS containing various concentrations of H<sub>2</sub>O<sub>2</sub>, by measuring the amount of encapsulated drug released in the buffer after particle degradation (Figure III.4a). Concentrations ranging from 0.1 to 1.0 mM of H<sub>2</sub>O<sub>2</sub> were chosen basing on the sensitivity of OxiDEX, which had previously showed degradation when incubated with H<sub>2</sub>O<sub>2</sub> 1.0 mM.<sup>[7]</sup> In 1 h, more than 60% of RIF was released with 1.0 mM of H<sub>2</sub>O<sub>2</sub> and even at low H<sub>2</sub>O<sub>2</sub> concentration (100 μM), still more than 14% of the drug was released by the end of the test. NPs were not degraded in PBS alone (RIF released < 1% after 6 h). The appearance of NPs suspensions confirmed the H<sub>2</sub>O<sub>2</sub> dependent degradation of the polymer: with increasing concentrations of H<sub>2</sub>O<sub>2</sub>, a yellow transparent solution can be observed, whereas a yellowish colloidal solutions could still be observed after 6 h of incubation in PBS (Figure III.4b), indicating the presence of solid NPs. These results proved that degradation of OxiDEX NPs was highly responsive to the level of H<sub>2</sub>O<sub>2</sub>. In addition, TEM images of the NPs suspension in the 1.0 mM of H<sub>2</sub>O<sub>2</sub> were taken at different time points to observe the evolution in the morphology of the NPs (Figure III.4c). Already after 15 min, the NPs lost their original spherical shape, and some were swollen or partially degraded. This effect progressed overtime, showing a clear degradation of the particles after 60 min.

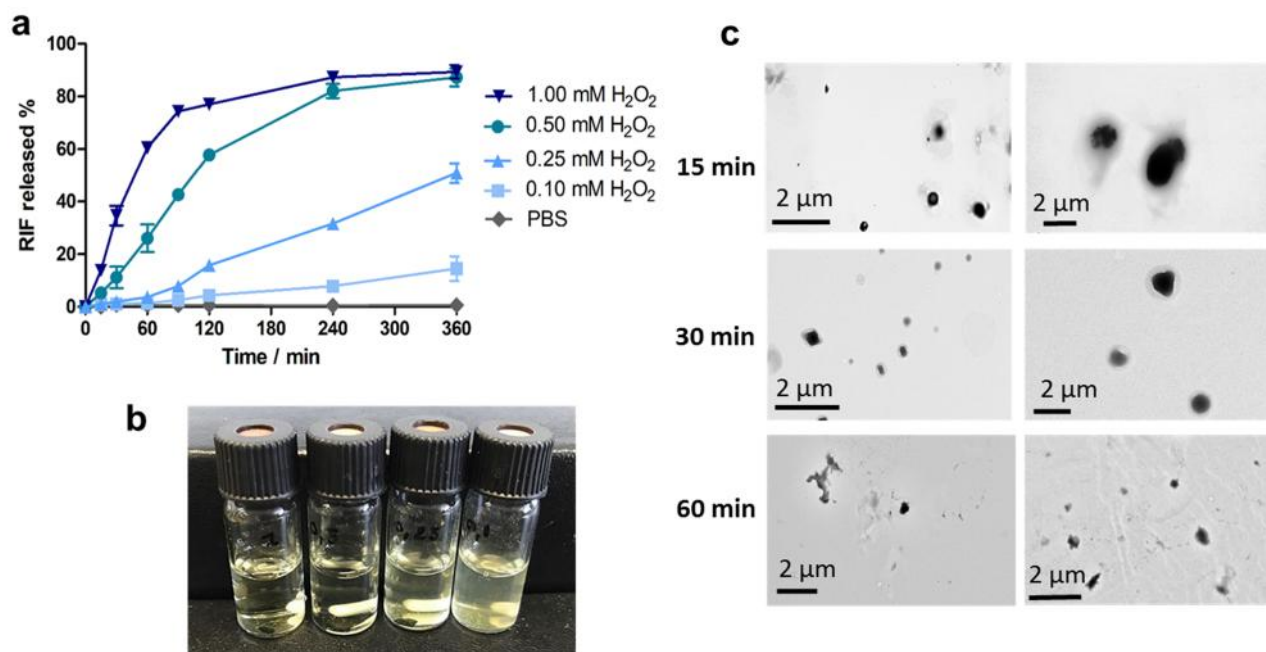


**Figure III.4.** (a) RIF release from OxiDEX NPs in PBS buffers with various concentrations of H<sub>2</sub>O<sub>2</sub>. Data represent mean ± S.D. (n = 3). (b) Appearance of the suspensions of RIF NPs in buffers with 1.0, 0.5, 0.25 and 0.1 mM of H<sub>2</sub>O<sub>2</sub> (from left to right). (c) TEM images of the RIF NPs suspension in 1.0 mM of H<sub>2</sub>O<sub>2</sub> at different time points.

**Characterization of nano-in-micro composites and *in vitro* drug release studies.** RIF NPs and CS-RIF NPs were encapsulated in a pH-responsive polymer MF grade of HPMCAS (HPMCAS-MF) to form nano-in-micro composites by microfluidics, named as RIF NPs@MF and CS-RIF NPs@MF, respectively. The preparation process is schematically illustrated in Figure III.1. This method allowed the production of MPs with spherical shape (Figure III.5a) and monodispersed particle size distribution, with prevalent size of  $53 \pm 3 \mu\text{m}$ . The distribution of NPs in the composites was studied by confocal microscopy (Figure III.5a). To enable the visualization, NPs were labelled with fluorescein isothiocyanate (FITC) and the outer HPMCAS-MF polymer layer was labelled with Nile red. Confocal images showed an efficient encapsulation of NPs in the composites. Moreover, the prevalence of yellow in the merged image indicated a co-localization of NPs and matrix, with a homogeneous distribution of the NPs within the polymeric matrix.

RIF NPs@MF and CS-RIF NPs@MF were immersed in simulated gastric fluid (SGF) at pH 1.2 and afterwards in PBS at pH 6.8 to evaluate the pH-responsive dissolution behaviour. As reported in Figure III.5b, composites kept their integrity after 2 h immersion in pH 1.2, showing no change of morphology. Differently, microparticles started to lose their shape already after 5 min at pH 6.8, and they were completely degraded when the immersion time was prolonged to 2 h. These results suggest that nano-in-micro composites based on HPMCAS-MF prepared by microfluidics are able to tolerate the harsh gastric conditions and to release the encapsulated NPs only at the typical intestinal pH (6.8).

In vitro drug release studies simulating the GI tract were carried out on the nano-in-micro composites (RIF NPs@MF and RIF CS-NPs@MF) and on a reference formulation, prepared by encapsulation of pure drug in the same enteric polymer HPMCAS-MF (RIF@MF), to better resemble the conventional commercial formulations. To evaluate the capability of the NPs to maintain the oxidation-responsive drug release after the encapsulation in the microcomposites, experiments in oxidative conditions (PBS with the addition of 1 mM of  $\text{H}_2\text{O}_2$ ) were also performed. The release profiles (Figure III.5c) showed that the MF matrix prevented the drug release at pH 1.2 in all samples.

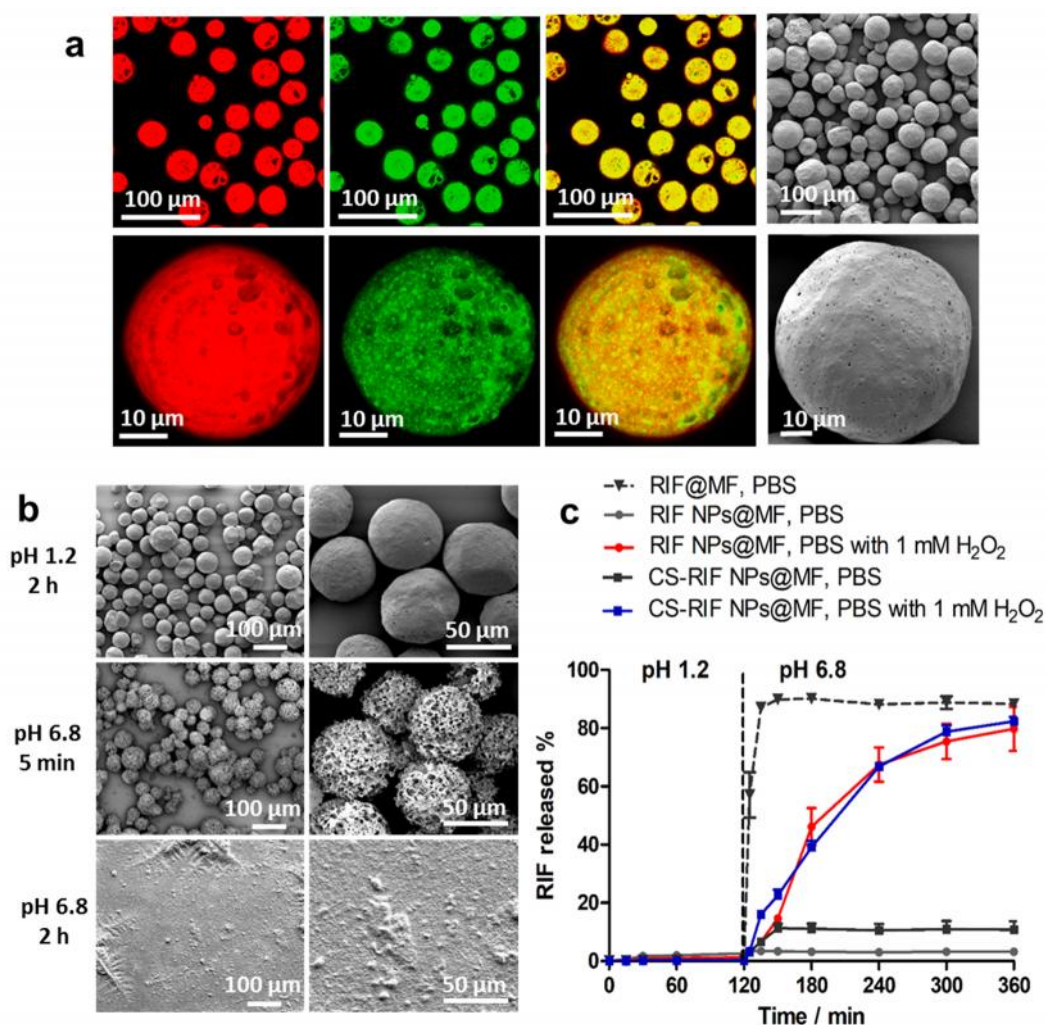


**Figure III.5.** (a) FITC-labelled NPs were encapsulated in HPMCAS-MF with the addition of Nile red. The confocal images showed (from left to right) the Nile red, FITC and the overlay channels. In addition, the surface of the particles was observed by scanning electron microscope (SEM). (b) SEM images of RIF NPs@MF after immersion in SGF (pH 1.2) for 2 h, and in PBS (pH 6.8) for 5 min and 2 h. (c) Drug release profiles of nano-in-micro composites and reference formulation consisted of RIF encapsulated in HPMCAS MF (RIF@MF) first in SGF for 2 h and then in PBS with or without H<sub>2</sub>O<sub>2</sub> for 6 h. Data represent mean  $\pm$  S.D. (n = 3).

The release behaviour at pH 6.8 showed important differences: the drug was released immediately in the case of RIF@MF, while the RIF encapsulated in OxiDEX NPs was gradually released over 4 h only in presence of H<sub>2</sub>O<sub>2</sub>. A controlled drug release is highly desired in IBD treatment, because it represents an advantage in terms of achieving the effective concentration required for local action and maintaining it over a sustained period of time. As expected, a very low drug amount (<10%) was released by the microcomposites in normal PBS buffer. It was interesting to notice that the coating with chitosan did not affect the dissolution behaviour.



**In vitro cytotoxicity studies.** The cytocompatibility of fabricated nanoparticles and nano-in-micro composites was evaluated on human colon carcinoma Caco-2 clone (C2BBe1) and human colon adenocarcinoma (HT29-MTX) cell lines, representing the enterocytes and the mucus-producing goblet cells of the intestine, respectively<sup>132</sup>. The time points 6 and 24 h were chosen for this study as they correspond to the typical time that the particles would travel in the small intestine and the whole GI tract, respectively<sup>122</sup>. Cytotoxicity results are shown in Figure III.6.

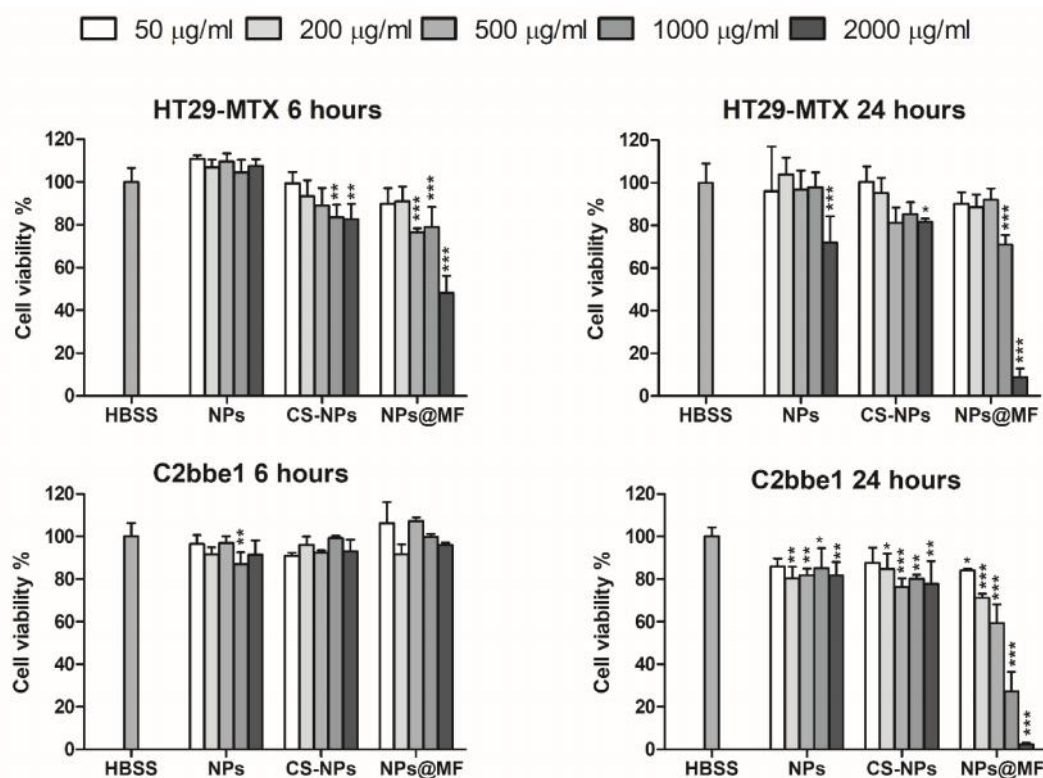


**Figure III.6.** Viability of C2BBe1 and HT29-MTX cells after 6 and 24 h incubation with different concentration of NPs, CS-NPs, and nano-in-micro composites (NPs@MF). The concentration of NPs@MF was calculated based on the amount of encapsulated NPs. Data represent mean  $\pm$  S.D. ( $n = 3$ ), and the level of significance was set at the probabilities of  $*p < 0.05$ ,  $**p < 0.01$ , and  $***p < 0.001$  compared to the control (HBSS).

OxiDEX NPs demonstrated to be safe for cells, even at very high concentrations ( $2000 \mu\text{g ml}^{-1}$ ), as cell viability was higher than 80% for both cell types for both time points, excluding the highest concentration of NPs incubated for 24 h with HT29-MTX cells. Compared to uncoated NPs, CS-NPs led to lower cell viability, probably because of the positive charge of the surface: however, the cell viability was still higher than 80% in all cases. Finally, the microcomposites showed the lowest viability. One possible explanation for this could be the very large amount of samples added in order to maintain fixed NPs concentration. Moreover, we should consider that in physiological conditions,

HPMCAS would be solubilized (it is soluble at pH > 6), and consequently, it would be quickly eliminated by physiological clearance. Thus, in the case of the final microcomposites, the experimental conditions were not fully representative of the *in vivo* situation, because the polymer remained in contact with cells during the whole experiment.

**Mucoadhesion of the particles to C2BBE1/HT29-MTX cell monolayers.** The interaction between NPs and intestinal cells was qualitatively studied by confocal laser scanning microscopy (CLSM). Wheat Germ Agglutinin-Alexa Fluor 594 conjugate (WGA-AF 594) was used to stain the mucus, as it binds to sialic acid and N-acetylglucosaminyl residues mainly localized in the mucus layer, which is particularly indicated when the objective is the evaluation of a mucoadhesive formulation.

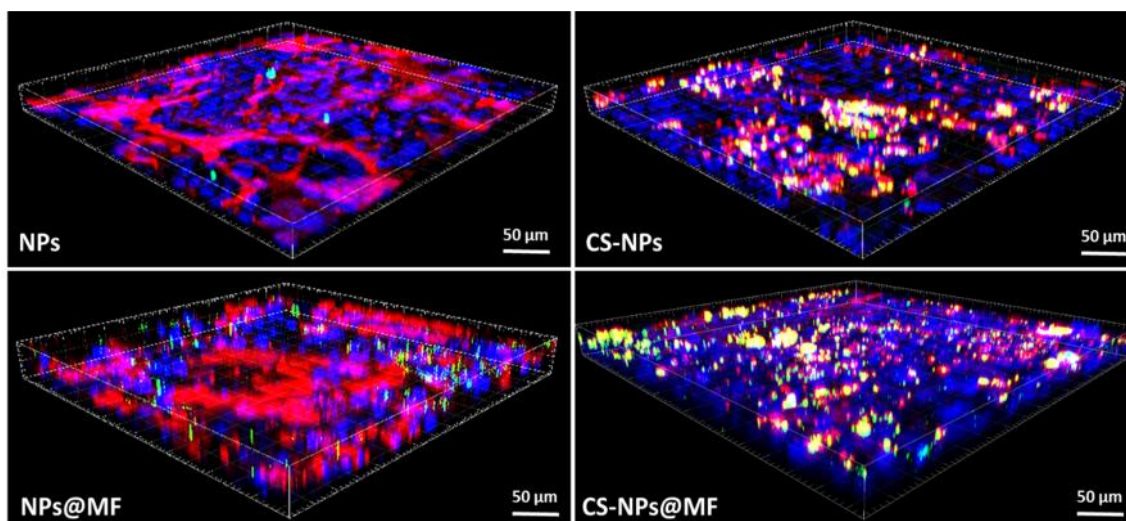


**Figure III.7.** 3D Confocal microscope images of C2BBE1/HT29-MTX monolayers treated with NPs and CS-NPs ( $250 \mu\text{g ml}^{-1}$ ) labelled with FITC after incubation with the cells at 37 °C for 4 h. Blue: cell nuclei stained with DAPI; Red: mucus layer stained with WGA-AF 594; green: FITC-labelled particles; and yellow: co-localization of NPs/CS-NPs and mucus.

As can be seen in Figure III.7, CLSM images showed no or minimal interactions between cells and OxIDEX NPs. The particles appeared as green, suggesting only a superficial adhesion to the cell monolayer, but no strong interaction with the mucus layer. Differently, for CS-coated NPs, more particles were observed on the cells. The larger amount of CS-NPs could be explained by the presence of CS on the NPs surface. The mucoadhesive properties of CS determined a high rate of interaction of CS-NPs with the co-cultured cells, thus decreasing the probability of washing away the particles during sample preparation. Electrostatic interactions of cationic CS with the negatively

charged mucin are the main reason for CS strong mucosal adhesion<sup>133</sup>. Notably, most CS-NPs appeared as yellow, indicating a co-localization with the red-stained mucins of the mucus layer on the surface of the monolayer and, thus, a preferential accumulation of CS-NPs on the mucus layer on the intestinal membrane.

**Drug permeability across C2bbe1/HT29-MTX cell monolayer.** After 21 days, the cell monolayers were completely differentiated and tight junction formed, as confirmed by TEER values stabilized at around 650  $\Omega\cdot\text{cm}^2$ . This model closely mimics the in vivo intestinal membrane<sup>134</sup>. Permeability curves and apparent permeability coefficients ( $P_{app}$ ) are reported in Figure III.8a,b, respectively. As observed from the permeation profiles, free RIF encapsulated in HPMCAS-MF showed the highest permeability, with a  $P_{app}$  of  $5.41\times 10^{-6}$ . RIF encapsulated in NPs@MF and CS-NPs@MF had very low permeability ( $5.26\times 10^{-7}$  and  $5.73\times 10^{-7}$ , respectively). The  $P_{app}$  values of RIF were significantly decreased after encapsulation into the OxiDEX NPs, indicating that the NPs were effective to limit the drug absorption through intestinal membrane and therefore decrease the drug amount in the systemic circulation.

Formulations were also tested with the addition of 1 mM of  $\text{H}_2\text{O}_2$  in the donor compartment, to simulate an oxidative extracellular condition. This condition with high-oxidative medium allows a complete release of the drug after degradation of the  $\text{H}_2\text{O}_2$ -sensitive NPs. Comparing the  $P_{app}$  in the two conditions, the permeability resulted enhanced in the case of oxidative conditions for all samples. In particular, for RIF NPs@MF and CS-RIF NPs@MF, only in the presence of oxidizing species in the medium the drug was released and slowly permeated through the cell monolayer. The drug permeability was higher in oxidative conditions also in the case of RIF@MF, despite the absence of the  $\text{H}_2\text{O}_2$ -sensitive polymer, suggesting that the presence of  $\text{H}_2\text{O}_2$  could influence the membrane integrity and contribute to increase drug permeation. Overall, the data indicate that the permeation of RIF may be drastically reduced by incorporation in OxiDEX NPs, especially in healthy conditions, representing an advantage in terms of unspecific absorption and systemic side effects.

After the permeability studies, the cell monolayers were observed under TEM (Figure III.8c,d). The morphology of the cell monolayers was similar for all conditions, and the incubation with RIF NPs@MF and CS-RIF NPs@MF did not affect the appearance of the microvilli, indicating that the formulations have no toxic effects on the cell monolayers under the present experimental conditions tested. TEM images also showed some spherical dots (marked with red arrows) on the

apical side of the monolayers near the microvilli, with dimensions quite similar to each other and in the range of the actual NPs (size around 100 nm). In particular, the dots seemed to be mainly attached to the cell monolayers or to remain in the close vicinity of the microvilli. It can be clearly noticed that more dots are present in the sample with CS-NPs, compared to the one with NPs, suggesting that the CS coating influenced the adhesiveness of the particles and the interactions with cells, thus confirming the results from confocal microscopy.

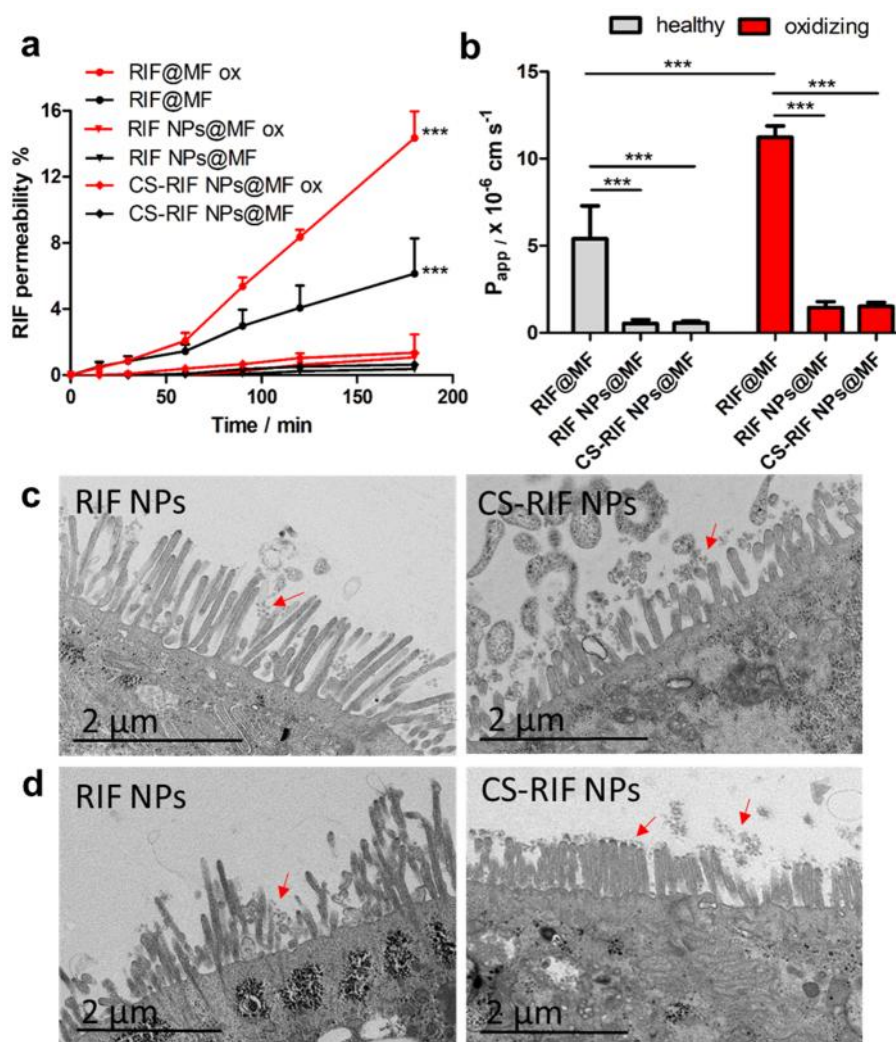


**Figure III.8.** (a) Permeation profiles of RIF across cell monolayers in normal or oxidizing (ox) conditions. The level of significance between the permeability of RIF@MF and the nano-in-micro composites (RIF NPs@MF and CS- RIF NPs@MF) in the same conditions were set at the probabilities of  $***p < 0.001$ . (b) Apparent permeability coefficient ( $P_{app}$ ) of RIF calculated from the drug permeation profiles. Data represent mean  $\pm$  S.D. ( $n = 3$ ). The level of significance was set the probability of  $***p < 0.001$ . TEM images of flat embedded sections of monolayers after permeability studies showing (c) RIF NPs and CS-RIF NPs interacting with the monolayers in healthy conditions and (d) with the monolayers simulating oxidizing conditions.

### III. Conclusion

In this study, we developed nano-in-micro composites to achieve an oxidation-responsive delivery of RIF for IBD treatment. A phenylboronic esters-modified dextran (OxiDEX) was successfully employed to prepare RIF-loaded NPs, which showed highly H<sub>2</sub>O<sub>2</sub>-responsive degradation and controlled drug release in the presence of physiologically relevant (equal to or higher than 100 μM) H<sub>2</sub>O<sub>2</sub> concentrations. The coating of NPs with CS significantly enhanced their stability in intestinal pH and their interactions with the intestinal mucosa, showing high mucoadhesive properties. Microfluidics allowed the encapsulation of NPs in HPMCAS, resulting in spherical and uniform microparticles able to protect the NPs from the harsh conditions of the stomach and to release them in the intestine. Compared to a traditional enteric formulation, the final composites showed ten times-decreased drug permeability across C2BBE1/HT29-MTX cell monolayer, indicating that OxiDEX NPs were effective to limit the drug permeation through intestinal epithelium, and therefore, representing an advantage in terms of unspecific absorption and systemic side effects. Overall, these results suggest that the prepared composite is a promising strategy for selective drug delivery in IBD treatment.

## Case study IV: An investigation into the release behavior of solid lipid microparticles in different simulated gastrointestinal fluids

### IV. Introduction

Despite the growing interest in solid lipid-based systems, particularly in solid lipid microparticles (SLMs), there is no specific compendial methods or regulations regarding the *in vitro* release studies for this drug delivery system. Dissolution testing of SLMs for oral use have been generally performed in accordance to standard methods reported both in the European Pharmacopoeia and in the United States one: paddle apparatus and pH 1.2 solution (or SGF-blank) or pH 6.8/7.2 buffer (or SIF-blank) as dissolution media <sup>135 136</sup>. The release of small molecules from liquid lipid-based formulations has been also investigated by means of lipolysis studies with pancreatin <sup>137 138</sup>. However, the digestion phase catalysed by enzymes can be reasonably considered to be crucial for the drug release only in the case of glyceride matrices, that are natural substrates of intestinal lipases. Lipid formulations of SLMs commonly include other types of excipients, which are not subjected to the action of lipases, such as fatty acids, fatty alcohols and, partially, waxes. Moreover, experimental conditions and parameters for lipolysis test vary among different groups and, despite recent efforts <sup>139</sup>, there is a lack of standardized *in vitro* methods for digestion tests <sup>140</sup>. Biorelevant media have been developed over the last decade and have demonstrated their appropriateness of predicting *in vivo* behaviour of drugs and of correlating *in vitro/in vivo/in silico* data <sup>141</sup>. In the case of lipid based-systems, suitable media which better reflect *in vivo* release characteristics of these dosage forms, especially in terms of hydrodynamics, have been developed <sup>142</sup>. Nevertheless, those media have been employed limited to liquid formulations <sup>143 144</sup>. In literature, only very few studies focused on the dissolution behaviour of oral delivered-solid lipid formulation.

Therefore, this research studied the release performance of SLMs in various updated biorelevant dissolution media simulating the conditions of the whole gastrointestinal tract (gastric tract and proximal human intestine). Three formulations of SLMs were produced using lipids belonging to different substance classes: fatty acids, triglycerides and waxes. The influence of the SLMs composition and the particle size in both biorelevant and compendial media was evaluated and compared. To assess the dissolution behavior of these delivery systems in various media, caffeine (CAF) was selected as water soluble model API in the perspective to study SLMs designed to deliver

orally water soluble active compounds, which can include for example, hydrophilic protein drugs. As the ability to differentiate among the classes of lipids in relation to their physico-chemical properties is an important prerequisite to formulating with lipids <sup>142</sup>, the present study intends to gain new insights into the release behaviour of different type of SLMs. In particular, the research aims to provide a comprehensive study, which takes into account not only the lipid class and the particle size, but also the GI tract section and the fasted/fed state.

#### IV. Experimental section

**Preparation of SLMs:** SLMs were prepared by spray congealing, using WPN as atomization device using three lipids: stearic acid (Fagron srl, Bologna), Compritol 888 ATO (Gattefossé, Milan, Italy) and carnauba wax (Fagron srl, Bologna). Briefly, the spray-congealing procedure consisted of the initial melting of the lipid carrier at the temperature 10°C above its melting point. CAF (Sigma Aldrich, Steinheim, Germany) was added to the molten carrier in order to obtain SLMs with a theoretical drug loading of 20% w/w and it was stirred up to obtain a suspension. Batch dimension was 10 g. The molten suspension was subsequently transferred into a temperature controlled feeding tank placed above the spray-congealing nozzle pre-heated to 10°C above the melting temperature of the carrier. The atomization of the molten suspension was then obtained at 4 bar air pressure and nozzle temperature ranged from 80 to 100°C, depending on the melting point of the carrier. The atomized molten droplets solidified into a cooling chamber at room temperature. Finally, SLMs were collected and stored in sealed polyethylene bottles at 4°C prior to analysis.

**SLMs characterization:** The morphological characteristics of MPs before and after dissolution testing were observed by SEM (ESEM Fei Quanta 200, Cambridge, UK) at 10 kV accelerating voltage. The size distribution of the MPs was evaluated by sieve analysis, using a vibrating shaker (Octagon Digital, Endecotts, London, UK) and four standard sieves (Scientific Instruments, Milan, Italy) of 100, 150, 250 and 500 µm. The determination of the CAF content into the SLMs was obtained using a procedure previously reported <sup>145 136 146</sup> and opportunely adapted according to the CAF properties (solubility, wavelength). Briefly, 50 mg of sample were accurately weighed and dissolved in 100 ml of phosphate buffer pH 6.8. The system was heated to melt the carrier and then shaken for 1 h. Finally, the solution was filtered, diluted with the same solvent and the drug content was assayed spectrophotometrically (UV-vis spectrophotometer mod. UV2, Unicam, Cambridge, UK) at 273 nm.

The drug loading of whole batches was assayed and the encapsulation efficiency was calculated as the ratio between the actual drug content and the theoretical amount of drug content in the MPs. Then the real drug content of the two size fractions (100-250  $\mu\text{m}$  and 250-500  $\mu\text{m}$ ) used for the dissolution tests was analysed in triplicate and the mean  $\pm$ SD was calculated.

***In vitro dissolution studies:*** *In vitro* release profiles were assessed using the Apparatus 2 (paddle apparatus) of the Eur. Ph. (Pharmatest, Steinheim, Germany) rotating at 75 rpm. Since lipid-based MPs, differently from other MPs (e.g. MPs based on hydrophilic materials), tend to float to the surface, the selected stirring rate was slightly higher than the usual speed rate (50 rpm), although still in the range recommended by the Pharmacopoeia<sup>63</sup>. A suitable amount of SLMs containing about 8 mg of CAF was added to 500 ml of dissolution media in order to have about 16  $\mu\text{g}/\text{ml}$  (the CAF solubility in water at 25°C is reported to be 1600  $\mu\text{g}/\text{ml}$ <sup>147</sup>). Six different dissolution media, maintained at 37°C, were used: pH 1.2 solution and pH 6.8 phosphate buffer, according to Eur. Pharm.; Fasted State Simulated Gastric Fluid (FaSSGF) at pH 1.6 prepared according to Vertzoni et al.<sup>148</sup>; Fed State Simulated Gastric Fluid (FeSSGF) at pH 5.0, using the composition indicated by Jantraid et al.<sup>76</sup> for the “middle” phase of gastric digestion; Fasted State Simulated Intestinal Fluid (FaSSIF-V2) at pH 6.5<sup>76</sup> and Fed State Simulated Intestinal Fluid (FeSSIF-V2) at pH 5.8 with and without the addition of pancreatin<sup>76</sup>, which combines, respectively, the pre and postprandial physiologically relevant parameters (pH, osmolarity, buffer capacity and bile components concentration) of early, medium and late phases of the digestion process. The composition of the various dissolution media and the CAF recovery (%) in every dissolution medium are summarised in **Table VI.1**. All the materials used for the preparation of the dissolution media were purchased from Sigma Aldrich (Steinheim, Germany). Long-life, UHT-treated 3.6% whole fat milk (Granarolo, Italy) was purchased commercially.



<i>Gastric media</i>	<i>Composition</i>	<i>CAF recovery (%)</i>
<b>pH 1.2 solution</b>	NaCl and HCl 0,2M	99.6 <sup>a</sup>
<b>FaSSGF, pH 1.6</b>	Sodium taurocholate (80 µM), Lecithin (20 µM), Pepsin (0.1 mg/ml), NaCl (34.2 mM), HCl qs pH 1.6, H <sub>2</sub> O qb ad 1l	98.5 <sup>a</sup>
<b>FeSSGF, pH 5</b>	NaCl (237.02 mM), Acetic acid (17.12 mM), Na acetate (29.75 mM), H <sub>2</sub> O qb ad 1l, UHT milk 3.6% fat (1:1 with buffer) and HCl qs pH 5	99.2 <sup>b</sup>
<i>Intestinal media</i>	<i>Composition</i>	
<b>pH 6.8 phosphate buffer</b>	K <sub>2</sub> HPO <sub>4</sub> , NaOH 0.2M	98.8 <sup>a</sup>
<b>FaSSIF-V<sub>2</sub>, pH 6.5*</b>	Sodium taurocholate (3 mM), Lecithin (2,2 mM), Maleic acid (19.12 mM), NaCl (68.62 mM), NaOH (34.8 mM), H <sub>2</sub> O qb ad 1l	99.7 <sup>b</sup>
<b>FeSSIF-V<sub>2</sub>, pH 5.8</b>	Sodium taurocholate (10 mM), Lecithin (2 mM), Glycerol mono-oleate (GMO) 5 mM, Sodium oleate 0.8 mM, Maleic acid (55.02 mM), NaCl (125.5 mM), NaOH (81.65 mM), H <sub>2</sub> O qb ad 1l  <i>In the case of addition of pancreatic lipase:</i>  Pancreatin (100 lipase USP unit/ml), CaCl <sub>2</sub> (5 mM)	99.0 <sup>b</sup>

<sup>a</sup> Spectrophotometrically assay

<sup>b</sup> HPLC assay

**Table IV.1:** Composition of the different dissolution media employed for the dissolution tests and CAF recovery (%) in every dissolution medium.

In the case of buffers and FaSSGF, during the dissolution test, the aqueous solution was filtered and continuously pumped (12.5 ml/min) to a flow cell in a spectrophotometer (UV2 Spectrometer, Unicam, Cambridge, UK). The amount of dissolved CAF in compendial media was analysed at 273 nm. The amount CAF dissolved in FeSSGF, FaSSIF-V2 and FeSSIF-V2 was assayed by HPLC due to the more complex composition of these media. Hence, during the dissolution tests, 2 ml of aliquots were withdrawn at predetermined time intervals (15, 30, 60, 90 and 120 min) from the dissolution medium and replaced with fresh medium. Particularly, for the dissolution test in FeSSGF, samples were pre-filtered through a 0,45 µm filter and diluted 9:1 with ice-cold trichloroacetic acid 12% v/v to precipitate milk proteins<sup>149</sup>. Sample were then vortexed and centrifugated at 10000 rpm for 12

min. The supernatant was filtered through a 0,2  $\mu\text{m}$  filter and injected in HPLC. For FaSSIF-V2 and FeSSIF-V2, the withdrawn samples were directly filtered through 0.2  $\mu\text{m}$  membrane filter and assayed by HPLC. For each formulation at least six replicates were performed and the mean  $\pm$ SD was reported. The release profiles were finally compared using the similarity factor,  $f_2$ .

**HPLC analysis:** The HPLC system consisted of two mobile phase delivery pumps (LC-10ADvp, Shimadzu, Japan), a UV-vis detector (SPD-10Avp, Shimadzu, Japan) and an autosampler (SIL-20A, Shimadzu, Japan). The method used for CAF quantification was adapted from literature<sup>149</sup> according to our instrument set-up. A reversed phase C12 column (Synergi MAX-RP, 4  $\mu\text{m}$ , 150 mm x 4.60 mm; Phenomenex, Bologna, Italy) was used as stationary phase, while the mobile phase consisted in 87.5% sodium acetate buffer (50mM, pH 4.0) and 12.5% acetonitrile. The injected volume was 20  $\mu\text{l}$  and the detection wavelength was set at 273 nm. The chromatographic run followed an isocratic method with a mobile phase flow rate of 1 ml/min. In these conditions the retention time of CAF was 5.8 minutes. The range of linear response was 0.5-30  $\mu\text{g/ml}$  and the  $R^2$  resulted  $\geq 0.999$  (Figure 1S). The limit of detection (LOD) and the limit of quantification (LOQ) resulted in 0.760  $\mu\text{g/ml}$  and 2,031  $\mu\text{g/ml}$ , respectively. In order to verify the suitability of the assay, the CAF recovery (%) into the various dissolution media was determined by dissolving pure CAF in every dissolution medium. The CAF recovery after filtration (and centrifugation in the case of FeSSGF) are shown in Table IV.1 and resulted  $\geq 99\%$  for every medium. Then, we selected the right amount of SLMs to have sink conditions and to ensure that every point of the dissolution testing was within the specified range of the analytical procedure.

#### IV. Results and discussion

**SLMs characterization.** SLMs containing a theoretical amount of CAF of 20% w/w were successfully produced by spray congealing, with yields higher than 80% for all formulations. CAF was completely encapsulated in all the formulations, with an efficiency very close to 100%. The particle size analysis (Table IV.2) shows a unimodal size distribution for all formulations with the mean particle size ranging from 100 to 250  $\mu\text{m}$  for F1 and F2. Differently, F3 presented higher dimensions, with the prevalent size fraction of 250-500  $\mu\text{m}$ . The drug content within the two more representative size fractions of microparticles, selected for the dissolution tests, resulted very close to 20% in both the size fractions of the three formulations (Table IV.2). SEM photographs (Figure IV.1) evidences that all formulations resulted in non-aggregated microparticles, perfectly round shaped with smooth surface in the case of F2 and F3, while F1 microparticles appeared a little bit more irregular. As the loaded API was dispersed and not solubilized in the lipid matrix, some CAF crystals can be noticed on the surface of SLMs, especially in F2 and F3.

Formulation	F1	F2	F3
<b>Excipient type</b>	Stearic acid	Compritol 888 ATO	Carnauba wax
<b>Yield (%)</b>	81.3	81.0	90.3
<b>Encapsulation efficiency (%) (overall batch)</b>	98.5	99.3	98.6
<b>Particle size distribution (% w/w)</b>			
< 100 $\mu\text{m}$	24.52	18.22	4.51
100-250 $\mu\text{m}$	<b>53.67</b>	<b>54.85</b>	28.17
250-500 $\mu\text{m}$	18.23	22.70	<b>51.84</b>
> 500 $\mu\text{m}$	3.58	4.23	15.48
<b>CAF content (% <math>\pm</math> SD, n=3)</b>			
100-250 $\mu\text{m}$	19.93 $\pm$ 0.63	20.64 $\pm$ 1.05	19.75 $\pm$ 0.51
250-500 $\mu\text{m}$	21.73 $\pm$ 0.46	21.34 $\pm$ 0.31	21.49 $\pm$ 0.27

**Table IV.2:** SLMs composition, process yield, encapsulation efficiency, particle size distribution and drug content of the size fractions used in the dissolution test.

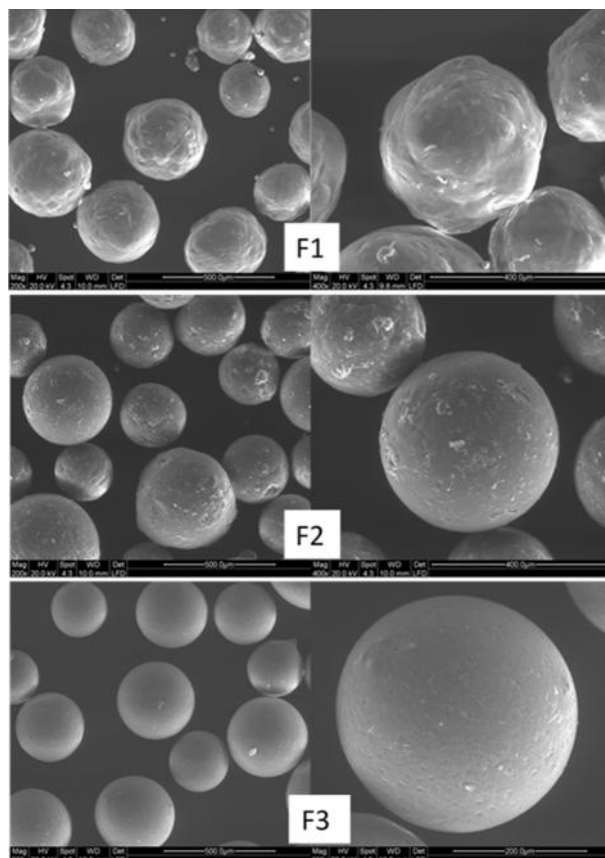


**Figure IV.1:** SEM pictures taken at different magnifications (200x and 400x) of F1, F2 and F3 SLMs with 250-500  $\mu\text{m}$  dimension.

**Dissolution behaviour of SLMs.** Dissolution of plain drug and different SLMs formulations were performed first in compendial media reflecting the gastric and the intestinal pH in order to evaluate the effect of the lipid formulation of the CAF release. Then, dissolution behaviour of each formulations was studied in biorelevant media simulating the primary gastrointestinal environments: fasted and fed gastric conditions, fasted and fed intestinal conditions. Finally, drug release profiles were compared by means of similarity factors ( $f_2$ ) and discussed. All the calculated  $f_2$  values are listed in Table IV.3.

<b>Section 1 - EFFECT OF SLMs COMPOSITION</b>						
<b>Compendial dissolution media</b>	Small size fraction			Large size fraction		
	F1 vs F2	F1 vs F3	F2 vs F3	F1 vs F2	F1 vs F3	F2 vs F3
Gastric (pH 1.2)	<b>48.2</b>	<b>32.8</b>	<b>46.2</b>	56.6	59.8	52.0
Enteric (pH 6.8)	<b>30.6</b>	<b>22.5</b>	49.5	<b>26.3</b>	<b>22.3</b>	58.6
<b>Section 2 - EFFECT OF THE DISSOLUTION MEDIUM</b>						
<b>Gastric media</b>	Small size fraction			Large size fraction		
	F1	F2	F3	F1	F2	F3
FASSGF vs pH 1.2 sol	79.1	73.2	66.9	64.8	83.6	68.5
FESSGF vs pH 1.2 sol	68.1	<b>39.8</b>	<b>50.2</b>	82.9	54.8	53.0
FASSGF vs FESSGF	66.8	<b>45.7</b>	56.3	72.2	58.9	65.5
<b>Intestinal media</b>	F1	F2	F3	F1	F2	F3
FASSIF-V <sub>2</sub> vs pH 6.8 buffer	<b>37.2</b>	<b>38.2</b>	<b>43.4</b>	<b>46.6</b>	<b>43.7</b>	54.8
FESSIF-V <sub>2</sub> vs pH 6.8 buffer	<b>42.1</b>	<b>30.6</b>	<b>24.7</b>	<b>35.4</b>	<b>38.3</b>	<b>37.8</b>
FASSIF-V <sub>2</sub> vs FESSIF-V <sub>2</sub>	59.4	54.7	<b>35.3</b>	52.5	68.1	<b>48.7</b>
<b>Section 3 - EFFECT OF THE PARTICLE SIZE</b>						
<b>Dissolution media</b>	Small size fraction vs large size fraction					
	F1	F2	F3			
Gastric (pH 1.2)	<b>26.2</b>	<b>40.0</b>	<b>41.0</b>			
FASSGF	<b>28.2</b>	<b>43.4</b>	<b>38.1</b>			
FESSGF	<b>27.8</b>	53.6	<b>42.0</b>			
Enteric (pH 6.8)	<b>31.1</b>	<b>35.9</b>	<b>39.1</b>			
FASSIF-V <sub>2</sub>	<b>28.9</b>	<b>31.6</b>	51.3			
FESSIF-V <sub>2</sub>	<b>40.4</b>	<b>27.8</b>	72.8			

**Table IV.3:** Calculated similarity factors ( $f_2$ ) (bold characters indicate significantly different profiles). **Section 1-Effect of the SLMs composition:** Pair-wise comparison of dissolution profiles in compendial media; **Section 2-Effect of the dissolution media:** Pair-wise comparison of dissolution profiles in gastric and enteric biorelevant media with respect to both compendial media for each formulation; **Section 3-Effect of the particle size:** Pair-wise comparison of dissolution profiles obtained from different size fractions for each formulation in the dissolution media.

**Effect of the SLMs composition.** CAF is a highly hydrophilic molecule with a log P equal to -0,07. Despite its character of weak basis, CAF is highly polar and thus very soluble in water even at higher pH levels. Accordingly, CAF is classified as belonging to BCS class I. In the dissolution tests, CAF completely dissolved within 5 min both at pH 1.2 (Figure IV.2a) and at pH 6.8. (Figure IV.2b), confirming a high and pH-independent water solubility. Comparing the dissolution profiles of SLMs in pH 1.2 (Figure IV.2a), all formulations considerably reduced the CAF dissolution. Overall, the best release-controlling formulation was F3. This can be easily explained considering the composition of carnauba wax, which contains highly hydrophobic substances <sup>150</sup>. Thus, this lipophilic excipient hardly allows water to penetrate into the microparticle matrix. In particular, smaller microparticles exhibited different dissolution profiles, as evidenced by the  $f_2$  values < 50 (Table 1 – Section 1); while, for bigger microparticles, the dissolution profile of all the formulations can be considered superimposable ( $f_2 > 50$ ). The results indicate that the lipid type had a significant influence on the drug release from smaller SLMs, while for bigger microparticles the effect of particle size prevailed on the lipid composition.

Dissolution profiles at pH 6.8 (Figure IV.2b) revealed an important change principally for F1 SLMs. As expected, while in the acidic harsh environment stearic acid provided F1 bigger microparticles with a good protection ability, the CAF release was no longer controlled in neutral-basic pH, where stearic acid is rather soluble: more than 80% of CAF was released after 30 min from F1 small fraction, and more than 90% was dissolved by the end of the test for both size fractions. According to Qi et al., 2008 <sup>151</sup>, an interaction between stearic acid microspheres and alkaline buffer resulted in acid soap formation. On the contrary, the CAF release profiles of both F2 and F3 SLMs was more controlled. Moreover, the difference between F2 and F3 dissolution profiles of the small size fraction resulted borderline significant (Table IV.3 Section 1).

These results indicate that, when SLMs are immerse in simple buffer solutions, the performance of the lipid matrix in controlling the CAF release profile was strongly affected by both the excipient composition and the SLMs particle size. Therefore, the performance of the two different size fractions, both suitable for oral administration, were further investigated using the biorelevant dissolution media, too.

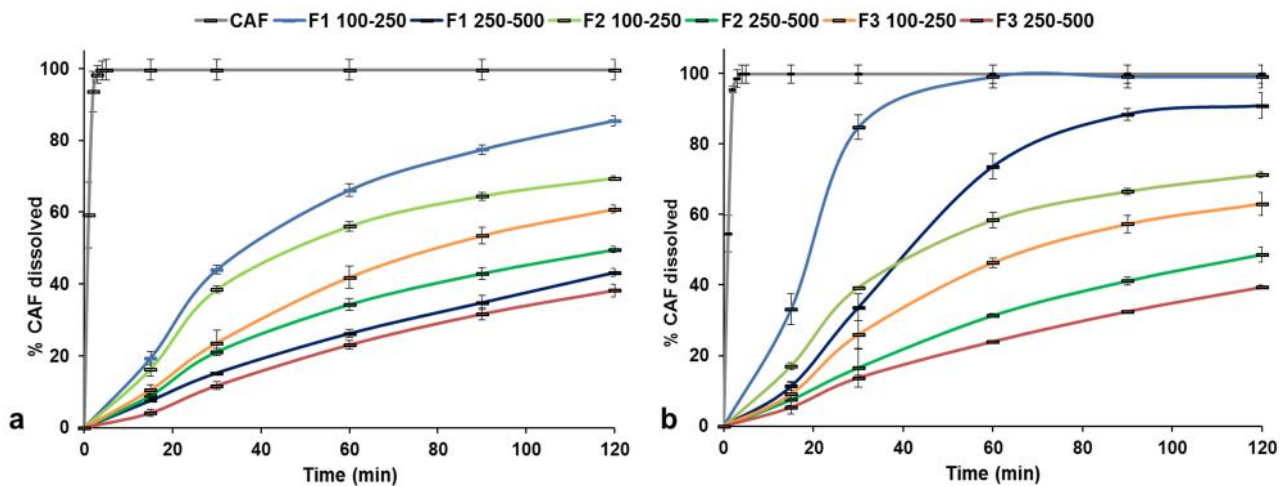


**Figure IV.2:** Dissolution profiles of pure drug and SLMs a) in buffer pH 1.2 and b) in phosphate buffer pH 6.8.

**Effect of the dissolution media: gastric conditions.** Raw CAF rapidly dissolved in both fasted and fed conditions whereby in the standard gastric solution, as indicated by the high amount of CAF recovered (Table 2S of the supplementary material) after few minutes of the dissolution test. Figure IV.3a,c,e shows the dissolution profiles of SLM formulations in different gastric conditions.

CAF release from F1 MPs (Figure IV.3a) was not influenced by the composition of the acidic medium, as both sizes exhibited the same profile using compendial buffer, FaSSGF and FeSSGF ( $f_2$  values are reported in Table 1-Section 2). Formulation F2 (Figure IV.3c) exhibited a clear influence of the fed state condition (increased viscosity) on the drug release. This phenomenon was emphasized for smaller particles (100-250  $\mu\text{m}$  size), which displayed the same dissolution profile in pH 1.2 and in FaSSGF ( $f_2 = 73.2$ ), while in the fed state the CAF release decreased: about 37% of CAF was dissolved within 30 min in buffer pH 6.8 and in FaSSGF, against only 22% dissolved in FeSSGF within the same time. Therefore, the dissolution profile resulted different ( $f_2 < 50$ ) from those displayed at pH 1.2 and in FaSSGF (Table IV.3-Section 2). Regarding the third formulation (Figure IV.3e), a slight decreased of drug release rate in the fed state conditions compared to the other media still happened. However, the CAF dissolution profiles from each particle size showed  $f_2$  values higher than 50 in all dissolution media (Table IV.3-Section 2).

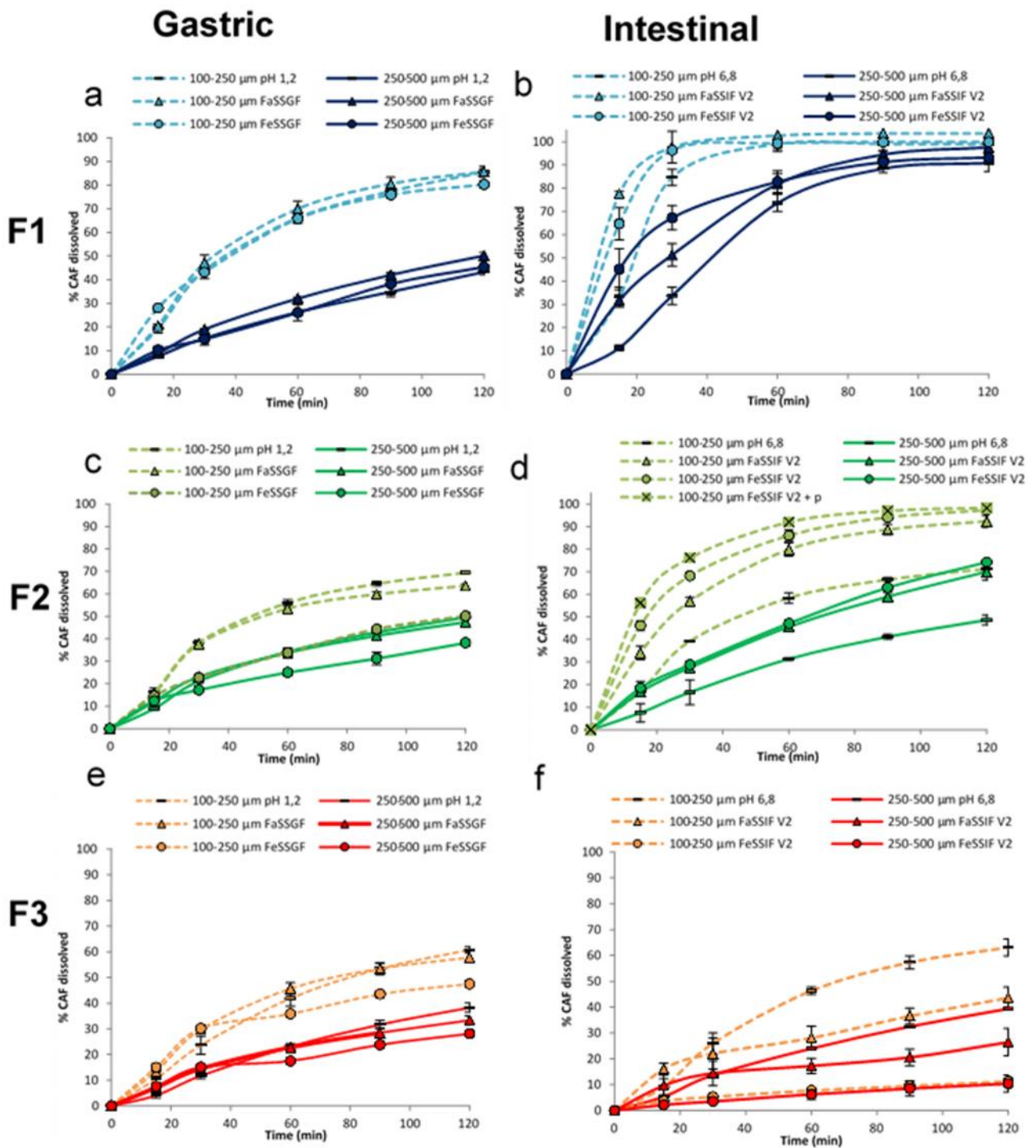


**Figure IV.3:** Release profiles of CAF in different gastric and intestinal dissolution media from SLMs F1 (a and b), F2 (c and d) and F3 (e and f).

In summary, the results evidenced that no substantial difference between the compendial and the biorelevant media simulating the fasted state occurred. Differently, the biorelevant media containing 50% of milk to simulate the fed state negatively influenced the drug dissolution, in a phenomenon known as “negative food effect” already reported. According to Andreas et al.<sup>152</sup>, the



BCS class I drug Zolpidem underwent a negative food effect when introduced into milk and FeSSGF. Explanations of this effect include (i) the formation of a hydrophobic layer of fat on the solid dosage form surface<sup>153</sup>, (ii) the higher viscosity of chyme compared to fasted state fluids<sup>154</sup> and (iii) the reduction of the diffusion coefficient of water caused by higher degree of interaction with the components of the food bolus<sup>155</sup>. In this study, the food effect in gastric environment demonstrated different influence depending on the chemical composition of the carrier, specifically in the order F2>F3>F1. The higher difference between pre and post-prandial gastric conditions for F2 compared to F3 SLMs may be explained considering the particle composition. In the case of carnauba wax-based SLMs, the major influence on the release is given by the lipophilicity of the matrix, rather than the viscosity of the fluid. On the contrary, F2 SLMs were mainly affected by fluid composition, as glyceryl behenate is a less lipophilic excipient. Moreover, the greater food effect observed on smaller particles may be attributed to the larger surface area of SLMs exposed to the fluids. The SEM pictures of CAF-loaded SLMs incubated in gastric media are reported in Table IV.4.

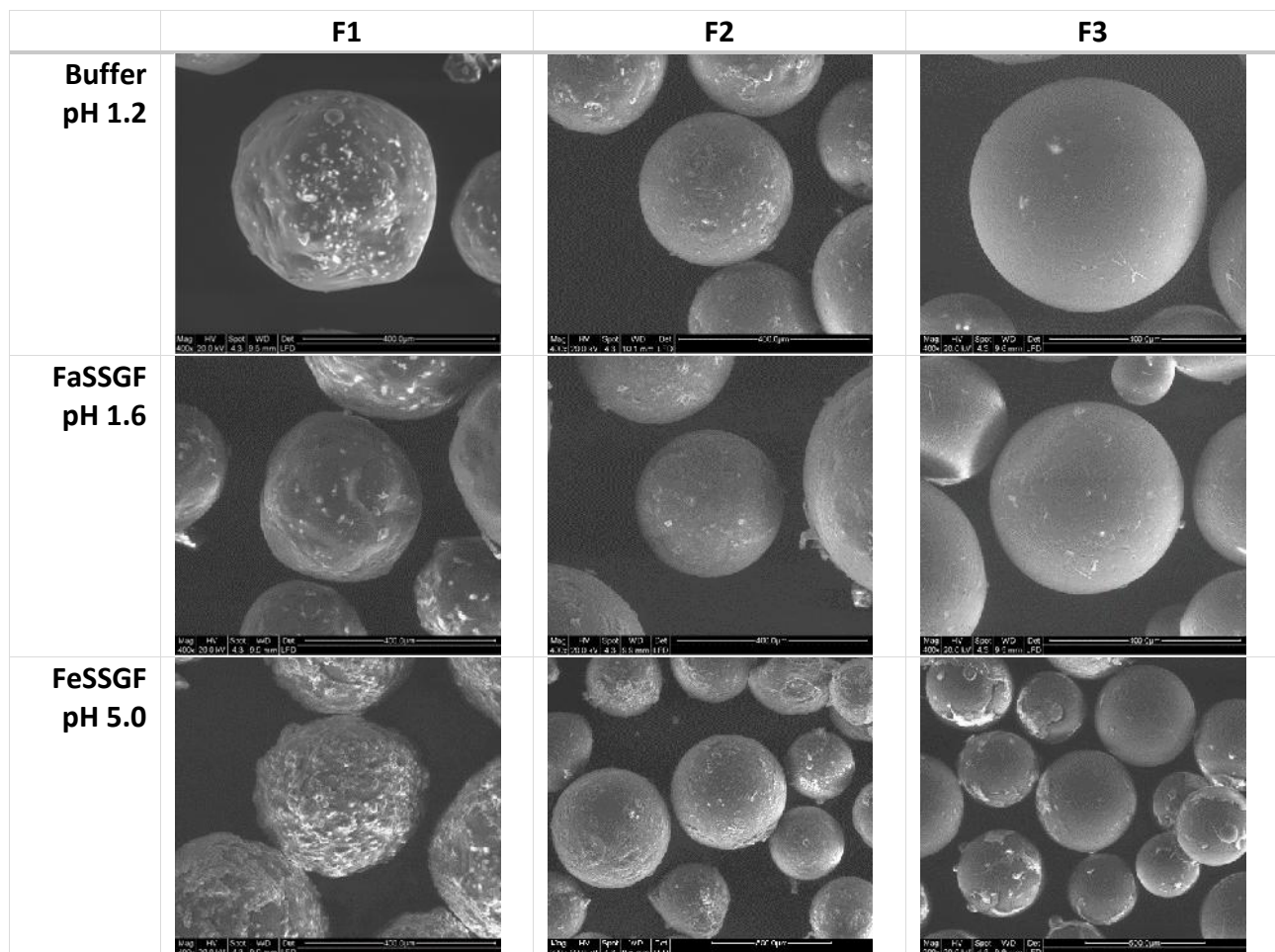


**Table IV.4:** SEM pictures of caffeine loaded SLMs (size fraction 250-500µm) incubated with different gastric media for 120 minutes taken at different magnifications (200x and 400x).

SEM pictures of F1 revealed the structure integrity of the SLMs and minor changes in the surface structure of the MPs after 120 minutes of incubation (Figure IV.4). In particular, the microspheres incubated in buffer pH 1.2 and FaSSGF resulted similar to the original ones, except for the presence of white spots on the surface. They are probably due to the presence of buffer salts remained on the particle surface after filtration, as inorganic material usually appears white under SEM analysis. Differently, the surface of F1 MPs treated with FeSSGF appeared more irregular and rough although the release profile of CAF in the three media was very similar, suggesting the deposition of the FeSSGF fluid composition onto the particle surface. MPs F2 showed no evident modification after exposure to the pH 1.2 solution and to FaSSGF. A more uneven surface and variable particle shape can be seen in the MPs incubated in FeSSGF. In all samples can be noticed the disappearance of CAF crystals, clearly visible on the particle surface before the test (Figure IV.1). Finally, the MPs surface of F3 was perfectly smooth after exposure to buffer pH 1.2 and FaSSGF and some CAF crystals can be still identified. After incubation in FeSSGF some irregular regions on particle surface appeared which might derive from an interaction between the SLMs surface and the milk components or, alternatively, they might be residuals of milk constituents.

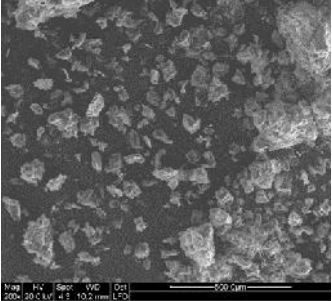
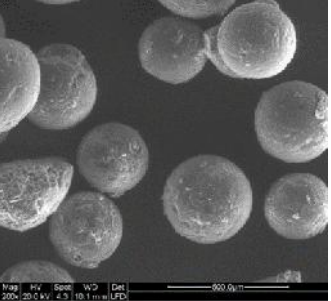
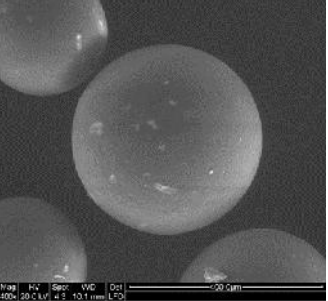
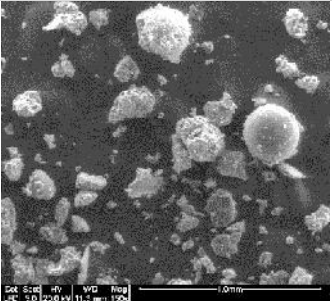
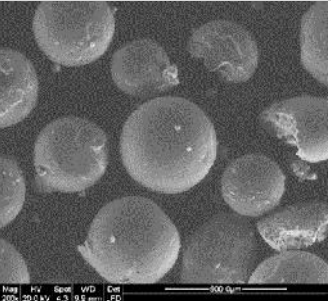
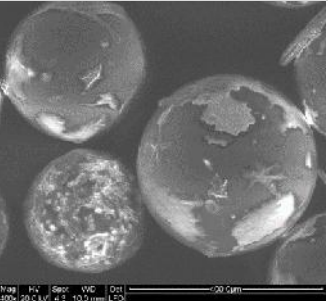
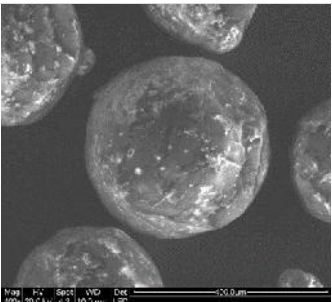
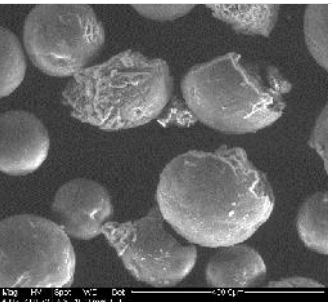
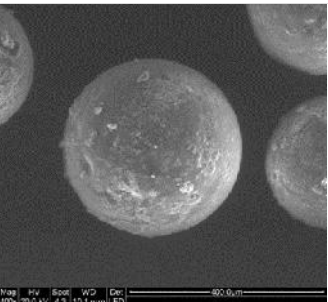
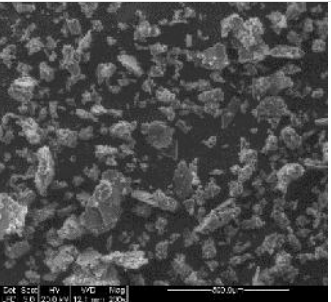
**Effect of the dissolution media: intestinal conditions.** The endogenously secreted bile mixture (bile salts, phospholipids, cholesterol) and the products of lipid hydrolysis (free fatty acids (FFAs), monoglycerides, and diglycerides) of the small bowel make the intestinal fluid a much more rich and complex media than a simple aqueous buffer <sup>156</sup>.

The dissolution of CAF was very fast in each fluid and the amount CAF recovered was  $\geq 99\%$  (Table IV.1). Our results regarding the drug release profiles from SLMs revealed remarkable differences in drug release profile replacing compendial media with biorelevant ones, as reported in Figure IV.3b,d,f. The dissolution profiles of F1 MPs (Figure IV.3b) evidenced that more than 85% of drug was released within 90 minutes in all the dissolution media, though bigger size SLMs better controlled the drug dissolution profile. Moreover, the presence of bile salts and phospholipids in the biorelevant media, acting as surfactants, further enhanced the drug dissolution with respect to the phosphate buffer. In particular, the CAF dissolution profiles of small and big size fractions in FaSSIF and FeSSIF resulted equivalent ( $f_2 > 50$ , Table 1-Section 2); whereas the dissolution profiles of small and big size fraction in buffer pH 6.8 differed significantly from both profiles obtained in FaSSIF and in FeSSIF ( $f_2 < 50$ , Table 1.-Section 2).

SEM images of SLMs after the dissolution test (Table IV.5) highlight important differences of particles morphology: in buffer pH 6.8 the F1 MPs resulted completely disintegrated by the end of the test. In the medium simulating the fasted state, the particles were only partially fragmented. Finally, in the medium simulating the fed state, SLMs were still intact showing a minor degradation process on the external surface. Those results may be explained considering the pH of the three dissolution media, with decreasing acidity from FeSSIF (5.8) to FaSSIF (6.5) to the compendial buffer (6.8). F1 MPs behaviour was likely to be strongly dependent on the pH because of the presence of free carboxylic groups. Nevertheless, the drug release is only partially associated with particles degradation at basic pH and, though the erosion mechanism prevailed, diffusion coexisted as well. Similar results have been already noticed for stearic acid MPs<sup>157</sup> and suggested that the release of cefuroxime axetil was dependent both on diffusion through the intact microspheres and changes in the physical integrity of the spheres, as a result of a reaction with the surrounding medium (pH<7). Moreover, it has been demonstrated<sup>158</sup> that in FaSSIF and FeSSIF concentrations of sodium taurocholate are above the CMC, indicating the theoretical presence of micelles. Thus, sodium taurocholate and lecithin mixed micelles could enhance drug molecules micelle interaction including solubilization capability as it occurs in vivo with bile salts in fasted and fed state. Also in this case, accelerated drug release rates in fasted and fed conditions can be related to the high bile salt and phospholipid content in the biorelevant fluids, which increased wetting and drug solubilisation.

The release of CAF from MPs F2 (Figure IV.3d) was faster in fed and fasted state simulated intestinal fluids than in the reference standard medium, especially for the smaller particle size. In particular, the dissolution profiles obtained in the biorelevant media resulted significant different from those at pH 6.8, for both particle size ( $f_2 < 50$ ). The difference between the profiles recorded in FaSSIF and FeSSIF were instead not significant for both size fractions (Table IV.3-Section 2). Therefore, dissolution from glyceryl behenate SLMs in the biorelevant media was influenced by the solubilization effect of surfactants in the medium. This effect has been already reported from Witzleb et al. for solid lipid extrudates containing the model drug praziquantel and cetyl palmitate and glyceryl monostearate as matrices<sup>159</sup>. The mixed micelles and vesicles present in the intraluminal environment of the postprandial state have solubilizing capacities also for lipophilic drugs<sup>160</sup>: e.g. the solubility of BCS class II compound carvedilol was found to increase significantly in simulated and human aspirated media of the fed state<sup>161</sup>. The small size fraction of F2 particles was then tested also in the fed medium with addition of pancreatin. As visible in Figure IV.3d, the

presence of pancreatic lipases further enhanced the drug release. This result suggested that glyceryl behenate SLMs are subjected to lipase-mediated degradation.

	F1	F2	F3
<b>Buffer pH 6.8</b>			
<b>FaSSIF pH 6.5</b>			
<b>FeSSIF pH 5.8</b>			
<b>FeSSIF pH 5.8 with pancreatin</b>			

**Table IV.5:** SEM pictures of CAF-loaded SLMs (size fraction 250-500  $\mu\text{m}$ ) taken after incubation with different intestinal media for 120 minutes.

SEM pictures of F2 MPs (Table IV.5) confirmed the dissolution results: F2 matrix was intact after 120 min incubation in buffer, whereas a massive erosion of the particles can be observed by the end of

the test in biorelevant media. The degradation of the particle became almost complete after exposure to the fed medium containing lipases, indicating that in vitro lipolysis had an effect not only on the particle surface but also on the whole particle structure.

The dissolution behaviour of formulation F3 in intestinal fluids is reported in Figure IV.3f. Carnauba wax further decrease the dissolution rate of CAF by reducing the erosion of the MPs and the water diffusion into the more hydrophobic delivery system <sup>162</sup>. Differently from the previous cases, the release of caffeine from F3 MPs was better controlled in the biorelevant media than in the compendial buffer for both particle sizes. Specifically, the release rate was decreased in the order buffer pH 6.8>FaSSIF>FeSSIF. Considering for example the small particles, their dissolution profile in compendial buffer resulted significantly different from both the one in FaSSIF and in FeSSIF ( $f_2 < 50$ , *Table 1-Section 2*). Comparing the dissolution rates in FaSSIF and FeSSIF, it can be seen that in the fed state the drug release was extremely slow, with only 11% and 10% of caffeine dissolved within 120 minutes for small and big particles, respectively. This “negative food effect” regarding intestinal conditions has been already noticed by Mason et al. <sup>163</sup>: it was found that caffeine was released more rapidly from HPMC matrices under fasted conditions compared to the fed ones. This phenomenon was explained considering the physical impedance of food on the transit of the dosage form or, alternatively, a reduced availability of water. The influence of food on drug dissolution has also been proved to depend on the physicochemical properties of the drug as well as on the drug concentration in the gut <sup>164</sup>. In our case, however, as drug and concentration were constant in all dissolution experiments, the difference in food effect observed between formulations F1/F2 and F3 can only be attributed to the formulation. In FaSSIF, F3 particles were actually easily wetted at the beginning of the dissolution test by the presence of bile salts, showing a moderate burst release in the first 15 minutes. Then, the drug release rate was decreased and only 43% of CAF was released at 120 minutes from small particles. On the contrary, buffer 6.8 enabled higher caffeine release with 63% released from the same particles in standard enteric buffer. Using FaSSIF, the dissolution behaviour of waxy matrixes was probably initially increased by a favourable wettability and then affected by the viscosity of the media. It can be hypothesized that FeSSIF medium, although its higher surfactants content, deeply penalized caffeine release from F3 MPs because of the presence of oily components, which tended to form a hydrophobic layer around F3 MPs, preventing caffeine solubilization. SEM images of F3 MPs after the test showed spherical particles with no traces of matrix degradation (*Table IV.5*).

Overall, it can be stated that in the case of fatty acid and triglyceride-based SLMs, the slowest caffeine release was obtained in the simple pH 6.8 phosphate buffer, while fed conditions significantly enhanced the drug release. Conversely, in the case of waxy-based SLMs the opposite behaviour was noticed.

**Effect of the particle size.** Generally, the bigger size fractions (250-500  $\mu\text{m}$ ) of all formulations mostly controlled the CAF dissolution than the smaller (100-250  $\mu\text{m}$ ) ones (Table IV.3-Section 3). Easily, the decreasing in CAF release with increasing particle size could be explained considering that the total effective surface area of small particles was larger than that of big ones, therefore more CAF crystals were exposed to the buffer media. At pH 1.2 the difference between SLMs dimensions was accentuate for formulation F1 rather than F2 and F3 (Table IV.3-Section 3). Independently from the composition, at enteric pH the dissolution performance of the two dimensional classes resulted significantly different, with analogous  $f_2$  values. Considering the biorelevant media that simulates the fasted gastric environment, in both fasted and fasted conditions, the profiles of larger particles were significantly different from those of smaller ones for all formulations, apart from formulation F2 in the postprandial conditions (Table IV.3-Section 3). Regarding the intestinal conditions, formulations F1 and F2 showed significant differences ( $f_2$  values always lower than 40) between the two particle size fractions, both in FaSSIF and FeSSIF. Differently, in F3 sample the dissolution profiles of small and big particles were similar (Table IV.3-Section 3).

Overall, the particle size of SLMs deeply influenced the dissolution performance: as expected, the release of caffeine was more efficiently controlled by the large MPs. In particular, the effect of particle size on dissolution depended on the formulation according to the previously stated different dissolution mechanisms: the fatty acid and the glyceride matrixes were thus overall more sensible to particle size variations, while the particle of carnauba wax showed less differences on varying particle dimensions.

#### IV. Conclusion

In summary, the results showed that the release profiles in the dissolution media simulating the gastric conditions (buffer pH 1.2, FaSSGF and FeSSGF) showed negligible differences, except for the smaller particles of tryglyceride-based SLMs which had a “negative food effect”. Therefore, the study of the dissolution behaviour of SLMs loaded with a water soluble drug, like caffeine, can be carried out indifferently both in the compendial medium and in the biorelevant gastric media. Differently, the dissolution performance and the morphological appearance of SLMs after passage in intestinal fluid (pH 6.8, FaSSIF-V2 and FeSSIF-V2) were deeply affected by the fluid composition. The presence of bile salts and lecithin as surfactants enhanced the drug release from fatty acid and triglyceride-based formulations, whereas the drug release from waxy-based SLMs was higher in the standard phosphate buffer. In addition, the triglyceride-based SLMs appeared fairly digested once the pancreatic lipase was added in FeSSIF-V<sub>2</sub> and the drug release from these SLMs was considerably enhanced. Moreover, contrary to what happened for small SLMs, the release behaviour of large SLMs was less affected by the media properties (viscosity and the presence of surfactants as bile salts and lecithin) and more dependent on the lipid excipient. Therefore, this research demonstrates that SLMs behaves differently according to their size and chemical composition in the examined intestinal dissolution media. Overall, the drug release from waxy-based SLMs is overestimated using phosphate buffer with respect to intestinal biorelevant media, while changing the matrix composition with fatty acids or triglycerides, the drug release is significant more controlled using the simple pH 6.8 buffer than FaSSIF and FeSSIF.

In conclusion, the study provides a better understanding of the release behaviour of SLMs in fluids simulating the real GI environment and proved the importance of using biorelevant media in the dissolution study for SLMs for predicting their behavior in the small intestine. Further, these results could be useful for an accurate design of a solid multiparticulated lipid-based delivery system for controlled drug release.

## Case study V: Spray congealed lipid microparticles for the local delivery of $\beta$ -galactosidase to the small intestine

### V. Introduction

In the present study  $\beta$ -Galactosidase (lactase), as an example of biomolecule that may need to be delivered orally for the treatment of lactose intolerance, was employed. Lactase is an enzyme occurring in the brush border membrane of the intestinal mucosa that hydrolyses lactose to galactose and glucose<sup>165</sup>. The development of formulations containing lactase has been driven by the fact that more than 70% of the world's population suffers from the inability to digest lactose or lactose containing products<sup>166</sup>. This condition is known as lactose intolerance, a very common disorder characterized by lactase deficiency<sup>167</sup>. In people who suffer from lactose intolerance, lactose is not digested in the small intestine and passes into the large intestine where it is fermented by microflora, causing the classic symptoms: abdominal pain and distension, bloating, flatulence, cramps, diarrhoea and nausea. The common therapeutic approach tends to exclude milk and dairy products from the diet, but the inadequate amounts of calcium, phosphate and vitamin D may lead to decreased bone mineral density and predispose to diseases such as osteoporosis<sup>168</sup>. Alternatively, the diet of lactose intolerants needs to be tied to the use of lactose-free or lactose-reduced dairy products. To overcome these limitations, several studies have been carried out to find out alternative approaches, such as the administration of exogenous  $\beta$ -galactosidase, which has proved to be effective in reducing the symptoms of lactose intolerance.<sup>169</sup> Lactase is actually marketed over-the-counter (OTC) as a chewable tablet or as food supplement. However, in a comparative assessment of the stability and activity of commercial lactase supplements<sup>170</sup>, none of the commercial preparations examined resulted an ideal supplemental lactase: incubation under simulated gastric conditions led to total inactivation of lactases in the case of products without enteric coating, whereas enteric-coated ones retained about 65% of the original activity.

Different technological strategies to achieve an effective lactase containing-formulation have been explored over the years including liposomes<sup>171</sup>, microcapsules based on enteric polymers<sup>172 173</sup>, surface-engineered nanoparticles<sup>174</sup>, electrospun polymeric fibers<sup>175</sup> and hydrogel beads<sup>176 177</sup>. Alternatively, lactase was chemically modified with PEG<sup>178</sup> and some acid-stable  $\beta$ -galactosidases were identified and purified<sup>179</sup>. In those works, the activity of the encapsulated enzyme in the



produced systems ranged from 60 to 80%, except from the electrospinning technique <sup>175</sup>, which showed the highest encapsulation efficiency (up to 97%). However, those formulations have never been studied in terms of release behaviour in simulated fluids or regarding the lactase residual activity after exposure to the gastric environment.

The present work proposes an alternative delivery system of encapsulated lactase through the production of SLMs using spray congealing. The study was designed in order to obtain a lipid-based solid oral formulation able to protect the acid labile enzyme from gastric pH and from digestive peptidases and alongside to deliver it to its physiological site of action, the small intestine. Among the lipid-based excipient listed as GRAS <sup>180</sup>, we focused on some commonly used long-chain glycerides and set up a preliminary screening based on the evaluation of their digestion in presence of physiological lipases. The rationale behind the experimental design was to find the acylglyceride which, in virtue of its lipophilic nature (low HBL), was able to protect the enzyme against gastric pH and pepsin. Meanwhile, it could be effectively emulsified by the bile salts and then digested by the intestinal physiological lipases, in order to selectively release the macromolecule directly in the site of action. Firstly, B-galactosidase from *Asp. Orizae* was characterized in terms of activity at different pH, kinetic analysis and proteolytic degradation by physiological proteases. Unloaded SLMs formulation were first prepared based on five different long-chain glycerides, then SLMs loaded with  $\beta$ -galactosidase were produced using the glyceride which showed the best response to pancreatic lipases (F1). A second formulation (F2) of lactase-loaded SLMs was obtained using as excipient the fatty acid that constitutes the chains of the glyceride used for F1. The two formulations were then compared with respect to process-related parameters (yield and encapsulation efficiency), morphological characteristics (particle size, shape and external appearance) and biopharmaceutical properties (stability under simulated gastric conditions and release studies in intestinal fluids) by means of biorelevant media to closely simulate the *in vivo* conditions.

## V. Experimental section

**Preparation of solid lipid microparticles (SLMs):** Microparticles were produced by spray congealing using WPN atomizer. For unloaded SLMs, five different long-chain glycerides with low melting point (less than 75°C) were tested: Glyceryl monostearate (Prabo srl, Cremona, Italy); Compritol 888 ATO and Precirol ATO 5 (Gattefossè, Milan, Italy); Dynasan 114 and Dynasan 118 (Sasol, Witten, Germany), whose properties are reported in Table V.1. The excipient was heated up to a temperature 5 °C above the melting point and loaded into the feeding tank of the spray congealing apparatus. The temperature of the nozzle was set 5 °C above the melting point of the carrier, whereas the inlet air pressure of the spray was set at 4.0 bar for all the formulations. The atomized molten droplets hardened during the fall into a cylindrical cooling chamber, which was held at room temperature. The glyceride resulted in the best formulation was then chosen as carrier for the encapsulation of lactase. Additionally, a second acid-based lipid formulation was produced for comparison purposes. In both cases,  $\beta$ -galactosidase from *Aspergillus Oryzae* (specific activity:  $\geq 8.0$  units/mg solid, used as received) was added as powder (5% w/w) into the melted carrier and magnetically stirred to obtain a stable suspension, which was loaded into the feeding tank. The inlet air pressure of the spray was set at 1.5 bar to obtain bigger SLMs. Finally, SLMs were collected from the bottom of the cooling chamber and stored in polyethylene closed bottles at 25°C. Enzyme-loaded SLMs were separated in two samples according to the particle size using test sieves with size of 50, 150 and 250  $\mu\text{m}$  (Scientific Instrument, Milan, Italy): the first one with dimensions in the range 50-150  $\mu\text{m}$  and the second with particle diameter from 150 to 250  $\mu\text{m}$ . The product yield (%) was also determined by dividing the quantity of SLMs recovered by the amount of enzyme and lipid loaded into the spray nozzle x 100.

**Lipase-induced degradation of SLMs:** The digestion of lipidic formulations results in the release of free fatty acids (FA) from acylglycerols, leading to a drop in the pH of the lipolysis medium.<sup>181</sup>

**Digestion buffer.** The preparation of the lipolysis buffer was based on previous reports<sup>140</sup> with a minor modification. The digestion buffer was composed by 50 mM Trizma® base, 50 mM maleic acid, 150 mM NaCl, 5 mM CaCl<sub>2</sub>, 5 mM taurocholic acid sodium salt hydrate (NaTC, Sigma Aldrich, Steinheim, Germany) 1.25 mM L- $\alpha$ -Phosphatidylcholine (L- $\alpha$ -PC, Sigma Aldrich, Steinheim, Germany) where the concentrations were chosen in order to reflect the typical concentrations in the small intestine. The pH of the lipolysis medium was adjusted at 6.8 with NaOH.

Concentrated pancreatin solution. The enzymatic suspension of lipase was prepared dissolving porcine pancreatic powder, which contained all the pancreatic lipolytic enzymes, in the digestion medium, at a concentration of 62.5 mg/ml (1000 USP units/ml). After vortexing until homogeneity, it was centrifuged at 4000 rpm for 15 min (Costar mini Centrifuge) and the supernatant was collected and freeze-dried in separated aliquots.

Lipolysis test. Unloaded lipid microparticles (100 mg) were added to a thermostated flask at 37°C containing 9 ml of lipolysis medium. After 5 min of equilibration, lipolysis was initiated by the addition of 1 ml of concentrated pancreatic solution to yield a lipase activity of 100 USP units (USPU)/mL<sup>138</sup>. The released free fatty acids (FFAs) were neutralized by manual titration with 0.1 M NaOH using phenolphthalein as indicator. During the entire experiment, pH was maintained in a range between 6 and 8 with the aid of the indicator, which is colourless in neutral conditions and turns pink in basic solutions (starting from pH 8.0). As reported by Armand et al. (1992), an optimum activity is observed in the pH range 6.5 to 8.0<sup>182</sup>. Control experiments (n = 3) were performed without any formulation, to correct for the amount of NaOH solution needed to neutralise the released acids as a result of the digestion of lecithin phospholipids or arising from the lipolysis of impurities in taurocholic acid and pancreatin.

The apparent extent of digestion was expressed as percentage of the maximum theoretical quantity of lipid susceptible to hydrolysis. This percentage was calculated from the volume of titrant consumed during the in vitro test, as expressed in Eq. 1:

$$\text{Extent of lipolysis (\%)} = \frac{V * 0.1 * MW}{n * P} * 100$$

where V is the volume (l) of titrant consumed during the digestion, 0.1 M is the concentration of the titrant, MW is the molecular weight (g/mol) of the lipid under investigation, n is the maximum quantity of FAs than can be released from one molecule of lipid and P is the weight (g) of the lipid.

Back titration. Taking into account the pKa of FAs released during the digestion, they might be only partially ionised at pH ranging from 6 to 8<sup>183</sup>. In order to calculate the total extent of lipolysis, back-titrations were performed, increasing the pH of the lipolysis buffer up to 11<sup>139</sup>. Control experiments without any triglyceride were carried out for this test as well.

**Lactase Activity Assay:** The activity of free enzyme was determined by a spectrophotometric assay based on the enzymatic cleavage of 2-Nitrophenyl  $\beta$ -D-galactopyranoside (ONPG, Sigma Aldrich, Steinheim, Germany), according to Shen et al. <sup>184</sup>, with little modification. ONPG is a colourless compound, which is hydrolyzed by  $\beta$  galactosidase to galactose (colorless) and 2-Nitrophenol (ONP, Sigma Aldrich, Steinheim, Germany), which is yellow if  $\text{pH} \geq 9$ . The amount of ONP can be evaluated spectrophotometrically at 410-420 nm. Firstly, enzyme solution (6 mg/ml in phosphate buffer pH 6.8) and substrate solution (20 mM in distilled water) were prepared and stored in the refrigerator for use. The enzyme solution (0.1 ml) was added then to 0.8 ml of buffer solution. After being incubated at 37°C for 10 min, the reaction was started by adding 0.4 ml ONPG solution. After 2 min at 37°C, the reaction was stopped by the addition of 2 ml 1M  $\text{Na}_2\text{CO}_3$  solution and the amount of ONP was measured directly at the maximum absorption wavelength (420 nm). Calibration curve of ONP was previously determined.

One unit of activity (U) is defined as the amount of enzyme that liberates 1  $\mu\text{mol}$  of product/min at 37°C. The activity was calculated following the equation (Eq. 2):

$$U = \frac{\text{Abs} * V(\text{ml}) * f}{\epsilon * l * t(\text{min})}$$

Where  $V$  (ml) is the volume of the incubation mixture after termination;  $f$  is the total dilution factor of the sample;  $\epsilon$  ( $\text{mM}^{-1} * \text{cm}^{-1}$ ) is the extinction coefficient,  $l$  (cm) is the path length and  $t$  is the incubation time. The enzyme activity was expressed as Specific activity (U/g), defined as enzyme activity per 1 g of enzyme <sup>175</sup>.

### **Lactase characterization:**

Lactase activity at different pH and kinetic analysis The effect of pH on enzyme activity was studied performing the activity assay using different buffer solutions. In particular, aliquots of enzyme solution (0.1 ml) were added to 0.8 ml of buffer at different pH values (1, 3, 5, 7 and 9). The kinetic analysis was performed on the free and encapsulated enzyme (F1 SLMs) using a direct kinetic spectrophotometric assay based on the enzymatic cleavage of ONPG, with a procedure similar to that used by Sheng et al <sup>174</sup>. Precisely, 0.25 ml of enzyme solution were added to 2.25 ml of 0.1M phosphate buffer pH 6.8 and incubated for 10 min. The reaction was started by adding 0.5 mL ONPG (1.5 mg/ml) and the concentration of ONP was monitored versus time by measuring the absorbance

at 420 nm.  $K_m$  and  $v_{max}$  parameters were determined by measuring enzyme activity at ONPG concentrations ranging from 0.5 to 8 mM. The kinetic constants were calculated from the Hanes-Woolf plot ( $[S]/v$  versus  $[S]$ ), where the intercept is  $K_m/v_{max}$  and the slope is  $1/v_{max}$ .

Lactase hydrolysis by digestive enzymes Proteolytic degradation of  $\beta$ -galactosidase was studied *in vitro* using both gastric and intestinal proteases, in order to assess the tendency of the enzyme to undergo degradation in the GI tract. In the first case lactase was incubated with pepsin (pepsin from porcine gastric mucosa, according to Ph.Eur., Sigma Aldrich, Steinheim, Germany) with a final concentration 0.1 mg/ml<sup>76</sup>, equivalent to 0.05 U/ml in 0.1 M sodium citrate buffer pH 3.0 at 37°C. For the intestinal digestive enzymes, the test was conducted in 0.1 M phosphate buffer (pH 6.8) at 37°C and pancreatin (pancreatin from porcine pancreas 8 × USP specifications, Sigma Aldrich, Steinheim, Germany), was employed to obtain a protease final concentration of 10 mg/ml<sup>185</sup>, corresponding to 2000 U/ml. The degradation over time was monitored incubating lactase for 10, 60 and 90 min in the above-mentioned conditions, followed by activity assay.

#### ***Lactase-loaded SLMs characterization:***

Morphological analysis Shape, surface morphology and dimensions of SLMs were assessed by means of Scanning Electron Microscopy (SEM). Samples were fixed on the sample holder with double-sided adhesive tape and examined by means of a scanning electron microscope ESEM Quanta 200 (Fei Company - Oxford Instruments) operating at 10,0 kV accelerating voltage.

Differential Scanning calorimetry (DSC) DSC measurements were performed using a Perkin-Elmer DSC 6 (Perkin Elmer, Beaconsfield, UK). The calibration of the instrument was performed with indium and lead for the temperature, and with indium for the measurement of the enthalpy. The samples, weighting 6-10 mg, were placed into the DSC under a nitrogen flux (20 ml/min) and heated from 25 to 150 °C at a scanning rate of 10 °C/min.

Enzyme content and encapsulation efficiency 15 mg of SLMs were soaked in 1.2 ml 0.1 M phosphate buffer at pH 6.8, heated to melt the carrier and to release all the enzyme and finally filtered through a paper filter (pore size 25-30  $\mu$ m) to obtain a solution without solid particles. An aliquot of 0.8 ml of this solution was used for the assay, which was performed using the procedure previously described. The measured activity of the encapsulated enzyme was compared to the activity of the

free enzyme in order to calculate the amount of enzyme loaded into the SLMs and the encapsulation efficiency.

*Stability of lactase-loaded SLMs under simulated gastric conditions* The effect of simulated gastric conditions on lactase activity was determined using a method similar to those of O'Connell and Walsh<sup>170</sup>. Free enzyme and SLMs (both size fractions of F1 and F2) were incubated for 30 minutes, which corresponds to the residence time in the stomach for multiparticulate solid dosage forms, as recommended by Klein et. al.<sup>186</sup>. The biorelevant media Fasted Simulated Gastric Fluid (FaSSGF) at pH 1.5 with and without pepsin<sup>76</sup> were used to test the protecting ability of the formulation to preserve the enzyme activity against the acidic pH and gastric proteases. The residual activity was measured and expressed as a percentage of the original activity (activity of a sample not exposed to any simulated digestive fluids). For the free enzyme, 0.1 ml of enzyme solution was incubated at 37°C in 0.6 ml of the gastric simulated fluids. After 30 minutes, the pH was adjusted to 6.8 using a concentrated buffer solution (Na<sub>2</sub>HPO<sub>4</sub> 0.5M), followed by activity assay. For the encapsulated enzyme, 15 mg of microparticles were incubated at 37°C in 1 ml of the gastric simulated fluids, under bland agitation. After 30 minutes, the pH was adjusted to 6.8 using the concentrated buffer solution, the sample was heated to melt the carrier and to release all the enzyme and finally filtered through a porous filter to obtain a solution without solid microparticles. An aliquot of 0.8 ml of this solution was used for the activity essay.

*In vitro release studies in simulated pre- and post-prandial intestinal fluids* About 10 mg of SLMs were immersed in 1,5 ml of the intestinal biorelevant media and incubated under bland agitation at 37°C. Fasted State Simulated Intestinal Fluid (FaSSIF V<sub>2</sub>) and Fed State Simulated Intestinal Fluid (FeSSIF V<sub>2</sub>) were prepared according to Jantrid et al.<sup>76</sup>. At determined time intervals, the sample was filtered to remove the SLMs and 0.8 ml were used for the activity assay.

**Statistical Analysis:** All results were expressed as mean ± standard deviation (S.D.). One-way analysis of variance (ANOVA) followed by the Bonferroni post-hoc test (GraphPadPrism, GraphPad software Inc., CA, USA) was used to analyze the data and the level of significance was set at the probabilities of \*p < 0.05, \*\*p < 0.01 and \*\*\*p < 0.001.

## V. Results and discussion

**Lipase-induced degradation of unloaded SLMs.** In order to select the best acylglycerol to be used in the preparation of lipase-loaded SLMs, a degradation study in presence of intestinal bile salts and intestinal lipase was set up. The test did not claim to mimic *in vivo* conditions, rather it came as a screening test able to discriminate whether a range of different lipid based systems would degrade in the presence of lipases. In particular, the aim of the screening was to investigate the influence of the chemical nature of the glyceride, both the length of the fatty acid chain and the degree of esterification (mono-, di- or tri-esters), on the emulsification and digestion. Moreover, the effect of SLMs size on the lipase-induced degradation was evaluated.

Excipient	Composition	Number of fatty acid chains	Number of C of the chain	HLB	MP (°C)
<b>Glyceryl monostearate</b>	Glyceryl monostearate	1	18	3-4	58-59
<b>Compritol 888 ATO</b>	Glyceryl dibehenate	2	22	2	71
<b>Precirol ATO 5</b>	Glyceryl distearate	2	18	2	61
<b>Dynasan 114</b>	Glyceryl trimyristate	3	14	-	55-58
<b>Dynasan 118</b>	Glyceryl tristearate	3	18	-	70-73

**Table V.1.** Characteristics of the acylglycerols used for the preparation of lipid microparticles

Effect of type of lipid. The test was performed on unloaded SLMs prepared with five different long-chain glycerides, whose properties are summarized in Table V.1. Eq. (1) was used to calculate the apparent extent of lipolysis at different time-points, which is shown in Figure V.1a, and the cumulative titrant volumes of both direct and back titrations are shown in Figure V.1b. The lipolysis of glyceryl trimyristate (Dynasan 114) SLMs resulted in the highest consumption of titrant, and thus in the highest apparent extent of lipolysis by direct titration. Differently from Dynasan 114, all other SLMs were hydrolyzed much more slowly. Moreover, the total extent of lipolysis was also lower, not exceeding the 70%. These results may be explained by considering the number of carbons in the FA chain of the lipid. Specifically, lipids with smaller chains lead to a higher pancreatic lipase activity and, thus, an increased lipolysis<sup>140,187,188</sup>. The explanation has been attributed to higher affinity of pancreatic lipase to lipids with shorter FA, because of the higher solubility and mobility of lipids with

smaller chain in comparison to longer chain-FA in the digestive interface <sup>159</sup>. Moreover, according to the specific mechanism of the hydrolysis, lipids with shorter chain length present better leaving groups (the corresponding carboxylates are more stable) compared to long-chained lipid, and thus the reaction at the active site of pancreatic lipase is faster <sup>140</sup>. Accordingly, Dynasan 114, the lipid with shorter chain (C14) among the tested ones, presented the highest degradation, followed by a slower but constant degradation of the lipids presenting chain of C18, and finally, glyceryl dibehenate (Compritrol 888ATO) SLMs, having the longest FA chain with 22 C, showed the slightest speed of hydrolysis as well as the lowest total lipolysis. Differently from the chain length, the degree of substitution of the glyceride seemed to not influence the lipolysis, since the three excipients with C18 chains (glyceryl monostearate, Precirol ATO 5 and Dynasan 118 that are mono-, di- and tri-glycerides of stearic acid, respectively) showed similar lipolysis profiles. Different reasons might contribute to this result. Firstly, lipids with C18 chains are long chain glycerides and lipases present poor catalytic activity towards them <sup>189</sup>. For this reason, the lipolysis profile is rather slow and thus it is more difficult to detect significant differences between samples. Secondly, the di- and tri-glycerides of stearic acid (Precirol ATO 5 and Dynasan 118) presents quite similar physicochemical properties and lipophilicity and thus it is reasonable to obtain similar lipolysis profiles; the corresponding monoglyceride is a little less lipophilic (it presents a higher HLB value, as shown in Table V.1) and thus more soluble in aqueous medium. Although a higher lipolysis should be expected for glyceryl monostearate due to its higher solubility, the lipolysis profile did not show a considerable increase. Nevertheless, it should be considered that the lower affinity of lipase towards monoglycerides compared to di- and tri-glycerides <sup>190</sup> might also have an important influence in the present study.

Overall, Dynasan 114 SLMs resulted the formulation with the highest response to pancreatic lipases and was therefore, selected as excipient to prepare loaded particles.



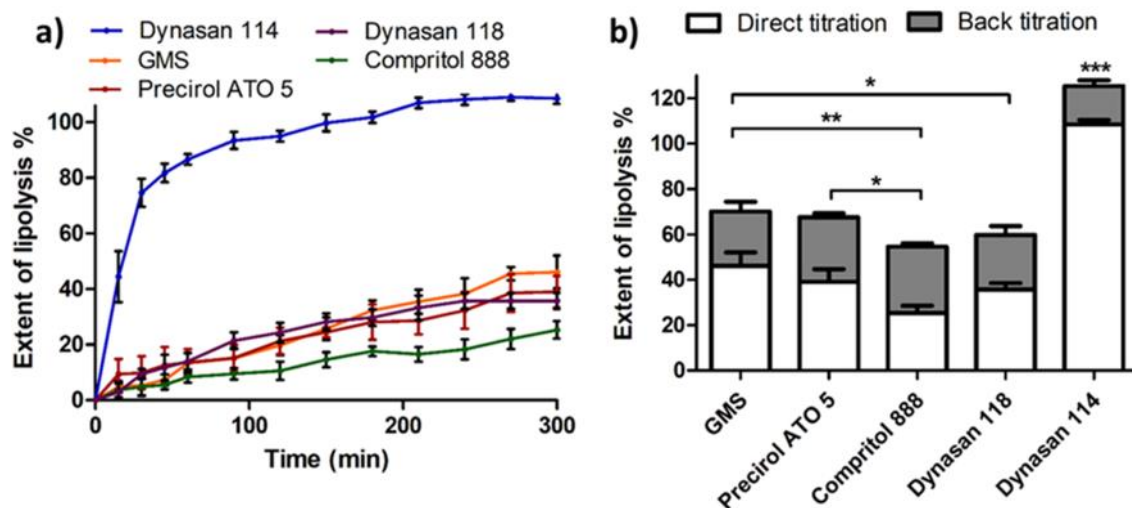


**Figure V.1.** Effect of the SLMs composition on lipolysis. (a) Apparent extent of lipolysis during the direct *in vitro* lipolysis of SLMs (size fraction 75-100  $\mu\text{m}$ ) prepared with different lipids. Values are expressed as means ( $n = 6$ )  $\pm$  SD. (b) Comparison of the total extent of lipolysis for the *in vitro* lipolysis of the SLMs (size fraction 75-100  $\mu\text{m}$ ) prepared with different lipids. White colours represent the apparent extent of lipolysis from the direct titration, while grey-shade areas represent the underestimated extent of lipolysis calculated after back-titration experiments. Values are expressed as means ( $n = 6$ )  $\pm$  SD, and the level of significance was set at the probabilities of \* $p < 0.05$ , \*\* $p < 0.01$ , and \*\*\* $p < 0.001$ .

Effect of SLMs size. The influence of the particle size on the lipase-induced degradation of SLMs was evaluated by testing Dynasan 114 SLMs with different particle size (Figure V.2). As clearly seen from Figure 2a, both SLMs showed a similar lipolysis profile, but with a different rate. Specifically, the lipolysis-time profiles were characterised by two distinct slopes, which indicates two different lipolysis rates. Pancreatic lipase initially hydrolyses triacylglycerides by attaching the first carbon (sn-1 position) and the third carbon (sn-3 position) forming two FAs and one 2-monoglyceride per triacylglyceride molecule. 2-Monoglyceride can spontaneously convert to 1- or 3-monoglyceride (isomerisation), which are subsequently lipolysed releasing the third FA and glycerol<sup>189</sup>. The point where the lipolysis curve changes slope corresponds approximately to the 66% value of the total lipolysis extent. It has been hypothesized that the first part of the curve represents the lipolysis of tri- and di- glycerides, while in the second part the isomerisation of 2-monoglycerid and subsequent lipolysis to glycerol and FA. Accordingly, the second part of the profile is the slowest because it involves two steps (isomerisation and hydrolysis) and lipases present lower affinity towards monoglycerides<sup>140</sup>. As expected, SLMs with diameter between 200 and 250  $\mu\text{m}$  showed slower lipolysis rate, particularly in the first part of the profile. The tendency to decrease lipolysis speed

with the increasing of particle size can be explained by considering that insoluble substrates (either solid or liquid) of lipases have to be emulsified in order to be hydrolyzed by the enzyme, which activity occurs at the oil–water interface<sup>191</sup>. Smaller SLMs were emulsified faster compared to bigger particles, thus increasing the specific surface area of emulsified triglycerides at the oil–water interface available for the enzymatic reaction.

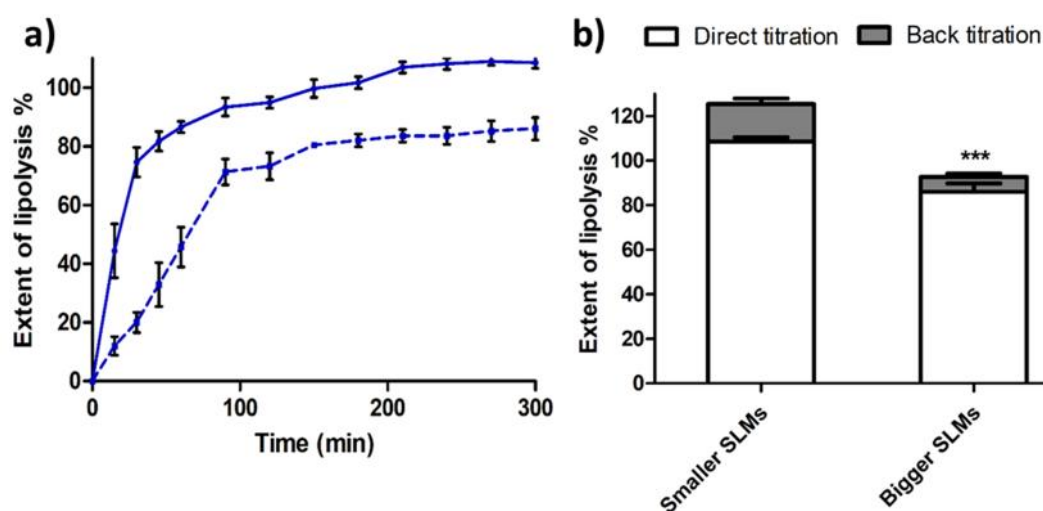


**Figure V.2** Effect of the SLMs size on lipolysis. Dynasan 114 SLMs with smaller size (diameters between 75 and 100  $\mu\text{m}$ ) were compared with SLMs with bigger size (diameters between 200 and 250  $\mu\text{m}$ ) a) Apparent extent of lipolysis of smaller SLMs (solid line) and bigger SLMs (dotted line). b) Total extent of lipolysis of smaller and bigger SLMs. White colours represent the apparent extent of lipolysis from the direct titration, while grey-shade areas represent the underestimated extent of lipolysis calculated after back-titration experiments. Values are expressed as means ( $n = 6$ )  $\pm$  SD, and the level of significance was set at the probabilities of \*\*\* $p < 0.001$ .

**Lactase characterization.** The enzyme's kinetic constants were determined by measuring the reaction speed at different ONPG concentrations. Figure V.3a showed that, as assumed,  $\beta$ -galactosidase followed Michaelis-Menten kinetic, which describes a hyperbolic relationship between reaction rate and concentration of substrate. As shown in Figure V.3b, the data of the free enzyme fitted in Hanes-Woolf plot ( $r^2 = 0.99335$ ), and the estimated kinetic parameters  $K_m$  and  $V_{max}$  were 1.80 mM and 0.039 units, respectively. Basing on those results, the  $\beta$ -galactosidase assay used in the following experiments was conducted using an excess of ONPG, in order to achieve the  $V_{max}$  of the enzyme. Beside the unprocessed lactase, also encapsulated lactase was analyzed using different ONPG concentrations to determine the effect of spray congealing on the kinetic behaviour of  $\beta$ -galactosidase. Results confirmed that the enzyme followed Michaelis-Menten kinetic even after

encapsulation, although a reduction of linearity ( $r^2$  value passed from 0.99335 to 0.93649) was observed. Nevertheless, the activity and overall kinetic characteristics of the enzyme were not affected by encapsulation in SLMs.

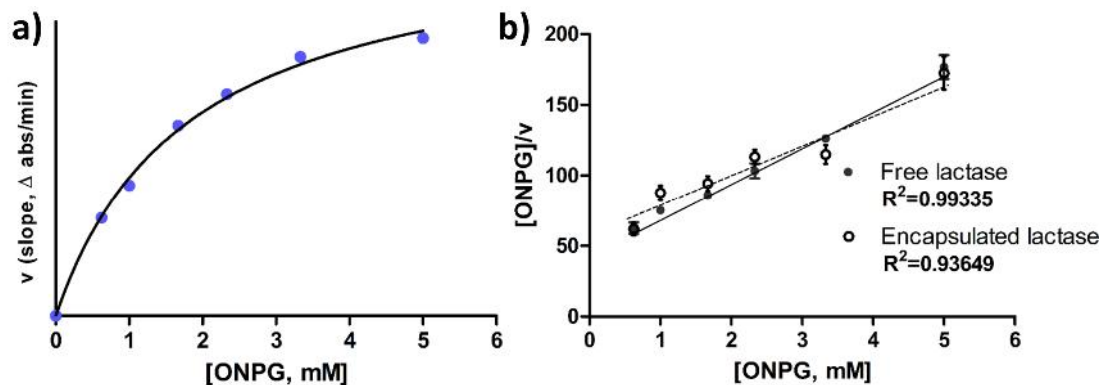


**Figure V.3.** (a) Effect of substrate concentration on lactase velocity (Michaelis-Menten plot). (b) Hanes-Woolf plot of  $\beta$ -galactosidase encapsulated in F1 SLMs compared with the unprocessed enzyme. Values are expressed as means ( $n = 3$ )  $\pm$  SD, and  $R^2$  values were calculated by linear regression analysis.

Measuring the activity of lactase at different pH, the results (Figure V.4a) showed that the optimum pH is in the range 3.0 – 5.0, with moderate activity up to pH 7.0 and a linear decrease in activity value moving toward more alkaline regions. Regarding acid conditions, the enzyme was almost completely inactivated at pH 1.0 and 2.0. The pH dependence data obtained were in accordance to those of Tanaka et al.<sup>192</sup>, who found a good activity in the pH range 4.0 - 9.0 and a pH optima of 4.5. Acid proteases secreted into the stomach (such as pepsin) and serine proteases present in duodenum (trypsin and chymotrypsin contained in pancreatic secretions) enable the digestion of proteins in food. These enzymes act by hydrolyzing the bonds between different aminoacid residues and, as a consequence, their effect on the protein structure can be complete or only partial<sup>193</sup>. It is therefore important to assess the degree of hydrolysis on our enzyme, in order to understand if its activity is affected by digestive enzymes. Figure V.4b showed the activity of  $\beta$ -galactosidase after exposure to pepsin and pancreatin. Incubation with pepsin caused no change in activity after 10 minutes, however a significant degradation of lactase occurred with longer exposure time. Specifically, after 60 and 90 minutes the residual activity was 9.1% and 8.4%, respectively. On the contrary, pancreatin induced a decrease in lactase activity already after 10 minutes, but prolonging the incubation, only a low further decrease in activity can be detected, passing from 85.7% to a constant residual activity value correspondent to 75%.

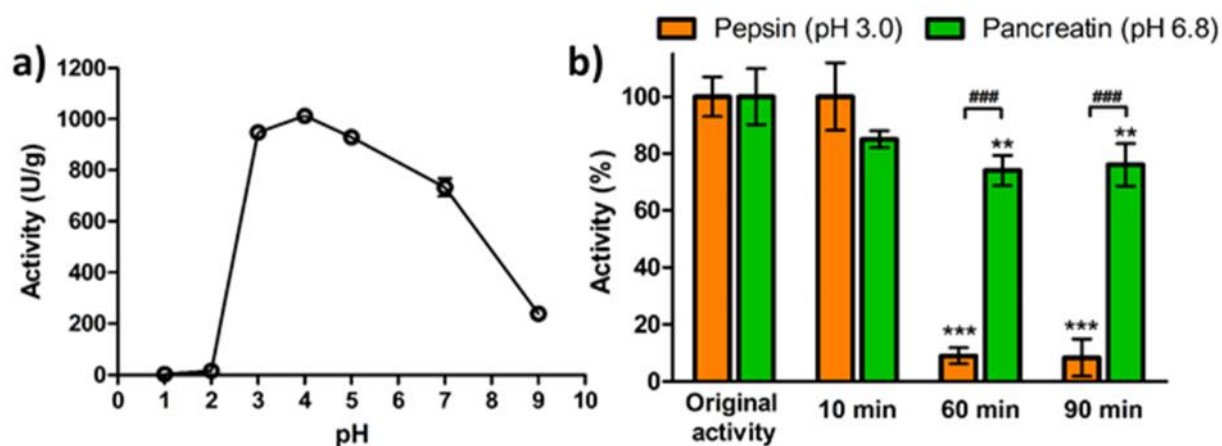


**Figure V.4.** (a) Effect of pH on lactase activity. Values are expressed as means ( $n = 3$ )  $\pm$  SD. (b) lactase residual activity after being hydrolysed for 10, 60 and 90 minutes by pepsin and pancreatic proteases. Data represent mean  $\pm$  S.D. ( $n = 3$ ), and the level of significance was set at the probabilities of  $**p < 0.01$ ,  $***p < 0.001$  compared to the lactase original activity and  $###p < 0.001$  comparing lactase activity after treatment with pepsin and pancreatin for the same incubation time.

**Lactase-loaded SLMs characterization.** SLMs loaded with  $\beta$ -galactosidase were produced using glyceryl trimyristate, which resulted in the best formulation (F1). For comparison, a second formulation of SLMs (F2) was then obtained using as excipient the fatty acid that constitutes the chains of the glyceride used in F1. Thus, the objective was to evaluate whether trimyristin was capable of a better gastric protection and enteric delivery than the correspondent free fatty acid.

The solid state of the excipient is a very important aspect to be considered as it can influence the release and protection ability of SLMs. SDC studies of raw materials and SLMs are shown in Figure V.5. The thermogram of myristic acid presented an endothermic peak at  $61^{\circ}\text{C}$ , corresponding to its melting point; very similar DSC curve was obtained for F2 SLMs, indicating the absence of polymorphic changes for this excipient. The thermogram of Dynasan 114 showed the melting peak of the lipid at  $59^{\circ}\text{C}$ , corresponding to its stable form. It is well-known that long-chains triglycerides exist at least in three key polymorphic forms identified by the lateral packing of their alkyl chains, the stable  $\beta$  form, and the metastable  $\alpha$  form and  $\beta'$ form<sup>194</sup> and melting-based processes can promote the conversion into the metastable forms. However, the DSC analysis of F1 SLMs performed immediately after preparation showed only a very small endothermic peak around  $33\text{--}35^{\circ}\text{C}$ , corresponding to the  $\alpha$  form of this excipient<sup>195</sup>, while the endothermic peak at  $60^{\circ}\text{C}$  indicated that the majority of the lipid recrystallized in its stable  $\beta$  form. The DSC of F1 SLMs was repeated after 7 days of storage, showing the disappearance of the peak of the  $\alpha$  form due to the complete

conversion of the excipient into the stable form. Thus, the solid state of both formulations F1 and F2 was characterised by the same stable polymorphic form and no significant changes in the lipid solid state occurred after spray congealing process.

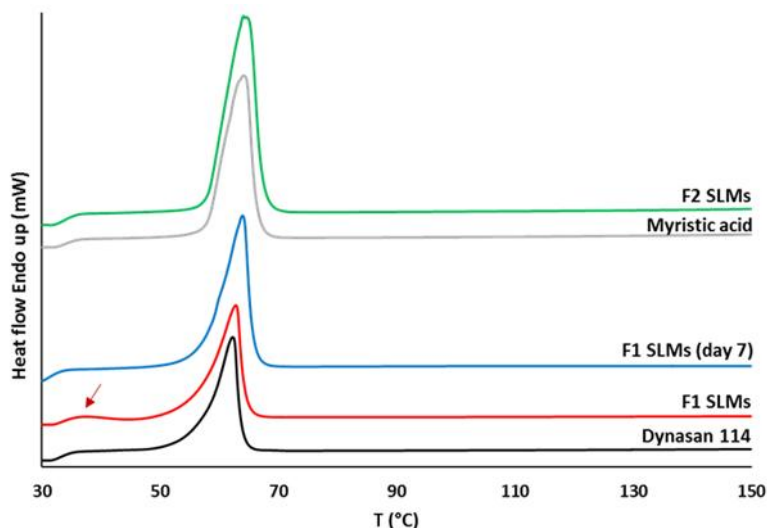


**Figure V.5.** DSC profiles of Dynasan 114, F1 SLMs (immediately after preparation and after 7 days of storage), myristic acid and F2 SLMs.

The SEM pictures of SLMs are shown in Figure V.6. F1 SLMs were spherical with quite smooth surface. Differently, the surface of F2 SLMs appeared rougher with some irregularities. No morphological differences were detected between unloaded and loaded particles.

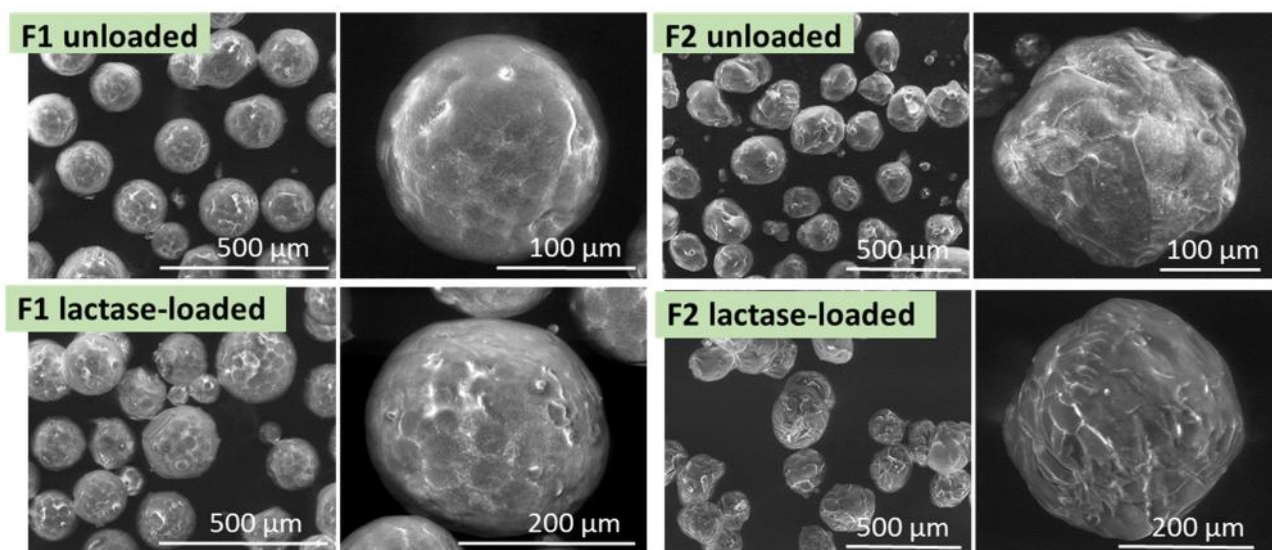


**Figure V.6.** SEM images of (a) unloaded F1 (b) lactase-loaded F1 (c) unloaded F2 and (d) lactase-loaded F2 SLMs at two different magnifications.

The encapsulation efficiencies of enzyme-loaded SLMs ranged from 95.6% to 108.1% (Table 2). As already noticed in previous studies involving spray congealing process<sup>40 196</sup>, a tendency of an increased encapsulation efficiency was observed with increasing particle size. One hypothesis could be that the drug loading increases with the particle size because drug powder is more easily encapsulated in big particles, while small particles result partially empty.

Formulation	Sample		Real enzyme content (% ± SD)	Encapsulation efficiency (% ± SD)
	Excipient	Particle size		
F1	Dynasan 114	50-150 µm	4.98 ± 0.22	99.63 ± 4.39
		150-250 µm	5.40 ± 0.33	108.06 ± 6.55
F2	Myristic acid	50-150 µm	4.78 ± 0.28	95.60 ± 5.52
		150-250 µm	5.20 ± 0.08	104.00 ± 1.52

**Table V.2.** Enzyme content and encapsulation efficiency of F1 and F2 SLMs.

### Biopharmaceutical properties of lactase-loaded SLMs.

Gastric environment. The effectiveness of SLMs as drug delivery system for the oral administration of β-galactosidase was examined simulating the pathway of the particles through the GI tract, by means of biorelevant media. Lactase supplements are usually administered 10-30 minutes before consuming the lactose-containing meal. For that reason, we decided to conduct the test in simulated pre-prandial gastric fluid (Fasted State Simulated Gastric Fluid, FaSSGF). Moreover, presenting a lower pH (1.6 instead of 5.0<sup>76</sup>), FaSSGF represent a more hostile environment with respect to Fed State Simulated Gastric Fluid (FeSSGF), therefore the study was carried out considered the worst possible scenario.

Exposure of free lactase to FaSSGF (Figure V.7) led to an almost complete inactivation of the enzyme, with only 3.8% residual activity in the fluid without gastric proteases, and 0.8% activity in the fluid containing pepsin. This result confirmed that lactase is subjected to inactivation caused by both low pH (as seen in the study of the lactase activity at different pH) and pepsin (as demonstrated in the hydrolysis test). Incubation of F1 SLMs in the same fluids resulted in 36.2% and 39.3% residual activity in the case of small particles, while the big size fraction showed 62.8% and 68.7% of activity after treatment in FaSSGF with and without pepsin, respectively. These results proved that glyceryl trimyristate-based SLMs were able to protect the hydrophilic macromolecules from gastric degradation. The significant difference ( $p < 0.001$ ) in the residual activity between the two particle

size fractions suggested that only the enzyme on the particle upon or close to the surface was inactivated by direct contact to the gastric fluid, while the enzyme loaded inside the particles was successfully preserved. Therefore, the protection ability of glyceryl trimyristate SLMs could be enhanced simply employing particles with bigger diameter in order to reduce the specific surface area. Differently, F2 microparticles displayed a poor protection ability against gastric conditions: only 17% and 14% of activity was retained in the small particles after exposure to FaSSGF with and without pepsin, respectively. These values were very similar to those recorded for the fraction 150-250  $\mu\text{m}$ , which corresponded to 16.4% of activity after incubation in FaSSGF with pepsin and 18.3% in the medium proteases-free. Since the residual activity values of lactase-loaded F2 SLMs did not differ significantly between the two size fractions, we can deduce that not only the surface enzyme was degraded, but also the enzyme contained in the inner part of the particles. Hence, it can be hypothesize that F2 microparticles were subjected to erosion and/or enzyme diffusion throughout the matrix.

In the light of these results, we can conclude that: I. SLMs with glyceryl trimyristate were able to protect the enzyme from gastric inactivation. As the enzyme present on particle surface was nonetheless inactivated by direct contact with the gastric fluid, the protection ability of SLMs resulted to be directly proportional to the microparticle size. SLMs with myristic acid were not able to protect lactase from gastric inactivation, regardless the particle size.

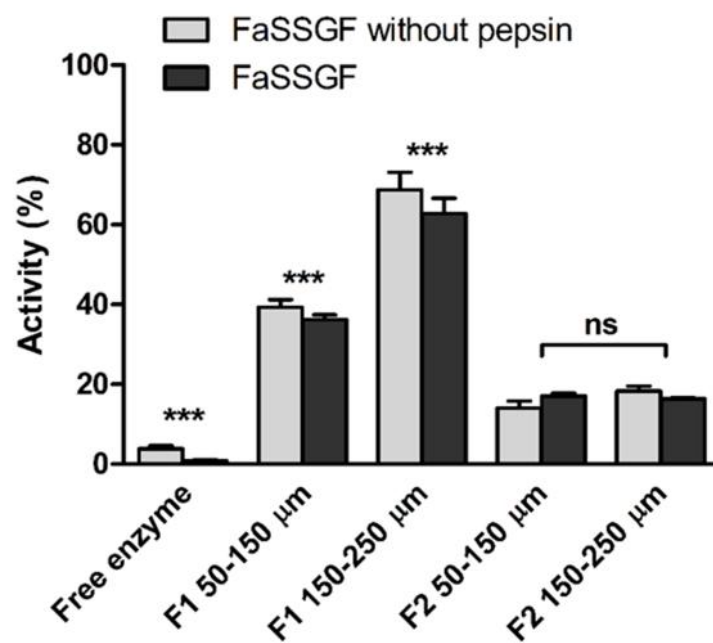


**Figure V.7.** Residual activity of lactase-loaded F1 and F2 SLMs after 30 minutes incubation in FaSSGF with and without pepsin. Data represent mean  $\pm$  S.D. ( $n = 3$ ), and the level of significance was set at the probabilities of  $***p < 0.001$  compared to all other samples and to the original activity (activity of a sample not exposed to any simulated digestive fluids, considered as 100%).

Intestinal environment. The ideal formulation has not only to protect the lactase in the gastric environment, but should also enable a prompt and consisted release of the enzyme directly in the site of action, such as the small intestine. Therefore, the release of lactase from SLMs was studied in both Fasted State Simulated Intestinal Fluid (FaSSIF) and Fed State Simulated Intestinal Fluid (FeSSIF), in order to consider both conditions and to evaluate the influence of bile salts, more concentrated in the fed conditions. Additionally, the post-prandial intestinal fluid contains partially digested fats forming a variety of different colloidal structures with the bile salt and lecithin including mixed micelles and oil droplets, present during digestion of fatty food, which can significantly influence the lactase release. In this study, only the big size fraction (150-250  $\mu\text{m}$ ) of F1 microparticles were tested, as this was the sample resulted in the best performance in the stability test under simulated gastric conditions, and it was compared with the same size fraction of F2 SLMs.

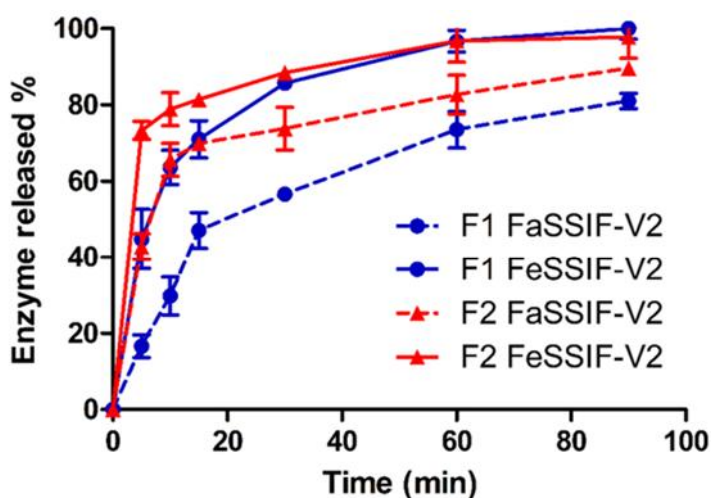


**Figure V.8.** Released profiles of lactase from F1 and F2 SLMs (size fractions 150-250  $\mu\text{m}$ ) in FaSSIF and FeSSIF. Values are expressed as means ( $n = 3$ )  $\pm$  SD.

Figure V.8 shows the release profiles of F1 and F2 SLMs in FaSSIF and FeSSIF. The release of lactase from F1 SLMs was consistent in the first 15 minutes of the test, with 47% and 71% of enzyme released in FaSSIF and FeSSIF, respectively. Although after 15 minutes the drug release rate was slightly reduced, after 90 minutes the enzyme released reached 81% in the medium simulating the



fasted state. Moreover, the totality of lactase contained in the SLMs was released in FeSSIF by the end of the test. The release profiles of F2 SLMs was even faster: in FaSSIF medium, 66% of enzyme was released after 10 minutes, followed by a constant increasing in the activity value detected, up to 90% of enzyme released after 90 minutes. As expected, when the release of lactase from F2 in FeSSIF was evaluated, we found the fastest release rate. At 10 minutes, 79% of enzyme was dissolved and a plateau was reached in the last 30 minutes, indicating the complete dissolution.

The higher release from F2 microparticles comparing to F1 can be explained considering the lipophilicity and therefore the wettability of the matrix. According to Koennings et al.<sup>197</sup>, wettability plays a decisive role in release of high molecular weight model compounds from triglyceride matrices. The presence of free carboxyl groups in the structure of the fatty acid makes this excipient a less lipophilic matrix and allows a better wettability and a consequent emulsification of the SLMs within the medium.

In the fed media, the release of the enzyme from both formulations was enhanced. The SLMs were finely dispersed in FeSSIF, suggesting increased wetting of the SLMs by the high content of lecithin, monoglycerides and bile salts in this medium, that can be considered as a “positive food effect”. Food effect can be described as an increase (positive food effect) or decrease (negative food effect) in the rate and extent of drug release and absorption in presence of food<sup>198</sup>. Christophersen et al.<sup>188</sup> studied the influence of fed state conditions on solid lipid particle systems for oral delivery of the peptide drug desmopressin and demonstrated that the drug release was accelerated in the medium containing oleic acid glycerides simulating fed state conditions. In particular, formulations made of different chain length-triglycerides showed a positive food effect. This suggested that lipid-based particulate systems are sensible to the presence of food in the GI tract, and specifically the composition of the fed state fluid can act enhancing the dispersion, solubilisation and/or erosion of a tryglyceride system. Lastly, the results confirmed that the administration of lactase-loaded SLMs after ingestion of food might significantly increase the release of drug.

## V. Conclusion

In this work, SLMs produced by spray congealing were evaluated as an innovative system for the encapsulation and oral delivery of  $\beta$ -galactosidase (lactase) in the small intestine. Spray congealing enabled the preparation of a feasible, non-toxic and inexpensive lipid formulation characterized by spherical, free-flowing microparticles with extremely good encapsulation efficiency values, always higher than 95%. Interestingly, the activity and the kinetic parameters of the enzyme were not affected by encapsulation in SLMs, demonstrating that the proposed technology caused no loss or degradation of lactase during the preparation process, due to the absence of solvent. In addition, incubation of SLMs in simulated gastric fluid with and without pepsin revealed a good protection ability for glyceryl trimyristate-based SLMs, property that resulted directly proportional to the particle size, whereas most enzyme was inactivated in the case of myristic acid-based SLMs. Lactase was promptly released in simulated intestinal environment, and an *in vitro* positive food effect was observed. In light of these results, we can conclude that spray congealed SLMs is an interesting alternative as vehicles for deliver an active enzyme to the small intestine and the advantages are mainly in the simplicity, feasibility and easy scalability of the preparation method as well as in the properties of the system obtained. In particular, SLMs are biocompatible, suitable for capsule filling and able to achieve a specific targeting of the active molecule in the small intestine, by exploiting the action of the physiological lipases in degrading the particle matrix and consequently the drug release.

In conclusion, the present study illustrated the potential of spray congealed lipid-based formulations to obtain a local delivery a biologic drug using tailor-made SLMs, by selecting appropriate lipid excipients and particle size.

## Case study VI: Glutathione-loaded solid lipid microparticles as innovative delivery system for oral antioxidant therapy

### VI. Introduction

Oxidative stress is defined as an imbalance between oxidant and antioxidant species, with overproduction of ROS and other free radicals, a disruption of redox signaling and/or molecular damage <sup>199</sup>. The GIT is a key source of ROS production. Despite the protective barrier provided by the epithelial layer, ingested materials and pathogens can cause inflammation by activating the intestinal epithelium, neutrophils and macrophages to produce inflammatory cytokines and other mediators that lead to inflammation and increasing oxidative stress <sup>200</sup>. ROS overproduction has been implicated in the pathogenesis of diverse gastrointestinal diseases including IBD, as seen in case study III, gastroesophageal reflux disease, gastritis, enteritis, colitis and associated cancers as well as pancreatitis and liver cirrhosis <sup>201</sup>. When the antioxidant capacity of the intestinal mucosa is compromised, the use of active substances able to eliminate ROS can be beneficial, either associated or not with anti-inflammatory medicines <sup>202</sup>.

Glutathione (GSH) is a water-soluble tripeptide composed of the amino acids glutamine, cysteine, and glycine. The thiol group is a potent reducing agent, rendering GSH one of the strongest physiological antioxidants <sup>203</sup>. Considering its high reactivity, the thiol group of GSH can be oxidized both enzymatically and non-enzymatically, especially when the pH is greater than 7 <sup>204</sup>, forming the corresponding glutathione disulfide (GSSG), which is devoid of radical scavenging activity. Moreover, as other peptides, GSH is likely to suffer both chemical and enzymatic hydrolysis by digestive enzymes during gastrointestinal transit following oral administration, with releasing of the free amino acids. Microencapsulation of GSH in a multiparticulate drug delivery system able to protect it against chemical and/or enzymatic degradation may enable the retention of its therapeutic properties following oral administration <sup>205</sup>.

In the case study V, it has been demonstrated that Dynasan 114-based SLMs produced by spray congealing are a promising strategy for the incorporation of a biologic drug into an orally delivered-systems with high encapsulation efficiency and gastric protection ability. Therefore, this study aims to encapsulate GSH in spray congealed triglycerides-based SLMs and to evaluate the potential of these delivery systems for the oral administration of GSH. Specifically, a triglyceride with longer

hydrophobic chains (Dynasan 118) and less subject to lipolysis (as shown in case study V) than Dynasan 114 was added into the SLMs composition in order to achieve a prolonged GSH release in the intestinal tract, which is desired in case of inflammation. The physicochemical characteristics (particle size and morphology, drug loading, solid state properties) and the release profiles of the SLMs were evaluated. Furthermore, the best formulation was used to perform *in vitro* cytotoxicity studies on HT29 cell line, in order to assess the cytocompatibility of SLMs with the intestinal membrane.

## VI. Experimental section

**Preparation of solid lipid microparticles (SLMs):** Two different MPs formulations were produced by spray congealing using WPN atomizer. In the first one (F1), Dynasan 114 (Sasol, Witten, Germany), was heated up to about 70°C, while in the second formulation (F2) Dynasan 114 and Dynasan 118 at a 1:1 weight ratio, were heated at about 75°C. SLMs were prepared either without drug (*unloaded-F1* and *unloaded-F2*, respectively), and with GSH (F1 and F2, respectively). In this case, GSH (Sigma Aldrich, Steinheim, Germany) was added as powder at a percentage of 5% w/w into the both melted carriers and magnetically stirred to obtain a stable suspension, which was loaded into the feeding tank. The temperature of the nozzle was set 5 °C above the melting point of the carrier, whereas the inlet air pressure of the spray was set at 1.5 bar. The atomized molten droplets hardened during the fall into a cylindrical cooling chamber, which was held at room temperature. Finally, SLMs were collected from the bottom of the cooling chamber and stored in polyethylene closed bottles at 4°C.

**HPLC analysis:** The HPLC system consisted of two mobile phase delivery pumps (LC-10ADvp, Shimadzu, Japan), a UV–vis detector (SPD-10Avp, Shimadzu, Japan) and an autosampler (SIL-20A, Shimadzu, Japan).

**Direct method.** An HPLC method for the simultaneous quantification of GSH and GSSG was developed. A reversed phase C18 column (Synergi Hydro RP, 4 µm, 150 mm x 4.60 mm; Phenomenex, Bologna, Italy) was used as stationary phase, while the mobile phase consisted in 95% potassium phosphate buffer (25mM, pH 2.7) and 5% methanol. The injected volume was 20 µl and the detection wavelength was set at 200 nm. The chromatographic run followed an isocratic method

with a mobile phase flow rate of 0.7 ml/min. In these conditions the retention times of GSH and GSSG were 4.1 and 6.4 minutes, respectively. The linearity ranges were obtained between 5 and 100 µg/ml ( $R^2=0.9999$ ) and 1 and 100 µg/ml ( $R^2=0.9998$ ) for GSH and GSSG, respectively.

***Derivatization method.*** For more complex media than simple saline buffers (e.g. biorelevant media), the direct method was not suitable for GSH determination because of the high signal of the matrix. Thus, a method based on the derivatization of GSH by 1,4-Naphthoquinone (NPQ, Sigma Aldrich, Steinheim, Germany) on the thiol group of GSH was carried out using a validated procedure<sup>206</sup>. Borate buffer solutions (pH 7.5; 250 mM) were prepared dissolving boric acid in water and adjusting the pH with sodium hydroxide. The derivatization reagent solution was prepared by dissolving NPQ (10 mM) in MeOH. An aliquot of 100 µl of the solution containing GSH (standard or sample) was added to 400 µl of borate buffer and treated with 100 µl of NPQ solution. The derivatization reaction was carried out under magnetic stirring in a micro-reaction vessel at room temperature and pH 7.5 for 2 min. Then, a 1.2 ml aliquot of the mobile phase was added. The stationary phase was a C18 column (Kinetex, 5 µm, 150 mm x 4.60 mm; Phenomenex, Bologna, Italy), the mobile phase consisted in 60% potassium phosphate buffer (25mM, pH 2.7) and 40% methanol with flow rate of 0.8 ml/min. The injected volume was 20 µl and the detection wavelength was set at 420 nm. Retention time of derivatised GSH was 6.7 min and the linearity range between 1 and 30 µg/ml with an  $R^2$  of 0.9959

#### ***GSH-loaded SLMs characterization:***

***Drug content determination.*** 20 mg of sample were accurately weighed and added to 5 ml of phosphate buffer pH 2.7. The system was heated to melt the carrier, shaken for 1 h and filtered to obtain a lipid solution, which was assayed by HPLC using the direct method.

***Morphological analysis.*** Shape and surface morphology of SLMs before and after dissolution testing were assessed by means of Scanning Electron Microscopy (SEM). Samples were fixed on the sample holder with double-sided adhesive tape and examined by means of a scanning electron microscope ESEM Quanta 200 (Fei Company - Oxford Instruments) operating at 20,0 kV accelerating voltage. The size distribution of the SLMs was evaluated by sieve analysis, using a vibrating shaker (Octagon Digital, Endecotts, London, UK) and four standard sieves (Scientific Instruments, Milan, Italy) of 100, 150, 250 and 500 µm. The more representative fraction was used for further experiments.

Differential Scanning calorimetry (DSC) DSC measurements were performed using a Perkin-Elmer DSC 6 (Perkin Elmer, Beaconsfield, UK). The calibration of the instrument was performed with indium and lead for the temperature, and with indium for the measurement of the enthalpy. The samples, weighting 6-10 mg, were placed into the DSC under a nitrogen flux (20 ml/min) and heated from 25 to 250 °C at a scanning rate of 10°C/min.

Hot Stage Microscopy (HSM) analysis. Physical changes in the samples during heating were monitored by HSM studies using a hot stage apparatus (Mettler-Toledo S.p.A., Novate Milanese, Italy) mounted on Nikon Eclipse E400 optical microscope connected to a Nikon Digital Net Camera DN100 for the image acquisition. The samples were equilibrated 25°C for 1 min and then heated at a scanning rate of 10°C/min in the desired ranges of temperature. The magnification was set at 10x.

Stability of GSH in gastric and intestinal pH. GSH (5 mg) was added to 20 ml of buffer pH 1.2 and pH 6.8 and incubated under bland agitation at 37°C. At determined time intervals, 1 ml of dissolution media was withdrawn, the sample was simply diluted and analysed by HPLC using the direct method.

In vitro release studies of SLMs in simulated intestinal fluids. Dissolution studies were performed both in compendial (buffer pH 6.8) and biorelevant media. Fasted State Simulated Intestinal Fluid (FaSSIF V<sub>2</sub>) and Fed State Simulated Intestinal Fluid (FeSSIF V<sub>2</sub>) were prepared according to Jantrid et al.<sup>76</sup>. About 60 mg of SLMs were immersed in 15 ml of the dissolution medium and incubated under bland agitation at 37°C. At determined time intervals, 0.5 ml of dissolution media was withdrawn by means of a membrane filter (800 µm size) to not remove the SLMs. 0.5 ml of fresh medium was added to keep the total volume constant. In case of simple buffer pH 6.8, the sample was simply diluted and analysed by HPLC using the direct method. In case of FaSSIF V<sub>2</sub> and FeSSIF V<sub>2</sub>, the derivatization method was employed. The sample was treated as described in the previous paragraph and assayed by HPLC.

***Evaluation of the antioxidant activity in vitro:*** To investigate the radical scavenging properties of GSH-loaded SLMs, 2,2-diphenyl-1-picrylhydrazyl (DPPH) was dissolved in ethanol to a final working concentration of 0.2 mM. DPPH solutions were supplemented with the 5 mg of SLMs (unloaded F1 and F2, GSH-loaded F1 and F2) in a micro-vials, protected from light with aluminium foil and incubated at 37°C for the 1 hour. The samples were assayed for DPPH amount by measuring the

absorbance at  $\lambda = 516$  nm (UV2 Spectrometer, Unicam). Three repetitions were performed per sample. DPPH 0.2 mM served as 100 % radical control, in comparison to the test samples. The ratio of free radical scavenging was calculated via normalization of the test sample absorbance to the absorbance of the DPPH alone as reported elsewhere<sup>207</sup>.

**Cell culture:** The colon cancer cell line HT29 was purchased from the American Type Culture Collection (Manassas, VA). HT29 cells were maintained in RPMI 1640 medium (Labtek Eurobio, Milan, Italy) supplemented with 10% fetal calf serum (Euroclone, Milan, Italy) and 2 mM glutamine (Sigma-Aldrich, St. Louis, MO) at 37° C and 5% CO<sub>2</sub>. HT29 cells were seeded at  $2 \times 10^4$  cells/cm<sup>2</sup> in a plastic well (60 cm<sup>2</sup>) and allowed to grow for 1 day before being exposed to treatments.

**In vitro cytotoxicity studies:** In order to estimate the effect of MPs on cell viability, MTT assay was performed as the reduction of tetrazolium salts is widely accepted as a reliable way to examine cell viability/proliferation<sup>208</sup>. Cells ( $2 \times 10^4$ / cm<sup>2</sup>) were incubated with different concentrations, in the range 50-2000 µg/mL of unloaded-MPs (F1 formulation, fraction with diameters between 100 and 200 µm) for 24h at 37°C. Cells were then incubated with 5 mg/mL MTT for 4 h at 37°C. At the end of the incubation, purple formazan salt crystals were formed and dissolved by adding the solubilisation solution (10% SDS, 0,01M HCl), then the plates were incubated overnight in humidified atmosphere (37°C, 5% CO<sub>2</sub>). The absorbance at 570 nm was measured in a multiwell plate reader (Wallac Victor2, Perkin-Elmer).

**Statistical Analysis:** All results were expressed as mean  $\pm$  standard deviation (S.D.). One-way analysis of variance (ANOVA) followed by the Bonferroni post-hoc test (GraphPadPrism, GraphPad software Inc., CA, USA) was used to analyze the data and the level of significance was set at the probabilities of \*p < 0.05, \*\*p < 0.01 and \*\*\*p < 0.001.

## VI. Results and discussions

**GSH-loaded SLMs characterization.** SLMs with Dynasan 114 (F1) were prepared as reference formulation, basing on previous results (Case study V). Additionally, a formulation with Dynasan 114 and Dynasan 118 in ratio 1:1 (F2) was prepared to evaluate the effect of a more hydrophobic excipient on the release characteristics of SLMs. Non-aggregated and spherical SLMs were obtained for both formulations, with drug loading values (Table VI.1) very close to the theoretical one (5% w/w) and thus demonstrating once again the high encapsulation efficiency of spray congealing process.

SLMs Samples	Constituents (% w/w)			Drug loading (% w/w)
	Dynasan 114	Dynasan 118	API	GSH
F1	95	-	5	5.09 ± 0.24
F2	48.5	48.5		5.18 ± 0.12

**Table VI.1.** Composition and GSH content of F1 and F2 SLMs.

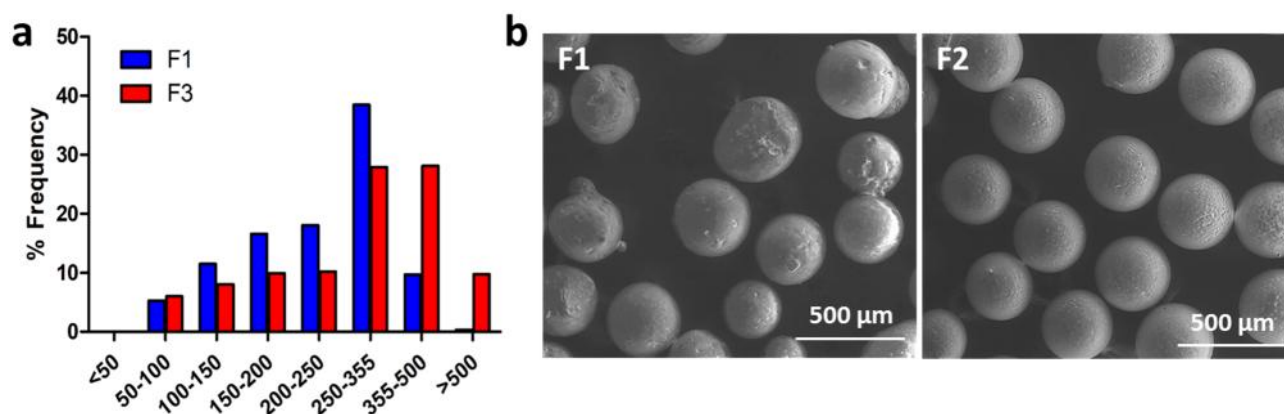


**Figure VI.1** (a) Size distribution and (b) SEM images of GSH-loaded F1 and F2 SLMs.

The particle size distribution of SLMs, reported in Figure VI.1a, showed Gaussian profile for both formulations. F1 SLMs had diameters comprised between 50 and 500  $\mu\text{m}$ , with prevalent size fraction 250-355  $\mu\text{m}$ . Differently, in case of F3 SLMs, the size distribution was shifted to higher dimensions, and the prevalent size fractions were both the 250-355  $\mu\text{m}$  and the 355-500  $\mu\text{m}$ . As visible in Figure VI.1b, SLMs were spherical and not aggregated. Whereas F1 showed some irregularities, F2 particle surface was more even and smooth. The difference in the particle morphology is related to the lipid composition, rather than to the characteristic of the encapsulated



compound. In fact, in case study V, Dynasan 114-based SLMs showed identical morphology, both unloaded or loaded with the biologic drug.

The DSC analysis is reported in Figure VI.2. Pure GSH showed a sharp endothermic peak at 205°C, indicating the melting of the drug. The same event at the same temperature was detected in both formulation of SLMs, despite the limited amount of GSH (5%) in the samples. In addition, F1 SLMs showed a single endothermic peak at 63°C attributed to the carrier melting, whereas in case of F3 the thermogram resulted much more complex, due to presence of two different components (Dynasan 114 and Dynasan 118). Moreover, additional DSC signals can originate from the formation of metastable polymorphic forms of the lipid excipient. As already mentioned, long-chains triglycerides exist at least in three polymorphic forms identified by the lateral packing of their alkyl chains, the stable  $\beta$  form, and the metastable  $\alpha$  form and  $\beta'$  form<sup>194</sup>. As a matter of fact melting-based processes can promote the conversion into the metastable forms. Four different endothermic signals related to the carrier melting were detected in F3 formulation immediately after preparation. The peak at highest temperature (69°C) can be attributed to the melting of the original polymorph of Dynasan 118. The small peak at the lowest temperature (around 37°) corresponded to the melting of the metastable  $\alpha$  form of Dynasan 114<sup>195</sup>. In between, two more signals can be observed at 51 and 60°C, respectively.

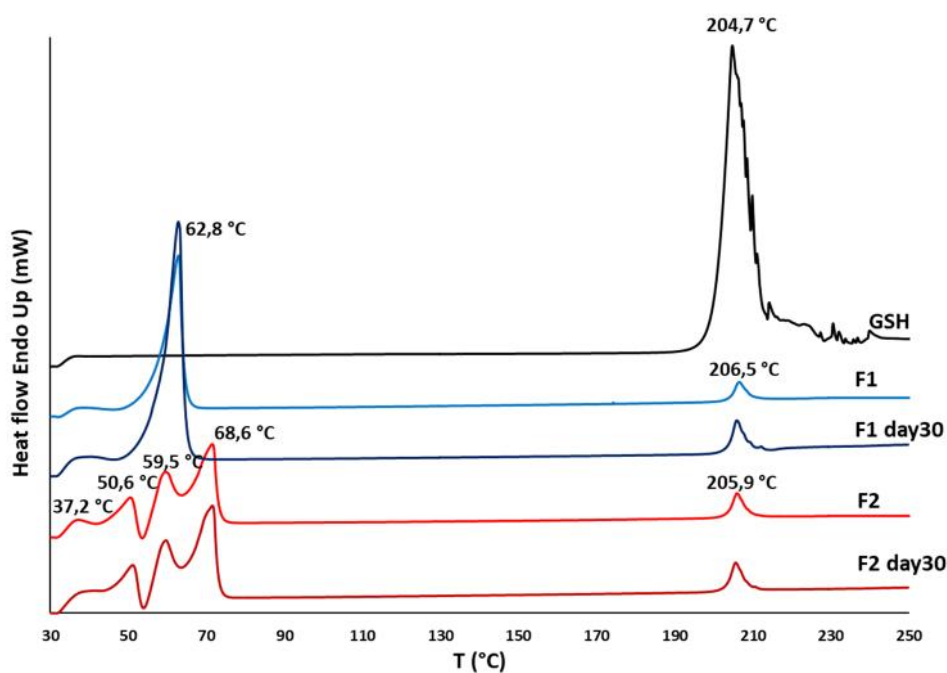


**Figure VI.2.** DSC analysis of GSH-loaded SLMs.

To better understand the DSC results of F3 formulation, DSC analysis of single raw materials, physical mixture Dynasan 114:Dynasan 118 (ratio 1:1) and correspondent SLMs were performed (Figure VI.3). The endothermic event at ca. 60°C can be attributed both to Dynasan 114 original  $\beta$  form ( $T_m$  of 63°C) and to the metastable  $\alpha$  form of Dynasan 118, formed during spray congealing process ( $T_m$  of 62°C). To the best of our knowledge, no data in the literature has been found in order to assign the endothermic event detected at ca. 51°C. In the DSC analysis of F3 SLMs performed after 1 months, the small peak at 37°C of the  $\alpha$  form of Dynasan 114 was no longer detectable, due to the complete conversion of the excipient into the stable form, whereas the other three peaks were unchanged.

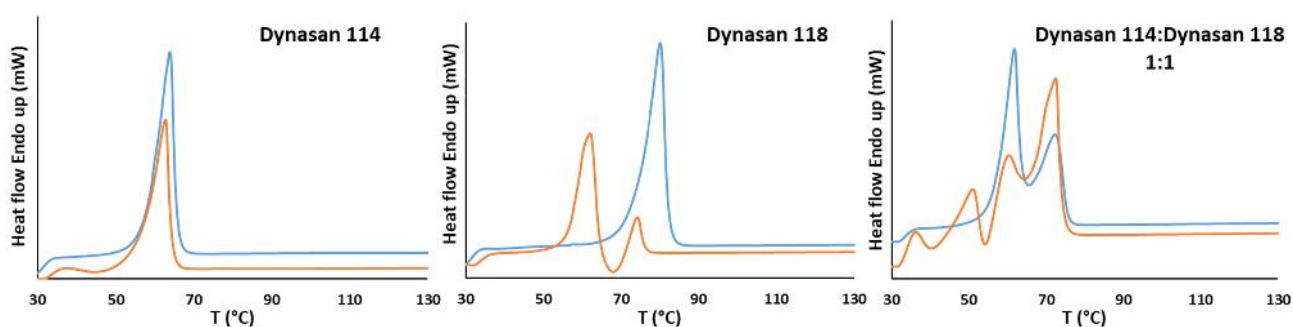


**Figure VI.3.** DSC of Dynasan 114, Dynasan 118 and Dynasan 114:Dynasan 118 (1:1 ratio) raw materials (blue curves) and SLMs prepared with the same excipients (orange curves). In case of Dynasan 114:Dynasan 118 (1:1 ratio), the sample was prepared as a physical mixture of the two excipients.

The HSM analysis of pure GSH showed needle-like crystals which melted at 203-205°C, followed by a change to darker colour, suggesting a probable decomposition. In case of SLMs, the melting of the carrier was observed starting from 55 and 64°C for F1 and F2, respectively. Afterwards, GSH crystals were observed into the melted particle matrix. Notably, the GSH crystals loaded into the SLMs showed unchanged morphology and melting temperature. It was interesting to notice that after melting, GSH was not miscible with the molten lipid, and the system remained as two liquid separate phases.

These results, taken together, suggest that the microencapsulation process did not cause any degradation and/or modification in GSH solid state and no interactions between drug and carrier were observed.

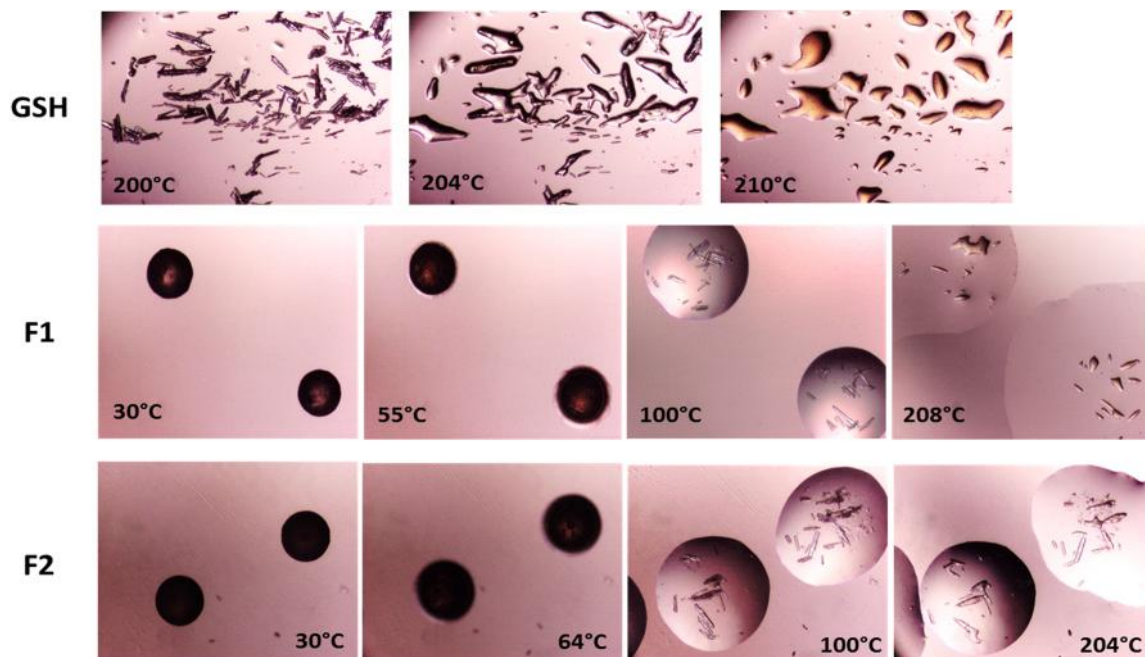


**Figure VI.3.** HSM images of GSH, F1 GSH and F2 GSH SLMs. The magnification was 10x.

**In vitro release studies.** To understand the behaviour of GSH in the GIT environments, dissolution studies of pure GSH were performed in buffer pH 1.2, simulating the gastric pH, and buffer 6.8, simulating the intestinal pH. As visible in Figure VI.4, in both cases GSH completely solubilized within the first 5 minutes, confirming its high water solubility. However, whereas at acidic pH the reduced form was stable over 4 hours, at pH 6.8 GSH amount decreased progressively due to the tripeptide oxidation. In fact, increasing amounts of GSSG were detected together with decreasing GSH levels in this dissolution medium, while at pH 1.2 the percentage of GSSG was always lower than 1%. The pH-dependent oxidation of GSH is in accordance with previous studies<sup>209 205</sup>.

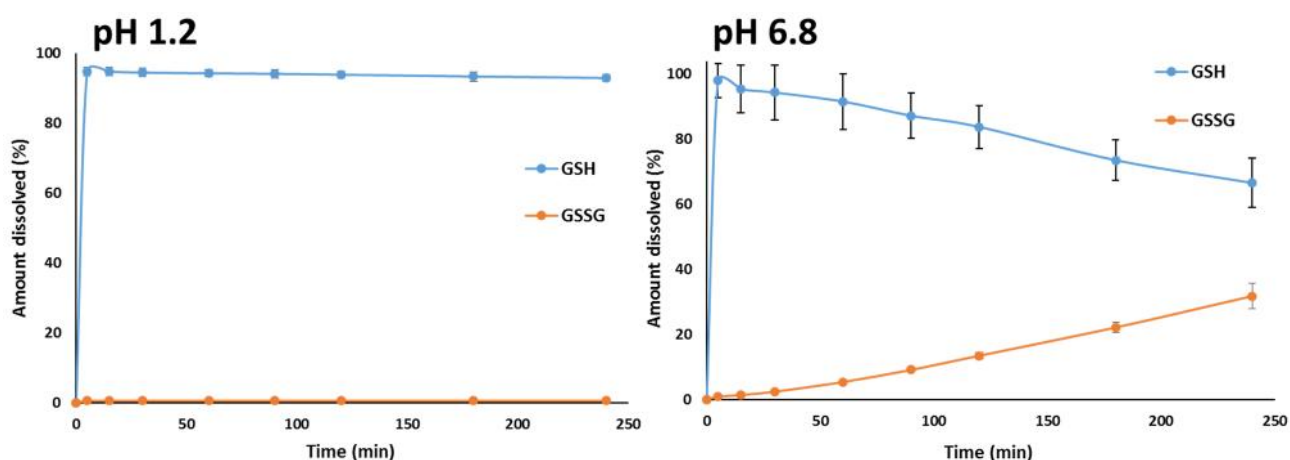


**Figure VI.4.** Dissolution profiles of pure GSH at pH 1.2 and pH 6.8 and its oxidation to GSSG. Values are expressed as means ( $n = 3$ )  $\pm$  SD.

The GSH release from SLMs was initially studied in buffer pH 6.8, simulating the intestinal pH (Figure VI.5). In the first 30 minutes, 31% and 26% of GSH was quickly released from F1 and F2, respectively, with low amount of GSSG (<4%). This initial burst release, observed from both formulations, was followed by a *plateau* in the concentration of measured GSH, as the amount of GSH released from the particles was equivalent to the amount of GSH oxidized. In fact, an increasing amount of GSSG was detected. After 90 minutes, the GSH concentration started to slowly decrease, indicating that the oxidation process was greater than the GSH release from the SLMs. Interestingly, the formulation composition did not seem to influence the amount of GSSG formed. However, the formulation F2 reduced the drug release, as expected, due to the more hydrophobic lipid carrier.

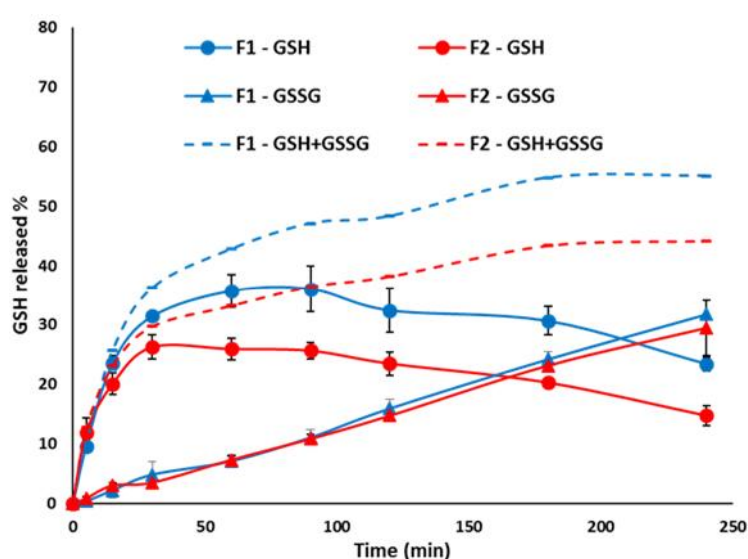


**Figure VI.5.** Dissolution profiles of F1 and F2 SLMs in phosphate buffer pH 6.8. The experimental amount of GSH and GSSG was measured by HPLC (solid lines). The total amount of drug released, calculated by summing the amount of GSH and GSSG at every time points, is also reported (dotted line). Values are expressed as means ( $n = 3$ )  $\pm$  SD.

To improve our understanding of the GSH release in the GIT, dissolution studies in biorelevant media were performed. Figure VI.6 showed the amount of GSH released from F1 and F2 SLMs in FaSSIF and FeSSIF, compared to those released in simple buffer pH 6.8. In fasted state, the GSH profile followed the same pattern of the one obtained in simple buffer, consisting in initial burst release, plateau phase and an ultimate slowly decrease. However, compared to buffer pH 6.8, a slight reduction in GSH amount was observed in FaSSIF for both formulations, probably due to the higher viscosity of this medium compared to a simple aqueous buffer. A similar behaviour was observed for carnauba wax based-MPs in case study IV. In case of F1 SLMs, the medium simulating the fed

state led to the faster drug release compared to the other media, in accordance with the release behaviour of lactase from Dynasan 114-based SLMs (case study V), where the highest drug released was observed in FeSSIF. This behaviour might be explained considering the effect of wettability and emulsification of lipid particles from the lecithin, monoglycerides and bile salts present in this medium. In the first 30 minutes, ca. 50% of GSH was released. Nevertheless, after 30 minutes, the GSH content decreased due to a fast oxidation, which was favoured by the components of the medium. GSH is characterized by the presence of the very reactive thiol group, which can react with many compounds to form a glutathione-adduct, with the function of removal of radical, peroxides and many xenobiotic compounds <sup>210</sup>. Differently, in case of formulation F2, the effect of enhanced GSH oxidation by FeSSIF prevailed over the enhanced release effect, and thus the total concentration of GSH measured during the test was quite low.

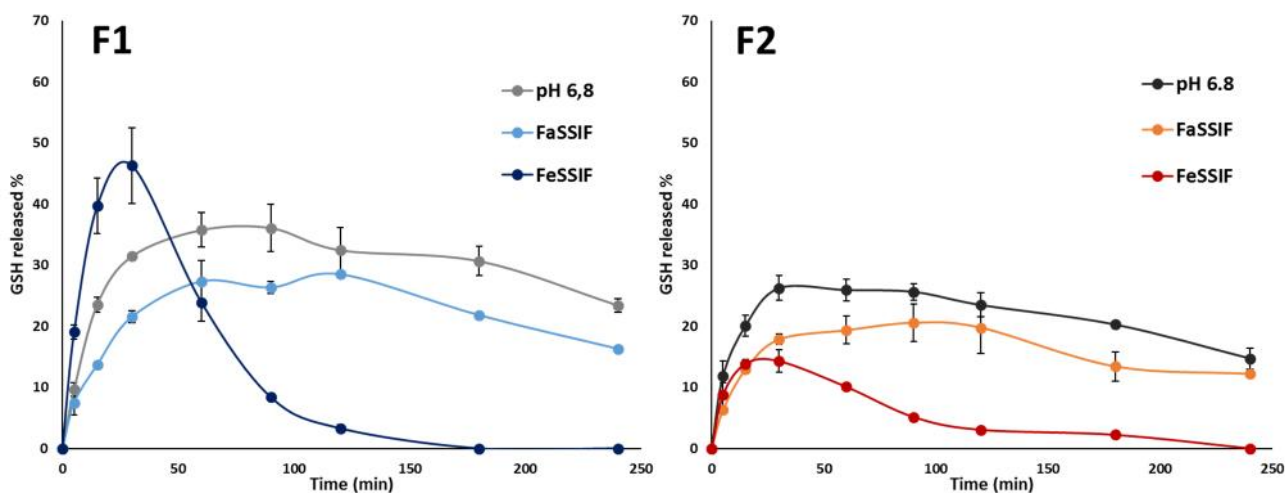


**Figure VI.6.** Dissolution profiles of GSH from F1 and F2 SLMs in phosphate buffer pH 6.8, FaSSIF-V<sub>2</sub> and FeSSIF-V<sub>2</sub>. Values are expressed as means (n = 3) ± SD.

The morphology of the particles after dissolution tests were observed by SEM and the images are reported in Figure VI.7. In the medium simulating the fasted state, the particles were partially intact and partially fragmented. It is interesting to notice that the SLMs did not lose their spherical shape and their original round morphology was still distinct. Notably, this feature was observed both in F1 and F2 SLMs in case of FaSSIF. Differently, in the medium simulating the fed state, only a small amount of SLMs were recovered at the end of the test, indicating that most particles were completely emulsified in the medium. By observing the particles, it is evident the loss of their spherical shape, suggesting an erosion of the lipid matrix by the FeSSIF, which seemed to mainly

lead to a degradation process on the external surface of SLMs. Moreover, numerous breakages and fractures were observed on the SLMs in this media, which were absent in case of FaSSIF.

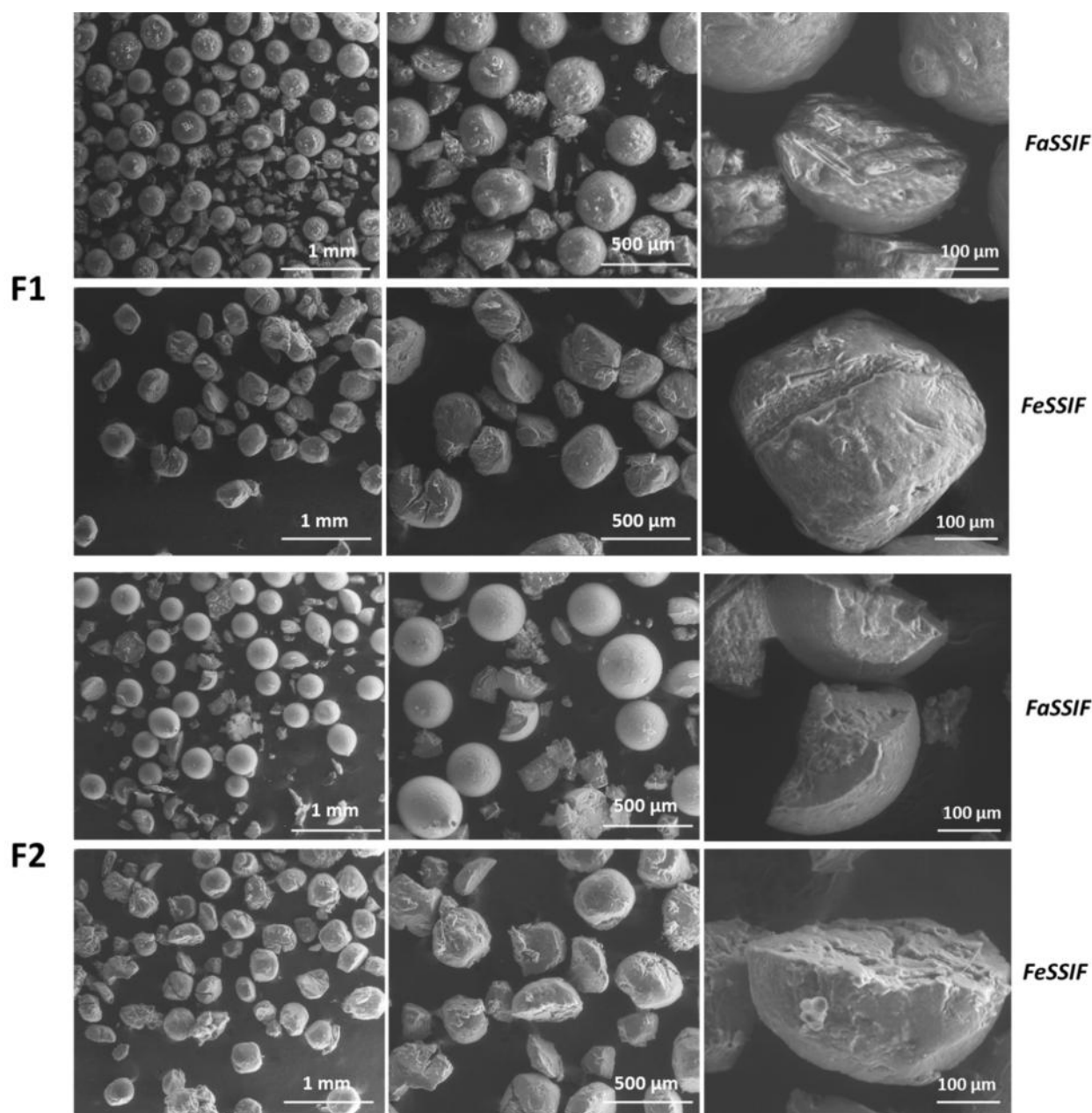


**Figure VI.7.** SEM images of the particles after the dissolution test in FaSSIF-V2 and FeSSIF-V2, at three different magnifications (80x, 160x and 600x).

The dissolution studies and SEM analysis performed at the end of the tests underlined important differences on the release of GSH and on the particle structure by using different biorelevant media. It was evidenced the critical stability of GSH in intestinal pH and its tendency to oxidize, especially in presence of complex buffers. However, this does not necessarily mean that the antioxidant activity of GSH would be prevented. As mentioned, the thiol group of GSH is involved in reduction

and conjugation reactions with mainly electrophilic or oxidizing species<sup>211</sup>. We should consider that in case of intestinal inflammation or other disease involving oxidative stress, the diseased sites are characterized by a high concentration of reactive species<sup>114 115</sup>. Therefore, when GSH is released from the SLMs close to the inflamed intestinal membrane, it will find a high oxidizing environment and it will readily react with the excess of oxidant species. Clearly, it is important to verify the antioxidant activity of our formulations as well as their citocompatibility with the intestinal cells.

**Evaluation of the antioxidant activity.** The ability of SLMs to scavenge ROS was study using DPPH, which gives fast detection of the antioxidant activity towards radical species and results are reported in Figure VI.8. Unloaded SLMs showed a slight effect on DPPH, with 82.7% and 82.4% of scavenging activity, for F1 and F2 SLMs, respectively. No significant differences between the two unloaded SLMs formulation were obtained. The antioxidant activity of GSH-loaded SLMs was significantly stronger ( $p < 0.001$  and  $p < 0.01$  for F1 and F2, respectively) than that of unloaded formulations. A good antioxidant activity towards radical species was observed, indicating the retention of anti-radical properties of GSH after microencapsulation. Specifically, F1 resulted in higher radical scavenging activity (49.4%) than F2 (53.9%).

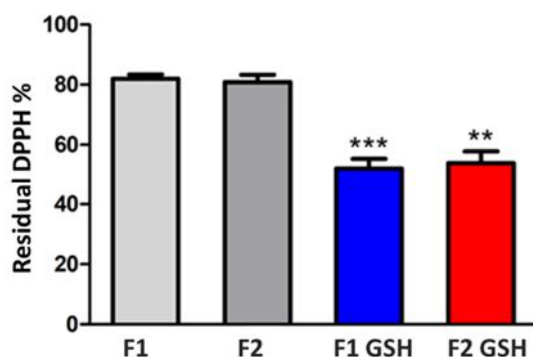


**Figure VI.8.** Antioxidant activity of unloaded and GSH-loaded SLM, measured with the decrease in absorbance of DPPH. Values are expressed as means ( $n = 3$ )  $\pm$  SD, and the level of significance between GSH-loaded SLMs and unloaded SLMs was set at the probabilities of  $**p < 0.01$ , and  $***p < 0.001$ .

**In vitro cytotoxicity studies.** To assess the feasibility of the use of SLMs for oral administration, the cytocompatibility of the formulation with the best performance (F1) was evaluated on human colon adenocarcinoma (HT29) intestinal cell line. As shown in Figure VI.9, concentrations ranging from 50 to 2000  $\mu\text{g}/\text{ml}$  resulted completely safe on cells, with viability values always close to 100% ( $p < 0.05$  compared to the control).

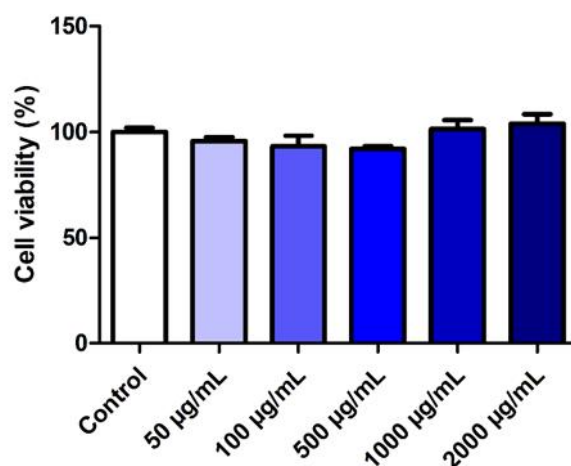


**Figure VI.9.** Viability of HT29 cells after 24 h incubation with different concentration of *unloaded*-F1 SLMs.

## VI. Conclusion

In this study reduced glutathione (GSH) was successfully encapsulated into SLMs by spray congealing. Dynasan 114 was used as main lipid carrier, alone (formulation F1) or in combination with a triglyceride with longer chains length, Dynasan 118 (formulation F2). SLMs showed excellent encapsulation efficiency values and no modification, loss or degradation of the tripeptide during the process. DSC and HSM analysis showed that GSH chemico-physical properties were maintained. It was also shown that variations in the lipid composition has the potential to modulate the drug release. Specifically, the presence of more hydrophobic lipid prolonged the drug release whereas the fastest GSH release was obtained by F1 SLMs and in fed state simulated intestinal medium (FeSSIF). Moreover, SLMs showed in vitro antioxidant activity towards radical species, with the best performance obtained by GSH-loaded F1 SLMs. Finally, the cytocompatibility of this formulation was tested on HT29 cells, confirming to be completely safe at concentrations up to 2000 µg/ml.

Overall, spray congealed SLMs confirmed to be a promising vehicle for the encapsulation and intestinal delivery of biotherapeutics.



#### 4. Concluding remarks

This thesis describes the development of innovative oral formulations to overcome poor drug bioavailability, which is currently one of the major challenges in the area of the pharmaceutical research. Specifically, MPs were successfully employed to improve the bioavailability of orally administered APIs, differing both from physicochemical properties and therapeutic purposes.

**Case studies I-II:** MPs based on hydrophilic carriers, such as Gelucire 50/13 and Gelucire 48/16, successfully improved the oral bioavailability of poorly water soluble drugs belonging to BCS class II. The bioavailability enhancement of Gelucires-based MPs relied on multiple mechanisms, including effects given by the hydrophilic carrier, such as improved wettability and micelle formation, and effects resulting from changes in the drug crystalline original state, specifically amorphisation, conversions into metastable polymorphs and crystals size reduction.

**Case study III:** MPs were successfully employed for the oral local delivery of an active compound for the treatment of IBD. In this case, an approach based on the encapsulation of nanoparticles into enteric polymeric MPs was adopted. The application of responsive materials allowed to achieve a selective drug delivery to the inflamed sites with limited systemic absorption.

**Case study IV-V-VI:** systems based on lipid carriers, called SLMs, were explored as strategy to achieve a local oral delivery of biologic drugs, specifically an enzyme and a peptide. In the development of oral biotherapeutics, one of the most challenging tasks to overcome is the loss of biological activity due to physical and chemical instabilities, which results in extremely poor bioavailability for this route. SLMs were able to protect the active compounds from the gastric degradation and release it closer to the target site by exploiting the action of bile salts and physiological lipases, which emulsified and degraded the lipid matrix promoting the drug release. The results highlighted that the release behaviour of these lipid systems should be studied in fluids simulating the real GI environment for accurately predict their behavior *in vivo*.

The applications of MPs illustrated in this dissertation thesis represent only a small part of all the possibilities that this delivery system can provide. The advantages of MPs include the use of biocompatible, low-cost and safe materials, and the benefits of multiparticulate dosage forms. Moreover, advances in solvent-free manufacturing technologies, such as spray congealing, for MPs production can further increase the interest on this delivery system. Concluding, MPs can provide a solid platform for the development of a number of oral formulations, representing a versatile drug delivery system able to address the different issues related to the poor oral bioavailability.

## References

1. Masaoka, Y., Tanaka, Y., Kataoka, M., Sakuma, S. & Yamashita, S. Site of drug absorption after oral administration: Assessment of membrane permeability and luminal concentration of drugs in each segment of gastrointestinal tract. *Eur. J. Pharm. Sci.* **29**, 240–250 (2006).
2. Golub, A. L., Ph, D., Frost, R. W. & Pharm, D. Physiologic considerations in drug absorption from the gastrointestinal tract. *J. Allergy Clin. Immunol.* **78**, 689–694 (1986).
3. Niess, J. H. & Reinecker, H.-C. Dendritic cells in the recognition of intestinal microbiota. *Cell. Microbiol.* **8**, 558–564 (2006).
4. AF, H. The continuing importance of bile acids in liver and intestinal disease. *Arch. Intern. Med.* **159**, 2647–2658 (1999).
5. Chow, S.-C. Bioavailability and Bioequivalence in Drug Development. *Wiley Interdiscip. Rev. Comput. Stat.* **6**, 304–312 (2014).
6. Charmot, D. Non-Systemic Drugs : A Critical Review. *Curr. Pharm. Des.* **18**, 1434–1445 (2012).
7. L. Amidon, G., HL, L., P. Shah, V. & Crison, J. A Theoretical Basis for a Biopharmaceutic Drug Classification: The Correlation of In Vitro Drug Product Dissolution and In Vivo Bioavailability. *Pharm. Res.* **12**, 413–420 (1995).
8. Shah, V. P. & Amidon, G. L. G.L. Amidon, H. Lennernas, V.P. Shah, and J.R. Crison. A theoretical basis for a biopharmaceutic drug classification: the correlation of in vitro drug product dissolution and in vivo bioavailability, *Pharm Res* **12**, 413-420, 1995--backstory of BCS. *AAPS J.* **16**, 894–8 (2014).
9. Lipinski, C. A., Lombardo, F., Dominy, B. W. & Feeney, P. J. Experimental and computational approaches to estimate solubility and permeability in drug discovery and development settings. *Adv. Drug Deliv. Rev.* **46**, 3–26 (2001).
10. Benet, L. Z., Hosey, C. M., Ursu, O. & Oprea, T. I. BDDCS, the Rule of 5 and drugability. *Adv. Drug Deliv. Rev.* **101**, 89–98 (2016).
11. Wu, C.-Y. & Benet, L. Z. Predicting Drug Disposition via Application of BCS: Transport/Absorption/Elimination Interplay and Development of a Biopharmaceutics Drug Disposition Classification System. *Pharm. Res.* **22**, 11–23 (2005).
12. Hurst, S., Loi, C.-M., Brodfuehrer, J. & El-Kattan, A. Impact of physiological, physicochemical and biopharmaceutical factors in absorption and metabolism mechanisms on the drug oral bioavailability of rats and humans. *Expert Opin. Drug Metab. Toxicol.* **3**, 469–489 (2007).
13. Dokoumetzidis, A., Kalantzi, L. & Fotaki, N. Predictive models for oral drug absorption: from in silico methods to integrated dynamical models. *Expert Opin. Drug Metab. Toxicol.* **3**, 491–505 (2007).
14. Desai, P. P., Date, A. A. & Patravale, V. B. Overcoming poor oral bioavailability using nanoparticle formulations – opportunities and limitations. *Drug Discov. Today Technol.* **9**, e87–e95 (2012).
15. Van de Waterbeemd, H., Smith, D. A., Beaumont, K. & Walker, D. K. Property-Based Design: Optimization of Drug Absorption and Pharmacokinetics. *J. Med. Chem.* **44**, 1313–1333 (2001).

16. Gomez-Orellana, I. Strategies to improve oral drug bioavailability. *Expert Opin. Drug Deliv.* **2**, 419–433 (2005).
17. Kawabata, Y., Wada, K., Nakatani, M., Yamada, S. & Onoue, S. Formulation design for poorly water-soluble drugs based on biopharmaceutics classification system: Basic approaches and practical applications. *Int. J. Pharm.* **420**, 1–10 (2011).
18. Guan, J. *et al.* Alginate as a potential diphase solid dispersion carrier with enhanced drug dissolution and improved storage stability. *Eur. J. Pharm. Sci.* **114**, 346–355 (2018).
19. Jermain, S. V, Brough, C. & Williams, R. O. Amorphous solid dispersions and nanocrystal technologies for poorly water-soluble drug delivery – An update. *Int. J. Pharm.* **535**, 379–392 (2018).
20. Goracinova, K., Glavas-dodov, M., Simonoska-crcarevska, M. & Geskovski, N. in *Inflammatory Bowel Disease – Advances in Pathogenesis and Management* (2007).
21. Koetting, M. C., Guido, J. F., Gupta, M., Zhang, A. & Peppas, N. A. PH-responsive and enzymatically-responsive hydrogel microparticles for the oral delivery of therapeutic proteins: Effects of protein size, crosslinking density, and hydrogel degradation on protein delivery. *J. Control. Release* **221**, 18–25 (2016).
22. Leader, B., Baca, Q. J. & Golan, D. E. Protein therapeutics: a summary and pharmacological classification. *Nat. Rev. Drug Discov.* **7**, 21 (2008).
23. Renukuntla, J., Vadlapudi, A. D., Patel, A., Boddu, S. H. S. & Mitra, A. K. Approaches for enhancing oral bioavailability of peptides and proteins. *Int. J. Pharm.* **447**, 75–93 (2013).
24. Bourganis, V., Karamanidou, T., Kammona, O. & Kiparissides, C. Polyelectrolyte complexes as prospective carriers for the oral delivery of protein therapeutics. *Eur. J. Pharm. Biopharm.* **111**, 44–60 (2017).
25. McClements, D. J. Encapsulation, protection, and delivery of bioactive proteins and peptides using nanoparticle and microparticle systems: A review. *Adv. Colloid Interface Sci.* **253**, 1–22 (2018).
26. Christophersen, P. C. *et al.* Characterization of particulate drug delivery systems for oral delivery of peptide and protein drugs. *Curr. Pharm. Des.* **21**, 2611–2628 (2015).
27. Moroz, E., Matorri, S. & Leroux, J. C. Oral delivery of macromolecular drugs: Where we are after almost 100 years of attempts. *Adv. Drug Deliv. Rev.* **101**, 108–121 (2016).
28. Maher, S., Mrsny, R. J. & Brayden, D. J. Intestinal permeation enhancers for oral peptide delivery. *Adv. Drug Deliv. Rev.* **106**, 277–319 (2016).
29. McCartney, F., Gleeson, J. P. & Brayden, D. J. Safety concerns over the use of intestinal permeation enhancers: A mini-review. *Tissue Barriers* **4**, 00–00 (2016).
30. Wang, J., Yadav, V., Smart, A. L., Tajiri, S. & Basit, A. W. Toward oral delivery of biopharmaceuticals: An assessment of the gastrointestinal stability of 17 peptide drugs. *Mol. Pharm.* **12**, 966–973 (2015).
31. Kumar, S., Jeet, K. & Ashish, B. Recent technological advancements in multiparticulate formulations: The smart drug delivery systems. *Asian J. Pharm.* **9**, S13–S25 (2018).

32. Campos, E. *et al.* Designing polymeric microparticles for biomedical and industrial applications. *Eur. Polym. J.* **49**, 2005–2021 (2016).
33. Subramanian, V. *Microspheres : technologies and global markets.* *BCC Res.* (2018).
34. Bertoni, S., Dolci, L. S., Albertini, B. & Passerini, N. Spray congealing: a versatile technology for advanced drug delivery systems. *Ther. Deliv.* **9**, 833–845 (2018).
35. Scalia, S., Young, P. M. & Traini, D. Solid lipid microparticles as an approach to drug delivery. *Expert Opin. Drug Deliv.* **12**, 1–17 (2014).
36. Vilos, C. & Velasquez, L. A. Therapeutic Strategies Based on Polymeric Microparticles. *J. Biomed. Biotechnol.* **2012**, 1–9 (2012).
37. Censi, R., Gigliobianco, M., Casadidio, C. & Di Martino, P. Hot Melt Extrusion: Highlighting Physicochemical Factors to Be Investigated While Designing and Optimizing a Hot Melt Extrusion Process. *Pharmaceutics* **10**, (2018).
38. Jaspert, S., Piel, G., Delattre, L. & Evrard, B. Solid lipid microparticles: formulation , preparation , characterisation , drug release and. *Expert Opin. Drug Deliv.* **2**, 75–87 (2005).
39. Klein, S. The Use of Biorelevant Dissolution Media to Forecast the In Vivo Performance of a Drug. *AAPS J.* **12**, 397–406 (2010).
40. Albertini, B., Passerini, N., Pattarino, F. & Rodriguez, L. New spray congealing atomizer for the microencapsulation of highly concentrated solid and liquid substances. *Eur. J. Pharm. Biopharm.* **69**, 348–357 (2008).
41. Barron, M. K., Young, T. J., Johnston, K. P. & Williams, R. O. Investigation of processing parameters of spray freezing into liquid to prepare polyethylene glycol polymeric particles for drug delivery. *AAPS PharmSciTech* **4**, 1–13 (2003).
42. Mackaplow, M. B., Zarraga, I. E. & Morris, J. F. Rotary spray congealing of a suspension : Effect of disk speed and dispersed particle properties. *J Microencapsul* **23**, 793–809 (2006).
43. Leach, W. T. *et al.* Encapsulation of Protein Nanoparticles Into Uniform-sized Microspheres Formed in a Spinning Oil Film. *AAPS PharmSciTech* **6**, 605–617 (2005).
44. Rodriguez, L. *et al.* Description and preliminary evaluation of a new ultrasonic atomizer for spray-congealing processes. *Int. J. Pharm.* **183**, 133–143 (1999).
45. Felder, C. B., Blanco-Prieto, M. J., Heizmann, J., Merkle, H. P. & Gander, B. Ultrasonic atomization and subsequent polymer desolvation for peptide and protein microencapsulation into biodegradable polyesters. *J. Microencapsul.* **20**, 553–567 (2003).
46. Wong, P. C. H., Heng, P. W. S. & Chan, L. W. A study on the solid state characteristics of spray-congealed glyceryl dibehenate solid lipid microparticles containing ibuprofen. *Drug Dev. Ind. Pharm.* **42**, 363–377 (2016).
47. Hallouard, F., Mehenni, L., Lahiani-Skiba, M., Anouar, Y. & Skiba, M. Solid Dispersions for Oral Administration : An Overview of the Methods for their Preparation. *Curr. Pharm. Des.* **22**, 1–17 (2016).

48. Nalamachu, S. & Wortmann, R. Role of Indomethacin in Acute Pain and Inflammation Management: A Review of the Literature. *Postgrad. Med.* **126**, 92–97 (2014).
49. Dalmoro, A. *et al.* Polymer-lipid hybrid nanoparticles as enhanced indomethacin delivery systems. *Eur. J. Pharm. Sci.* **121**, 16–28 (2018).
50. Aloisio, C., G. de Oliveira, A. & Longhi, M. Cyclodextrin and Meglumine-Based Microemulsions as a Poorly Water-Soluble Drug Delivery System. *J. Pharm. Sci.* **105**, 2703–2711 (2016).
51. Mehanna, M. M., Alwattar, J. K. & Elmaradny, H. A. Optimization, physicochemical characterization and in vivo assessment of spray dried emulsion: A step toward bioavailability augmentation and gastric toxicity minimization. *Int. J. Pharm.* **496**, 766–779 (2015).
52. Sant, V. P., Smith, D. & Leroux, J.-C. Novel pH-sensitive supramolecular assemblies for oral delivery of poorly water soluble drugs: Preparation and characterization. *J. Control. Release* **97**, 301–312 (2004).
53. Ford, J. L. & Rubinstein, M. H. Phase equilibria and dissolution rates of indomethacin-polyethylene glycol 6000 solid dispersions. *Pharm. Acta Helv.* **53**, 327–332 (1978).
54. Bikiaris, D. N. Solid dispersions, Part II: new strategies in manufacturing methods for dissolution rate enhancement of poorly water-soluble drugs. *Expert Opin. Drug Deliv.* **8**, 1663–1680 (2011).
55. Leuner, C. & Dressman, J. Improving drug solubility for oral delivery using solid dispersions. *Eur. J. Pharm. Biopharm.* **50**, 47–60 (2000).
56. Huang, S. & Williams, R. O. Effects of the Preparation Process on the Properties of Amorphous Solid Dispersions. *AAPS PharmSciTech* **19**, 1971–1984 (2017).
57. Liu, X., Feng, X., Williams, R. O. & Zhang, F. Characterization of amorphous solid dispersions. *J. Pharm. Investig.* **48**, 19–41 (2018).
58. Chella, N. & Tadikonda, R. Melt dispersion granules: formulation and evaluation to improve oral delivery of poorly soluble drugs – a case study with valsartan. *Drug Dev. Ind. Pharm.* **41**, 888–897 (2015).
59. Jammula, S. *et al.* Design and characterization of cefuroxime axetil biphasic floating minitables. *Drug Deliv.* **22**, 125–135 (2015).
60. de Oliveira Eloy, J., Saraiva, J., de Albuquerque, S. & Marchetti, J. M. Solid dispersion of ursolic acid in Gelucire 50/13: a strategy to enhance drug release and trypanocidal activity. *AAPS PharmSciTech* **13**, 1436–45 (2012).
61. Passerini, N. *et al.* A new approach to enhance oral bioavailability of Silybum Marianum dry extract: Association of mechanochemical activation and spray congealing. *Phytomedicine* **19**, 160–168 (2012).
62. Van Duong, T. & Van den Mooter, G. The role of the carrier in the formulation of pharmaceutical solid dispersions. Part II: amorphous carriers. *Expert Opin. Drug Deliv.* **13**, 1681–1694 (2016).
63. *European Pharmacopoeia 9th Edition, 2.9.3. Dissolution test for solid dosage forms.*
64. Simovic, S. *et al.* Dry Hybrid Lipid–Silica Microcapsules Engineered from Submicron Lipid Droplets and

- Nanoparticles as a Novel Delivery System for Poorly Soluble Drugs. *Mol. Pharm.* **6**, 861–872 (2009).
65. Surwase, S. A. *et al.* Indomethacin: New polymorphs of an old drug. *Mol. Pharm.* **10**, 4472–4480 (2013).
  66. Kaneniwa, N., Otsuka, M. & Hayashi, T. Physicochemical characterization of Indomethacin polymorphs and the transformation kinetics in ethanol. *Chem. Pharm. Bull.* **33**, 3447–3455 (1985).
  67. Passerini, N. *et al.* Characterization of Carbamazepine - Gelucire 50/13 Microparticles Prepared by a Spray-Congeaing Process Using Ultrasounds. *J. Pharm. Sci.* **91**, 699–707 (2002).
  68. Passerini, N., Albertini, B., Perissutti, B. & Rodriguez, L. Evaluation of melt granulation and ultrasonic spray congealing as techniques to enhance the dissolution of praziquantel. *Int. J. Pharm.* **318**, 92–102 (2006).
  69. Fini, A., Cavallari, C. & Ospitali, F. Raman and thermal analysis of indomethacin / PVP solid dispersion enteric microparticles. *Eur. J. Pharm. Biopharm.* **70**, 409–420 (2008).
  70. Martins, R. M. *et al.* The effect of homogenization method on the properties of carbamazepine microparticles prepared by spray congealing carbamazepine microparticles prepared by spray congealing. *J Microencapsul* **30**, 692–700 (2013).
  71. El Hadri, M. *et al.* Lyotropic behavior of Gelucire 50/13 by XRD, Raman and IR spectroscopies according to hydration. *Chem. Phys. Lipids* **200**, 11–23 (2016).
  72. Van Duong, T. *et al.* Polymorphism of Indomethacin in Semicrystalline Dispersions: Formation, Transformation, and Segregation. *Mol. Pharm.* **15**, 1037–1051 (2018).
  73. Strachan, C. J., Rades, T. & Gordon, K. C. A theoretical and spectroscopic study of  $\gamma$ -crystalline and amorphous indometacin. *J. Pharm. Pharmacol.* **59**, 261–269 (2007).
  74. Kistenmacher, T. J. & Marsh, R. E. Crystal and molecular structure of an antiinflammatory agent, indomethacin, 1-(p-chlorobenzoyl)-5-methoxy-2-methylindole-3-acetic acid. *J. Am. Chem. Soc.* **94**, 1340–1345 (1972).
  75. Elkhodairy, K. A., Barakat, N. S. & El-Shazli, G. Effect of type and concentration of release-retarding vehicles on the dissolution rate of diltiazem hydrochloride from liquisolid compact. *J. Drug Deliv. Sci. Technol.* **22**, 189–195 (2012).
  76. Jantratid, E., Janssen, N., Reppas, C. & Dressman, J. B. Dissolution media simulating conditions in the proximal human gastrointestinal tract: An update. *Pharm. Res.* **25**, 1663–1676 (2008).
  77. Ahuja, N., Katare, O. P. & Singh, B. Studies on dissolution enhancement and mathematical modeling of drug release of a poorly water-soluble drug using water-soluble carriers. *Eur. J. Pharm. Biopharm.* **65**, 26–38 (2007).
  78. Ferretti, V. *et al.* Indomethacin Co-Crystals and Their Parent Mixtures: Does the Intestinal Barrier Recognize Them Differently? *Mol. Pharm.* **12**, 1501–1511 (2015).
  79. Kim, J. Y. & Ku, Y. S. Enhanced absorption of indomethacin after oral or rectal administration of a self-emulsifying system containing indomethacin to rats. *Int. J. Pharm.* **194**, 81–89 (2000).

80. Acosta, E. Bioavailability of nanoparticles in nutrient and nutraceutical delivery. *Curr. Opin. colloid interface Sci.* **14**, 3–15 (2009).
81. Jung, M.-S. *et al.* Bioavailability of indomethacin-saccharin cocrystals. *J. Pharm. Pharmacol.* **62**, 1560–1568 (2010).
82. Van Duong, T. *et al.* Spectroscopic Investigation of the Formation and Disruption of Hydrogen Bonds in Pharmaceutical Semicrystalline Dispersions. *Mol. Pharm.* **14**, 1726–1741 (2017).
83. Chambin, O. & Jannin, V. Interest of multifunctional lipid excipients: case of Gelucire 44/14. *Drug Dev. Ind. Pharm.* **31**, 527–34 (2005).
84. V. Jannin, M. Di Cuia, S. Chevrier, A. Faure, Y. Chavant, C. Voutsinas, F. D. Characterization of new self-emulsifying excipient to expand formulation options for poorly soluble drugs: Gelucire 48/16. in *AAPS 2012*.
85. Gupta, S., Kesarla, R. & Omri, A. Formulation strategies to improve the bioavailability of poorly absorbed drugs with special emphasis on self-emulsifying systems. *ISRN Pharm.* **2013**, 848043 (2013).
86. Chambin, O. *et al.* Influence of drug polarity upon the solid-state structure and release properties of self-emulsifying drug delivery systems in relation with water affinity. *Colloids Surfaces B Biointerfaces* **71**, 73–78 (2009).
87. Breitzkreitz, M. C., Sabin, G. P., Polla, G. & Poppi, R. J. Characterization of semi-solid Self-Emulsifying Drug Delivery Systems (SEDDS) of atorvastatin calcium by Raman image spectroscopy and chemometrics. *J. Pharm. Biomed. Anal.* **73**, 3–12 (2013).
88. Albertini, B., Di Sabatino, M., Melegari, C. & Passerini, N. Formulation of spray congealed microparticles with self-emulsifying ability for enhanced glibenclamide dissolution performance. *J. Microencapsul.* **32**, 181–192 (2015).
89. Khan, N. & Craig, D. Q. M. The influence of drug incorporation on the structure and release properties of solid dispersions in lipid matrices. *J. Control. Release* **93**, 355–368 (2003).
90. Xiao, Y., Wang, S., Chen, Y. & Ping, Q. Self-emulsifying bifendate pellets: preparation, characterization and oral bioavailability in rats. *Drug Dev. Ind. Pharm.* **39**, 724–732 (2013).
91. Zingone, G. & Rubessa, F. Release of carbamazepine from solid dispersions with polyvinylpyrrolidone/vinylacetate copolymer (PVP/VA). *S.T.P. Pharma Sci. J.* **4**, 122–127 (1994).
92. Gupta, S., Chavhan, S. & Sawant, K. K. Self-nanoemulsifying drug delivery system for adefovir dipivoxil: Design, characterization, in vitro and ex vivo evaluation. *Colloids Surfaces A Physicochem. Eng. Asp.* **392**, 145–155 (2011).
93. Devani, M., Ashford, M. & Craig, D. Q. M. The emulsification and solubilisation properties of polyglycolysed oils in self-emulsifying formulations. *J. Pharm. Pharmacol.* **56**, 307–316 (2010).
94. Li, P. *et al.* Effect of combined use of nonionic surfactant on formation of oil-in-water microemulsions. *Int. J. Pharm.* **288**, 27–34 (2005).
95. Mukherjee, T. & Plakogiannis, F. M. Development and oral bioavailability assessment of a

- supersaturated self-microemulsifying drug delivery system (SMEDDS) of albendazole. *J. Pharm. Pharmacol.* **62**, 1112–1120 (2010).
96. Zhao, Y., Bao, Y., Wang, J. & Rohani, S. In situ focused beam reflectance measurement (FBRM), attenuated total reflectance fourier transform infrared (ATR-FTIR) and Raman characterization of the polymorphic transformation of carbamazepine. *Pharmaceutics* **4**, 164–178 (2012).
  97. Park, M. W. & Yeo, S. Do. Antisolvent crystallization of carbamazepine from organic solutions. *Chem. Eng. Res. Des.* **90**, 2202–2208 (2012).
  98. Thirunahari, S., Aitipamula, S., Chow, P. S. & Tan, R. B. H. Conformational polymorphism of tolbutamide: A structural, spectroscopic, and thermodynamic characterization of Burger's Forms I-IV. *J. Pharm. Sci.* **99**, 2975–2990 (2010).
  99. Paus, R., Hart, E., Ji, Y. & Sadowski, G. Solubility and Caloric Properties of Cinnarizine. *J. Chem. Eng. Data* **60**, 2256–2261 (2015).
  100. Gu, C., Rao, D., Gandhi, R. B., Hilden, J. o. n. & Raghavan, K. Using a Novel Multicompartment Dissolution System to Predict the Effect of Gastric pH on the Oral Absorption of Weak Bases with Poor Intrinsic Solubility. *J. Pharm. Sci.* **94**, 199–208 (2005).
  101. Grzesiak, A. L., Lang, M., Kim, K. & Matzger, A. J. Comparison of the Four Anhydrous Polymorphs of Carbamazepine and the Crystal Structure of Form I. *J. Pharm. Sci.* **92**, 2260–2271 (2003).
  102. Kobayashi, Y., Ito, S., Itai, S. & Yamamoto, K. Physicochemical proprieties and bioavailability of carbamazepine polymorphs and dehydrate. *Int. J. Pharm.* **193**, 137–146 (2000).
  103. Aparecida, M. *et al.* Thermoanalytical studies of carbamazepine: hydration/ dehydration, thermal decomposition, and solid phase transitions. *Brazilian J. Pharm. Sci.* **50**, 877–884 (2014).
  104. Perissutti, B., Rubessa, F. & Princivalle, F. Solid dispersions of carbamazepine with Gelucire 44/14 and 50/13. *S.T.P. Pharma Sci. J.* **10**, 479–484 (2000).
  105. Parambil, J. V., Poornachary, S. K., Hinder, S. J., Tan, R. B. H. & Heng, J. Y. Y. Establishing template-induced polymorphic domains for API crystallisation: the case of carbamazepine. *CrystEngComm* **17**, 6384–6392 (2015).
  106. Martins, R. M., Siqueira, S., Machado, M. O. & Freitas, L. A. P. The effect of homogenization method on the properties of carbamazepine microparticles prepared by spray congealing. *J. Microencapsul.* **30**, 692–700 (2013).
  107. Rustichelli, C. *et al.* Solid-state study of polymorphic drugs: Carbamazepine. *J. Pharm. Biomed. Anal.* **23**, 41–54 (2000).
  108. Lampman, G. M., Pavia, D. L. & Kriz, G. S. *Introduction to Spectroscopy.* (2009).
  109. Hasegawa, G. *et al.* Reevaluation of solubility of tolbutamide and polymorphic transformation from Form I to unknown crystal form. *Int. J. Pharm.* **369**, 12–18 (2009).
  110. Türk, M. & Bolten, D. Polymorphic properties of micronized mefenamic acid, nabumetone, paracetamol and tolbutamide produced by rapid expansion of supercritical solutions (RESS). *J.*



*Supercrit. Fluids* **116**, 239–250 (2016).

111. Kimura, K., Hirayama, F. & Uekama, K. Characterization of Tolbutamide Polymorphs ( Burger ' s Forms II and IV ) and Polymorphic Transition Behavior. *J. Pharm. Sci.* **88**, 385–391 (1999).
112. Siqueira Jørgensen, S., Rades, T., Mu, H., Graeser, K. & Müllertz, A. Exploring the utility of the Chasing Principle: influence of drug-free SNEDDS composition on solubilization of carvedilol, cinnarizine and R3040 in aqueous suspension. *Acta Pharm. Sin. B* **9**, 194–201 (2019).
113. Tian, T., Wang, Z. & Zhang, J. Pathomechanisms of Oxidative Stress in Inflammatory Bowel Disease and Potential Antioxidant Therapies. *Oxid. Med. Cell. Longev.* **2017**, 18 (2017).
114. Simmonds, N. J. *et al.* Chemiluminescence assay of mucosal reactive oxygen metabolites in inflammatory bowel disease. *Gastroenterology* **103**, 186–196 (1992).
115. Lih-Brody, L. *et al.* Increased oxidative stress and decreased antioxidant defenses in mucosa of inflammatory bowel disease. *Dig. Dis. Sci.* **41**, 2078–2086 (1996).
116. Wilson, D. S. *et al.* Orally delivered thioketal nanoparticles loaded with TNF- $\alpha$ -siRNA target inflammation and inhibit gene expression in the intestines. *Nat. Mater.* **9**, 923–928 (2010).
117. Lamprecht, A., Schäfer, U. & Lehr, C. M. Size-dependent bioadhesion of micro- and nanoparticulate carriers to the inflamed colonic mucosa. *Pharm. Res.* **18**, 788–793 (2001).
118. Song, C.-C., Ji, R., Du, F.-S. & Li, Z.-C. Oxidation-Responsive Poly(amino ester)s Containing Arylboronic Ester and Self-Immolative Motif: Synthesis and Degradation Study. *Macromolecules* **46**, 8416–8425 (2013).
119. de Gracia Lux, C. *et al.* Biocompatible polymeric nanoparticles degrade and release cargo in response to biologically relevant levels of hydrogen peroxide. *J. Am. Chem. Soc.* **134**, 15758–15764 (2012).
120. Zhang, D. *et al.* Biocompatible Reactive Oxygen Species (ROS)-Responsive Nanoparticles as Superior Drug Delivery Vehicles. *Adv. Healthc. Mater.* **4**, 69–76 (2014).
121. Broaders, K. E., Grandhe, S. & Fréchet, J. M. J. A biocompatible oxidation-triggered carrier polymer with potential in therapeutics. *J. Am. Chem. Soc.* **133**, 756–758 (2011).
122. Hua, S., Marks, E., Schneider, J. J. & Keely, S. Advances in oral nano-delivery systems for colon targeted drug delivery in inflammatory bowel disease : Selective targeting to diseased versus healthy tissue. *Nanomedicine Nanotechnology, Biol. Med.* **11**, 1117–1132 (2015).
123. Sartor, R. B. Review article: the potential mechanisms of action of rifaximin in the management of inflammatory bowel diseases. *Aliment. Pharmacol. Ther.* **43**, 27–36 (2016).
124. Guslandi, M. Rifaximin in the treatment of inflammatory bowel disease. *World J. Gastroenterol.* **17**, 4643–4646 (2011).
125. Li, W. *et al.* Microfluidic assembly of a nano-in-micro dual drug delivery platform composed of halloysite nanotubes and a pH-responsive polymer for colon cancer therapy. *Acta Biomater.* **48**, 238–246 (2017).

126. Hidalgo, T., Bellido, E., Avila, J., Asensio, M. C. & Salles, F. Chitosan-coated mesoporous MIL- 100 ( Fe ) nanoparticles as improved bio-compatible oral nanocarriers. *Sci. Rep.* **100**, 1–14 (2017).
127. Coco, R. *et al.* Drug delivery to inflamed colon by nanoparticles : Comparison of different strategies. *Int. J. Pharm.* **440**, 3–12 (2013).
128. Liu, D., Bimbo, L. M., Mäkilä, E., Villanova, F. & Kaasalainen, M. Co-delivery of a hydrophobic small molecule and a hydrophilic peptide by porous silicon nanoparticles. *J. Control. Release* **170**, 268–278 (2013).
129. Li, X., Zhu, J., Man, Z., Ao, Y. & Chen, H. Investigation on the structure and upconversion fluorescence of Yb(3+)/Ho(3+) co-doped fluorapatite crystals for potential biomedical applications. *Sci. Rep.* **4**, 4446 (2014).
130. Lin, X., Han, P., Dong, S. & Li, H. RSC Advances Preparation and application of bacteriophage- loaded chitosan microspheres for controlling *Lactobacillus plantarum* contamination in bioethanol fermentation. *RSC Adv.* **5**, 69886–69893 (2015).
131. Mansur, H. S., Mansur, A. A. P., Curti, E. & De Almeida, M. V. Functionalized-chitosan/quantum dot nano-hybrids for nanomedicine applications: towards biolabeling and biosorbing phosphate metabolites. *J. Mater. Chem. B* **1**, 1696–1711 (2013).
132. Araújo, F. & Sarmiento, B. Towards the characterization of an in vitro triple co-culture intestine cell model for permeability studies. *Int. J. Pharm.* **458**, 128–134 (2013).
133. Sogias, I. A., Williams, A. C. & Khutoryanskiy, V. V. Why is Chitosan Mucoadhesive? *Biomacromolecules* **9**, 1837–1842 (2008).
134. Walter, E., Janich, S., Roessler, B. J., Hilfinger, J. M. & Amidon, G. L. HT29-MTX/Caco-2 Cocultures as an in Vitro Model for the Intestinal Epithelium: In Vitro–in Vivo Correlation with Permeability Data from Rats and Humans. *J. Pharm. Sci.* **85**, 1070–1076 (1996).
135. Di Sabatino, M., Albertini, B., Kett, V. L. & Passerini, N. Spray congealed lipid microparticles with high protein loading: Preparation and solid state characterisation. *Eur. J. Pharm. Sci.* **46**, 346–356 (2012).
136. Passerini, N. *et al.* Development of microparticles for oral administration of the non-conventional radical scavenger IAC and testing in an in fl ammatory rat model. *Int. J. Pharm.* **512**, 126–136 (2016).
137. Hønborg, N. & Mullertz, A. A dynamic in vitro lipolysis model I . Controlling the rate of lipolysis by continuous addition of calcium. *Eur. J. Pharm. Sci.* **14**, 115–122 (2001).
138. Kilic, M. & Dressman, J. A simplified method to screen for in-vivo performance of oral lipid formulations. *J. Pharm. Pharmacol.* **66**, 615–623 (2014).
139. Williams, H. D. *et al.* Toward the Establishment of Standardized In Vitro Tests for Lipid-Based Formulations , Part 1 : Method Parameterization and Comparison of In Vitro Digestion Profiles Across a Range. *J. Pharm. Sci.* **101**, 3360–3380 (2012).
140. Benito-gallo, P. *et al.* Chain length affects pancreatic lipase activity and the extent and pH – time profile of triglyceride lipolysis. *Eur. J. Pharm. Biopharm.* **93**, 353–362 (2015).

141. Vertzoni, M. *et al.* Dissolution media simulating the intraluminal composition of the small intestine : physiological issues and practical aspects. *J. Pharm. Pharmacol.* **56**, 453–462 (2004).
142. Jantratid, E., Janssen, N., Chokshi, H., Tang, K. & Dressman, J. B. Designing biorelevant dissolution tests for lipid formulations : Case example – Lipid suspension of RZ-50. *Eur. J. Pharm. Biopharm.* **69**, 776–785 (2008).
143. Griffin, B. T. *et al.* Comparison of in vitro tests at various levels of complexity for the prediction of in vivo performance of lipid-based formulations : Case studies with fenofibrate. *Eur. J. Pharm. Biopharm.* **86**, 427–437 (2014).
144. Pestieau, A., Krier, F., Brouwers, A., Streel, B. & Evrard, B. Selection of a discriminant and biorelevant in vitro dissolution test for the development of fenofibrate self-emulsifying lipid-based formulations. *Eur. J. Pharm. Sci.* **92**, 212–219 (2016).
145. Albertini, B., Di Sabatino, M., Melegari, C. & Passerini, N. Formulating SLMs as oral pulsatile system for potential delivery of melatonin to pediatric population. *Int. J. Pharm.* **469**, 67–79 (2014).
146. Matos-jr, F. E., Di, M., Passerini, N., Favaro-trindade, C. S. & Albertini, B. Development and characterization of solid lipid microparticles loaded with ascorbic acid and produced by spray congealing. *Food Res. Int.* **67**, 52–59 (2015).
147. *Sigma Aldrich data sheet, available online on [https://www.sigmaaldrich.com/content/dam/sigmaaldrich/docs/Sigma-Aldrich/Product\\_Information\\_Sheet/c0750pis.pdf](https://www.sigmaaldrich.com/content/dam/sigmaaldrich/docs/Sigma-Aldrich/Product_Information_Sheet/c0750pis.pdf).*
148. Vertzoni, M., Pastelli, E., Psachoulas, D., Kalantzi, L. & Reppas, C. Estimation of Intragastric Solubility of Drugs: In What Medium? *Pharm. Res.* **24**, 909–917 (2007).
149. Williams, H. D., Barrett, D. A., Ward, R., Hardy, I. J. & Melia, C. D. A liquid chromatography method for quantifying caffeine dissolution from pharmaceutical formulations into colloidal , fat-rich media. *J. Chromatogr. B* **878**, 1739–1745 (2010).
150. Go, E. H. Release and diffusional modeling of metronidazole lipid matrices. *Eur. J. Pharm. Biopharm.* **63**, 331–339 (2006).
151. Qi, S., Deutsch, D. & Craig, D. Q. M. An Investigation into the Mechanisms of Drug Release From Taste-Masking Fatty Acid Microspheres. *J. Pharm. Sci.* **97**, 3842–3854 (2008).
152. Andreas, C. J. *et al.* Mechanistic investigation of the negative food effect of modified release zolpidem. *Eur. J. Pharm. Sci.* **102**, 284–298 (2017).
153. Davis, J., Burton, J., Connor, A. L., Macrae, R. & Wilding, I. R. Scintigraphic Study to Investigate the Effect of Food on a HPMC Modified Release Formulation of UK-294,315. *J. Pharm. Sci.* **98**, 1568–1576 (2009).
154. Cvijić, S., Parojčić, J. & Langguth, P. Viscosity-mediated negative food effect on oral absorption of poorly-permeable drugs with an absorption window in the proximal intestine: In vitro experimental simulation and computational verification. *Eur. J. Pharm. Sci.* **61**, 40–53 (2014).
155. Brouwers, J. *et al.* Food-dependent disintegration of immediate release fosamprenavir tablets : In vitro evaluation using magnetic resonance imaging and a dynamic gastrointestinal system. *Eur. J. Pharm. Biopharm.* **77**, 313–319 (2011).

156. Borkar, N. *et al.* Investigating the correlation between in vivo absorption and in vitro release of fenofibrate from lipid matrix particles in biorelevant medium. *Eur. J. Pharm. Sci.* **51**, 204–210 (2014).
157. Robson, H. J., Craig, D. Q. M. & Deutsch, D. An investigation into the release of cefuroxime axetil from taste-masked stearic acid microspheres Part 1: The influence of the dissolution medium on the drug release profile and the physical integrity of the microspheres. *Int. J. Pharm.* **190**, 183–192 (1999).
158. Xie, X. *et al.* Micelle dynamic simulation and physicochemical characterization of biorelevant media to reflect gastrointestinal environment in fasted and fed states. *Eur. J. Pharm. Biopharm.* **88**, 565–573 (2014).
159. Witzleb, R., Müllertz, A., Kanikanti, V., Hamann, H. & Kleinebudde, P. Dissolution of solid lipid extrudates in biorelevant media. *Int. J. Pharm.* **422**, 116–124 (2012).
160. Raman, S. & Polli, J. E. Prediction of positive food effect : Bioavailability enhancement of BCS class II drugs. *Int. J. Pharm.* **506**, 110–115 (2016).
161. Stappaerts, J., Wuyts, B., Tack, J., Annaert, P. & Augustijns, P. Human and simulated intestinal fluids as solvent systems to explore food effects on intestinal solubility and permeability. *Eur. J. Pharm. Sci.* **63**, 178–186 (2014).
162. Nart, V. *et al.* Carnauba wax as a promising excipient in melt granulation targeting the preparation of mini-tablets for sustained release of highly soluble drugs. *Mater. Sci. Eng. C* **70**, 250–257 (2017).
163. Mason, L. M. *et al.* Use of the Dynamic Gastric Model as a tool for investigating fed and fasted sensitivities of low polymer content hydrophilic matrix formulations. *Int. J. Pharm.* **510**, 210–220 (2016).
164. Awai, Y. K., Ujii, Y. F., Abata, F. T., To, J. I. & Etsugi, Y. M. Analysis of Food Effects on Oral Drug Absorption Considering Micelle Interaction and Solubilization by Bile Micelles. *Drug Metab. Pharmacokinet.* **26**, 1–2 (2011).
165. Maksimainen, M. M., Lampio, A., Mertanen, M., Turunen, O. & Rouvinen, J. The crystal structure of acidic  $\beta$ -galactosidase from *Aspergillus oryzae*. *Int. J. Biol. Macromol.* **60**, 109–115 (2013).
166. Husain, Q.  $\beta$  Galactosidases and their potential applications : a review. *Crit. Rev. Biotechnol.* **30**, 41–62 (2010).
167. European Food Safety Authority (EFSA), Parma, I. Scientific Opinion on lactose thresholds in lactose intolerance and galactosaemia. *EFSA J.* **8**, 1–29 (2010).
168. Bayless, T. M., Brown, E., Paige, D. M. & Paige, D. M. Lactase Non-persistence and Lactose Intolerance. *Curr Gastroenterol Rep* **19**, 23 (2017).
169. Montalto, M. *et al.* Management and treatment of lactose malabsorption. *World J. Gastroenterol.* **12**, 187–191 (2006).
170. O’Connell, S. & Walsh, G. Physicochemical Characteristics of Commercial Lactases Relevant to Their Application in the Alleviation of Lactose Intolerance. *Appl. Microbiol. Biotechnol.* **134**, 179–191 (2006).
171. Kim, C., Chung, H., Lee, M., Choi, L. & Kim, M. Development of dried liposomes containing b -

galactosidase for the digestion of lactose in milk. *Int. J. Pharm.* **183**, 185–193 (1999).

172. Alavi, A. K., Squillante, E. & Mehta, K. A. Formulation of enterosoluble microparticles for an acid labile protein. *J. Pharm. Pharm. Sci.* **5**, 234–244 (2002).
173. Squillante, E., Morshed, G., Bagchi, S. & Mehta, K. A. Microencapsulation of beta-galactosidase with Eudragit L-100. *J. Microencapsul.* **20**, 153–67 (2003).
174. Sheng, Y., He, H. & Zou, H. Poly(lactic acid) nanoparticles coated with combined WGA and water-soluble chitosan for mucosal delivery of  $\beta$ -galactosidase. *Drug Deliv.* **21**, 370–8 (2014).
175. Wagner, I. *et al.* Stable formulation of protein-type drug in electrospun polymeric fiber followed by tableting and scaling-up experiments. *Polym. Adv. Technol.* **26**, 1461–1467 (2015).
176. Zhang, Z., Zhang, R., Chen, L. & McClements, D. J. Encapsulation of lactase (b-galactosidase) into k-carrageenan-based hydrogel beads: Impact of environmental conditions on enzyme activity. *Food Chem.* **200**, 69–75 (2016).
177. Zhang, Z., Zhang, R. & McClements, D. J. Lactase ( b -galactosidase ) encapsulation in hydrogel beads with controlled internal pH microenvironments : Impact of bead characteristics on enzyme activity. *Food Hydrocoll.* **67**, 85–93 (2017).
178. Liu, M. *et al.* Molecular Sieving on the Surface of a Protein Provides Protection Without Loss of Activity. *Adv. Funct. Mater.* **23**, 2007–2015 (2012).
179. O’Connell, S. & Walsh, G. A novel acid-stable, acid-active b-galactosidase potentially suited to the alleviation of lactose intolerance. *Appl. Microbiol. Biotechnol.* **86**, 517–524 (2010).
180. Becker, K., Salar-behzadi, S. & Zimmer, A. Solvent-Free Melting Techniques for the Preparation of Lipid-Based Solid Oral Formulations. *Pharm. Res.* **32**, 1519–1545 (2015).
181. Jannin, V. *et al.* In vitro lipolysis tests on lipid nanoparticles : comparison between lipase / co-lipase and pancreatic extract In vitro lipolysis tests on lipid nanoparticles : comparison between lipase / co-lipase and pancreatic extract. *Drug Dev. Ind. Pharm.* **9045**, (2015).
182. Armand, M. *et al.* Effects of droplet size , triacylglycerol composition , and calcium on the hydrolysis of complex emulsions by pancreatic lipase : an in vitro study. *J. Nutr. Biochem.* **3**, 333–341 (1992).
183. Fernandez, S. *et al.* Lipolysis of the semi-solid self-emulsifying excipient Gelucire® 44/14 by digestive lipases. *Biochim. Biophys. Acta J.* **1781**, 367–375 (2008).
184. Sun, S., Dong, L., Xu, X. & Shen, S. Immobilization of  $\beta$  -galactosidase from *Aspergillus Oryzae* on Macroporous PloyGMA Newly Prepared. *Int. J. Chem.* **2**, 89–96 (2010).
185. Sarti, F., Barthelmes, J., Iqbal, J., Hintzen, F. & Bernkop-schnürch, A. Intestinal enzymatic metabolism of drugs. *J. Pharm. Pharmacol.* **63**, 392–399 (2011).
186. Klein, S., Stein, J. & Dressman, J. Site-specific delivery of anti-inflammatory drugs in the gastrointestinal tract: an in-vitro release model. *J. Pharm. Pharmacol.* **57**, 709–719 (2005).
187. Christophersen, P. C. *et al.* Solid lipid particles for oral delivery of peptide and protein drugs I –

- Elucidating the release mechanism of lysozyme during lipolysis. *Eur. J. Pharm. Biopharm.* **85**, 473–480 (2013).
188. Christophersen, P. C. *et al.* Solid Lipid Particles for Oral Delivery of Peptide and Protein Drugs II - The Digestion of Trilaurin Protects Desmopressin from Proteolytic Degradation. *Pharm. Res.* 1–9 (2014). doi:10.1007/s11095-014-1337-z
  189. Sek, L., Porter, C. J. H., Kaukonen, A. M. & Charman, W. N. Evaluation of the in-vitro digestion profiles of long and medium chain glycerides and the phase behaviour of their lipolytic products. *J. Pharm. Pharmacol.* **54**, 29–41 (2002).
  190. Brockerhoff, H. Substrate specificity of pancreatic lipase. *Biochim. Biophys. Acta* **159**, 296–303 (1968).
  191. N’Goma Bakala, J.-C., Amara, S., Dridi, K., Jannin, V. & Carrière, F. Understanding the lipid-digestion processes in the GI tract before designing lipid-based drug-delivery systems. *Ther. Deliv.* **3**, 105–124 (2012).
  192. Tanaka, Y., Kagamiishi, A., Horiuchi, T. & Kiuchi, A. Purification and properties of beta-galactosidase from *Aspergillus oryzae*. *J. Biochem.* **77**, 241–247 (1975).
  193. Fuhrmann, G. & Leroux, J.-C. Improving the stability and activity of oral therapeutic enzymes-recent advances and perspectives. *Pharm. Res.* **31**, 1099–105 (2014).
  194. Da Silva, E., Bresson, S. & Rousseau, D. Characterization of the three major polymorphic forms and liquid state of tristearin by Raman spectroscopy. *Chem. Phys. Lipids* **157**, 113–119 (2009).
  195. Bunjes, H., Westesen, K. & Koch, M. H. J. Crystallization tendency and polymorphic transitions in triglyceride nanoparticles. *Int. J. Pharm.* **129**, 159–173 (1996).
  196. Albertini, B., Passerini, N. & Gonza, M. L. Effect of Aerosil R on the properties of lipid controlled release microparticles. *J. Control. Release* **100**, 233–246 (2004).
  197. Koennings, S., Berié, A., Tessmar, J., Blunk, T. & Goepferich, A. Influence of wettability and surface activity on release behavior of hydrophilic substances from lipid matrices. *J. Control. Release* **119**, 173–181 (2007).
  198. Kollipara, S. & Gandhi, R. K. Pharmacokinetic aspects and in vitro – in vivo correlation potential for lipid-based formulations. *Acta Pharm. Sin. B* **4**, 333–349 (2014).
  199. Sies, H. Oxidative stress: a concept in redox biology and medicine. *Redox Biol.* **4**, 180–183 (2015).
  200. Bhattacharyya, A., Chattopadhyay, R., Mitra, S. & Crowe, S. E. Oxidative Stress: An Essential Factor in the Pathogenesis of Gastrointestinal Mucosal Diseases. *Physiol. Rev.* **94**, 329–354 (2014).
  201. Kim, Y. J., Kim, E.-H. & Hahm, K. B. Oxidative stress in inflammation-based gastrointestinal tract diseases: Challenges and opportunities. *J. Gastroenterol. Hepatol.* **27**, 1004–1010 (2012).
  202. Moura, F. A., de Andrade, K. Q., dos Santos, J. C. F., Araújo, O. R. P. & Goulart, M. O. F. Antioxidant therapy for treatment of inflammatory bowel disease: Does it work? *Redox Biol.* **6**, 617–639 (2015).
  203. Townsend, D. M., Tew, K. D. & Tapiero, H. The importance of glutathione in human disease. *Biomed.*

*Pharmacother.* **57**, 145–155 (2003).

204. Camera, E. & Picardo, M. Analytical methods to investigate glutathione and related compounds in biological and pathological processes. *J. Chromatogr. B* **781**, 181–206 (2002).
205. Trapani, A. *et al.* Eudragit RS 100 microparticles containing 2-hydroxypropyl- $\beta$ -cyclodextrin and glutathione : Physicochemical characterization , drug release and transport studies. *Eur. J. Pharm. Sci.* **30**, 64–74 (2007).
206. Themelis, T., Gotti, R. & Gatti, R. Journal of Pharmaceutical and Biomedical Analysis A novel hydrophilic interaction liquid chromatography method for the determination of underivatized amino acids in alimentary supplements. *J. Pharm. Biomed. Anal.* **145**, 751–757 (2017).
207. Newland, B. *et al.* Synthesis of ROS scavenging microspheres from a dopamine containing poly( $\beta$ -amino ester) for applications for neurodegenerative disorders. *Biomater. Sci.* **4**, 400–404 (2016).
208. Cole, S. P. Rapid chemosensitivity testing of human lung tumor cells using the MTT assay. *Cancer Chemother. Pharmacol.* **17**, 259–263 (1986).
209. Kutscher, H., Stein, S. & Sinko, P. Nonenzymatic , Self-Elimination Degradation Mechanism of Glutathione. *Chem. Biodivers.* **6**, 527–539 (2009).
210. Forman, H. J., Zhang, H. & Rinna, A. Glutathione: Overview of its protective roles, measurement, and biosynthesis. *Mol. Aspects Med.* **30**, 1–12 (2009).
211. Pompella, A., Visvikis, A., Paolicchi, A., Tata, V. De & Casini, A. F. The changing faces of glutathione, a cellular protagonist. *Biochem. Pharmacol.* **66**, 1499–1503 (2003).